

UNIVERSIDADE DE SÃO PAULO
INSTITUTO DE QUÍMICA
Programa de Pós-Graduação em Ciências Biológicas (Bioquímica)

BRUNO BARROS QUELICONI

**Bicarbonato/CO₂ Aumenta Dano
em Isquemia-Reperfusão: da
observação inicial à caracterização
molecular**

São Paulo

Data do Depósito na SPG:
05/09/2014

BRUNO BARROS QUELICONI

**Bicarbonato/CO₂ Aumenta Dano em Isquemia-
Reperusão: da observação inicial à caracterização
molecular**

*Tese apresentada ao Instituto de Química da
Universidade de São Paulo para obtenção do
Título de Doutor em Ciências (Bioquímica)*

Orientadora: Profa. Dra. Alicia Juliana Kowaltowski

São Paulo
2014

Agradecimentos

Gostaria de agradecer as pessoas que fizeram essa tese possível e contribuíram direta ou indiretamente para que fosse completada.

À Mônica Shizuka Takahashi, por estar sempre comigo, aguentando eu falar do laboratório o tempo todo, suportar todas as minhas ambições e viagens e sempre me dar a oportunidade de ser uma pessoa melhor e crescer ao seu lado.

Aos meus pais e avó, Flávio, Rosana e Nilda, por sempre apoiarem minha decisão de seguir a carreira científica, incentivar meus sonhos e me suportar financeiramente sempre que precisei.

À Alicia Kowaltowski, que foi uma ótima orientadora me dando liberdade para desenvolver o meu trabalho, mas sempre me ajudando a construir minha carreira da melhor maneira possível com sugestões e todo o incentivo que eu poderia receber.

A todos os colaboradores que tive durante o doutorado, em especial ao Julio Ferreira e Juliane Campos, por me darem a oportunidade de trabalhar com exercício, algo que sempre desejei e me introduzirem a diversos assuntos que hoje são partes fundamentais da minha formação; à Ohara Augusto e Sandra Vaz que foram fundamentais no início desse trabalho; ao Keith Nehrke e Paul Brookes, por me receberem em Rochester e me ajudarem sempre que precisei deles; à Roberta Gottlieb por me receber em San Diego e Los Angeles e me introduzir a novas e interessantes ideias e campos científicos.

À Thire Marazzi, uma ótima aluna e amiga que me ensinou muito sobre a visão médica dos diversos problemas que estudamos juntos.

A todos técnicos, colegas e ex-colegas dos laboratórios e institutos onde trabalhei que através do constante suporte, de discussões sobre experimentos, ideias e hipóteses me ensinaram sobre seus campos e linhas de pesquisas, a planejar bons experimentos, e mais importante, que boa ciência não se faz sozinho.

À FAPESP, CNPq, ASBMB e NHI, sem os quais não haveria suporte financeiro para todos os trabalhos que foram desenvolvidos e por me suportarem durante os anos do doutorado.

Epígrafe

"Science is not about building a body of known 'facts'. It is a method for asking awkward questions and subjecting them to a reality-check, thus avoiding the human tendency to believe whatever makes us feel good. " T. Pratchett

RESUMO

Queliconi, B.B. **Bicarbonato/CO₂ Aumenta Dano em Isquemia-Reperfusão: da observação inicial à caracterização molecular.** 2014, 143p. Tese (Doutorado) - Programa de Pós-Graduação em Ciências (Bioquímica). Instituto de Química, Universidade de São Paulo, São Paulo.

Bicarbonato é uma importante espécie química para os seres vivos, sendo o principal tampão celular, além de apresentar uma negligenciada atividade redox. Isquemia é um evento no qual existe inibição do aporte de nutrientes e oxigênio, sendo a reperfusão o retorno do fluxo de nutrientes e oxigênio, que é acompanhada por alta produção de radicais livres e morte celular. Nessa tese estudamos o efeito da presença de bicarbonato durante a isquemia-reperfusão. Em nosso modelo nós mantivemos o pH constante e modulamos a quantidade de bicarbonato enquanto células, órgãos e animais foram submetidos a isquemia-reperfusão. Utilizamos condições sem a presença de bicarbonato, a concentração basal sanguínea e uma concentração mais alta simulando o acúmulo de bicarbonato em condições isquêmicas. Nesses diversos modelos mostramos que a presença de bicarbonato aumenta o dano provocado por isquemia-reperfusão e provoca um aumento do acúmulo de proteínas oxidadas. A presença do bicarbonato não modifica a respiração, produção de espécies reativas de oxigênio, ou a morfologia mitocondrial, também não detectamos mudança na atividade do proteossoma e nos indicadores de autofagia geral. Entretanto detectamos um acúmulo de marcadores autofágicos na fração mitocondrial indicando inibição da mitofagia. Essa inibição foi confirmada ao detectarmos o acúmulo de uma proteína degradada especificamente por mitofagia enquanto não houve mudança em outra degradada pelo proteossoma. Além disso, ao inibirmos farmacologicamente a autofagia, reproduzimos o fenótipo causado pelo bicarbonato mesmo na sua ausência. Em conclusão, a presença de bicarbonato é deletéria em condições de isquemia/reperfusão devido a inibição da mitofagia.

Palavras-chave: Bicarbonato, Isquemia, Coração, Mitocôndria, Espécies reativas de oxigênio, Mitofagia

ABSTRACT

Queliconi, B.B. **Bicarbonate/CO₂ Increase Damage in Ischemia-Reperfusion Injury: from observation to molecular characterization.** 2014, 143p. PhD Thesis - Graduate Program in Biochemistry. Instituto de Química, Universidade de São Paulo, São Paulo.

Bicarbonate is an important molecule in all living being, acting as the main cellular buffer. However, its biological and redox activity has been mostly neglected to date. Ischemia is an event in which an inhibition of nutrient availability and oxygen flow occurs, while reperfusion is the return of nutrients and oxygen, accompanied of a burst of reactive oxygen species production and cell death. Here, we studied the effects of bicarbonate during cardiac ischemia-reperfusion. In our model, we kept the pH stable and changed the concentration of the bicarbonate. We then subjected cells, organs and animals to ischemia-reperfusion under conditions where there was no presence, basal blood concentration or a higher concentration of bicarbonate. In these diverse models, we found that the presence of bicarbonate increased damage after a ischemia-reperfusion, and promoted the accumulation of oxidized proteins. Bicarbonate did not change respiration, production of reactive oxygen species or the morphology of the mitochondria. There were also no changes in proteasome activity and in global autophagy markers, although there was an accumulation of mitophagy markers. We also found that mitophagy was responsible for the increased damage observed, since pharmacological inhibiting of autophagy abolished the increased damage caused by the presence of bicarbonate. In conclusion the presence of bicarbonate is deleterious in ischemia-reperfusion due mitophagy inhibition.

Keywords: Bicarbonate, Ischemia, Heart, Mitochondria, Reactive oxygen species, Mitophagy

LISTA DE ABREVIATURAS E SIGLAS

BPM – Batimentos por minuto

CK – Creatina quinase

CCCP - Carbonilcianeto m-clorofenil-hidrazona

CoxIV - Subunidade IV da citocromo C oxidase

DTT - Ditioneitol

DNPH – 2,4 - Dinitrofenilhidrazina

EROs – Espécies reativas de oxigênio

HRP - Peroxidase de raiz forte tipo 1

IR – Isquemia-reperfusão

min – Minuto(s)

NOS - sintase de óxido nítrico

s – Segundos

SDS - Dodecil sulfato de sódio

SOD – Superóxido dismutase

sIR – Simulação de isquemia-reperfusão

sIR(CN⁻) - Simulação de isquemia-reperfusão utilizando cianeto

TTC - 2,3,5-triphenil-tetrazolium

WB – Western Blot

Sumário

1. Introdução	11
1.1. Isquemia cardíaca	11
1.2. Tampão bicarbonato	12
1.3. Espécies reativas de oxigênio	13
1.4. Dinâmica mitocondrial	15
1.5. Autofagia/Mitofagia	16
2. Objetivos	18
3. Materiais e Métodos	19
3.1. Materiais	19
3.2. Isolamento de mitocôndrias de coração de rato	19
3.3. Tampão de experimento	20
3.4. Produção de H ₂ O ₂	20
3.5. Consumo de oxigênio em mitocôndrias	21
3.6. Corações de ratos isolados	21
3.7. Medidas hemodinâmicas	22
3.8. Cálculo da área infartada	22
3.9. Dosagem da liberação de creatina quinase (CK)	22
3.10. Cultivo de células HL-1	23
3.11. Quantificação de pH utilizando BCECF-AM	23
3.12. Simulação de isquemia/reperfusão em células HL-1	24
3.13. Viabilidade celular usando brometo de etídio	25
3.14. Extração proteica	26
3.15. Western Blot	26
3.16. Dosagem de proteína	28
3.17. Imunohistoquímica em células HL-1	28
3.18. Atividade do proteassoma	29
3.19. RT-PCR	29
3.20. <i>Caenorhabditis elegans</i>	29
3.21. Anóxia-jejum (IR) em <i>C. elegans</i>	30
3.22. <i>C. elegans</i> teste de resposta a toque	30
3.23. Microscopia do neurônio mecanosensor em <i>C. elegans</i>	31

3.24. Análise estatística	31
4. Resultados	32
4.1. Caracterização do dano causado pela presença de bicarbonato na IR	32
4.2. Identificação das mudanças moleculares no dano causado pela presença de bicarbonato na IR	43
5. Discussão	58
5.1. Caracterização do dano causado pela presença de bicarbonato na IR	58
5.2. Identificação das mudanças moleculares no dano causado pela presença de bicarbonato na IR	59
6. Conclusões	65
7. Referências	66
Apêndice	74
Ap.1. Pharmacological and physiological stimuli do not promote Ca ²⁺ -sensitive K ⁺ channel activity in isolated heart mitochondria, doi: 10.1016/j.cardiores.2006.11.035	74
Ap.2. Mitochondrial Ion Transport Pathways: Role in Metabolic Diseases, doi: 10.1016/j.bbabi.2009.12.017	83
Ap.3. Redox regulation of the mitochondrial K(ATP) channel in cardioprotection, doi: 10.1016/j.bbamcr.2010.11.005	90
Ap.4. Mitochondrial compartmentalization of redox processes, doi: 10.1016/j.freeradbiomed.2012.03.008	97
Ap.5. Bicarbonate modulates oxidative and functional damage in ischemia-reperfusion, doi: 10.1016/j.freeradbiomed.2012.11.007	105
Ap.6. Exercise training restores cardiac protein quality control in heart failure, doi: 10.1371/journal.pone.0052764	113
Ap.7. An anoxia-starvation model for ischemia/reperfusion in <i>C. elegans</i> , doi: 10.3791/51231	125
Ap.8. Aldehyde dehydrogenase 2 activation in heart failure restores mitochondrial function and improves ventricular function and remodelling, doi: 10.1093/cvr/cvu125	133
Súmula Curricular	144

1. Introdução

1.1 - *Isquemia cardíaca*

Na isquemia cardíaca ocorre um declínio no aporte de sangue ao tecido cardíaco, levando a um déficit de substratos energéticos e oxigenação. Os danos provocados pelo processo de isquemia acontecem majoritariamente no momento do retorno da circulação, a reperfusão (Bolli, 1998; Facundo et al., 2006), quando há um aumento na produção de espécies reativas de oxigênio (EROs), principalmente provenientes da cadeia de transporte de elétrons mitocondrial (Zweier et al., 1987; Vanden Hoek et al., 1997; Wang et al., 2008; Chen e Zweier, 2014).

Existem diversos fatores que influenciam no dano final provocado pelo processo de isquemia-reperfusão (IR), e algumas técnicas que permitem que esse dano seja reduzido. A modulação da produção de EROs é de essencial importância no dano final provocado pela IR (Facundo et al., 2005; Sun et al., 2005; Quarrie et al., 2011). A produção de EROs na IR é essencialmente mitocondrial (Vanden Hoek et al., 1998), sendo controlada por diversos fatores, incluindo proteínas com sensores redox (Facundo et al., 2007; Queliconi et al., 2011). Outro ponto de controle da mitigação dos danos na IR está relacionado à dinâmica mitocondrial e a autofagia (Gottlieb e Mentzer, 2010).

1.2 - Tampão bicarbonato

O tampão bicarbonato ($\text{HCO}_3^-/\text{CO}_2$), presente no ambiente intra quanto extracelular com concentrações de 14,5 e 25 mM, respectivamente, ainda é pouco estudado em processos redox apesar de estudos demonstrarem que ele estimula reações de oxidação, peroxidação e nitração em biomoléculas (Hodgson e Fridovich, 1976; Berlett et al., 1990; Radi et al., 1993; Zhang, 2000; Bonini e Augusto, 2001; Liochev e Fridovich, 2002; Stadtman et al., 2005; Trindade et al., 2006; Ezraty et al., 2011; Queliconi et al., 2013) e que sua concentração é aumentada até 4 vezes durante a isquemia (Khuri et al., 1985). Existem diversos mecanismos conhecidos que levam à produção do radical bicarbonato (Fig. 1), mas não existe um consenso sobre os mecanismos de reação que levam à oxidação estimulada por $\text{HCO}_3^-/\text{CO}_2$. Sabe-se que não existe transferência de oxigênio nas reações de oxidação e que a presença de radicais de nitrogênio aumenta o dano (Augusto et al., 2002; Radi, 2004).

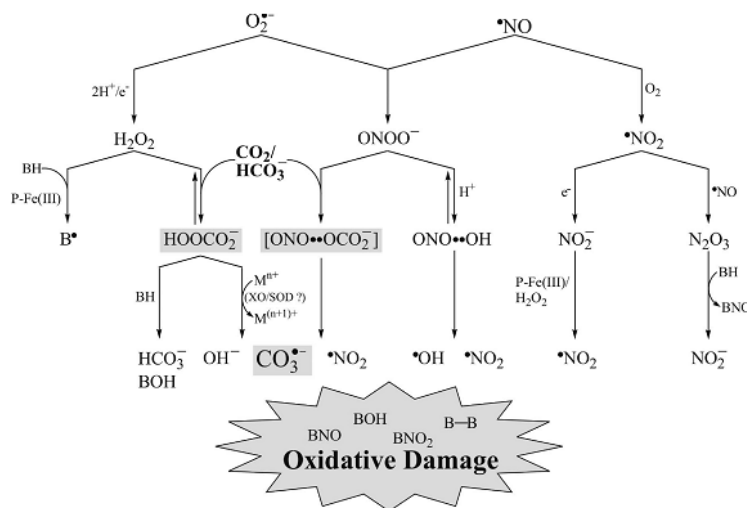


Fig. 1 – Esquema com mecanismos de formação do radical carbonato (extraído de Medinas et al 2007)

Recentemente nós demonstramos que o aumento da concentração de $\text{HCO}_3^-/\text{CO}_2$ aumenta o dano provocado por IR (Queliconi et al., 2013). Nossos dados mostram a viabilidade de usar o modelo de isquemia-reperfusão para estudar a importância do par $\text{HCO}_3^-/\text{CO}_2$.

1.3 - Espécies reativas de oxigênio

EROs têm importância tanto em condições patológicas quanto na fisiologia celular (Lebuffe et al., 2003; Palmer et al., 2007; Kowaltowski et al., 2009; Nadtochiy et al., 2009). As EROs mitocondriais são produzidas principalmente pelo vazamento de elétrons em sua cadeia de transporte de elétrons ou por desidrogenases presentes na matriz (Boveris e Chance, 1973; Turrens, 2003; Starkov et al., 2004; Tahara et al., 2007; Figueira et al., 2013). Fora da mitocôndria, EROs podem ser produzidas por outras enzimas, como a sintase de óxido nítrico (NOS), NADPH oxidase e xantina oxidase (Dröge, 2002).

A principal ERO produzida na mitocôndria é o radical ânion superóxido ($\text{O}_2^{\cdot-}$). Sua remoção é feita pela superóxido dismutase (SOD1 e 2) (McCord e Fridovich, 1969), que dismuta o radical superóxido a peróxido de hidrogênio. O H_2O_2 produzido pode ser removido por enzimas mitocondriais ou citosólicas, que incluem a catalase e peroxiredoxinas (Turrens, 2003; Figueira et al., 2013), ou reagir com Fe^{2+} e através da reação de Fenton produzindo $\text{OH}^{\cdot} + \text{OH}^{\cdot}$ (Halliwell e Gutteridge, 1992). Além disso, $\text{O}_2^{\cdot-}$ não dismutado pode reagir com diversas macromoléculas, oxidando-as, ou produzir outras espécies radicalares (Medinas et al., 2007).

EROs geradas pela mitocôndria em excesso podem causar danos a diferentes componentes celulares, como DNA (mitocondrial e nuclear), lipídios, carboidratos e proteínas. Esses danos podem levar a uma perda ou alteração de função dessas biomoléculas. Por esse motivo, EROs são uma importante fonte de dano em diversas condições patológicas, como doenças degenerativas e eventos isquêmicos (para revisão (Balaban et al., 2005; Halestrap et al., 2007)).

EROs produzidos em baixas concentrações pela mitocôndria podem funcionar como sinalizadores, regulando a atividade e a expressão de diversas enzimas e atividades celulares incluindo ciclo celular e controle transcricional (Palmer et al., 1977; Ignarro et al., 1987; Yoon et al., 2002; Cai, 2005). Quando presentes em concentrações maiores provocam a ativação de respostas contra estresse (Chandel et al., 1998; Yoon et al., 2002), incluindo a produção/regeneração dos sistemas antioxidantes (Jin et al., 2005).

Pre e pós condicionamento são eventos especialmente sensíveis à sinalização redox (Forbes et al., 2001; Facundo et al., 2007; Penna et al., 2009). Diversos sistemas e proteínas envolvidas nos eventos de proteção são ativadas por EROs. O sistema autofágico (Satoo et al., 2009), PKCs (principalmente PKC ϵ e PKC δ) (Liu et al., 2008), e o canal de potássio mitocondrial sensível por ATP (Facundo et al., 2007; Queliconi et al., 2011) são algumas proteínas reguladas.

1.4 - Dinâmica mitocondrial

As mitocôndrias estão constantemente se fissionando e fundindo dentro das células. Esse processo permite troca de conteúdo da matriz mitocondrial e está envolvido em processos como ciclo celular, proteção contra dano, aumento da necessidade energética entre outros (Twig et al., 2008), sendo chamado de dinâmica mitocondrial. A dinâmica mitocondrial é essencial para o desenvolvimento (Chen et al., 2011) e está intimamente ligada ao controle de qualidade mitocondrial e a diversas condições patológicas, como infarto do miocárdio, insuficiência cardíaca e diabetes (Ong e Hausenloy, 2010; Sebastián et al., 2012). Sua regulação acontece através da ativação das GTPases mitofusina 1 e 2, Drp1 e OPA1 (Hyde et al., 2010).

Existem diversos estímulos que levam à ativação da fissão ou da fusão mitocondrial. A fusão é estimulada pela alta demanda energética (Westermann, 2012), pelo período G1-S da divisão celular (Mitra et al., 2009) e é necessária para o ciclo de controle de qualidade mitocondrial (Twig e Shirihai, 2011). A fissão está aumentada no período M da divisão celular (Arakaki et al., 2006), em condições de dano celular (Brady et al., 2006), durante período de baixa demanda energética (Westermann, 2012) e é necessária para que ocorra autofagia mitocondrial (Twig et al., 2008).

A alteração da dinâmica pode causar um aumento do dano celular em condições patológicas (Ma et al., 2012). Desse modo a dinâmica mitocondrial tem um importante papel no dano causado por IR, sendo um centro de modulação do mesmo, ao estar intimamente ligada ao controle de qualidade mitocondrial, à recuperação de mitocôndrias danificadas e à produção de EROs (Hyde et al., 2010).

1.5 - Autofagia/Mitofagia

A autofagia é um processo onde organelas são incorporadas em lisossomos e destruídas. Esse processo tem como principais funções a remoção de organelas danificadas (Twig et al., 2008) e a produção de energia em condições de jejum extremo (Kuma et al., 2004; Mizushima et al., 2004).

A autofagia mitocondrial recebe um nome específico, mitofagia. Esse processo é essencial para o funcionamento celular, pois é através dela que mitocôndrias danificadas são removidas do citosol (Twig et al., 2008). O funcionamento correto da mitofagia é essencial para o pré-condicionamento (Huang et al., 2010) e está desregulado em diversas cardiopatias (Ma et al., 2012).

Algumas enzimas necessárias para a mitofagia são conhecidas, como LC3, ATG5, ATG12, p62 e Parkin (Gottlieb e Mentzer, 2010), entretanto até recentemente existiam poucas ferramentas disponíveis para o seu estudo *in vivo* e por consequência pouco se entendia sobre sua regulação e importância.

O desenvolvimento de uma proteína LC3 acoplada a uma GFP (LC3-GFP) permitiu que fossem realizados estudos *in vivo* (Gottlieb e Mentzer, 2010; Mizushima et al., 2011). A LC3 é uma proteína essencial para a mitofagia, servindo como marcador e selecionando qual mitocôndria deve sofrer autofagia. Utilizando-a, é possível seguir a mitocôndria até sua fusão com o lisossomo onde será degradada.

A ativação da mitofagia é protetora em IR (Huang et al., 2010) e sua inibição causa um aumento de proteínas e organelas danificadas (Huang et al., 2010). No último

caso, esse acúmulo pode levar a um aumento da produção de EROs e a um aumento do dano em IR (Hyde et al., 2010).

2. Objetivo

O objetivo desse trabalho é entender como bicarbonato modula o dano causado por um evento de isquemia–reperfusão.

3. Materiais e Métodos

3.1. Materiais: Todos os reagentes utilizados eram de qualidade analítica ou maior, sendo a maioria comprado da Sigma ou da Merck. Peroxidase de raiz forte tipo 1 (HRP) foi preparada em H₂O, enquanto Amplex Red (Invitrogen), rotenona, antimicina A e carbonilcianeto m-clorofenil-hidrazona (CCCP) foram preparados em DMSO. ADP/ATP, malato/glutamato e succinato foram preparados em H₂O e tiveram seu pH acertado para 7 usando NaOH. Todas as soluções estoques foram mantidas congeladas até o uso.

3.2. Isolamento de mitocôndrias de coração de rato: O isolamento foi feita como já descrito anteriormente (Cancherini et al., 2007; Tahara et al., 2009; Queliconi et al., 2011): a extração é realizada sobre gelo e em equipamentos com temperatura regulada para 4°C, e consiste em retirar o coração de um rato (idade entre 2-2,5 meses) e colocá-lo em uma solução A (sacarose 300 mM, Hepes 10 mM, EGTA 2 mM, pH = 7,2) onde é lavado para retirar o excesso de sangue. Em seguida a solução é trocada adicionando a solução A contendo protease (0,1 mg/mL), para facilitar a quebra do tecido e picando finamente até os pedaços atingirem 2 mm de comprimento. Após, lava-se com a solução A contendo albumina bovina (BSA, 1 mg/mL). Depois a suspensão é passada 5 vezes por um homogenizador tipo potter manual (Kontes Dounce Tissue Grinder, pistão A). Com esse homogeneizado, fazemos a primeira centrifugação de 5 min a 600 g. Pegamos o sobrenadante e seguimos para uma segunda centrifugação de 10 min a 10.000 g. Descartamos o sobrenadante, resuspendemos o precipitado na solução A e recentrifugamos por 10 min a 10.000 g. Descartamos o sobrenadante e resuspendemos o precipitado em um volume pequeno (150-200 µL) de solução A

contendo BSA (1 mg/mL), que serve como suporte proteico para a suspensão mitocondrial e como inibidor competitivo para proteases contaminantes.

A extração de mitocôndrias de corações congelados seguiu o mesmo protocolo com leve modificações. Foram usados 300 mg de tecido ao invés do tecido cardíaco inteiro e não foi utilizada protease.

3.3. Tampão de experimento: Todos os experimentos utilizando mitocôndrias isoladas (exceto a calibração do potencial de membrana e inchamento mitocondrial) foram feitos em tampão descrito anteriormente (Tahara et al., 2009) contendo 125 mM de sacarose, 65 de mM KCl, 10 mM de HEPES, 2 mM de fosfato inorgânico, 2 mM de $MgCl_2$, 2 mM de succinato, 1 mM de malato/glutamato, 200 μM de EGTA, e 0.01% de BSA, ajustado para pH 7,2 com NaOH, utilizando 0,125 mg de proteína/mL.

Nos experimentos onde houve mudança na concentração de CO_2 , o tampão continha 20 mM de HEPES e o pH foi acertado após o equilíbrio com o CO_2 .

3.4. Produção de H_2O_2 : A produção de H_2O_2 foi medida utilizando o sistema Amplex Red (25 μM)/horseradish peroxidase (HRP - 0,5 U/mL) (Zhou et al., 1997; Tahara et al., 2009). O ensaio foi feito a 37°C com agitação contínua em um Fluorescence Spectrophotometer F-2500 da Hitachi utilizando 563 nm de excitação e 587 nm de emissão. A leitura é sempre iniciada com tampão de experimento e Amplex Red/HRP seguido da adição de mitocôndrias. A calibração foi feita com concentrações conhecidas de H_2O_2 ($A_{240} = 43,6 M^{-1}cm^{-1}$) em tampão de experimento com Amplex Red/HRP sem mitocôndrias.

3.5. Consumo de oxigênio em mitocôndrias: O consumo de oxigênio mitocondrial foi medido através do uso de um eletrodo de Clark (OROBOROS Oxygraph-2k) (Tahara et al., 2009). O controle respiratório foi determinado adicionando a mitocôndrias suspensas em tampão de experimento, com curtos intervalos, ADP (0,2 mM, pH = 7,2), oligomicina (1 μ g/mL) e CCCP (1 μ M). O controle respiratório foi calculado dividindo a taxa de consumo de oxigênio no estado 3 (com ADP) pelo estado 4 (com oligomicina). O experimento foi realizado utilizando o tampão de experimento a 37°C e com agitação contínua.

3.6. Corações de ratos isolados: Ratos Sprague-Dawley com idade entre 2 e 2,5 meses foram sacrificados tendo seu coração rapidamente retirado e colocado em tampão Krebs (em mM, NaCl 118; NaHCO₃ 25; KH₂PO₄ 1,2; KCl 4,7; MgSO₄ 1,2; CaCl₂ 1,25; glicose 10; Hepes 20) gelado (4°C) (Facundo et al., 2007; Queliconi et al., 2013). Nesse tampão, a aorta foi presa a uma cânula e colocada em um sistema Langendorff com tampão de Krebs (a 37°C equilibrado com gás de interesse). Corações em que o tempo entre o sacrifício do animal e a colocação no Langendorff ultrapassou 2,5 min foram descartados.

Para obter as condições experimentais desejadas, nós alteramos a composição do tampão de Krebs para aumentar ou diminuir a presença de bicarbonato sem que houvesse alterações no pH. Na condição de 0% de CO₂ a quantidade de NaHCO₃ foi reduzida a zero e o gás de equilíbrio era composto de 100% de O₂. Na condição de 5% de CO₂ a quantidade de NaHCO₃ foi de 25 mM e o gás de equilíbrio era composto por 5% de CO₂ e 95% de O₂. Na condição de 10% de CO₂ a quantidade de NaHCO₃ foi de 66 mM e o gás de equilíbrio era composto por 10% de CO₂ e 90% de O₂.

3.7. Medidas hemodinâmicas: As medidas hemodinâmicas foram obtidas através do uso de um eletrodo de pressão acoplado a um sistema Powerlab da AdInstruments. A diferença de pressão desenvolvida e os batimentos por minuto (BPM) foram medidos através da utilização de um balão de látex inflado com H₂O com aproximadamente 2,5 mm de diâmetro conectado a um transdutor de pressão. Os pontos apresentados são médias dos últimos 3 min antes do ponto temporal determinado no gráfico.

3.8. Cálculo da área infartada: Após o processo de isquemia/reperfusão o coração foi cortado manualmente entre 2 a 4 fatias transversais e incubado em 1% de 2,3,5-triphenyl-tetrazolium (TTC) diluído em PBS por 15 min no escuro. Em seguida as fatias foram escaneadas e a área infartada e total foi medida usando o programa Image J (<http://rsbweb.info.nih.gov/ij/>).

3.9. Dosagem da liberação de creatina quinase (CK): A dosagem da liberação de CK foi feita coletando o perfusato do coração isolado no minuto anterior ao indicado. Em HL-1 o sobrenadante foi coletado e uma alíquota da proteína total celular foi coletada para normalização. A atividade da CK foi mensurada através da taxa de redução do NAD⁺. A absorbância do NADH (340 nm) foi medida a cada 20 s entre os tempos 5 e 10 min após o início da reação a 37°C utilizando um SpectraMax M3 da Molecular Probes. O ensaio foi realizado em placas de 96 poços utilizando o kit Doles CK-NAC ou Sekisui CK-SL, 4 µl de amostra e 200 µl do meio de reação (ADP 20 mM, AMP 5 mM, diadenosina pentafofato 10 mM, NAD⁺ 2 mM, HK 3 µkat/L, G6P-DH 3 µkat/L, n-acetil cisteína 20 mM, creatina fosfato 30 mM, glicose 20 mM, acetato de magnésio 10 mM, EDTA 2 mM e imidazol 100 mM; pH = 7,3). A partir dos pontos obtidos foi feita uma regressão linear e calculada a quantidade de NADH produzido utilizando $\Delta A = \epsilon \Delta C$,

onde ΔA = |inclinação da regressão linear|, ε = coeficiente de extinção do NADH ($6,220 \text{ M}^{-1}\text{cm}^{-1}$), l = caminho ótico (altura do líquido total na placa) e $\Delta C = \Delta [\text{NADH}^+]$. O resultado foi apresentado considerando que 1 unidade de enzima reduz $1 \mu\text{M}$ de NADH por minuto.

3.10. Cultivo de células HL-1: Como modelo de cardiomiócitos em cultura utilizamos células HL-1 (Claycomb et al., 1998) gentilmente doadas pelo Prof. Claycomb. As células foram cultivadas como descrito em seu laboratório em meio Claycomb com adição de norepinefrina e glutamina. Os experimentos foram conduzidos quando a confluência atingia 90%.

3.11. Quantificação de pH utilizando BCECF-AM: O pH intracelular foi medido utilizando a sonda intracelular BCECF-AM, com modificações no método já descrito (Rink et al., 1982; Johnson e Nehrke, 2010). Células foram tripisinizadas e resuspensas a uma concentração de 10^6 células por mL no tampão experimental de interesse contendo 5 mM de BCECF-AM. Incubadas por 90 min, foram centrifugadas a 300 g por 5 min e resuspensas em tampão experimental sem BCECF-AM. As leituras foram feitas utilizando um espectrofluorímetro Hitachi P-4500 (emissão 535 nm, excitação escaneada de 400 nm a 550 nm). Após a medida da fluorescência basal, a calibração foi feita adicionando 10 mg/mL de nigericina, permitindo a troca de prótons através da membrana citoplasmática. Em seguida foi adicionado excesso de NaOH seguido de excesso de HCl para promover alcalinização máxima e acidificação máxima, respectivamente. O pH foi então calculado como indicado pelo fabricante, utilizando a fórmula $[\text{H}^+] = K_a((R - R_A)/(R_B - R))(F_{A(\lambda,2)}/F_{B(\lambda,2)})$, onde K_a é 0,00911882, R é a razão da

intensidade de fluorescência (F) entre $F_{(\lambda_1)}/F_{(\lambda_2)}$ entre dois comprimentos de onda, λ_1 , 490 nm, e λ_2 , 440 nm, onde o subscrito A e B representam os valores após acidificação e alcalinização, respectivamente. A sonda apresenta uma mudança de fluorescência ao redor de 470 nm enquanto o ponto ao redor de 440 não sofre alterações coma mudança de pH permitindo um ponto de referência para calibrar a sonda.

3.12. Simulação de isquemia/reperfusão em células HL-1: Utilizamos dois protocolos distintos para promover simulação de isquemia/reperfusão em HL-1. O protocolo inicial se utilizava de cianeto e deoxiglicose nas células em suspensão (sIR(CN⁻)) (Facundo et al., 2006; Queliconi et al., 2013). Para tanto foram utilizados um tampão para isquemia contendo NaCl 137 mM; Hepes 20 mM; taurina 20 mM; creatina 5 mM; KCl 5,4 mM; MgCl₂ 1 mM; piruvato de sódio 5 mM; CaCl₂ 1 mM; deoxi-glicose 2 mM; cianeto de potássio 10 mM; pH=7,4, e um para reperfusão contendo NaCl 137 mM; Hepes 20 mM; taurina 20 mM; creatina 5 mM; KCl 5,4 mM; MgCl₂ 1 mM; piruvato de sódio 5 mM; CaCl₂ 1 mM; glicose 22 mM; pH=7,4. A isquemia consistia em incubar as células por 90 min no tampão de isquemia. A reperfusão era realizada peletando as células (centrifugadas por 5 min a 300g) e resuspendendo-as em tampão de reperfusão por 5 min. No tempo determinado, as células foram centrifugadas por 5 min a 300g e processadas para extração proteica. Em ambos os casos as células eram mantidas na concentração de 10⁶ células/mL e as incubações ocorriam a 37°C. Controles foram feitos para certificar que a respiração retorna a níveis próximos ao controle após a mudança de tampão.

O segundo método de isquemia consistia em utilizar um GazPak (BD Bioscience – New Jersey) para remover o oxigênio e promover isquemia. Nesse caso utilizamos células aderidas em placas que são seladas em um saco plástico que tem a sua atmosfera trocada por uma condição anóxica, adicionando um agente consumidor de oxigênio (distribuído junto ao GazPak) para acelerar o consumo de O₂. As células eram incubadas em tampão de isquemia (NaCl 137 mM; Hepes 20 mM; taurina 20 mM; creatina 5 mM; KCl 5,4 mM; MgCl₂ 1 mM; piruvato de sódio 5 mM; CaCl₂ 1 mM; 2 mM de deoxi-glicose; pH = 7,4) por 150 min. Após a isquemia as células eram removidas, e o tampão trocado pelo tampão de reperfusão (NaCl 137 mM; Hepes 20 mM; taurina 20 mM; creatina 5 mM; KCl 5,4 mM; MgCl₂ 1 mM; piruvato de sódio 5 mM; CaCl₂ 1 mM; 22 mM de glicose e pH = 7,4) e as células então eram coletadas aos 5 min da reperfusão.

Em ambas as condições os tampões foram preparados como descrito para os corações isolados. Eles eram equilibrados com a fase gasosa contendo 0, 5 ou 10% de CO₂ com N₂ para isquemia ou O₂ para a reperfusão. O pH era acertado após o equilíbrio.

3.13. Viabilidade celular usando brometo de etídio: Fizemos análise de viabilidade celular a partir da fluorescência do brometo de etídio conforme descrito no laboratório anteriormente (Facundo et al., 2006). As células foram utilizadas a 10⁶ células/mL e 2 mL foram retirados do experimento para leitura em um Spectrofluorímetro Hitachi F-4500 (excitação 365 nm e emissão 580 nm). Após a leitura basal foi adicionado 50 mM brometo de etídio para leitura das células mortas seguida da adição de 1% de Triton X-100 para leitura da fluorescência total.

3.14. Extração proteica: A extração de proteínas foi feita como descrito anteriormente (Churchill e Mochly-Rosen, 2007; Campos et al., 2012; Queliconi et al., 2013). Células foram peletadas ou raspadas da placa e o tecido cardíaco foi cortado em tampão de extração (Tris 150 mM, EGTA 10 mM, EDTA 5 mM, pH=7.5), contendo inibidores de proteinase e fosfatase. As células foram passadas por uma seringa de detecção de 27G e o tecido cardíaco foi processado em um potter. O lisado foi congelado a -80°C até o momento de uso.

Proteínas extraídas para análise de atividade do proteassoma não continham inibidores de proteinase ou fosfatase.

Proteínas extraída de *C. elegans* foram extraídas usando um tampão de extração (Tris-HCl 200 mM, DTT 100 mM, glicerol 20%, SDS 10%, e inibidores de proteinase, pH 8). Após incubação no tampão passaram por 3 ciclos de congelamento e descongelamento, foram centrifugados a 600 g por 5 min e congelados em -80°C até o uso.

3.15. Western Blots: As proteínas preparadas para Western Blot (WB) foram aliquotadas e processadas no momento da extração. Para quantificação de proteína carbonilada foi realizada derivatização com 2,4 -dinitrofenilhidrazina (DNPH) antes das análises, como descrito anteriormente (da Cunha et al., 2011; Queliconi et al., 2013). Após a dosagem de proteínas, as amostras (máx. 4 mg/mL de proteína) foram incubadas com SDS 24% e 3 mM de 2,4- DNPH em ácido tricloroacético (TFA) 10% (recém-preparado; ambos em proporção 1:1 com a amostra,) durante 30 min no escuro a temperatura ambiente. As soluções foram neutralizadas com uma mistura contendo

Tris-HCl 2 M, glicerol 30% e mercaptoetanol 19% pH 7,4 (1 ul de amostra: 0,75 neutralizante). Em cada gel foi corrido 5 µg de proteína por amostra.

Amostras para detecção de outras proteínas foram dosadas e diluídas em tampão de amostra (Tris-HCl 200 mM; glicerol 40%; SDS 8%; mercaptoetanol 2%; azul de bromofenol 0,04%; pH 6,8) utilizando 30 µg de proteína em cada amostra.

Em ambos os casos as amostras foram diluídas em tampão de amostra, fervidas por 5 minutos e submetidas à eletroforese em gel desnaturante de poliacrilamida (5% gel de empacotamento; 15% gel de resolução). As proteínas foram transferidas para a membrana de PVDF (4h à 400 mV, 4°C) e procedeu-se a coloração inespecífica com corante Ponceau (usado como controle de carregamento).

O bloqueio foi feito incubando as membranas com agitação em 5% de BSA em TBST por 1 hora. A incubação com anticorpo primário foi feita durante a noite (4°C) seguida por 3 lavagens de 20 min, incubação com o anticorpo secundário (diluído 1:5000, calbiochem ligado à HRP) por 1 hora seguido de 3 lavagens de 20 min, quando as membranas foram expostas. A diluição dos anticorpos primários foi feita em tampão de bloqueio nas seguintes concentrações – proteína carbonilada (Anti-DNHPH - 1:5000); anti-nitrotirosina (1:3000); anti-metioninasulfóxido (1:3000); P-Akt (1:2000); anti-ubiquitina (1:1000); anti-LC3 (1:1000); anti-p62 (1:1000); anti-Beclin1 (1:1000); anti-Drp1 (1:1000); anti-Parkin (1:1000); anti-Atg4b (1:1000); anti-Tom70 (1:1000); anti-CoxIV (1:1000). A membrana foi revelada utilizando quimioluminescência ao incubar em SuperSignal West Pico Chemiluminescent Substrate da Thermo Scientific. A exposição foi feita em filme fotográfico Kodak e revelado em câmera escura. Após o

filme foi escaneado e a densitometria das bandas foi realizada com o auxílio do programa Image J.

O controle de carregamento foi feito quantificando a intensidade da marcação de Ponceau na coluna inteira. Para tal secamos a membrana após a transferência incubamos com Ponceau por 5 min, em seguida lavamos o excesso e secamos a membrana. A membrana foi escaneada e a quantificação foi feita com o auxílio do programa Image J.

3.16. Dosagem de proteínas: Todas as dosagens de proteínas utilizadas nos trabalhos foram realizadas utilizando a técnica colorimétrica de Bradford em microplacas como descrita pelo fabricante. Brevemente, 10 μ l de amostra foram adicionados a 190 μ l de Bradford. A curva de calibração foi feita para cada leitura e consistia dos pontos 0; 0,05; 0,1; 0,2; 0,3; 0,5 mg de BSA/mL. Os pontos da curva foram feitos utilizando 10 μ l da solução de BSA correspondente em 190 μ l de Bradford. A leitura foi feita em 590 nm em um SpectraMax M3 da Molecular Probes.

3.17. Imunocitoquímica em células HL-1: Células HL-1 (Claycomb et al., 1998; Queliconi et al., 2013) foram cultivadas durante 2 dias em placas de 35 mm com fundo de vidro (25k de células por placa). Nos momentos indicados as placas tiveram o meio removido e foi adicionado PFA 4% por 15 min a temperatura ambiente. As placas foram incubadas em PBS por 5 min (repetido 3 vezes) e meio de bloqueio (PBS, 0,1% Tween 20, 1% BSA) foi adicionado e deixado por 30 min. Na sequência o tampão de bloqueio foi removido e as células foram incubadas em anticorpo primário (diluição 1:100, em tampão de bloqueio) e deixadas durante a noite a 4°C. No dia seguinte a placa foi

incubadas em PBS por 5 min (repetido 3 vezes) e incubada em anticorpo secundário (diluição 1:250, em tampão de bloqueio) por 1 hora, seguido de 3 incubações de 5 min em PBS por 5 min. A última incubação continha DAPI diluído 10^4 vezes (solução estoque 1 $\mu\text{g}/\text{mL}$).

3.18. Atividade do proteassoma: A atividade do proteassoma foi medida através da quantificação do aumento de fluorescência (Ex 380 nm/ Em 460 nm) provocado pela quebra do peptídeo Suc-Leu-Leu-Val-Tyr-AMC (Enzo Life Sciences BML-P802-0005). A quantificação foi realizada em um leitor de placas M2 da Molecular Devices a 37°C com medições a cada 30 s durante 30 min. Para a leitura foram usados 10 μg de amostra diluído em tampão Tris-Mg (50 mM Tris, 5 mM MgCl_2 , pH = 7,5) na presença de 125 nM de Suc-Leu-Leu-Val-Tyr-AMC.

3.19. RT-PCR: PCR de tempo real (RT-PCR) do gene LC3 foi feito como descrito anteriormente (Lin et al., 2012). Brevemente, mRNA foi isolado (GenElute™ Direct mRNA Miniprep Kits - Sigma-Aldrich, DMN10-1KT) do tecido cardíaco de rato e transformado em DNA usando iScript (Biorad – Hercules, CA). 10 ng desse DNA foi utilizado em cada reação de RT-PCR utilizando o 10 ng de primer (FP: CGGGTGGATTAGGCAGAGATG e RP: CCAGCACCCAAAAGAGCAAG, eficiência de 72%) e Sybr green super mix como descrito pelo fabricante. O experimento foi feito e quantificado utilizando um CFX96 da Biorad e os dados são apresentados como ΔCT .

3.20. *Caenorhabditis elegans*: A criação de *C. elegans* foi feita como descrita anteriormente (Brenner, 1974; Queliconi et al., 2013, 2014). *C. elegans* foram criados usando técnicas padrões a 20°C em placas de Agar com meio de cultura normal

(NGM). A sincronização de jovens adultos foi usada nos experimentos e feita através da sincronização da colocação dos ovos. As linhagens usadas foram selvagem (Bristol – N2) e KWN85 (*him-5(e1490)V, uls22(Pmec-18::GFP)V*).

3.21. Anóxia-jejum (IR) em *C. elegans*: IR em *C. elegans* foi simulado usando anóxia-jejum (20 h) seguido de reoxigenação e alimentação (24 h) como descrito anteriormente (Scott et al., 2002; Wojtovich et al., 2012; Queliconi et al., 2013, 2014). *C. elegans* jovem adultos (3 dias de idade) foram coletados das placas de NGM e lavados 3 vezes quando resuspenso em M9 (KH_2PO_4 22 mM, Na_2HPO_4 42 mM, NaCl 86 mM, MgSO_4 1 mM, pH 7,0) suplementado com HEPES 20 mM e com fase gasosa igual à usada na isquemia (pH corrigido para 7). Os vermes foram incubados em 100 μL de M9 em um microtubo aberto a 26°C por 20 h sob atmosfera de 100% de N_2 ou de atmosfera de 90% N_2 + 10% CO_2 . Após a IR os *C. elegans* foram movidos com uma mínima quantidade de M9 para uma nova placa com comida (bactérias) por 24 h onde foram contados os vermes vivos e através de um experimentador cego foi feito o teste de sensibilidade ao toque. Para maiores detalhes consultar Queliconi et al. (2014).

3.22. Teste de resposta ao toque em *C. elegans*: Após 24 h de recuperação, *C. elegans* que sobreviveram foram movidos para uma nova placa onde, usando um cílio preso a um extensor, foi medida a resposta ao toque. A resposta ao toque foi feita tocando-se levemente a lateral do verme na região dos neurônios mecanosensores e verificando se isso causa a mudança de direção.

3.23. Microscopia do neurônio mecanosensor em *C. elegans*: Após as 24 h de recuperação, animais vivos foram anestesiados utilizando 0,1% de tetrakisole e 0,1% de tricaina (EMS, Hatfield, PA, USA), transferidos para lâmina com um suporte de agarose (2% agarose em M9) e observados em 20 min sob uma lamínula. Foi utilizado um microscópio Nikon Eclipse TE2000-U (Nikon USA, Melville, NY, USA), com uma Polychrome V monochromator (TILL Photonics, Gräfelfing, Germany), e Cooke Sensicam CCD (PCO-TECH, Romulus, MI, USA) coordenados utilizando o software TILLvisION, para se obter as imagens de fluorescência (470 nm excitação/535 nm emissão) sob uma objetiva a óleo de 100x.

3.24. Análise estatística: Todos os experimentos mostrados tem ao menos 3 repetições e os gráficos são apresentados com o desvio padrão do erro. Os dados apresentados em grupos maiores que 2 foram analisados utilizando 1-way ANOVA com pós-teste de Bonferroni e os dados comparando 2 grupos foram analisados usando teste de t-student. As análises foram feitas utilizando o GraphPad Prism 5.

4. Resultados

4.1 – Caracterização do dano causado pela presença de Bicarbonato na IR

Nós iniciamos os experimentos certificando que nossa condição experimental não estava alterando o pH intracelular. Utilizando a sonda de pH BCECF-AM, incubamos células como descrito nos Matérias e Métodos e medimos o pH citoplasmático após 95 minutos, obtendo sempre o mesmo pH em ambas as condições (Figura 2).

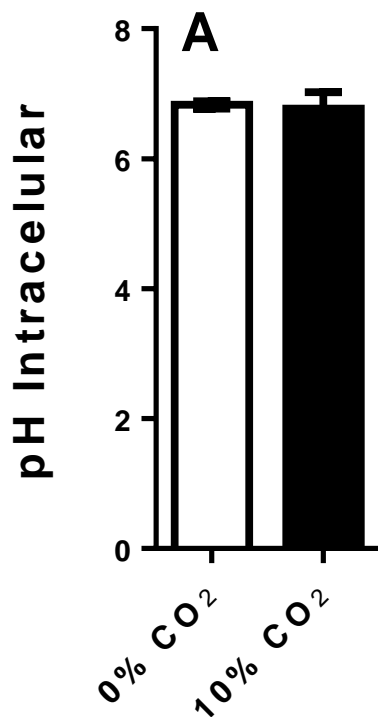


Fig. 2 – O pH intracelular não é alterado pela presença de bicarbonato – pH citosólico foi medido usando BCECF como descrito nos Materiais e Métodos. Células HL-1 foram incubadas por 120 min em tampão na ausência de bicarbonato (0 % CO₂) ou contendo 10% de HCO₃⁻/CO₂.

Nós olhamos a seguir para o efeito do bicarbonato em condições controle e sob isquemia-reperfusão. Para tanto utilizamos um modelo utilizado anteriormente no

laboratório, estabelecido por Facundo e colaboradores (Facundo et al., 2005). Nesse modelo utilizamos inibições químicas da cadeia respiratória utilizando cianeto (CN^-) e deoxiglicose para inibir a glicólise. Usando esse dois compostos, conseguimos mimetizar o processo de isquemia onde existe inibição da cadeia respiratória e da glicólise devido à inibição de consumo dos substratos. O processo de reperfusão é iniciado ao se trocar o meio por outro sem os inibidores e com glicose presente. Esse modelo representa bem os eventos isquêmicos já que é possível utilizá-lo para mimetizar pré-condicionamento e eventos que protegem tecidos contra dano isquêmico (Facundo et al., 2005, 2007).

Submetemos as células a diversos tempos de sIR(CN^-) na ausência de bicarbonato e concluímos que subter as células a um período de 90 min produzia a quantidade de morte desejada (~30%), semelhante a usada anteriormente no laboratório (Facundo et al., 2005). Seguimos utilizando uma condição sem bicarbonato (0%) e uma com alto bicarbonato (10% de CO_2). O controle (utilizando somente o tampão de reperfusão) não apresentou diferenças na morte entre os dois grupos (Fig. 3A). Ao submetermos os grupos à sIR(CN^-) obtivemos uma diferença significativa na morte celular após a reperfusão (95 min) (Fig. 3B).

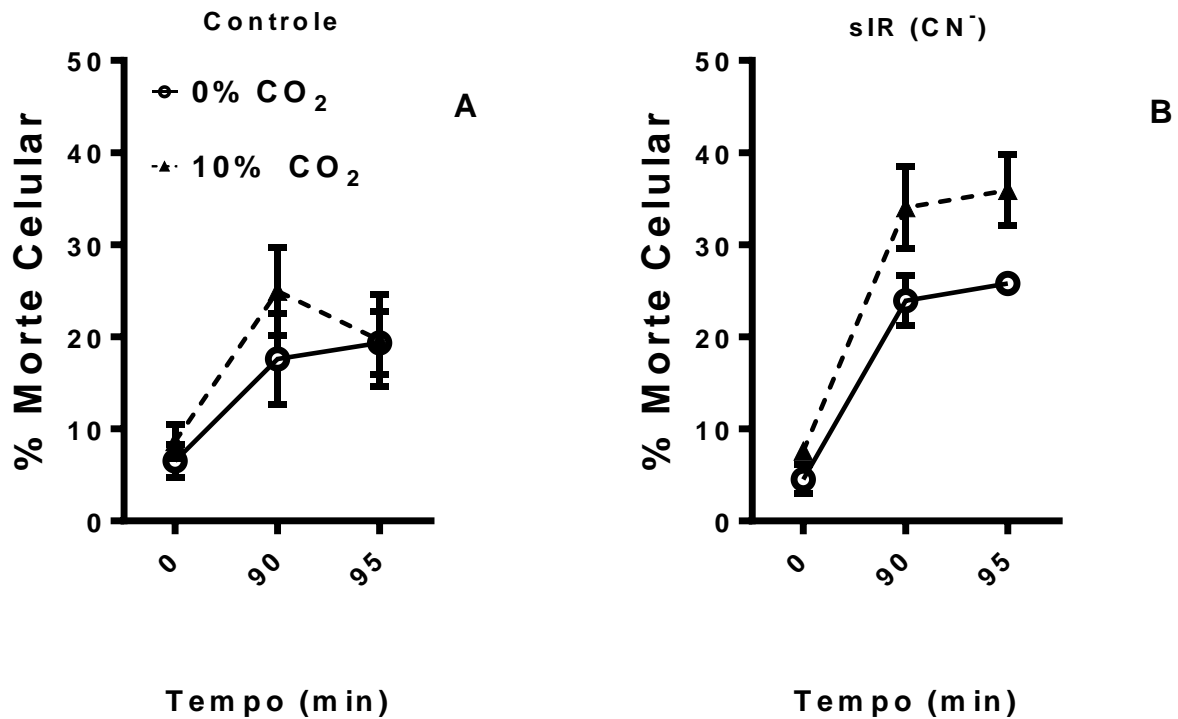


Fig. 3 – A presença de bicarbonato aumenta morte celular após sIR(CN⁻) – Células HL-1 foram incubadas somente com tampão de reperfusão (A) ou submetidas a sIR(CN⁻) (B) na ausência (0% CO₂) ou presença (10% CO₂) de bicarbonato. A morte celular foi medida através da utilização da fluorescência do brometo de etídeo como descrito nos Matérias e Métodos.

Devido à atividade redox do par HCO₃⁻/CO₂, medimos a quantidade de proteínas carboniladas nas nossas amostras para verificar se haviam danos oxidativos associados ao processo. Os dados (Fig. 4) mostraram um significativo aumento da quantidade de proteínas carboniladas a durante a reperfusão e um aumento significativamente maior no grupo exposto ao bicarbonato (10%) e a sIR(CN⁻).

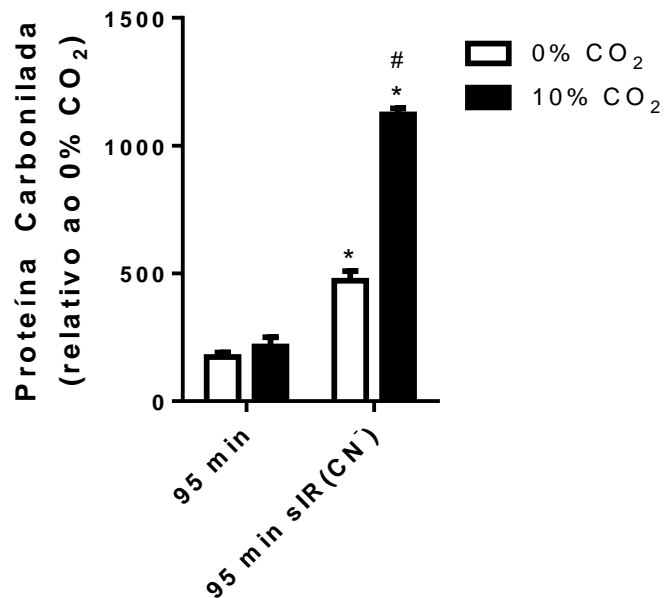


Fig. 4 – A presença de bicarbonato aumenta a quantidade de proteínas carboniladas durante a reperfusão – Proteína carbonilada foi medida através de WB como descrito nos Materiais e Métodos. Células HL-1 foram incubadas por 95 min em tampão sem (0% CO₂) ou com bicarbonato (10% CO₂) em tampão controle (95 min) ou submetidas a sIR(CN⁻) (95 min sIR(CN⁻)). *, p<0,05 em relação ao controle não isquêmico; #, p<0,05 em relação ao 0% CO₂ – sIR(CN⁻)

Seguida a caracterização em células, utilizamos corações isolados de ratos em um sistema Langendorff para testar se os mesmos efeitos detectados se reproduziriam em um modelo de isquemia reperfusão mais complexo. Para tanto usamos as modificações nos tampões e o protocolo de isquemia descritos nos Materiais e Métodos, graficamente representados na figura 4.

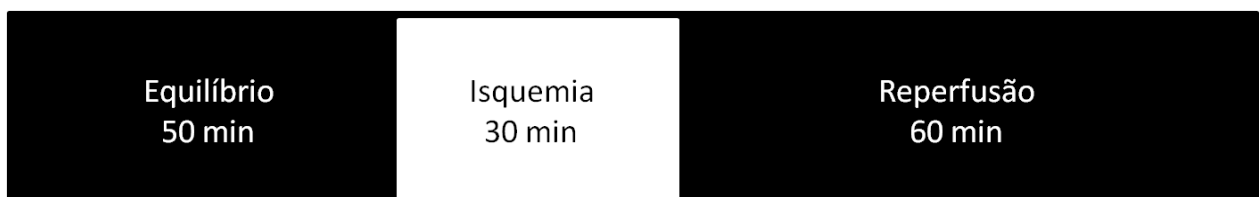


Fig. 5 - Esquema do tempo de isquemia e reperfusão utilizado nos corações isolados de ratos.

Para medir o dano utilizamos parâmetros funcionais (batimentos por minuto – BPM e pressão desenvolvida no ventrículo esquerdo) e área de tecido morto do coração utilizando 2,3,5-triphenil-tetrazolium (TTC), como descrito nos Materiais e Métodos. Em corações controles não expostos à IR não detectamos nenhuma diferença nos parâmetros medidos (Fig. 6).

Ao expor os corações ao protocolo isquêmico obtivemos uma significativa deterioração dos parâmetros cardíacos na presença de 10% de CO₂ (Fig. 7). Houve declínio na velocidade de batimentos (Fig. 7A) e na pressão desenvolvida no ventrículo (Fig. 7B). Os corações expostos a 5% de CO₂ apresentaram uma piora inicial mas que é recuperada no decorrer da reperfusão, entretanto os corações expostos ao tampão com 10% de CO₂ não se recuperaram durante todo o período de reperfusão. A queda em ambos os parâmetros indica que esse coração teria significativa perda de sua funcionalidade.

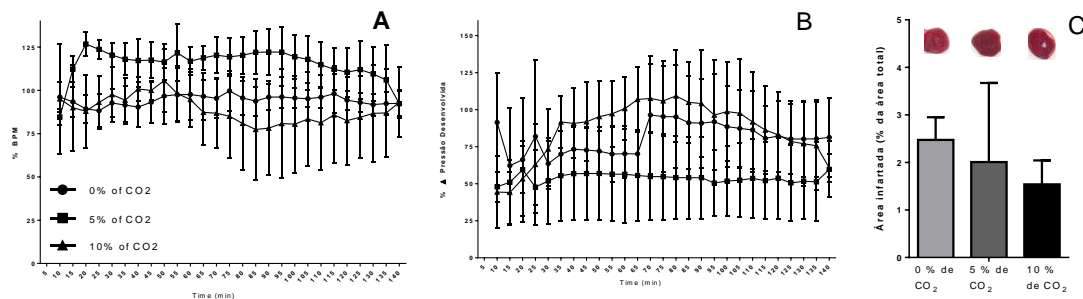


Fig. 6 – Corações de ratos perfundidos com diferentes concentrações de bicarbonato/CO₂ não apresentam diferença sobre o BPM (A), pressão de perfusão (B) e área infartada (C). Corações de ratos foram perfundidos por 140 min usando diferentes concentrações de bicarbonato/CO₂. O tampão de perfusão foi adaptado para cada condição como descrito nos Materiais e Métodos. BPM (A) e pressão de perfusão (B) estão representados relativo ao ponto médio do tratamento com 5% de CO₂ no tempo 50 min. (C) Ao final da reperfusão os corações foram retirados e cortados em 2 a 4 fatias coradas em TTC 1%. As fatias foram escaneadas e a área infartada e a total foram medidas com o auxílio do programa Image J. A área infartada foi apresentada relativa à área total do corte.

Os corações expostos a uma concentração maior de bicarbonato também apresentaram um aumento da área infartada (Fig. 7C), mas não apresentaram diferenças quando não submetidos a IR (Fig. 6C). Seguimos analisando a oxidação proteica nos corações isolados. Como é um modelo mais complexo e com maior quantidade de proteína total, conseguimos medir a quantidade de carbonilação, metionina sulfóxido e nitro-tirosina como marcadores adicionais de dano oxidativo.

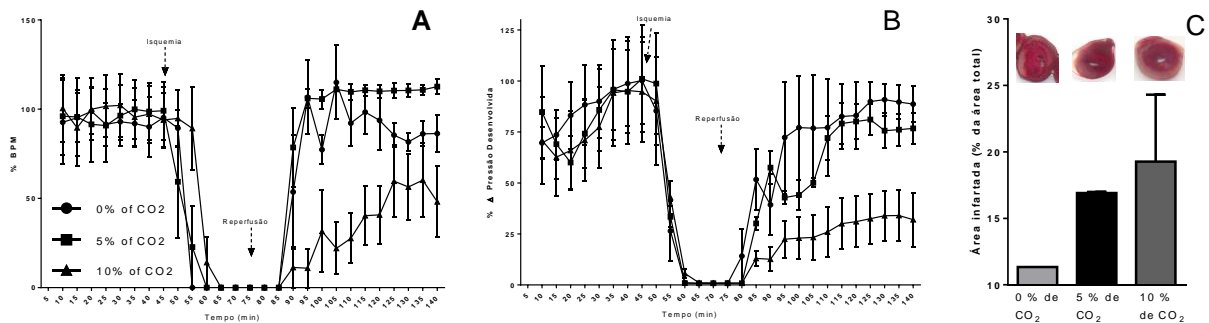


Fig. 7 – Corações de ratos infartados submetidos a diferentes concentrações de bicarbonato/CO₂ apresentam piora na recuperação do BPM (A) e pressão de perfusão (B) e maior área infartada (C). Corações de ratos foram submetidos a 30 minutos de isquemia seguida de 60 min de reperfusão usando diferentes concentrações de bicarbonato/CO₂. O tampão de perfusão foi adaptado para cada condição como descrito nos materiais e métodos. O BPM (A) e pressão de perfusão (B) estão representados relativo ao ponto médio do tratamento com 5% de CO₂ no tempo 50 min. (C) Ao final da reperfusão os corações foram retirados e cortados em 2 a 4 fatias coradas em TTC 1%. As fatias foram escaneadas e a área infartada e a total foram medidas com o auxílio do programa Image J. A área infartada foi apresentada relativa à área total do corte.

Não detectamos nenhuma alteração nas condições de oxidação proteica nos corações controles promovida por IR, mas detectamos um aumento na quantidade de proteína carbonilada e metionina sulfóxido (Fig. 8A e B) e um aumento na quantidade de nitro-tirosina (Fig. 8C).

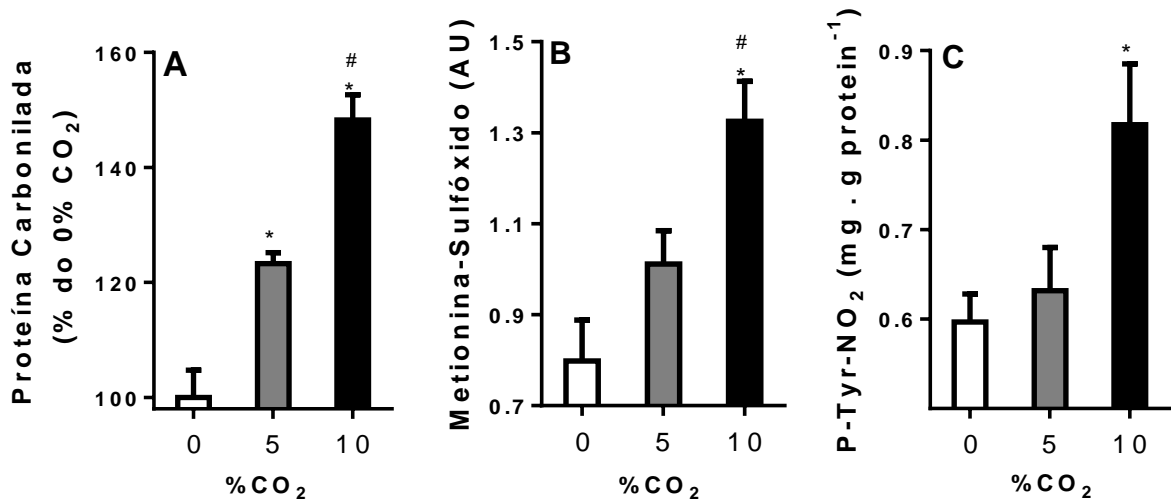


Fig. 8 - Corações de ratos infartados submetidos a diferentes concentrações de bicarbonato/CO₂ apresentam acúmulo de espécies oxidadas. Corações de ratos foram submetidos a 30 minutos de isquemia seguida de 60 min de reperfusão usando diferentes concentrações de bicarbonato/CO₂. O tampão de perfusão foi adaptado para cada condição como descrito nos Materiais e Métodos. Ao final do experimento isolamos as proteínas dos corações e dosamos a quantidade de proteína carbonilada (A), metionina sulfóxido (B) e nitro-tirosina (C) através de Western blots como descrito nos Materiais e Métodos. *, p<0,05 em relação ao 0% CO₂; #, p<0,05 em relação ao 5% CO₂.

Seguimos tentando identificar se essa diferença era causada pela ativação de alguma via de sinalização protetora. Para tanto analisamos a quantidade de Akt fosforilada (Fig. 9), como um indicativo de ativação das defesas celulares e concluímos que a presença do bicarbonato não modifica a capacidade de ativação de cascatas de proteção celular. Para detectarmos se a nitração das proteínas surte um efeito importante, utilizamos L-NAME (inibidor da nítrico óxido sintase) e expusemos os corações a isquemia na presença (10%) ou ausência de bicarbonato (0%) (Fig. 10). A inibição da produção de óxido nítrico não provocou mudanças no fenótipo, indicando que esse radical não participa do dano causado pelo bicarbonato.

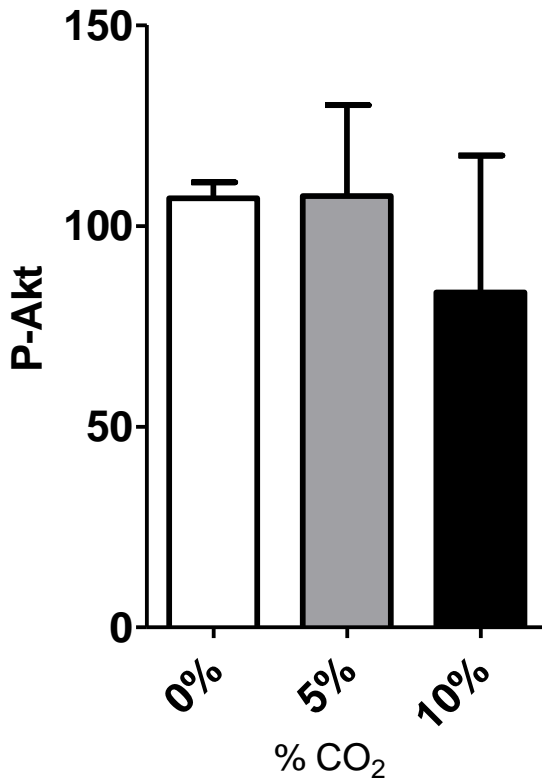


Fig. 9 – Quantidades de P-Akt não em corações perfundidos na presença de diferentes concentrações de CO₂. A ativação de Akt foi quantificada usando WB para P-Akt em corações não isquêmicos, após perfusão por 2h e 20 min com diferentes concentrações de HCO₃⁻/CO₂.

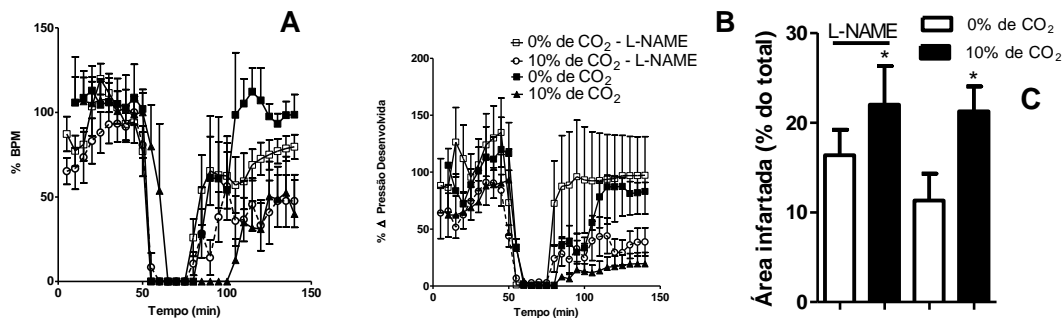


Fig. 10 – Corações de ratos submetidos a IR na presença de L-NAME apresentam um aumento do dano na presença de bicarbonato. Corações de ratos foram submetidos a 30 minutos de isquemia seguida de 60 min de reperfusão usando diferentes concentrações de bicarbonato/CO₂. O tampão de perfusão foi adaptado para cada condição como descrito nos Materiais e Métodos na presença de L-NAME (200 μM - adicionando 5 min antes da isquemia e mantido até o fim da reperfusão). (A) BPM, (B) pressão desenvolvida e (C) área infartada (medida ao fim da reperfusão). *, p < 0,05 em relação ao 0% CO₂.

Todos os nossos modelos estudados até o momento envolviam derivados de tecido cardíaco. Para testar modelos não cardíacos, utilizamos um modelo não mamífero e de animal inteiro, *C. elegans*. Assim conseguimos testar os efeitos das diferentes concentrações de bicarbonato no dano causado por IR em um modelo distinto, permitindo melhor confirmação dos eventos.

Desenvolvemos esse modelo em colaboração com o laboratório de Keith Nerhke da *University of Rochester* em Rochester, no estado de *New York* nos Estados Unidos. Utilizamos um modelo de isquemia reperfusão em *C. elegans* descrito inicialmente por Scott (Scott et al., 2002) que foi adaptado e posteriormente publicado por nós (Queliconi et al., 2014). A isquemia em *C. elegans* consiste em 20 horas de privação de oxigênio e alimentos (Anoxia-Jejum) seguidas de 24 horas de recuperação em ambiente com alimento e O₂ ambiente (Fig. 11).



Fig. 11 - Esquema temporal de anóxia-jejum, modelo de IR em *C. elegans*.

Nós não detectamos um aumento de mortalidade nos vermes, somente uma tendência no acúmulo de espécies oxidadas de proteínas (Fig. 12A e B). Entretanto detectamos uma significativa deterioração na resposta dos vermes ao exame de toque (Fig. 12C).

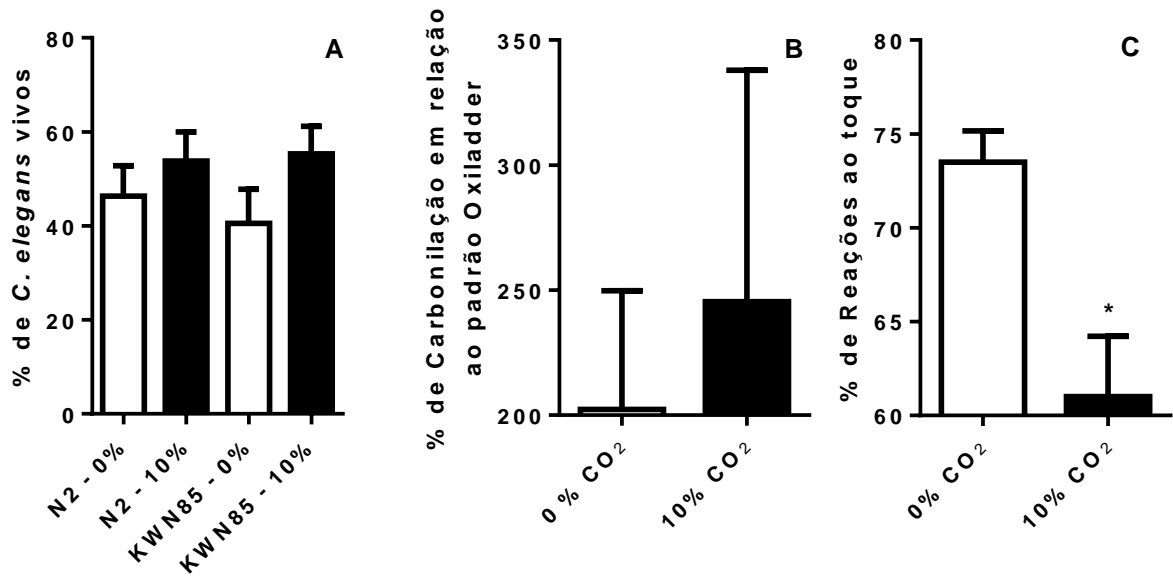


Fig. 12 – 10% CO₂ diminui a capacidade de resposta a toque em *C. elegans* submetidos a anóxia-jejum sem alterar viabilidade – (A) Viabilidade pós recuperação em *C. elegans* submetidos a anóxia-jejum na presença ou ausência de bicarbonato como descrito nos Materiais e Métodos. N2 é a linhagem selvagem, e KWN85 é uma linhagem que apresenta expressão de GFP nos neurônios mecanosensores. (B) Quantidade de proteínas carboniladas foram medidas como descrito nos Materiais e Métodos em *C. elegans* após a recuperação de anóxia-jejum na ausência (0%) ou presença (10%) de bicarbonato. (C) Resposta ao estímulo por toque in *C. elegans* vivos após a recuperação de anóxia-jejum na ausência (0%) ou presença (10%) de bicarbonato. *, $p < 0,05$ em relação ao 0% CO₂.

Os neurônios mecanosensores responsáveis pela resposta específica ao toque são conhecidos em *C. elegans*. Utilizando animais que expressam GFP na membrana citosólica (linhagem KWN85) analisamos a morfologia dos mesmos (Fig. 13). Esses neurônios apresentavam diversas modificações no axônio, como abnormalidades (Fig.13A) (não linearidade do axônio) e pontuações (Fig.13B) (estruturas semelhantes a bubble apoptótico). A quantificação nos mostrou uma grande concentração dessas modificações no grupo exposto ao bicarbonato (Fig. 13).

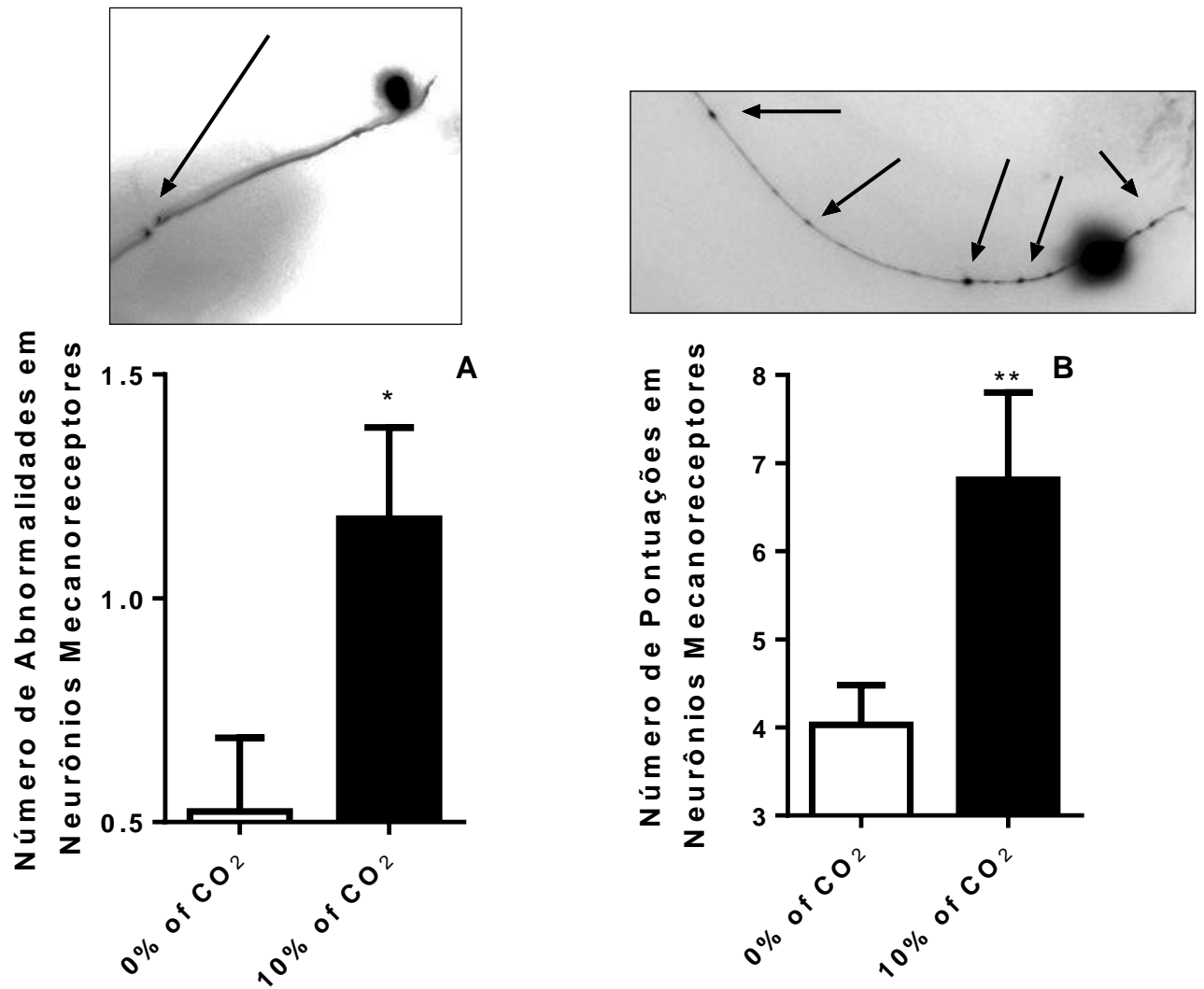


Fig. 13 - 10% CO₂ aumenta modificações nos neurônios mecanosensores - Neurônios mecanosensores de *C. elegans* (KWN85) foram analisados em vermes sobreviventes sob anestesia após a recuperação de anóxia-jejum na ausência (0%) ou presença (10%) de bicarbonato. (A) Anormalidades como a presença de processos tortuosos (B) Formação de agregados de GFP na membrana dos neurônios mecanosensores. *, $p < 0,05$ em relação ao 0% CO₂.

4.2 - Identificação das mudanças moleculares promovidas pela presença de bicarbonato na IR

Com a demonstração de que o aumento de dano provocado pela presença do bicarbonato na IR ocorria em modelos muito distintos, analisamos a fisiologia mitocondrial em busca do mecanismo responsável pelo do aumento do dano. Para tanto utilizamos mitocôndrias isoladas de coração de ratos que foram expostas as diferentes concentrações de bicarbonato.

Os tampões de experimento foram previamente equilibrados com a fase gasosa de interesse e o pH foi checado antes do início do experimento. Iniciamos medindo produção de H_2O_2 através da utilização do fluoróforo Amplex Red na presença de peroxidase de raiz forte (HRP). Medimos a produção utilizando condições experimentais diferentes para produzir baixas ou altas concentrações de oxidantes mitocondriais (Fig. 14).

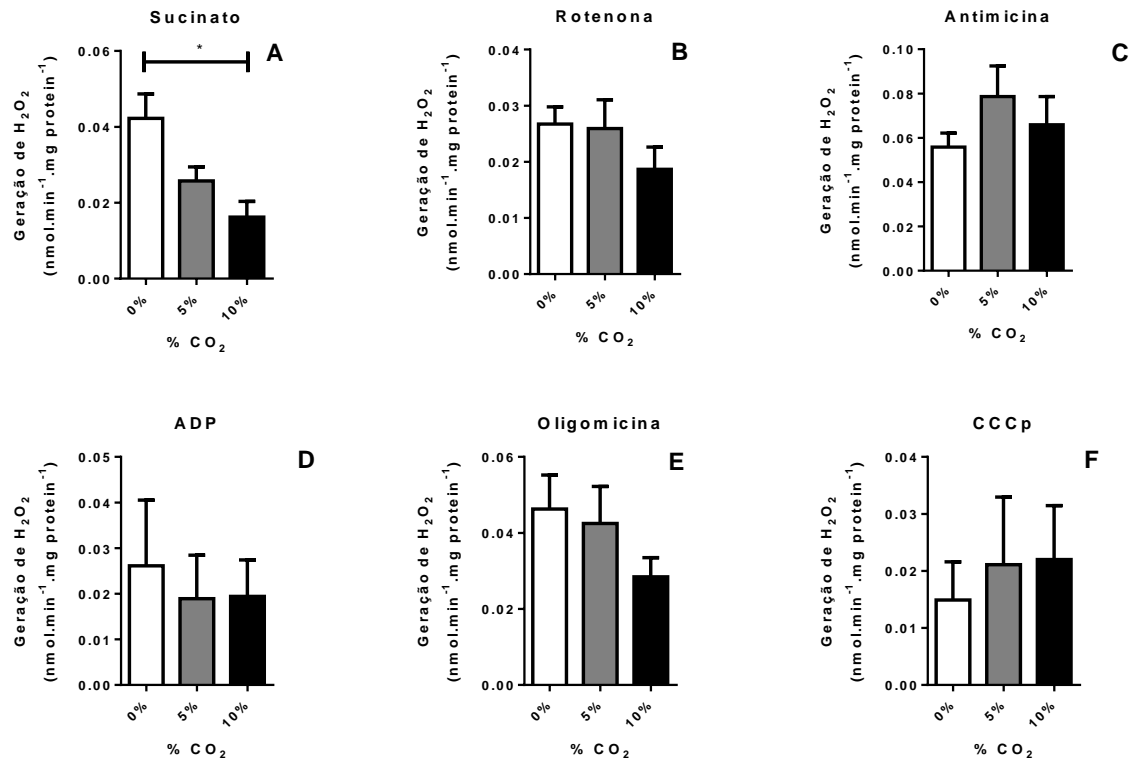


Fig. 12 – Produção de H₂O₂ não é aumentada pela presença de HCO₃⁻/CO₂ em mitocôndrias isoladas. Mitocôndrias foram isoladas de coração de rato e incubadas com diferentes concentrações de HCO₃⁻/CO₂ e a produção de H₂O₂ foi medida como descrito nos Materiais e Métodos. As condições foram (A) presença de succinato (2 mM) (B) succinato 2 mM e rotenona 2 μM (C) succinato 2 mM, rotenona 2 μM e antimicina 1 μg/mL (D) succinato 2 mM e ADP 0,2 mM (E) succinato 2 mM, ADP 0,2 mM e oligomicina 1 μg/mL (F) succinato 2 mM, ADP 0,2 mM, oligomicina 1 μg/mL e CCCP 1 μM. *, p < 0,05 em relação ao 0% CO₂.

Apesar de não haver um aumento na produção total de H₂O₂, poderia haver uma alta porcentagem de EROs em relação ao oxigênio consumido. Para verificar essa hipótese nós medimos as velocidades respiratórias em paralelo à produção de H₂O₂ e analisamos a velocidade respiratória e a taxa de produção de peróxido por oxigênio consumido (Fig. 15 e 16).

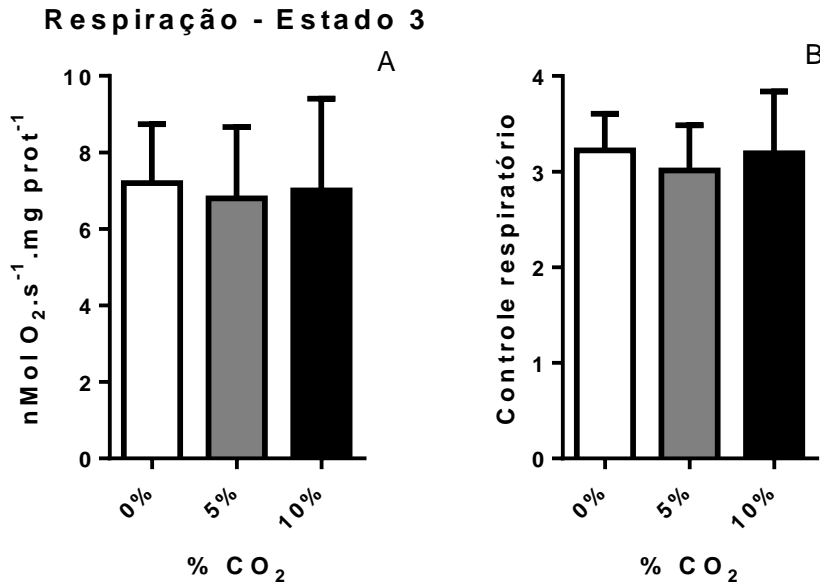


Fig. 15 – Diferentes quantidades de CO₂ não alteram a velocidade respiratória e o acoplamento em mitocôndrias isoladas de coração de rato. Mitocôndrias foram isoladas de coração de ratos e incubadas em tampões (0,125 mg/mL de proteína mitocondrial em 125 mM de sacarose, 65 de mM KCl, 10 mM de HEPES, 2 mM de fosfato inorgânico, 2 mM de MgCl₂, 2 mM de succinato, 200 μM de EGTA, e 0.01% de BSA, pH 7,2) com diferentes concentrações de HCO₃⁻/CO₂. (A) velocidade respiratória (na presença de ADP) (B) Controle Respiratório (V_{ADP}/V_{Oligo}), determinado como descrito nos Materiais e Métodos.

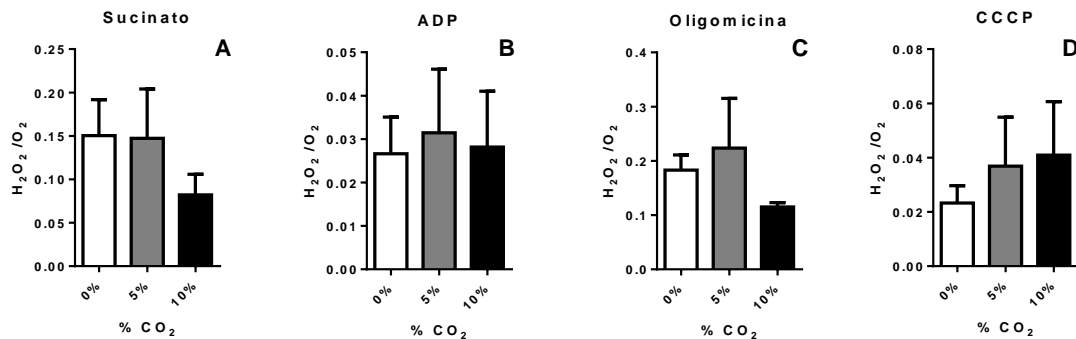


Fig. 16 – Razão H₂O₂/O₂ não é alterada pela presença de diferentes concentrações de HCO₃⁻/CO₂ em mitocôndrias isoladas. Mitocôndrias foram isoladas de coração de rato e incubadas com diferentes concentrações de HCO₃⁻/CO₂ e a produção de H₂O₂ foi medida como descrito nos Materiais e Métodos. As condições foram (A) presença de succinato 2 mM (B) succinato 2 mM e ADP 0,2 mM (C) succinato 2 mM, ADP 0,2 mM e oligomicina 1 μg/mL (D) succinato 2 mM, ADP 0,2 mM, oligomicina 1 μg/mL e CCCP 1 μM.

Em nenhuma das condições analisadas obtivemos uma diferença que explicasse um aumento da concentração de proteínas oxidadas. A atividade redox do par HCO₃⁻

/CO₂ permite a produção de diversos radicais não detectáveis utilizando Amplex Red e HRP. Dessa maneira decidimos olhar diretamente para a quantidade de proteínas oxidadas. Para tanto incubamos mitocôndrias isoladas de coração de rato em tampão de experimento equilibrado com a quantidade desejada de bicarbonato na presença de condições com baixa (succinato) e alta produção de peróxido (succinato + antimicina). Incubamos inicialmente as mitocôndrias por 30 min (Fig. 17) e não obtivemos a diferença detectada anteriormente.

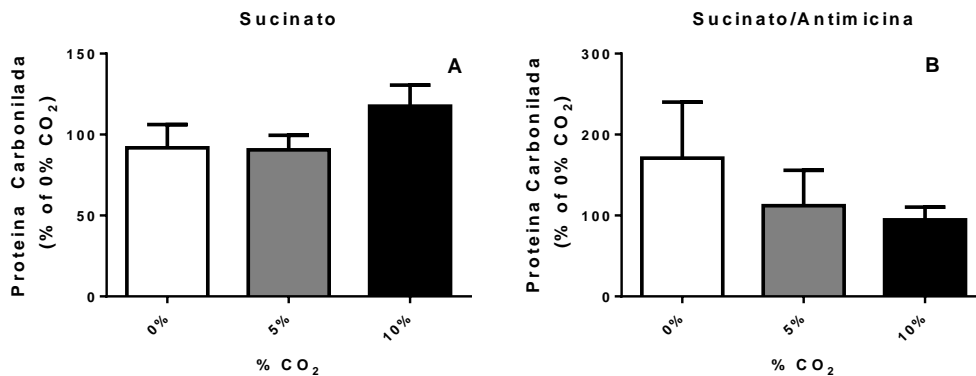


Fig. 17 – Quantidade de proteína carbonilada em mitocôndrias incubadas durante 30 minutos em diferentes concentrações de HCO₃⁻/CO₂ na presença de succinato (A) ou succinato e antimicina (B). Mitocôndrias de coração 0,5 mg/mL de ratos foram incubadas por 30 min em tampão de experimento (veja Materiais e Métodos) na presença de succinato 2 mM (A) ou succinato 2 mM e antimicina 1 µg/mL (B) proteínas carboniladas quantificadas por western blots.

Uma possibilidade para falta de diferença seria a exposição ao um tempo muito longo, o que levaria ao consumo máximo de oxigênio e a mascarar as diferenças. Para resolver essa questão nós refizemos o experimento usando uma menor quantidade de proteína mitocondrial e um tempo menor, de 10 minutos (Fig. 18). Mesmo nas novas condições não detectamos diferenças.

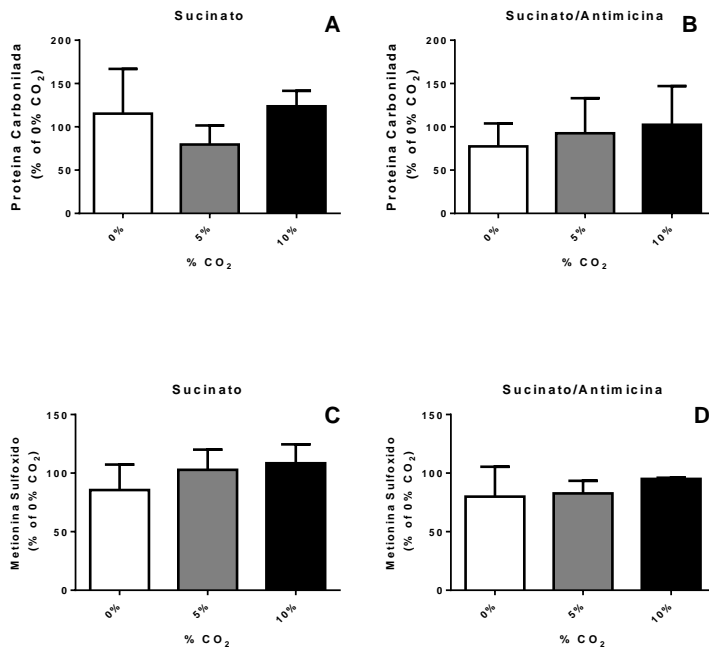


Fig. 18 – Oxidação proteica de mitocôndrias incubadas com diferentes concentrações de $\text{HCO}_3^-/\text{CO}_2$ em diversas condições. Mitocôndrias de coração de rato 0,125 mg/mL foram incubadas por 10 min em na presença de succinato 2 mM (A e C), succinato 2 mM e antimicina 1 $\mu\text{g}/\text{mL}$ (B e D). Após a incubação a quantidade de proteína carbonilada (A e B) e de resíduos de metionina sulfoxido (C e D) foram quantificadas por WB.

Sem detectar diferenças em organelas isoladas, voltamos a utilizar sistemas celulares completos. Inicialmente utilizamos o protocolo de sIR para olhar para a rede mitocondrial. Marcamos as rede mitocondrial utilizando imunofluorescência para a subunidade IV da citocromo C oxidase (CoxIV). Isso nos permitiu analisar a rede mitocondrial em condições controles e após sIR (Fig. 19). Não conseguimos detectar diferenças causadas pela presença (10%) ou ausência de bicarbonato (0%).

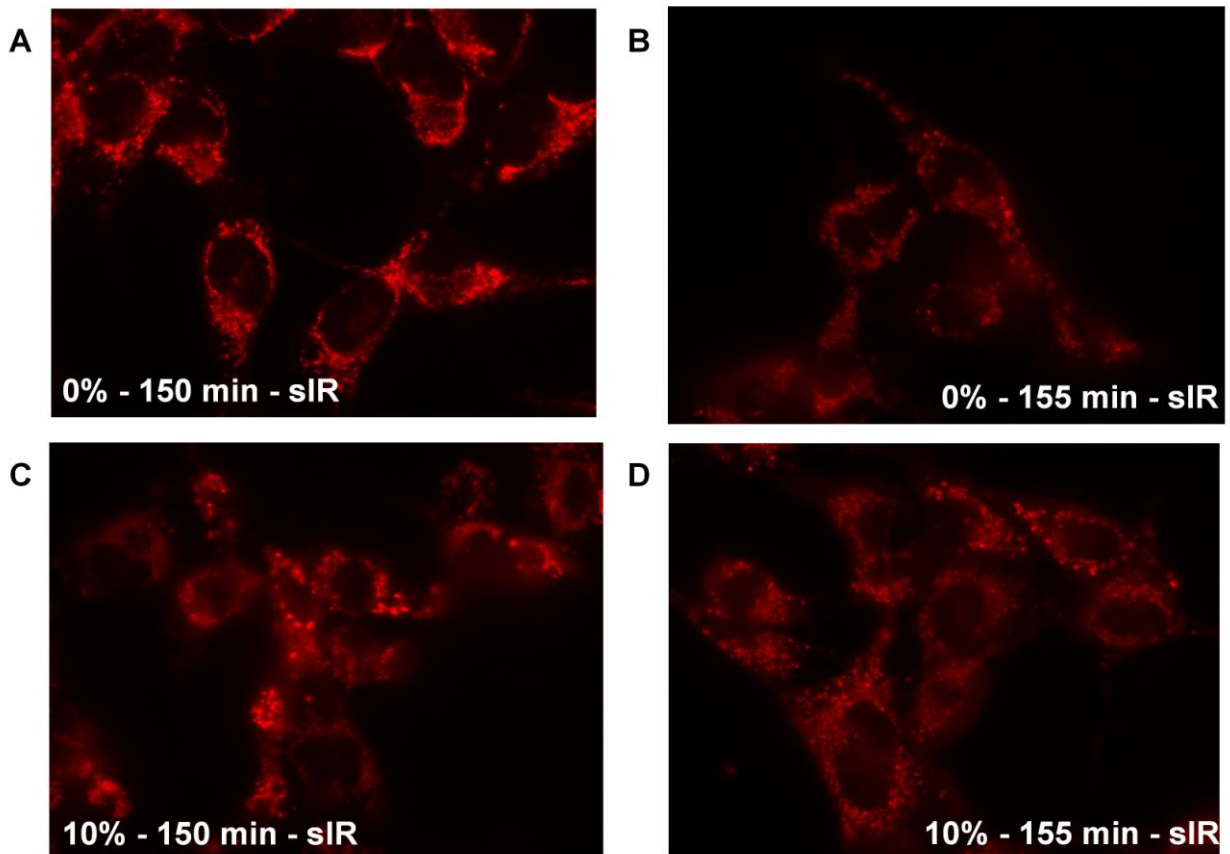


Fig. 19 – Imunofluorescencia para CoxIV na presença ou ausência de $\text{HCO}_3^-/\text{CO}_2$. Células HL-1 foram crescidas em placas de de 35 mm com fundo de vidro e submetidas a sIR na ausência (0% - A e B) ou presença (10% - C e D) de $\text{HCO}_3^-/\text{CO}_2$ antes (150 min – A e C) ou após a reperusão (155 min – B e D).

Outro fator que poderia influenciar o dano celular seria uma mudança na atividade do sistema protossoma-ubiquitina. Iniciamos analisando a quantidade de ubiquitina em células após sIR, na presença (10%) ou ausência de bicarbonato (0%) (Fig. 20A). Detectamos um aumento significativo da quantidade de ubiquitina na presença de 10% de CO_2 . O aumento da quantidade de ubiquitina pode ser devido a uma perda de atividade do proteassoma. Seguimos analisado a atividade do proteassoma em HL-1 antes e após a sIR (Fig. 20B) e nos em corações isolados de rato submetidos a IR (Fig. 20C), entretanto não houve mudanças na atividade do proteassoma na presença ou ausência de bicarbonato.

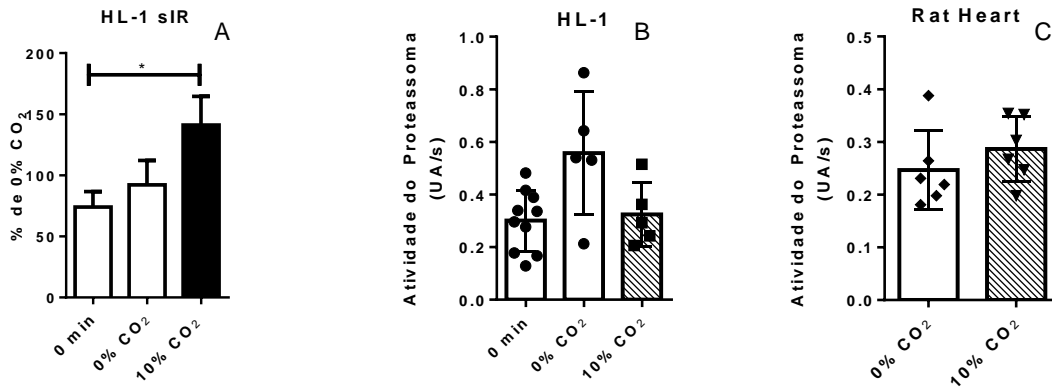


Figura 20 – Ubiquitina é acumulada na presença de bicarbonato, mas não muda a atividade do proteassoma – Células HL-1 foram submetidas a sIR na ausência ou presença de bicarbonato e a quantidade de ubiquitina foi medida na proteína total através de WB (A) Atividade do proteassoma foi medida como descrito nos Materiais e Métodos no extrato celular de HL-1 submetida a sIR (B) e em extrato dos corações submetidos a sIR (C).

Outro sistema envolvido com degradação de proteínas oxidadas e danificadas é o sistema autofágico. Para estudar esse mecanismo nós firmamos uma colaboração com o laboratório da professora Roberta Gottlieb do hospital Cedars-Sinai em Los Angeles, nos Estados Unidos. Nessa parte do projeto nós utilizamos corações isolados de ratos e células HL-1 como modelos. Os corações foram submetidos a um protocolo semelhante ao descrito anteriormente (Queliconi et al., 2013). Utilizamos 30 min de estabilização seguidos de 30 min de isquemia e 15 min de reperfusão (IR). As células HL-1 foram submetidas à isquemia-reperfusão simulada (sIR), com duração de 150 min de isquemia e 5 minutos de reperfusão, utilizando um sistema GazPak para obter um ambiente anóxico e utilização de deoxiglicose para inibição da via glicolítica (Perry et al., 2011).

A quantificação da morte celular foi feita medindo a atividade da creatina kinase (CK) (Fig. 21). A atividade da CK foi medida no perfusato dos corações de rato a cada

minuto durante os 5 min iniciais da reperfusão. Nas células HL-1, a atividade de CK foi medida no sobrenadante e no extrato total (atividade sobrenadante + atividade das células aderidas) e a proporção da atividade no sobrenadante pela atividade total foi considerada como % de morte celular. A presença de bicarbonato provocou um aumento na liberação de CK em ambos os modelos (Fig. 21) condizendo com os outros indicadores de morte celulares que obtivemos anteriormente (Queliconi et al., 2013).

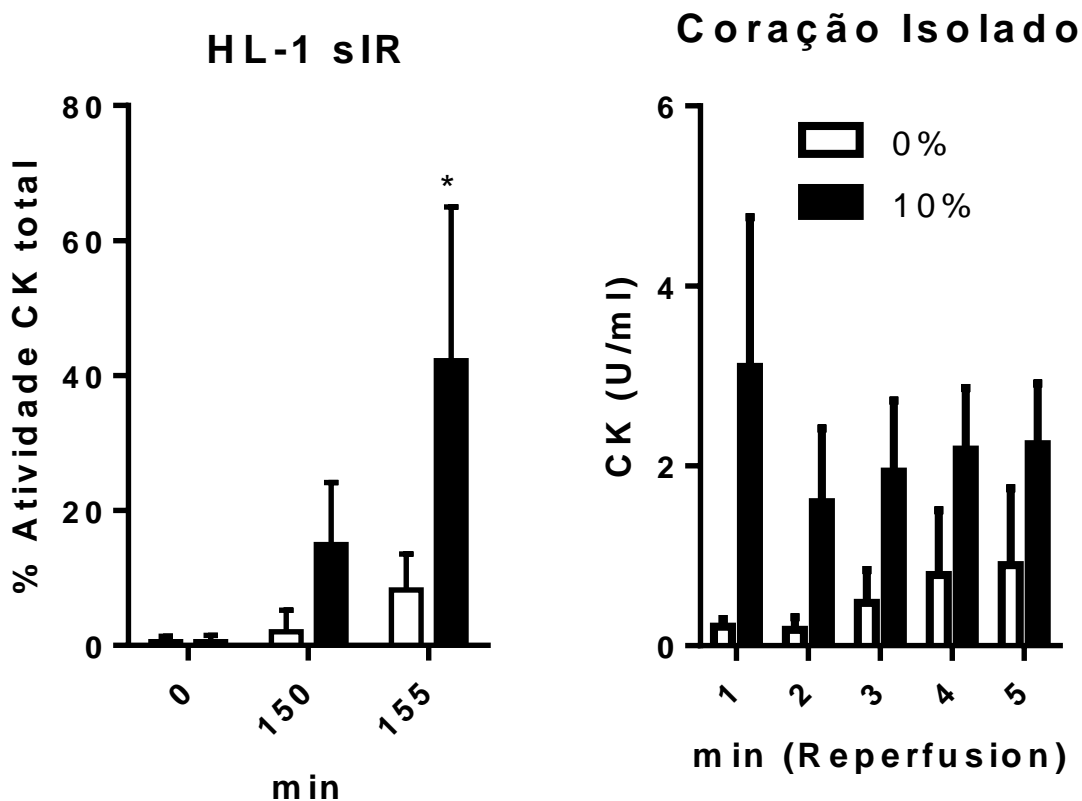


Figura 21 – Bicarbonato aumento o dano após dano por isquemia-reperfusão. A medida do dano foi feita pela atividade da creative kinase (CK) liberada. (A) % de CK total no sobrenadante de células HL-1 no tempo 0, pré-reperfusão (150 min) e pós reperfusão (155 min) (B) Liberação de CK no perfusato de corações de ratos isolados submetidos à IR como descrito nos Materiais e Métodos.

Confirmamos também que o acúmulo de proteínas oxidadas podia ser reproduzido no novo modelo (Fig. 22, 3 e 7).

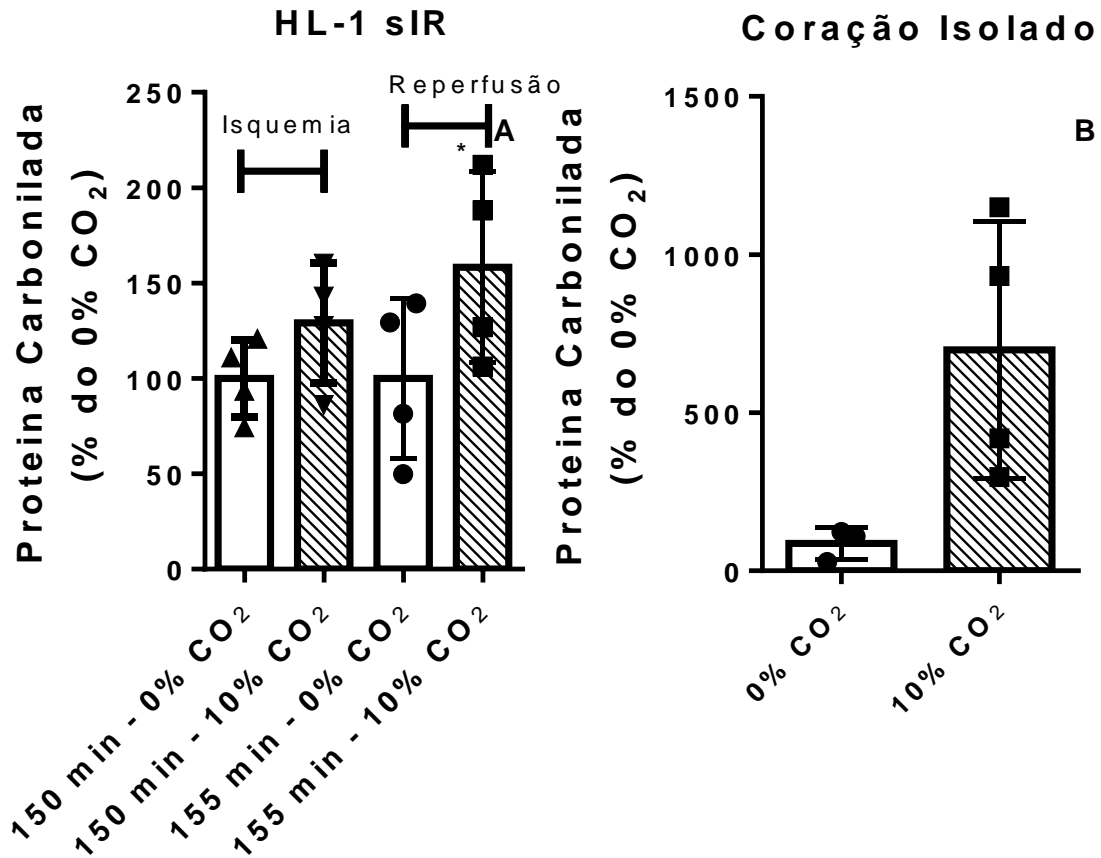


Figura 22 – Acúmulo de proteínas carboniladas após IR na ausência de (0% CO₂) ou presença de bicarbonato (10% CO₂)- (A) Células HL-1 foram submetidas a sIR e coletadas na isquemia (150 min) e após a 5 min de reperusão (155 min) na presença ou ausência de bicarbonato como descrito nos Materiais e Métodos. (B) Corações isolados foram submetidos a IR e proteína carbonilada foi medida como descrito nos materiais e métodos * , p<0,05 em relação ao 0% CO₂.

Começamos a analisar o sistema autofágico medindo a quantidade de LC3 I e II. Não detectamos diferenças significativas na quantidade de proteína LC3 ou seus subtipos (Fig. 23 A-F). Usando RT-PCR (Fig. 23G) conseguimos detectar um aumento da quantidade de mRNA de LC3 nos corações isolados de ratos.

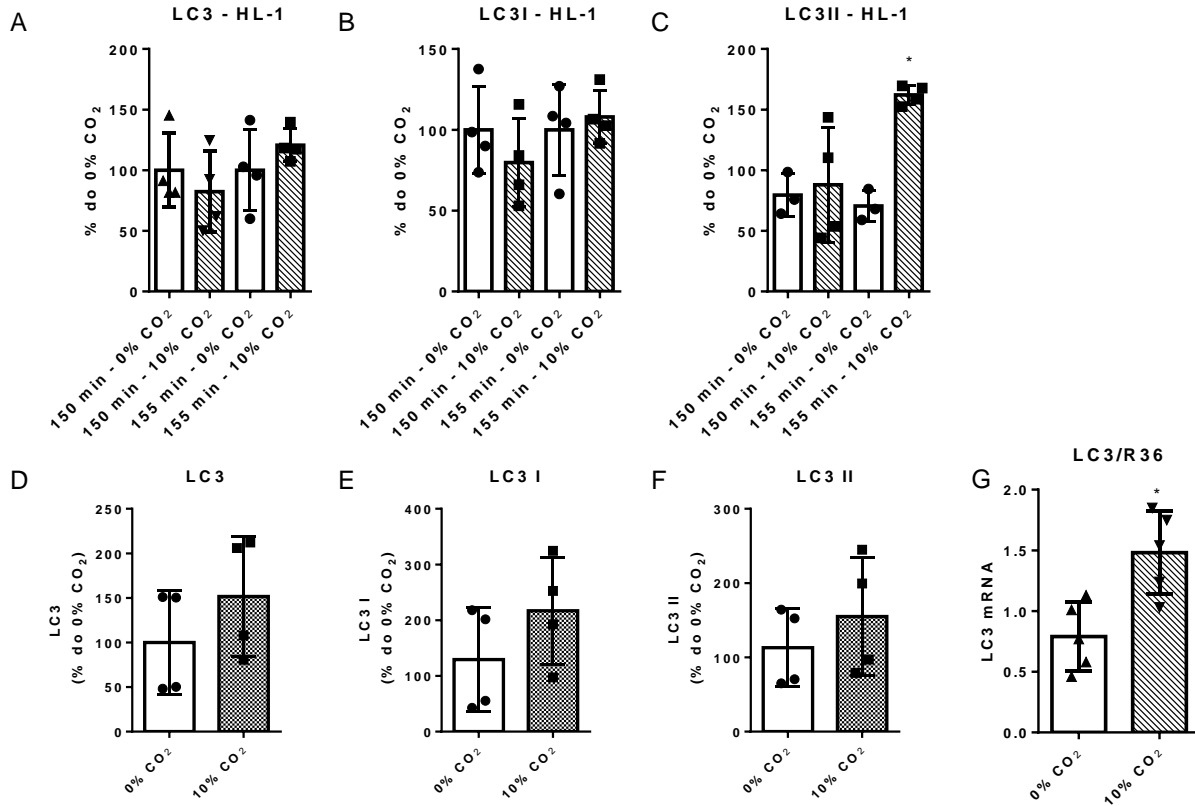


Figura 23 – A quantidade de LC3 não muda na presença ou ausência de bicarbonato – A quantidade LC3 foi medida usando WB como descrito nos Materiais e Métodos. (A-C) Células HL-1 foram submetidas a sIR na presença ou ausência de bicarbonato. (D-F) Corações de rato submetidos a IR na presença ou ausência de bicarbonato, (G) A quantidade de mRNA foi medida como descrito nos Materiais e Métodos de corações de rato submetidos a IR na presença ou ausência de bicarbonato. *, $p < 0,05$ em relação ao 0% CO₂.

Outro importante marcador da cascata autofágica é p62. Uma depleção de p62 em geral indica fluxo autofágico aumentado enquanto seu acúmulo em geral indica inibição. Utilizando extrato total das células HL-1, nós detectamos uma diminuição da quantidade de p62 (Fig. 24A), o que se repetiu quando medimos a quantidade de p62 na fração citosólica dos corações infartados (Fig. 24B). Entretanto, a quantidade de p62 na fração mitocondrial (Fig. 24C) se apresentou significativamente aumentada.

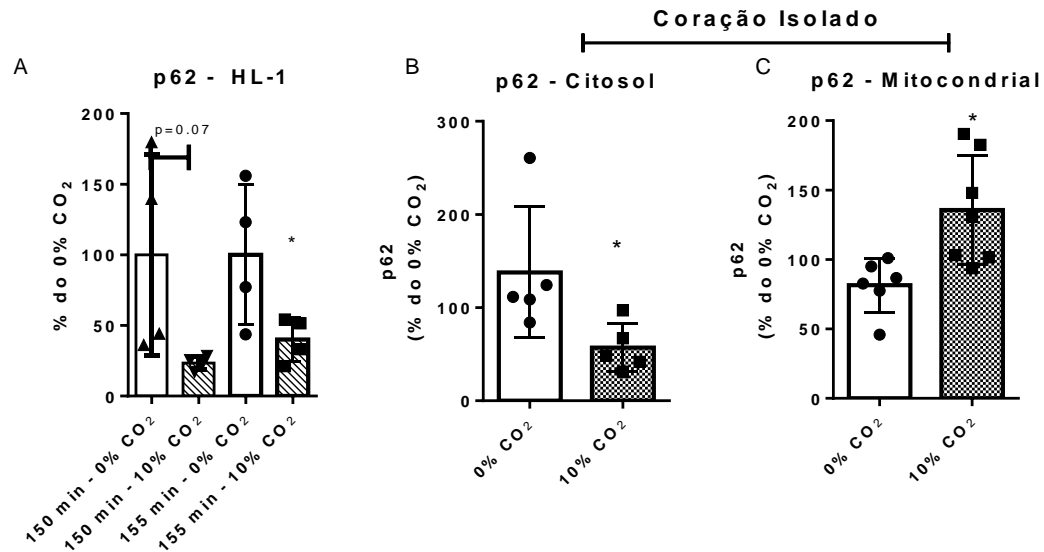


Figura 24 – Quantidade de p62 diminuí no citosol e aumenta na fração mitocondrial – A quantidade de p62 foi medida usando WB como descrito nos Materiais e Métodos. (A) Células HL-1 foram submetidas a SIR na presença ou ausência de bicarbonato. Corações de rato submetidos a IR na presença ou ausência de bicarbonato e fracionados em (B) citosol e (C) mitocôndrias. *, $p < 0,05$ em relação ao 0% CO₂.

Para nos certificarmos que as modificações na fração mitocondrial eram consistentes, medimos outros marcadores ligados à mitofagia. A quantidade de Beclin1 apresenta o padrão oposto de p62, estando aumentada no citosol e diminuída na fração mitocondrial (Fig. 25A e B). Beclin1, quando clivada (Fig. 25C), é um indicativo de aumento de sinalização apoptótica. Porém, não conseguimos detectar diferenças em sua clivagem, o que indica que o processo de morte observado não está ligado a um aumento de apoptose por essa via.

Drp1 é uma enzima necessária para a fragmentação mitocondrial e para iniciar o processo de mitofagia. Na presença de bicarbonato ela apresentou um aumento na fração citosólica e na fração mitocondrial (Fig. 25D e E).

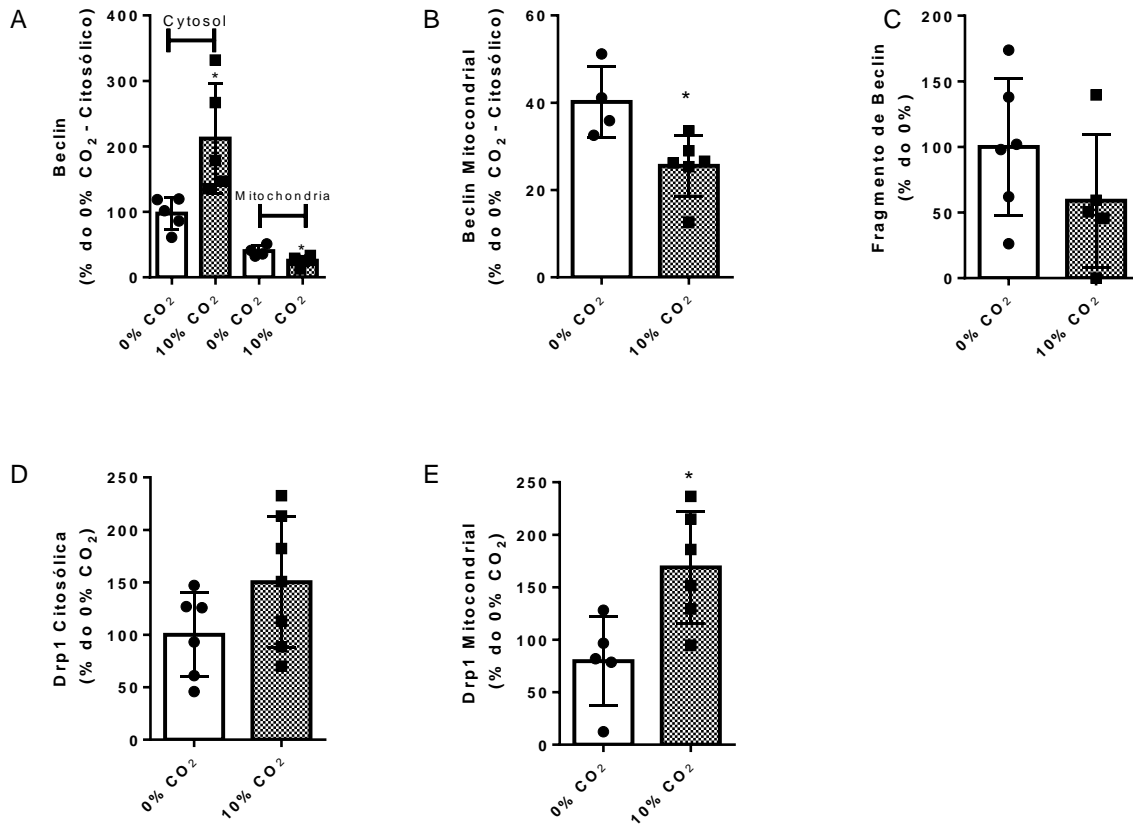


Figura 25 – Presença de bicarbonato aumenta marcadores de mitofagia – Beclin1 foi quantificada usando WB em células HL-1 submetidas à SIR na presença ou ausência de bicarbonato (A) e em frações de corações de ratos submetidos a IR na presença ou ausência de bicarbonato. Fração citosólica (B) e mitocondrial (C). Drp1 foi quantificada por WB em fração de corações de ratos submetidos a IR na presença ou ausência de bicarbonato. Fração citosólica (D) e mitocondrial (E). Os WB foram feitos como descrito nos Materiais e Métodos. *, $p < 0,05$ em relação ao 0% CO₂.

Parkin é uma ubiquitina ligase, que poderia ser responsável pelas modificações detectadas na quantidade de ubiquitina. Outra proteína importante é ATG4, responsável pela remoção de LC3. Analisamos a expressão dessas duas proteínas por WB (Fig. 26). Em ambos os casos não detectamos mudanças.

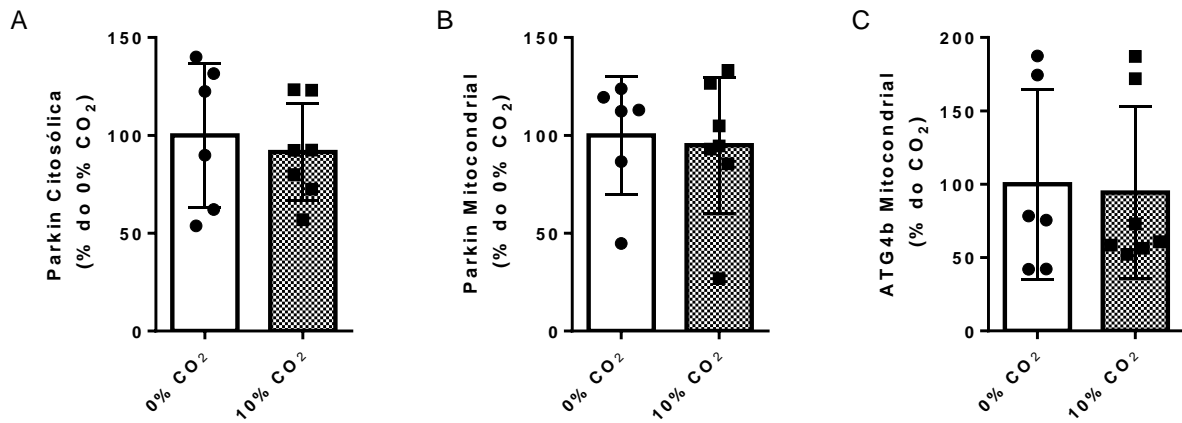


Figura 26 – Presença ou ausência de bicarbonato não muda a quantidade de Parkin ou ATG4b – A quantidade de Parkin e ATG4b foi medida usando WB em frações de corações de rato expostos a IR na presença ou ausência de bicarbonato. Parkin nas frações citosólica (A), mitocondrial (B) e ATG4b na fração mitocondrial (C). Os WB foram feitos como descrito nos Materiais e Métodos.

Para verificar se a mitofagia está inibida, analisamos a quantidade de proteínas que são degradadas especificamente pelo sistema ubiquitina-proteassoma (TOM70) e proteínas degradadas pelo sistema autofágico (CoxIV). Detectamos um acúmulo de CoxIV (Fig. 27B), mas não TOM70 (Fig. 27A), indicando que somente a via autofágica está inibida.

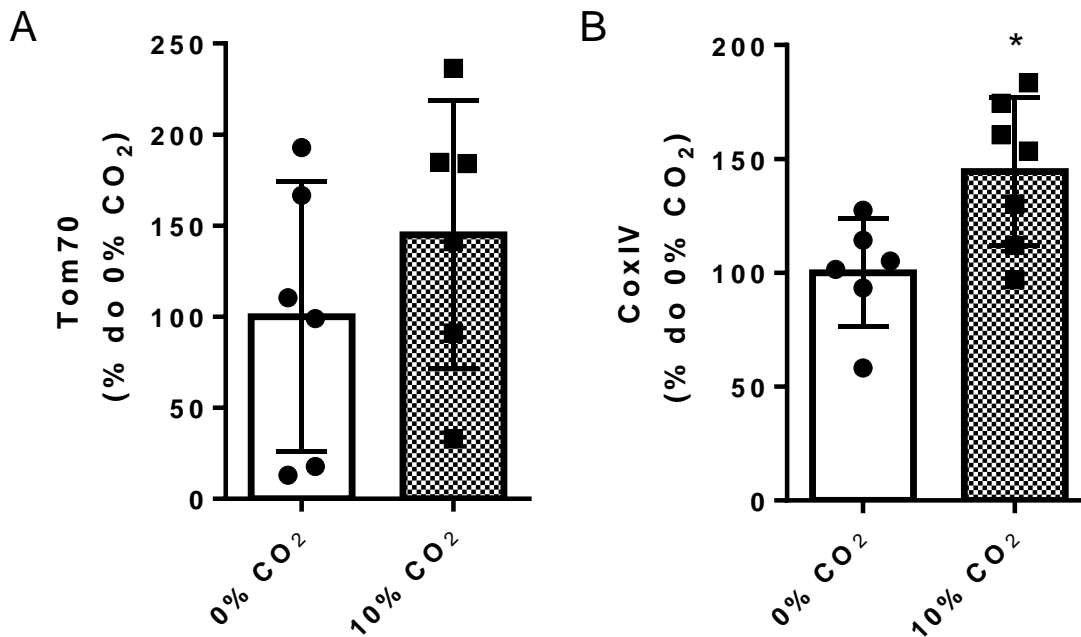


Figura 27 – A presença de bicarbonato não muda quantidade de TOM70, mas causa acúmulo de CoxIV – Lisados totais de coração de rato expostos a IR na presença ou ausência de bicarbonato foram testados para Tom70 e CoxIV usando WB como descrito nos Materiais e Métodos. *, $p < 0,05$ em relação ao 0% CO₂.

Se a inibição da mitofagia é a responsável pelo aumento de dano causado pela presença de bicarbonato, a inibição do processo autofágico deveria desaparecer com a diferença de dano causado pelo tratamento com bicarbonato. Utilizamos bafilomicina A para inibir a acidificação do lisossomo e sua consequente fusão com o autofágossomo. Submetemos células HL-1 a sIR na presença de Bafilomicina A (Fig. 28) na presença (10%) ou ausência de bicarbonato (0%) (Fig. 28). O grupo contendo bicarbonato não apresentou mudanças no dano, mas o grupo que não continha bicarbonato apresentou um dano maior. É interessante ressaltar que não há diferença entre o grupos 0% + Bafilomicina / 10% / 10 + Bafilomicina, mas essa é significativa quando comparada com o 0%. Isso mostra que a inibição da autofagia não aumenta o dano causado pelo

bicarbonato, mas causa um dano de proporções similares no grupo que não contém bicarbonato, suportando a hipótese de que a inibição da mitofagia é a causa do aumento de dano promovido pelo bicarbonato.

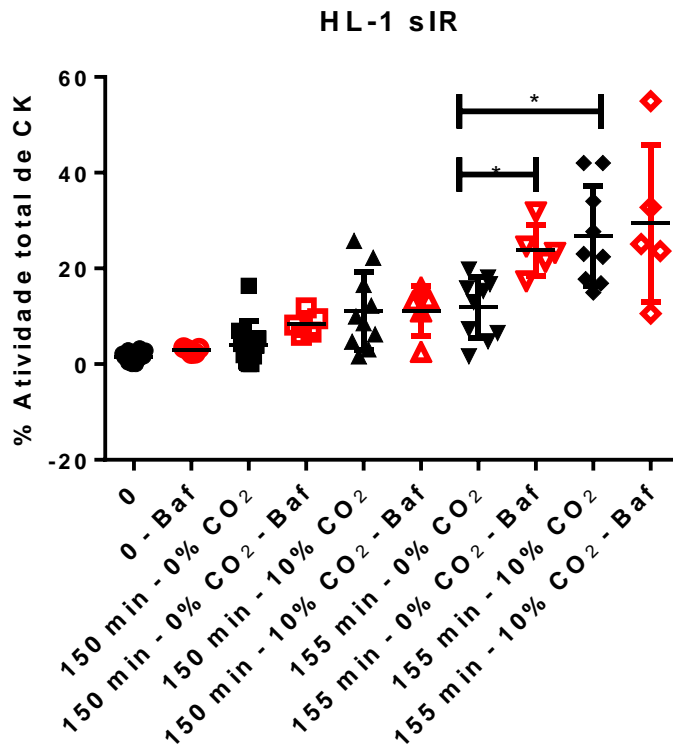


Figura 28 – Bafilomicina A causa um aumento de liberação de CK na ausência de bicarbonato, mas não na presença de bicarbonato – Células HL-1 foram incubadas na presença de Bafilomicina A (Baf) (em vermelho) ou DMSO (em preto) por 2 h antecedendo o experimento e submetidas a sIR como descrito nos Materiais e Métodos. A liberação de CK foi medida sobre condições basais (0 min), antes da reperfusão (150 min) e 5 min após a reperfusão (155 min). *, $p < 0,05$ em relação ao indicado.

5. Discussão

5.1 – Caracterização do dano causado pela presença de bicarbonato na IR

Esse trabalho se iniciou pela constatação de que há aumento do dano causado por isquemia/reperfusão pela presença de $\text{HCO}_3^-/\text{CO}_2$. Os dados que caracterizam esse efeito estão compreendidos entre as figuras 2-15 discutidos em detalhes no trabalho publicado e em anexo (Ap.5) (Queliconi et al., 2013). Aqui faremos uma breve discussão dos dados já publicados e focaremos na discussão do mecanismo responsável, ainda não publicado.

A presença do bicarbonato causa um aumento do dano provocado por IR sem que haja modificações nas condições basais. Estudos anteriores utilizando bicarbonato mostram que a presença um aumento do bicarbonato poderia ser protetora (Heijnen et al., 2002; Imahashi et al., 2007), entretanto esses estudos não se preocuparam em manter o pH constante. Essa proteção descrita pode se dever principalmente a reperfusão acida, que já foi descrita como protetora em condições de IR (Inserte et al., 2008) devido a um menor gasto energético pela bomba de Na^+/K^+ (Imahashi et al., 2007).

Nós analisamos a influência da presença de bicarbonato mantendo o pH intra e extra celular constante. Nossos dados são coerentes com diversos estudos mostrando toxicidade devido a um aumento de CO_2 (Ezraty et al., 2011) e que o par $\text{HCO}_3^-/\text{CO}_2$ permite e catalisa a produção de espécies radicalares mais reativas (Medinas et al., 2007).

Nós estudamos a possibilidade da reação de radicais derivados do par $\text{HCO}_3^-/\text{CO}_2$ reagir com NO^* (Fig. 10) e danificar a NOS ou a NADPH oxidase, criando um fluxo constante de superóxido que poderia ser a origem do dano (Santos et al., 2009). Nenhum desses fatores demonstrou ser necessário para o aumento do dano. Dessa maneira seguimos para um estudo detalhado das diversas possíveis fontes que provocariam o aumento do dano.

5.2 – Identificação das mudanças moleculares envolvidas no dano causado pela presença de bicarbonato na IR

Parâmetros bioenergéticos e redox mitocondriais podem ser facilmente alterados pela mudança de carga iônica pela diferença de pH entre o espaço intermembranas e a matriz (Nicholls, 2002; Kumar et al., 2011). Ao analisar a respiração, produção de EROs, a quantidade de proteínas oxidadas formadas em situação de estresse oxidativo e a forma da rede mitocondrial, não conseguimos detectar nenhuma diferença (Fig. 14-19). O mais intrigante desses dados é a falta de detecção de um acúmulo de proteínas oxidadas em organelas isoladas (Fig. 17 e 18), já que esse foi um dado consistente observado nos experimentos com sistemas celulares e é conhecido que o bicarbonato pode aumentar a toxicidade de outras espécies radicalares (Medinas et al., 2007).

A falta de lesões oxidativas no sistema de organelas isoladas nos fez levantar a hipótese de que a diferença não estava na produção de EROs, mas na remoção dos danos provocados por essas espécies. A degradação proteica em células é mediada pelo sistema proteassoma-ubiquitina e sistema autofágico. O proteassoma é considerado a principal via de degradação de proteínas danificadas e mal

formadas/dobradas (da Cunha et al., 2011; Livnat-Levanon e Glickman, 2011). Sabe-se que o aumento da atividade do proteassoma reduz o danos associados a IR (Churchill et al., 2010). Nós detectamos um aumento da quantidade de ubiquitinação na presença de bicarbonato (Fig. 20A). O acúmulo de ubiquitina pode ser causado pela inibição da degradação ou um aumento da ubiquitinação das proteínas. Infelizmente, o grande número de ubiquitin-ligases (Livnat-Levanon e Glickman, 2011) e sua ligação transiente com os alvos e organelas torna difícil quantificar a atividade das mesmas.

Seguimos medindo a atividade do proteassoma em extratos de células HL-1 submetidas à isquemia na presença ou ausência de bicarbonato (Fig. 20B) e de corações que foram submetidos a IR na presença ou ausência de bicarbonato (Fig. 20C). Não detectamos nenhuma diferença na atividade do proteassoma que explicasse as diferenças na quantidade de ubiquitina.

O processo autofágico também se utiliza de ubiquitina como marcador e iniciador (Geng e Klionsky, 2008; Suen et al., 2010; Huang et al., 2011; Kubli et al., 2013; Bingol et al., 2014). Os nossos dados iniciais indicavam uma tendência de acúmulo de LC3 (Fig. 23 A-C, E-G), com um significativo aumento da quantidade de LC3II na sua forma ativa na presença de bicarbonato em células HL-1 submetidas a IR (Fig. 23G). Detectamos também um aumento significativo de mRNA de LC3 nos corações expostos ao bicarbonato (Fig. 23D). Esses dados são um indicativo de que a autofagia pode estar inibida. A inibição da degradação pode ser causada por problemas na detecção dos alvos, estruturação do autofagossomo, fusão com o lisossomo e na degradação do conteúdo dentro do autofagolisossomo (Gottlieb et al., 2011; Mizushima et al., 2011; Kobayashi e Liang, 2014). Iniciamos olhando para a quantidade de uma proteína acessória que permite a identificação dos alvos a serem degradados, p62 (Fig. 24).

A quantidade detectada no extrato celular total aparece diminuída na presença de bicarbonato (Fig. 24A), e o mesmo se repete quando analisamos a fração citosólica dos corações de ratos. Esse dano parece inconsistente com a quantidade de LC3 (Fig. 23), entretanto quando analisamos a quantidade de p62 na fração mitocondrial dos corações de rato detectamos um aumento na quantidade de p62 mitocondrial.

O acúmulo de p62 na fração mitocondrial pode indicar um problema especificamente no processo de mitofagia. Essa hipótese seria condizente com os dados anteriores já que o acúmulo de mitocôndrias danificadas causaria um aumento de dano oxidativo nas células provocando um aumento de proteínas oxidadas. Para nos certificarmos se o processo mitofágico estava realmente inibido medimos outros marcadores. Utilizando corações de rato fracionados submetidos a IR e expostos ou não ao bicarbonato, medimos a quantidade e a translocação de Beclin e de Drp1 (Fig. 25). Beclin apresentou um aumento na fração citosólica (Fig. 25A) e uma diminuição na fração mitocondrial (Fig. 25B). Beclin1 é essencial para mitofagia e sua presença é essencial para a translocação de outros fatores necessários para a mitofagia (Wirawan et al., 2010; Choubey et al., 2014). Esse dado reforça que a mitocôndria não está sendo degradada de modo eficiente porque não está recebendo todos os fatores necessários, e a presença da mesma quantidade de Beclin1 clivada (Fig. 25C) indica que a inibição da mitofagia não está ocorrendo devido a um aumento de sinalização para apoptose (Wirawan et al., 2010).

Drp1 é uma proteína importante para a fissão mitocondrial, um passo que normalmente precede a mitofagia. A fissão mitocondrial é necessária para que as mesmas possam ser englobadas pela autofagossomo e Drp1 interage com Parkin para estimular a mitofagia (Buhlman et al., 2014). Na presença de bicarbonato houve um

aumento da quantidade de Drp1 citosólica (Fig. 25D) e translocada para a fração mitocondrial (Fig. 25E) indicando um acúmulo de Drp1 que seria degradada junto com as mitocôndrias danificadas.

O aumento de Drp1 e o decréscimo de Beclin1 poderiam indicar um defeito na marcação das mitocôndrias que seriam degradadas, já que ambas são translocadas para a mitocôndria, portanto poderiam haver mudanças em proteínas que marcam as mitocôndrias a serem degradadas, como Parkin e Atg4b. Analisamos ambas e não detectamos nenhuma diferença (Fig. 26). Essas proteínas apresentam uma ligação transiente com as mitocôndrias danificadas e isso pode ter dificultado a detecção. Entretanto a quantidade aumentada de ubiquitina pode indicar que não temos problemas Parkin (uma das muitas ubiquitinas ligase celulares), e o leve aumento de LC3 pode indicar que ATG4b também funciona corretamente. Portanto, a falta de diferença não nos fornece informações adicionais.

Essencialmente, a mitofagia promove a degradação de proteínas mitocondriais. Entretanto nem todas são degradadas pelo sistema autofágico e algumas são degradadas pelo sistema proteassoma ubiquitina (Vincow et al., 2013). Dessa maneira nós analisamos Tom70 e CoxIV (Fig. 27) como representantes da degradação do sistema proteassoma-ubiquitina e do sistema autofágico respectivamente.

A quantificação por WB se deu em extrato total para que não houvesse influência da purificação mitocondrial, que poderia separar uma subpopulação mitocondrial. A quantidade de Tom70 (Fig. 27A) não apresentou diferenças significativas, o que condiz com a atividade normal do sistema proteassoma analisada anteriormente (Fig. 20). A quantidade de CoxIV (Fig. 27B) aparece aumentada, o que também condiz com os dados mostrando inibição da mitofagia.

Ainda não existem meios de se modular positivamente ou negativamente a mitofagia de maneira específica. Os meios de ativação do sistema autofágico total também não são específicos e apresentam diversos efeitos indiretos (Dolman et al., 2013). Por isso inibimos o sistema autofágico utilizando bafilomicina A, uma droga que inibe a acidificação do lisossomo, o que impede a degradação proteica e a fusão do autofagossomo com o lisossomo. Após a inibição submetemos células HL-1 a sIR na presença ou ausência de bicarbonato e medimos a morte celular (Fig. 28). Com isso conseguimos mostrar que a inibição do sistema autofágico aumenta a morte de células submetidas a sIR na ausência de $\text{HCO}_3^-/\text{CO}_2$ ao mesmo nível daquelas expostas à sIR com $\text{HCO}_3^-/\text{CO}_2$. Esse dado adiciona à hipótese de que a presença de bicarbonato inibe a mitofagia, mostrando que a inibição da autofagia total exerce o mesmo efeito que a presença do bicarbonato nas células HL-1. Os dados estão esquematizados na fig. 29.

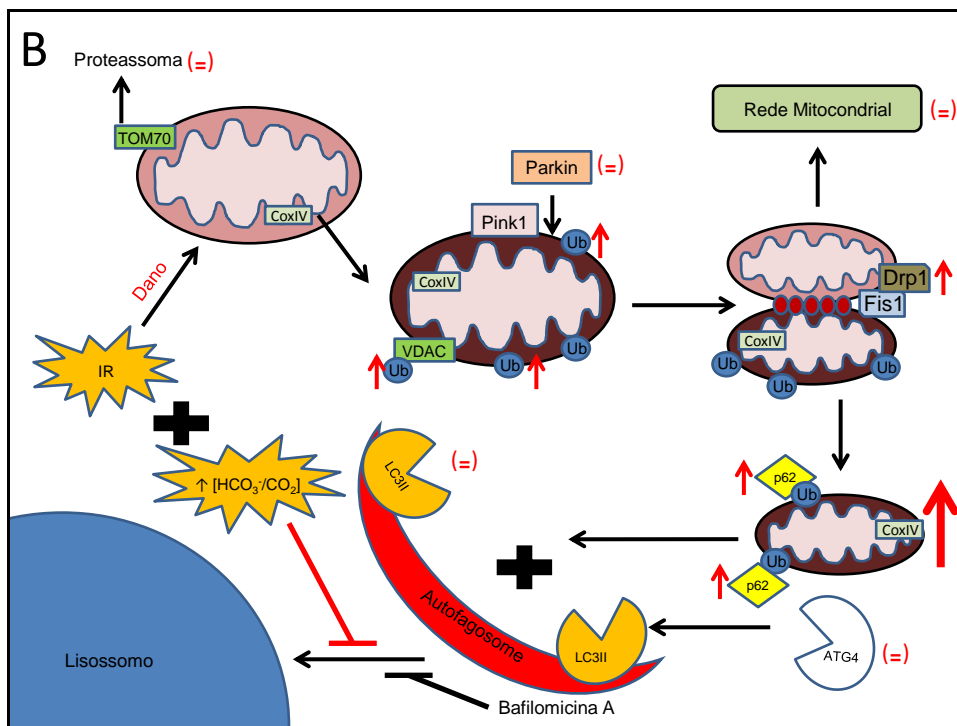
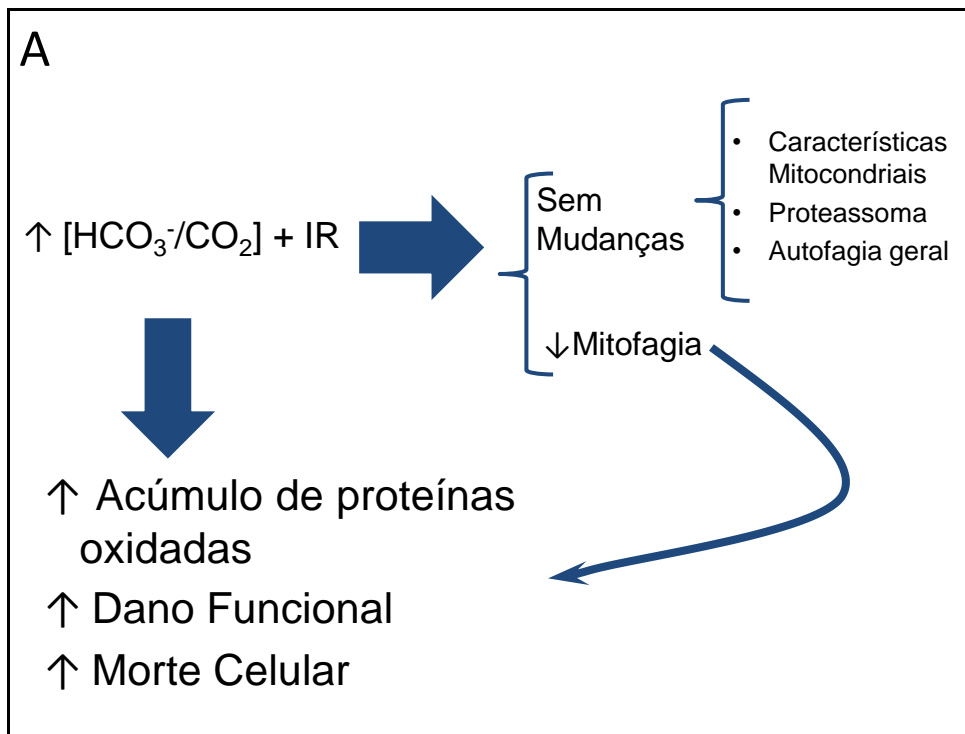


Figura 29 – Esquema geral e mecânico dos efeitos da presença de bicarbonato na IR – (A) Esquema das modificações observadas na presença de bicarbonato e IR (B) Detalhe das modificações na mitofagia que levam ao danos observados na parte A., em vermelho as modificações detectadas nesse estudo.

6. Conclusões

Nosso trabalho demonstra que a presença de bicarbonato durante IR aumenta o dano celular em diversos modelos. Mostramos também que esse dano é causado por uma inibição da mitofagia.

Resumidamente,

- $\uparrow[\text{HCO}_3^-/\text{CO}_2]$ + IR causa um aumento do dano e morte celular acompanhado de um acúmulo de proteínas oxidadas
- $\uparrow[\text{HCO}_3^-/\text{CO}_2]$ não modifica o fenótipo mitocondrial
- $\uparrow[\text{HCO}_3^-/\text{CO}_2]$ e $\uparrow[\text{HCO}_3^-/\text{CO}_2]$ + IR não modifica a atividade do proteassoma
- $\uparrow[\text{HCO}_3^-/\text{CO}_2]$ + IR provoca um aumento da quantidade de ubiquitina
- $\uparrow[\text{HCO}_3^-/\text{CO}_2]$ + IR não muda marcadores de autofagia gerais $\uparrow[\text{HCO}_3^-/\text{CO}_2]$ + IR provoca acúmulo de marcadores de autofagia na mitocôndria (mitofagia), e modifica a relação entre proteínas degradadas pelo proteassoma e por mitofagia (TOM70 e CoxIV)
- A inibição da autofagia produz dano semelhante à presença de bicarbonato, sem alterar o dano causado na presença de bicarbonato

7. Referências

- Arakaki, N., Nishihama, T., Owaki, H., Kuramoto, Y., Suenaga, M., Miyoshi, E., Emoto, Y., Shibata, H., Shono, M., and Higuti, T. (2006). Dynamics of mitochondria during the cell cycle. *Biol. Pharm. Bull.* 29, 1962–1965.
- Augusto, O., Bonini, M.G., Amanso, A.M., Linares, E., Santos, C.C.X., and De Menezes, S.L. (2002). Nitrogen dioxide and carbonate radical anion: two emerging radicals in biology. *Free Radic. Biol. Med.* 32, 841–859.
- Balaban, R.S., Nemoto, S., and Finkel, T. (2005). Mitochondria, oxidants, and aging. *Cell* 120, 483–495.
- Berlett, B.S., Chock, P.B., Yim, M.B., and Stadtman, E.R. (1990). Manganese(II) catalyzes the bicarbonate-dependent oxidation of amino acids by hydrogen peroxide and the amino acid-facilitated dismutation of hydrogen peroxide. *Proc. Natl. Acad. Sci. U. S. A.* 87, 389–393.
- Bingol, B., Tea, J.S., Phu, L., Reichelt, M., Bakalarski, C.E., Song, Q., Foreman, O., Kirkpatrick, D.S., and Sheng, M. (2014). The mitochondrial deubiquitinase USP30 opposes parkin-mediated mitophagy. *Nature*.
- Bolli, R. (1998). Why myocardial stunning is clinically important. *Basic Res. Cardiol.* 93, 169–172.
- Bonini, M.G., and Augusto, O. (2001). Carbon dioxide stimulates the production of thiyl, sulfinyl, and disulfide radical anion from thiol oxidation by peroxynitrite. *J. Biol. Chem.* 276, 9749–9754.
- Boveris, B.A., and Chance, B. (1973). The Mitochondrial Generation of Hydrogen Peroxide. *134*, 707–716.
- Brady, N.R., Hamacher-Brady, A., and Gottlieb, R. a (2006). Proapoptotic BCL-2 family members and mitochondrial dysfunction during ischemia/reperfusion injury, a study employing cardiac HL-1 cells and GFP biosensors. *Biochim. Biophys. Acta* 1757, 667–678.
- Brenner, S. (1974). The genetics of *Caenorhabditis elegans*. *Genetics* 77, 71–94.
- Buhlman, L., Damiano, M., Bertolin, G., Ferrando-Miguel, R., Lombès, A., Brice, A., and Corti, O. (2014). Functional interplay between Parkin and Drp1 in mitochondrial fission and clearance. *Biochim. Biophys. Acta* 1843, 2012–2026.
- Cai, H. (2005). Hydrogen peroxide regulation of endothelial function: origins, mechanisms, and consequences. *Cardiovasc. Res.* 68, 26–36.
- Campos, J.C., Queliconi, B.B., Dourado, P.M.M., Cunha, T.F., Zambelli, V.O., Bechara, L.R.G., Kowaltowski, A.J., Brum, P.C., Mochly-Rosen, D., and Ferreira, J.C.B. (2012). Exercise training restores cardiac protein quality control in heart failure. *PLoS One* 7, e52764.

Cancherini, D. V, Queliconi, B.B., and Kowaltowski, A.J. (2007). Pharmacological and physiological stimuli do not promote Ca(2+)-sensitive K⁺ channel activity in isolated heart mitochondria. *Cardiovasc. Res.* 73, 720–728.

Chandel, N.S., Maltepe, E., Goldwasser, E., Mathieu, C.E., Simon, M.C., and Schumacker, P.T. (1998). Mitochondrial reactive oxygen species trigger hypoxia-induced transcription. *Proc. Natl. Acad. Sci.* 95, 11715–11720.

Chen, Y.-R., and Zweier, J.L. (2014). Cardiac mitochondria and reactive oxygen species generation. *Circ. Res.* 114, 524–537.

Choubey, V., Cagalinec, M., Liiv, J., Safiulina, D., Hickey, M. a, Kuum, M., Liiv, M., Anwar, T., Eskelinen, E.-L., and Kaasik, A. (2014). BECN1 is involved in the initiation of mitophagy: It facilitates PARK2 translocation to mitochondria. *Autophagy* 10, 1105–1119.

Churchill, E.N., and Mochly-Rosen, D. (2007). The roles of PKCdelta and epsilon isoenzymes in the regulation of myocardial ischaemia/reperfusion injury. *Biochem. Soc. Trans.* 35, 1040–1042.

Churchill, E.N., Ferreira, J.C., Brum, P.C., Szweda, L.I., and Mochly-Rosen, D. (2010). Ischaemic preconditioning improves proteasomal activity and increases the degradation of deltaPKC during reperfusion. *Cardiovasc. Res.* 85, 385–394.

Claycomb, W.C., Lanson, N. a, Stallworth, B.S., Egeland, D.B., Delcarpio, J.B., Bahinski, a, and Izzo, N.J. (1998). HL-1 cells: a cardiac muscle cell line that contracts and retains phenotypic characteristics of the adult cardiomyocyte. *Proc. Natl. Acad. Sci. U. S. A.* 95, 2979–2984.

Da Cunha, F.M., Demasi, M., and Kowaltowski, A.J. (2011). Aging and calorie restriction modulate yeast redox state, oxidized protein removal, and the ubiquitin-proteasome system. *Free Radic. Biol. Med.* 51, 664–670.

Dolman, N.J., Chambers, K.M., Mandavilli, B., Batchelor, R.H., and Janes, M.S. (2013). Tools and techniques to measure mitophagy using fluorescence microscopy. *Autophagy* 9, 1653–1662.

Dröge, W. (2002). Free radicals in the physiological control of cell function. *Physiol. Rev.* 82, 47–95.

Ezraty, B., Chabalier, M., Ducret, A., Maisonneuve, E., and Dukan, S. (2011). CO(2) exacerbates oxygen toxicity. *EMBO Rep.* 1–6.

Facundo, H.T.F., de Paula, J.G., and Kowaltowski, A.J. (2005). Mitochondrial ATP-sensitive K⁺ channels prevent oxidative stress, permeability transition and cell death. *J. Bioenerg. Biomembr.* 37, 75–82.

Facundo, H.T.F., Carreira, R.S., de Paula, J.G., Santos, C.C.X., Ferranti, R., Laurindo, F.R.M., and Kowaltowski, A.J. (2006). Ischemic preconditioning requires increases in

reactive oxygen release independent of mitochondrial K⁺ channel activity. *Free Radic. Biol. Med.* 40, 469–479.

Facundo, H.T.F., de Paula, J.G., and Kowaltowski, A.J. (2007). Mitochondrial ATP-sensitive K⁺ channels are redox-sensitive pathways that control reactive oxygen species production. *Free Radic. Biol. Med.* 42, 1039–1048.

Figueira, T.R., Barros, M.H., Camargo, A. a, Castilho, R.F., Ferreira, J.C.B., Kowaltowski, A.J., Sluse, F.E., Souza-Pinto, N.C., and Vercesi, A.E. (2013). Mitochondria as a source of reactive oxygen and nitrogen species: from molecular mechanisms to human health. *Antioxid. Redox Signal.* 18, 2029–2074.

Forbes, R.A., Steenbergen, C., and Murphy, E. (2001). Diazoxide-induced cardioprotection requires signaling through a redox-sensitive mechanism. *Circ. Res.* 88, 802–809.

Geng, J., and Klionsky, D.J. (2008). The Atg8 and Atg12 ubiquitin-like conjugation systems in macroautophagy. “Protein modifications: beyond the usual suspects” review series. *EMBO Rep.* 9, 859–864.

Gottlieb, R. a, and Mentzer, R.M. (2010). Autophagy during cardiac stress: joys and frustrations of autophagy. *Annu. Rev. Physiol.* 72, 45–59.

Gottlieb, R.A., Mentzer, R.M., and Linton, P. (2011). Impaired mitophagy at the heart of injury. *Autophagy* 7, 1573–1574.

Halestrap, A.P., Clarke, S.J., and Khaliulin, I. (2007). The role of mitochondria in protection of the heart by preconditioning. *Biochim. Biophys. Acta* 1767, 1007–1031.

Halliwell, B., and Gutteridge, J.M. (1992). Biologically relevant metal ion-dependent hydroxyl radical generation. An update. *FEBS Lett.* 307, 108–112.

Heijnen, B.H.M., Elkhouloufi, Y., Straatsburg, I.H., and Van Gulik, T.M. (2002). Influence of acidosis and hypoxia on liver ischemia and reperfusion injury in an in vivo rat model. *J. Appl. Physiol.* 93, 319–323.

Hodgson, E.K., and Fridovich, I. (1976). The mechanism of the activity-dependent luminescence of xanthine oxidase. *Arch. Biochem. Biophys.* 172, 202–205.

Vanden Hoek, T.L., Li, C., Shao, Z., Schumacker, P.T., and Becker, L.B. (1997). Significant levels of oxidants are generated by isolated cardiomyocytes during ischemia prior to reperfusion. *J. Mol. Cell. Cardiol.* 29, 2571–2583.

Vanden Hoek, T.L., Becker, L.B., Shao, Z., Li, C., and Schumacker, P.T. (1998). Reactive oxygen species released from mitochondria during brief hypoxia induce preconditioning in cardiomyocytes. *J. Biol. Chem.* 273, 18092–18098.

Huang, C., Yitzhaki, S., Perry, C.N., Liu, W., Giricz, Z., Mentzer, R.M., and Gottlieb, R. (2010). Autophagy induced by ischemic preconditioning is essential for cardioprotection. *J. Cardiovasc. Transl. Res.* 3, 365–373.

- Huang, C., Andres, A.M., Ratliff, E.P., Hernandez, G., Lee, P., and Gottlieb, R. (2011). Preconditioning involves selective mitophagy mediated by Parkin and p62/SQSTM1. *PLoS One* 6, e20975.
- Hyde, B.B., Twig, G., and Shirihai, O.S. (2010). Organellar vs cellular control of mitochondrial dynamics. *Semin. Cell Dev. Biol.* 21, 575–581.
- Ignarro, L.J., Buga, G.M., Wood, K.S., Byrns, R.E., and Chaudhuri, G. (1987). Endothelium-derived relaxing factor produced and released from artery and vein is nitric oxide. *Proc. Natl. Acad. Sci. U. S. A.* 84, 9265–9269.
- Imahashi, K., Mraiche, F., Steenbergen, C., Murphy, E., and Fliegel, L. (2007). Overexpression of the Na⁺/H⁺ exchanger and ischemia-reperfusion injury in the myocardium. *Am. J. Physiol. Heart Circ. Physiol.* 292, H2237–47.
- Inserte, J., Barba, I., Hernando, V., Abellán, A., Ruiz-Meana, M., Rodríguez-Sinovas, A., and Garcia-Dorado, D. (2008). Effect of acidic reperfusion on prolongation of intracellular acidosis and myocardial salvage. *Cardiovasc. Res.* 77, 782–790.
- Jin, Z., Zhou, H., Cecchini, G., Gray, M.O., and Karliner, J.S. (2005). MnSOD in mouse heart: acute responses to ischemic preconditioning and ischemia-reperfusion injury. *Am. J. Physiol. Heart Circ. Physiol.* 288, H2986–94.
- Johnson, D., and Nehrke, K. (2010). Mitochondrial fragmentation leads to intracellular acidification in *Caenorhabditis elegans* and mammalian cells. *Mol. Biol. Cell* 21, 2191–2201.
- Khuri, S.F., Kloner, R.A., Karaffa, S.A., Marston, W., Taylor, A.D., Lai, N.C., Tow, D.E., and Barsamian, E.M. (1985). The significance of the late fall in myocardial PCO₂ and its relationship to myocardial pH after regional coronary occlusion in the dog. *Circ. Res.* 56, 537–547.
- Kobayashi, S., and Liang, Q. (2014). Autophagy and mitophagy in diabetic cardiomyopathy. *Biochim. Biophys. Acta.*
- Kowaltowski, A.J., de Souza-Pinto, N.C., Castilho, R.F., and Vercesi, A.E. (2009). Mitochondria and reactive oxygen species. *Free Radic. Biol. Med.* 47, 333–343.
- Kubli, D. a, Zhang, X., Lee, Y., Hanna, R. a, Quinsay, M.N., Nguyen, C.K., Jimenez, R., Petrosyan, S., Murphy, A.N., and Gustafsson, A.B. (2013). Parkin protein deficiency exacerbates cardiac injury and reduces survival following myocardial infarction. *J. Biol. Chem.* 288, 915–926.
- Kuma, A., Hatano, M., Matsui, M., Yamamoto, A., Nakaya, H., Yoshimori, T., Ohsumi, Y., Tokuhiya, T., and Mizushima, N. (2004). The role of autophagy during the early neonatal starvation period. *Nature* 432, 1032–1036.
- Kumar, S., Flacke, J., Kostin, S., Appukuttan, A., Reusch, H.P., and Ladilov, Y. (2011). SLC4A7 sodium bicarbonate co-transporter controls mitochondrial apoptosis in ischaemic coronary endothelial cells. *Cardiovasc. Res.* 89, 392–400.

- Lebuffe, G., Schumacker, P.T., Shao, Z.-H., Anderson, T., Iwase, H., and Vanden Hoek, T.L. (2003). ROS and NO trigger early preconditioning: relationship to mitochondrial KATP channel. *Am. J. Physiol. Heart Circ. Physiol.* 284, H299–308.
- Lin, T.-C., Chen, Y., Kensicki, E., Li, A.Y.-J., Kong, M., Li, Y., Mohny, R.P., Shen, H., Stiles, B., Mizushima, N., et al. (2012). Autophagy: resetting glutamine-dependent metabolism and oxygen consumption. *Autophagy* 8, 1477–1493.
- Liochev, S.I., and Fridovich, I. (2002). Copper, zinc superoxide dismutase and H₂O₂. Effects of bicarbonate on inactivation and oxidations of NADPH and urate, and on consumption of H₂O₂. *J. Biol. Chem.* 277, 34674–34678.
- Liu, Y., Yang, X.-M., Iliodromitis, E.K., Kremastinos, D.T., Dost, T., Cohen, M. V, and Downey, J.M. (2008). Redox signaling at reperfusion is required for protection from ischemic preconditioning but not from a direct PKC activator. *Basic Res. Cardiol.* 103, 54–59.
- Livnat-Levanon, N., and Glickman, M.H. (2011). Ubiquitin-proteasome system and mitochondria - reciprocity. *Biochim. Biophys. Acta* 1809, 80–87.
- Ma, X., Liu, H., Foyil, S.R., Godar, R.J., Weinheimer, C.J., Hill, J. a, and Diwan, A. (2012). Impaired autophagosome clearance contributes to cardiomyocyte death in ischemia/reperfusion injury. *Circulation* 125, 3170–3181.
- McCord, J.M., and Fridovich, I. (1969). The utility of superoxide dismutase in studying free radical reactions. I. Radicals generated by the interaction of sulfite, dimethyl sulfoxide, and oxygen. *J. Biol. Chem.* 244, 6056–6063.
- Medinas, D.B., Cerchiaro, G., Trindade, D.F., and Augusto, O. (2007). The carbonate radical and related oxidants derived from bicarbonate buffer. *IUBMB Life* 59, 255–262.
- Mitra, K., Wunder, C., Roysam, B., Lin, G., and Lippincott-Schwartz, J. (2009). A hyperfused mitochondrial state achieved at G1-S regulates cyclin E buildup and entry into S phase. *Proc. Natl. Acad. Sci. U. S. A.* 106, 11960–11965.
- Mizushima, N., Yamamoto, A., Matsui, M., Yoshimori, T., and Ohsumi, Y. (2004). In vivo analysis of autophagy in response to nutrient starvation using transgenic mice expressing a fluorescent autophagosome marker. *Mol. Biol. Cell* 15, 1101–1111.
- Mizushima, N., Yoshimori, T., and Ohsumi, Y. (2011). The role of Atg proteins in autophagosome formation. *Annu. Rev. Cell Dev. Biol.* 27, 107–132.
- Nadtochiy, S.M., Baker, P.R.S., Freeman, B.A., and Brookes, P.S. (2009). Mitochondrial nitroalkene formation and mild uncoupling in ischaemic preconditioning: implications for cardioprotection. *Cardiovasc. Res.* 82, 333–340.
- Nicholls, D. (2002). Bioenergetics.
- Ong, S.-B., and Hausenloy, D.J. (2010). Mitochondrial morphology and cardiovascular disease. *Cardiovasc. Res.* 88, 16–29.

- Palmer, J.W., Tandler, B., and Hoppel, C.L. (1977). Biochemical properties of subsarcolemmal and interfibrillar mitochondria isolated from rat cardiac muscle. *J. Biol. Chem.* *252*, 8731–8739.
- Palmer, L.A., Doctor, A., Chhabra, P., Sheram, M.L., Laubach, V.E., Karlinsey, M.Z., Forbes, M.S., Macdonald, T., and Gaston, B. (2007). S-nitrosothiols signal hypoxia-mimetic vascular pathology. *J. Clin. Invest.* *117*, 2592–2601.
- Penna, C., Mancardi, D., Rastaldo, R., and Pagliaro, P. (2009). Cardioprotection: a radical view Free radicals in pre and postconditioning. *Biochim. Biophys. Acta* *1787*, 781–793.
- Perry, C.N., Huang, C., Liu, W., Magee, N., Carreira, R.S., and Gottlieb, R. a (2011). Xenotransplantation of mitochondrial electron transfer enzyme, Ndi1, in myocardial reperfusion injury. *PLoS One* *6*, e16288.
- Quarrie, R., Cramer, B.M., Lee, D.S., Steinbaugh, G.E., Erdahl, W., Pfeiffer, D.R., Zweier, J.L., and Crestanello, J. a (2011). Ischemic preconditioning decreases mitochondrial proton leak and reactive oxygen species production in the postischemic heart. *J. Surg. Res.* *165*, 5–14.
- Queliconi, B.B., Wojtovich, A.P., Nadtochiy, S.M., Kowaltowski, A.J., and Brookes, P.S. (2011). Redox regulation of the mitochondrial K(ATP) channel in cardioprotection. *Biochim. Biophys. Acta* *1813*, 1309–1315.
- Queliconi, B.B., Marazzi, T.B.M., Vaz, S.M., Brookes, P.S., Nehrke, K., Augusto, O., and Kowaltowski, A.J. (2013). Bicarbonate modulates oxidative and functional damage in ischemia-reperfusion. *Free Radic. Biol. Med.* *55*, 46–53.
- Queliconi, B.B., Kowaltowski, A.J., and Nehrke, K. (2014). An anoxia-starvation model for ischemia/reperfusion in *C. elegans*. *J. Vis. Exp.* *2*.
- Radi, R. (2004). Nitric oxide, oxidants, and protein tyrosine nitration. *Proc. Natl. Acad. Sci. U. S. A.* *101*, 4003–4008.
- Radi, R., Cosgrove, T.P., Beckman, J.S., and Freeman, B. a (1993). Peroxynitrite-induced luminol chemiluminescence. *Biochem. J.* *290 (Pt 1)*, 51–57.
- Rink, T.J., Tsien, R.Y., and Pozzan, T. (1982). Cytoplasmic pH and free Mg²⁺ in lymphocytes. *J. Cell Biol.* *95*, 189–196.
- Santos, C.X.C., Tanaka, L.Y., Wosniak, J., and Laurindo, F.R.M. (2009). Mechanisms and implications of reactive oxygen species generation during the unfolded protein response: roles of endoplasmic reticulum oxidoreductases, mitochondrial electron transport, and NADPH oxidase. *Antioxid. Redox Signal.* *11*, 2409–2427.
- Satoo, K., Noda, N.N., Kumeta, H., Fujioka, Y., Mizushima, N., Ohsumi, Y., and Inagaki, F. (2009). The structure of Atg4B-LC3 complex reveals the mechanism of LC3 processing and delipidation during autophagy. *EMBO J.* *28*, 1341–1350.

Scott, B. a, Avidan, M.S., and Crowder, C.M. (2002). Regulation of hypoxic death in *C. elegans* by the insulin/IGF receptor homolog DAF-2. *Science* 296, 2388–2391.

Sebastián, D., Hernández-Alvarez, M.I., Segalés, J., Sorianello, E., Muñoz, J.P., Sala, D., Waget, A., Liesa, M., Paz, J.C., Gopalacharyulu, P., et al. (2012). Mitofusin 2 (Mfn2) links mitochondrial and endoplasmic reticulum function with insulin signaling and is essential for normal glucose homeostasis. *Proc. Natl. Acad. Sci. U. S. A.* 109, 5523–5528.

Stadtman, E.R., Arai, H., and Berlett, B.S. (2005). Protein oxidation by the cytochrome P450 mixed-function oxidation system. *Biochem. Biophys. Res. Commun.* 338, 432–436.

Starkov, A. a, Fiskum, G., Chinopoulos, C., Lorenzo, B.J., Browne, S.E., Patel, M.S., and Beal, M.F. (2004). Mitochondrial alpha-ketoglutarate dehydrogenase complex generates reactive oxygen species. *J. Neurosci.* 24, 7779–7788.

Suen, D.-F., Narendra, D.P., Tanaka, A., Manfredi, G., and Youle, R.J. (2010). Parkin overexpression selects against a deleterious mtDNA mutation in heteroplasmic cybrid cells. *Proc. Natl. Acad. Sci. U. S. A.* 107, 11835–11840.

Sun, H.-Y., Wang, N.-P., Kerendi, F., Halkos, M., Kin, H., Guyton, R.A., Vinten-Johansen, J., and Zhao, Z.-Q. (2005). Hypoxic postconditioning reduces cardiomyocyte loss by inhibiting ROS generation and intracellular Ca²⁺ overload. *Am. J. Physiol. Heart Circ. Physiol.* 288, H1900–8.

Tahara, E.B., Barros, M.H., Oliveira, G. a, Netto, L.E.S., and Kowaltowski, A.J. (2007). Dihydrolipoyl dehydrogenase as a source of reactive oxygen species inhibited by caloric restriction and involved in *Saccharomyces cerevisiae* aging. *FASEB J.* 21, 274–283.

Tahara, E.B., Navarete, F.D.T., and Kowaltowski, A.J. (2009). Tissue-, substrate-, and site-specific characteristics of mitochondrial reactive oxygen species generation. *Free Radic. Biol. Med.* 46, 1283–1297.

Trindade, D.F., Cerchiaro, G., and Augusto, O. (2006). A Role for Peroxymonocarbonate in the Stimulation of Biothiol Peroxidation by the Bicarbonate / Carbon Dioxide Pair. 1475–1482.

Turrens, J.F. (2003). Mitochondrial formation of reactive oxygen species. *J. Physiol.* 552, 335–344.

Twig, G., and Shirihai, O.S. (2011). The interplay between mitochondrial dynamics and mitophagy. *Antioxid. Redox Signal.* 14, 1939–1951.

Twig, G., Hyde, B., and Shirihai, O.S. (2008). Mitochondrial fusion, fission and autophagy as a quality control axis: the bioenergetic view. *Biochim. Biophys. Acta* 1777, 1092–1097.

Vincow, E.S., Merrihew, G., Thomas, R.E., Shulman, N.J., Beyer, R.P., MacCoss, M.J., and Pallanck, L.J. (2013). The PINK1-Parkin pathway promotes both mitophagy and

selective respiratory chain turnover in vivo. *Proc. Natl. Acad. Sci. U. S. A.* 110, 6400–6405.

Wang, W., Fang, H., Groom, L., Cheng, A., Zhang, W., Liu, J., Wang, X., Li, K., Han, P., Zheng, M., et al. (2008). Superoxide flashes in single mitochondria. *Cell* 134, 279–290.

Westermann, B. (2012). Bioenergetic role of mitochondrial fusion and fission. *Biochim. Biophys. Acta* 1817, 1833–1838.

Wirawan, E., Vande Walle, L., Kersse, K., Cornelis, S., Claerhout, S., Vanoverberghe, I., Roelandt, R., De Rycke, R., Verspurten, J., Declercq, W., et al. (2010). Caspase-mediated cleavage of Beclin-1 inactivates Beclin-1-induced autophagy and enhances apoptosis by promoting the release of proapoptotic factors from mitochondria. *Cell Death Dis.* 1, e18.

Wojtovich, A.P., DiStefano, P., Sherman, T., Brookes, P.S., and Nehrke, K. (2012). Mitochondrial ATP-sensitive potassium channel activity and hypoxic preconditioning are independent of an inwardly rectifying potassium channel subunit in *Caenorhabditis elegans*. *FEBS Lett.* 586, 428–434.

Yoon, S., Yun, C., and Chung, A. (2002). Dose effect of oxidative stress on signal transduction in aging. *Mech. Ageing Dev.* 123, 1597–1604.

Zhang, H. (2000). Bicarbonate Enhances the Hydroxylation, Nitration, and Peroxidation Reactions Catalyzed by Copper, Zinc Superoxide Dismutase. Intermediacy of Carbonate Anion Radical. *J. Biol. Chem.* 275, 14038–14045.

Zhou, M., Diwu, Z., Panchuk-Voloshina, N., and Haugland, R.P. (1997). A stable nonfluorescent derivative of resorufin for the fluorometric determination of trace hydrogen peroxide: applications in detecting the activity of phagocyte NADPH oxidase and other oxidases. *Anal. Biochem.* 253, 162–168.

Zweier, J.L., Flaherty, J.T., and Weisfeldt, M.L. (1987). Direct measurement of free radical generation following reperfusion of ischemic myocardium. *Proc. Natl. Acad. Sci. USA* 84, 1404–1407.

Apêndice

Ap.1. Pharmacological and physiological stimuli do not promote Ca^{2+} -sensitive K^+ channel activity in isolated heart mitochondria



Cardiovascular Research 73 (2007) 720–728

Cardiovascular
Research

www.elsevier.com/locate/cardiores

Pharmacological and physiological stimuli do not promote Ca^{2+} -sensitive K^+ channel activity in isolated heart mitochondria

Douglas V. Cancherini, Bruno B. Queliconi, Alicia J. Kowaltowski*

Departamento de Bioquímica, Instituto de Química, Universidade de São Paulo, São Paulo, SP, Brazil

Received 13 July 2006; received in revised form 23 November 2006; accepted 27 November 2006

Available online 30 November 2006

Time for primary review 25 days

Abstract

Objective: Mitochondrial calcium-activated K^+ (mito K_{Ca}) channels have been described as channels that are activated by Ca^{2+} , inner mitochondrial membrane depolarization and drugs such as NS-1619. NS-1619 is cardioprotective, leading to the assumption that this effect is related to the opening of mito K_{Ca} channels. Here, we show several weaknesses in this hypothesis.

Methods: Isolated mitochondria from rat hearts were tested for evidence of mito K_{Ca} activity by analyzing functional parameters in K^+ -rich and K^+ -free media.

Results: NS-1619 promoted mitochondrial depolarization both in K^+ -rich and K^+ -free media. Respiratory rate increments were also seen in the presence of NS-1619 for both media. In parallel, NS-1619 promoted respiratory inhibition, as evidenced by respiratory measurements in state 3. Mitochondrial volume measurements conducted using light scattering showed that NS-1619 led to swelling, in a manner unaltered by inhibitors of mito K_{Ca} channels, antagonists of adenosine triphosphate-sensitive potassium channels or inhibitors of the permeability transition. Swelling was also maintained when K^+ in the media was substituted with tetraethylammonium (TEA^+), which is not transported by any known K^+ carrier. Electron microscopy experiments gave support to the idea that NS-1619-induced mitochondrial swelling took place in the absence of K^+ . In addition to testing the pharmacological effects of NS-1619, we attempted, unsuccessfully, to promote mito K_{Ca} activity by altering Ca^{2+} concentrations in the medium and inducing mitochondrial uncoupling.

Conclusion: Our data indicate that NS-1619 promotes non-selective permeabilization of the inner mitochondrial membrane to ions, in addition to partial respiratory inhibition. Furthermore, we found no specific K^+ transport in isolated heart mitochondria compatible with mito K_{Ca} opening, whether by pharmacological or physiological stimuli. Our results indicate that NS-1619 has extensive mitochondrial effects unrelated to mito K_{Ca} and suggest that tissue protection mediated by NS-1619 may occur through mechanisms other than activation of these channels.

© 2006 European Society of Cardiology. Published by Elsevier B.V. All rights reserved.

Keywords: Oxygen consumption; K^+ channel; Ischemia; Mitochondria; Preconditioning

1. Introduction

Myocardial cells present increased resistance to ischemic insults when previously exposed to brief, non-lethal ischemia, a phenomenon known as ischemic preconditioning [1]. This suggests that myocytes possess an evolutionarily selected, endogenous machinery of protection against ischemia. Ischemic preconditioning involves several redundant signaling cascades and end effectors (reviewed in [2,3]), a finding that attests to the importance of these mechanisms. A thorough understanding of the cardioprotective events

Abbreviations: NS-1619, 1,3-dihydro-1-[2-hydroxy-5-(trifluoromethyl)phenyl]-5-(trifluoromethyl)-2H-benzimidazol-2-one; 5-HD, 5-hydroxydecanoate; CCCP, carbonyl cyanide *m*-chloro phenyl hydrazone; DNP, dinitrophenol; CsA, cyclosporin A; EGTA, ethylene glycol bis(2-aminoethyl ether)-*N,N,N',N'*-tetraacetic acid; mito K_{Ca} , mitochondrial ATP-sensitive K^+ channels; mito K_{ATP} , mitochondrial calcium-activated K^+ channels; Pax; paxilline; TEA^+ , tetraethylammonium ion; S.E.M., standard error of the mean; TMPD, *N,N,N,N*-tetramethyl-*p*-phenylene-diamine

* Corresponding author. Av. Prof. Lineu Prestes, 748, Cidade Universitária, São Paulo, SP, 05508-900, Brazil. Fax: +55 11 38155579.

E-mail address: alicia@iq.usp.br (A.J. Kowaltowski).

0008-6363/\$ - see front matter © 2006 European Society of Cardiology. Published by Elsevier B.V. All rights reserved.
doi:10.1016/j.cardiores.2006.11.035

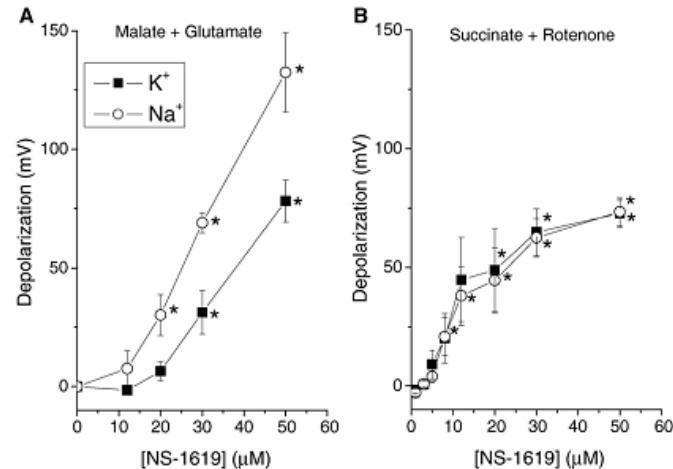


Fig. 1. NS-1619 depolarizes mitochondria suspended in both K^+ - and Na^+ -rich media. Rat heart mitochondria (0.25 mg protein/mL) were incubated in working buffer containing Na^+ (O) or K^+ (■) as the main cation, in the presence of 5 μ M safranin O and 1 μ g/mL oligomycin. In Panel A, 5 mM glutamate and 5 mM malate were used as substrates. In Panel B, 2 mM succinate and 1 μ M rotenone were present. Membrane potentials were measured before and after the addition of NS-1619, and the average depolarization (in mV) \pm S.E.M. of 4–7 repetitions was plotted. *, $p < 0.05$ in comparison to control.

2.4. Experimental conditions

Mitochondrial volume, oxygen consumption and membrane potential measurements were performed in a working buffer containing 2 mM $MgCl_2$ and K^+ salts of Cl^- (150 mM), phosphate (2 mM) and K^+ -HEPES (5 mM), pH 7.2. Where indicated, experiments were also performed in buffers of similar composition, in which all K^+ salts were replaced by Na^+ or tetraethylammonium (TEA^+) salts. Further additions are mentioned in the figure legends. All experiments were conducted at 37 °C, with continuous stirring.

2.5. Mitochondrial swelling

Changes in 90° light scattering, reflecting changes in mitochondrial volume [21], were followed using a temperature-controlled Hitachi F4500 spectrofluorometer operating with continuous stirring at excitation and emission wavelengths of 520 nm, with 2.5 nm slits. Light scattering decrease was calculated for each sample by taking the difference of scattered light between an early and a late time interval (3.5 to 6.5 s, and 220 to 230 s, respectively, after mitochondrial injection), and normalizing it to the scattered light at the early time interval. Light scattering decreases were calculated in the presence and absence of the pharmacological agents tested, both in K^+ or TEA^+ media, and the ratio was used as final data.

2.6. $NAD(P)^+/NAD(P)H$ redox state

Fluorescence levels at 352 nm excitation and 464 nm emission, in which $NAD(P)H$, but not $NAD(P)^+$, fluo-

resces, were measured over time using a Hitachi F4500 spectrofluorometer.

2.7. Mitochondrial membrane potential estimation

Mitochondrial membrane potentials were estimated by following safranin O (5 μ M) fluorescence [22] at 495 nm excitation and 586 nm emission on a Hitachi F4500 spectrofluorometer. A calibration curve was constructed using the K^+ ionophore valinomycin (0.1 ng/mL) and known K^+ additions, assuming matrix K^+ concentrations were 150 mM [23].

2.8. Measurement of mitochondrial respiration

Oxygen consumption was measured using a computer-interfaced Clark-type oxygen electrode from Hansatech Instruments, equipped with magnetic stirring.

2.9. Transmission electron microscopy

Mitochondria (0.6 mg protein/mL) were incubated for 240 or 150 s in working buffer containing either K^+ or TEA^+ as the main cation, respectively, in the presence of 1 μ g/mL oligomycin, 5 mM malate and 5 mM glutamate. A shorter incubation time was used for TEA^+ because it is not extruded from the mitochondrial matrix, producing larger matrix volume increases, and eventually outer membrane rupture [24]. Suspended mitochondria were centrifuged at 16,500 \times g for 2 min and fixed first in 100 mM cacodylate buffer with 2% glutaraldehyde and then in 2% osmium tetroxide. The samples were dehydrated through a series of 70–100%

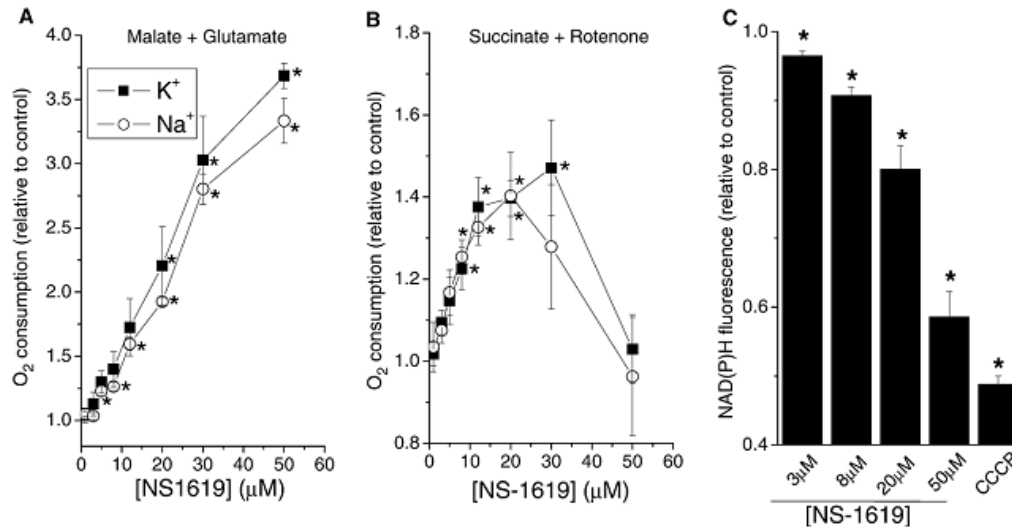


Fig. 2. NS-1619 increases non-phosphorylating respiratory rates. Mitochondria (0.3 mg protein/mL) were incubated in working buffer containing Na⁺ (O) or K⁺ (■) as the main cation, in the presence of 1 μg/mL oligomycin and (Panel A) 5 mM glutamate plus 5 mM malate, (Panel B) 2 mM succinate plus 1 μM rotenone or (Panel C) 2 mM succinate, 5 mM glutamate, 5 mM malate and 2 mM pyruvate. Changes in oxygen consumption (Panels A and B) or NAD(P)H fluorescence (Panel C) upon the addition of NS-1619 (as indicated) or 1 μM CCCP (Panel C) were recorded and plotted relative to control in the absence of NS-1619 and CCCP, as averages ± S.E.M. of 3–6 repetitions. *, $p < 0.05$ in comparison to control.

ethanol solutions and incubated in propylene oxide prior to infiltration with Spurr resin [25]. The samples then were embedded in 100% Spurr resin and polymerized at 72 °C. Ultrathin 70 to 80 nm sections were cut and stained with

uranyl acetate and lead nitrate. Sections were examined with a Jeol Jem-1010 transmission electron microscope at 80 kV.

2.10. Data analysis

Experiments depict averages and standard errors of the mean (Figs. 1, 2, 3 and 4B) or representative results (Figs. 4A, 5 and 6) from at least three similar repetitions. NS-1619-induced depolarizations were evaluated by one-sample *t*-test comparisons against 0 mV. NS-1619-induced changes in control-normalized respiratory rates, light scattering decreases or NAD(P)H fluorescence were compared to 1, again by one sample *t*-tests. Since we were not interested in all pairwise comparisons, only in comparing treated groups to controls (in what is usually named planned comparisons) we used *t*-tests rather than ANOVA.

3. Results

Increases in inner mitochondrial membrane permeability to K⁺ ions decrease the inner membrane potential and the H⁺ electrochemical potential, since K⁺ is positively charged and exchanged for H⁺ by mitochondrial K⁺/H⁺ exchangers [11,26]. The extent of inner membrane depolarization is proportional to K⁺ transport rates. In the case of mitoK_{Ca} channels, inner membrane potential changes should be pronounced, since the conductance and abundance of these channels is significant [12,13]. We measured the effects of NS-1619 on mitochondrial inner membrane potentials, in

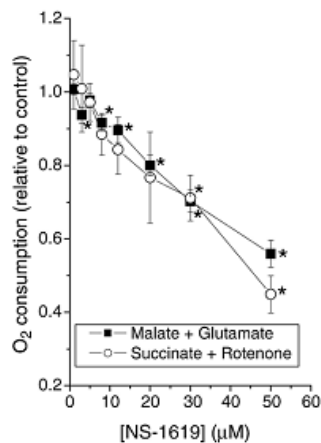


Fig. 3. NS-1619 promotes maximal respiratory rate inhibition. Mitochondria (0.3 mg protein/mL) were incubated in working buffer in the presence of 2 mM ADP and (O) 2 mM succinate plus 1 μM rotenone or (■) 5 mM glutamate and 5 mM malate. Respiratory rates were recorded before and after the addition of NS-1619, and the inhibitory effect was calculated relative to the basal oxygen consumption rate and presented as averages ± S.E.M. of 3–13 repetitions. *, $p < 0.05$ in comparison to control.

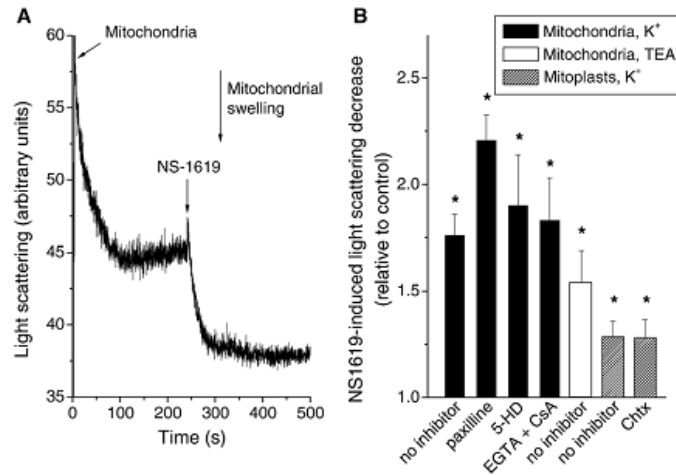


Fig. 4. NS-1619 promotes mitochondrial swelling. Mitochondria or mitoplasts (0.2 mg protein/mL) were incubated in working buffer containing K^+ or TEA^+ , as indicated, as the main cation and 1 μ M oligomycin, 5 mM glutamate and 5 mM malate. In Panel A, 20 μ M NS-1619 was added to K^+ -rich buffer after initial mitochondrial volume stabilization. In Panel B, light scattering decreases in K^+ (full bars) or TEA^+ (empty bar) media promoted by 20 μ M NS-1619 were measured, in the presence of no further addition (no inhibitor), 1 mM EGTA plus 1 μ M cyclosporin A (EGTA + CsA), 5 μ M paxilline or 300 μ M 5-hydroxydecanoate (5-HD), as indicated. The striped columns represent experiments in which swelling induced by NS-1619 was followed in mitoplasts (see Materials and methods) in the presence or absence of 100 nM charybdotoxin (Chtx). Data represent averages \pm S.E.M. of 3–20 repetitions. *, $p < 0.05$ in comparison with the respective (K^+ or TEA^+ /mitochondria or mitoplast) control.

order to assess possible depolarizations promoted by $mitoK_{Ca}$ (Fig. 1). Mitochondria were incubated in the presence of the ATP synthase inhibitor oligomycin, so changes in oxidative phosphorylation could not affect the measurements. Either malate plus glutamate (Panel A) or succinate (plus rotenone, Panel B) were used as respiratory substrates. We found that NS-1619 induced a concentration-dependent inner mitochondrial membrane depolarization, which was statistically significant at concentrations above 20 μ M (malate plus glutamate) or 8 μ M (succinate). This finding is in line with a previous description of mitochondrial depolarization induced by NS-1619 in glioma cells [18,19] and heart [20], and with the high conductance of $mitoK_{Ca}$ [12,13]. However, the depolarization did not change if the main medium cation was K^+ (■) or Na^+ (○), suggesting it does not reflect $mitoK_{Ca}$ channel activity, since these channels are specific for K^+ [12].

Possible causes for the depolarization observed with NS-1619 could be respiratory inhibition and/or mitochondrial uncoupling, so we investigated the effects of this drug on mitochondrial respiratory rates, also in the presence of added oligomycin (Fig. 2A and B, note difference in scale). In the presence of malate plus glutamate as substrates (Panel A), NS-1619 induced a strong increase in respiratory rates which was statistically significant at concentrations as small as 5 μ M and, at 50 μ M, reached levels more than three times higher than controls. Again, the effect observed was not altered by the cation (Na^+ , ○, or K^+ , ■) used as osmotic support. Furthermore, increments in respiratory rates pro-

moted by 20 μ M NS-1619 (2.15 ± 0.19 , $n=6$) were unaltered by the presence of $mitoK_{Ca}$ antagonist paxilline (5 μ M, 2.14 ± 0.23 , $n=3$), indicating they are not attributable to the activity of this channel.

Increments in respiratory rates were also observed when succinate (plus rotenone) was used as a substrate (Panel B), at NS-1619 concentrations ranging from 3 to 30 μ M. Interestingly, higher NS-1619 concentrations reversed the increments in respiratory rates observed at lower concentrations, suggesting the drug may not only lead to uncoupling, but may also promote respiratory inhibition (see below).

The uncoupling effect of NS-1619 was also confirmed by measuring mitochondrial NAD(P) redox state (Fig. 2C). We found that the addition of this drug to mitochondria energized by both succinate and NADH-linked substrates in the presence of oligomycin lead to significant oxidation of NAD(P)H, resulting in decreased fluorescence, which was significant at NS-1619 concentrations as low as 3 μ M. The effect was dose-dependent and, at high NS-1619 concentrations, almost equivalent to that of the classical mitochondrial uncoupler CCCP.

As mentioned above, the results in Fig. 2B suggest NS-1619 may not lead only to mitochondrial uncoupling, but may also promote respiratory inhibition. Indeed, many lipophilic drugs such as NS-1619 are inhibitors of mitochondrial electron transport when used in high concentrations [9]. However, the data from Fig. 2B are not ideal to uncover a respiratory inhibition effect since maximal respiratory rates were not present, and experimental errors

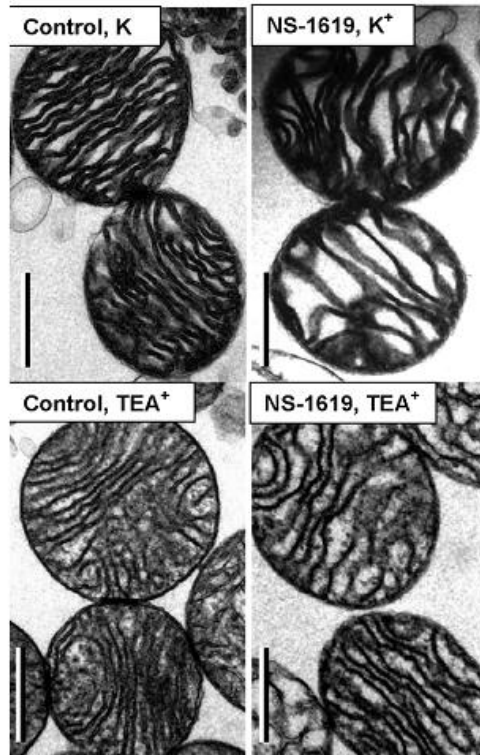


Fig. 5. NS-1619-induced changes in mitochondrial morphology. The figure depicts electron micrographs of mitochondria (magnification=30,000; scale bar length=500 nm) incubated in K^+ or TEA^+ media. In the rightmost Panels, 50 μM NS-1619 was present. Samples are typical areas of at least 5 images collected under the same experimental conditions.

were large. To investigate the respiratory effect further, we measured oxygen consumption in mitochondria in which maximum respiratory rates were induced by adding ADP (Fig. 3). Under these conditions, respiratory inhibition was promoted by NS-1619 at concentrations as low as 8 μM , with either malate plus glutamate (■) or succinate (○) as substrates. The similar extent of respiratory inhibition in the presence of substrates that reduce either complex I or II suggests that a downstream point in the electron transport chain, such as complex III or IV, is affected by this drug.

In order to investigate the site of respiratory inhibition further, we tested the effect of NS-1619 on respiration supported by 200 μM TMPD plus 2 mM ascorbate, which donate electrons directly to complex IV, bypassing complex III. Under these conditions, 50 μM NS-1619 reduced the maximum respiratory activity by $12.1 \pm 1.3\%$ ($n=4$). Since 45% to 55% respiratory inhibition was observed with complex I or II-reducing substrates, this results suggests that, while complex IV contributes to the respiratory inhibition observed, at least part of the respiratory inhibition

promoted by NS-1619 originates from effects of this drug on complex III. Altogether, our data show that, in addition to promoting uncoupling, NS-1619 inhibits mitochondrial respiration.

NS-1619 promoted mitochondrial uncoupling independently of the cation used in the media, suggesting it may promote non-selective inner membrane permeabilization instead of activating a cation transporter. To investigate this possibility, we measured light scattering of isolated mitochondria (Fig. 4), which is decreased as the organelles swell due to the uptake of ions and water [16]. Fig. 4A shows a typical light scattering trace over time. Mitochondria added to K^+ -rich media swell rapidly, taking up K^+ ions lost during the isolation process [6], until they reach a steady state. We found that the addition of NS-1619 lead to further mitochondrial swelling, confirming that this drug increases inner membrane permeability to K^+ , and not only to H^+ , as indicated by the data in Figs. 1 and 2. Interestingly, the effect of NS-1619 (Fig. 4B) was also observed in buffer in which K^+ ions were substituted by TEA^+ (empty column), a cation which is not transported by any known mitochondrial carrier, and blocks several types of K^+ channels [27]. This indicates that the effect of NS-1619 is not ion selective, and cannot be ascribed to the activation of a K^+ channel. Indeed, the effect of NS-1619 was not prevented by $mitoK_{Ca}$ antagonist paxilline (5 μM). The $mitoK_{Ca}$ antagonist charybdotoxin was also ineffective in preventing NS-1619-induced swelling, even when used in mitoplast preparations (mitochondria devoid of outer membranes, striped columns), a condition in which this toxin is fully accessible to the inner mitochondrial membrane. Finally, $mitoK_{ATP}$ inhibitors ATP (1 mM, data not shown) and 5-hydroxydecanoate (300 μM , Fig. 4B) or 1 mM EGTA plus 1 μM cyclosporin A, inhibitors of the mitochondrial permeability transition (a form of non-selective inner mitochondrial membrane permeabilization [28,29]) did not prevent swelling induced by NS-1619. These results indicate that the effect of this drug is to promote non-selective inner membrane permeabilization to ions in a manner independent of K^+ channels or the permeability transition.

In order to confirm our volume measurements using a more direct technique, we performed transmission electron microscopy on mitochondria incubated in the presence or absence of NS-1619 (Fig. 5). Normal mitochondrial conformations (Leftmost Panels) were altered by the addition of NS-1619 (Rightmost Panels), which caused largely enhanced matrix volumes and intercrystal spaces, with decreased electron-density compared to controls. This effect occurred independently of the ion used as osmotic support, confirming that NS-1619 has significant effects on mitochondrial structure which are unrelated to selective K^+ transport.

Our results up to this point do not uncover any evidence of the activity of a $mitoK_{Ca}$ channel, due mainly to undesirable effects of NS-1619. We thus decided to investigate possible mitochondrial effects of this channel

involved in ischemic preconditioning will certainly contribute toward the development of newer therapeutic interventions designed to prevent tissue damage in ischemic diseases.

Mitochondrial adenosine triphosphate (ATP)-sensitive K^+ channels (mitoK_{ATP}) are an established part of the endogenous protective machinery mediating ischemic preconditioning. Indeed, ischemic preconditioning is prevented by mitoK_{ATP} channel antagonists [4–6] and mimicked by a variety of agonists [5,7,8]. When opened, these channels promote significant mitochondrial matrix expansion and mild inner membrane potential reduction [9]. These effects of K^+ entry through mitoK_{ATP} channels are thought to protect tissues by modulating the production of reactive oxygen species and avoiding the loss of cellular high energy phosphates (such as ATP and phosphocreatine) and the accumulation of matrix Ca^{2+} , resulting in the prevention of mitochondrial permeability transition (reviewed in [10,11]). All these protective mechanisms result from K^+ transport across the inner mitochondrial membrane, the primary consequence of mitoK_{ATP} opening. Indeed, despite the fact that some pharmacological regulators of mitoK_{ATP} present toxic effects, they have been shown to act on a selective K^+ transport pathway in isolated heart mitochondria [9].

Recently, a second type of K^+ channel, the mitochondrial calcium-sensitive K^+ channel (mitoK_{Ca}), has been identified as another possible mediator of ischemic cardioprotection. Patch clamp experiments show that the opening probability of this channel increases in response to Ca^{2+} and depolarization [12,13]. These stimuli are observed under physiological conditions such as high cardiac work, and pathophysiological conditions such as ischemia. Thus, it is possible that mitoK_{Ca} could be activated during ischemic preconditioning. Indeed, there is initial evidence that mitoK_{Ca} channels may be involved in protection mediated by preconditioning, based on effects of putative mitoK_{Ca} blockers [14]. Further evidence for the cardioprotective role of mitoK_{Ca} is based on the finding that 1,3-dihydro-1-[2-hydroxy-5-(trifluoromethyl)phenyl]-5-(trifluoromethyl)-2H-benzimidazol-2-one (NS-1619), an activator of plasma membrane big conductance calcium-sensitive K^+ channels, leads to protection against ischemia in perfused hearts and cardiac cells [13–16]. However, the specificity of NS-1619 toward mitoK_{Ca} opening was not extensively verified. Indeed, although single-channel recordings of mitoK_{Ca} in glioma [12] and rat heart [13,17] mitoplasts have been conducted, there is no evidence NS-1619 activates currents under these conditions. Instead, the effect of NS-1619 was tested on mitochondrial K^+ uptake using a K^+ -sensitive probe [13], an experimental setting which may be influenced by factors distinct from a regulated and selective K^+ entry pathway. Furthermore, there is some evidence in the literature that NS-1619 may have mitochondrial effects unrelated to K^+ transport, such as respiratory inhibition [18–20].

This work evaluated NS-1619 effects in isolated mitochondria, an experimental setting that allows for more detailed examination of bioenergetic effects and specificity of this drug. Surprisingly, we found that NS-

1619 does not promote K^+ transport attributable to a channel or a specific proteinaceous cation transporter. Instead, this drug promotes non-selective ion transport across the inner mitochondrial membrane, in addition to respiratory inhibition. Furthermore, we demonstrate that measurable effects of mitoK_{Ca} opening cannot be obtained in isolated mitochondria by elevation of extramitochondrial Ca^{2+} or depolarization, the suggested physiological activators of this channel.

2. Materials and methods

2.1. Materials

All reagents used were analytical grade or better, and deionized water was used for all aqueous solutions. Respiratory substrates (pyruvate, malate, glutamate and succinate), ATP and EGTA stock solutions were prepared in water and buffered with the main cation used in the experimental media. NS-1619, paxilline and cyclosporin A stock solutions were prepared in DMSO; charybdotoxin and 5-hydroxydecanoate solutions (in deionized water) were prepared fresh the day of the experiment.

2.2. Mitochondrial isolation

All animal studies were approved by the *Comissão de Ética em Cuidado e Uso Animal* and conform with the *Colégio Brasileiro de Experimentação Animal* and the Guide for the Care and Use of Laboratory Animals published by the USA National Institutes of Health. Hearts were rapidly removed from adult (2 month) Sprague–Dawley rats weighing between 250 and 350 g, finely minced and homogenized in ice-cold buffer containing 300 mM sucrose, 0.1% BSA, and Na^+ salts of HEPES (10 mM) and EGTA (2 mM), pH 7.2. The suspension was then centrifuged at $800\times g$ for 7 min, and the resulting supernatant was centrifuged at $9500\times g$ for 10 min. The final pellet was resuspended in 300–500 μ l of the same buffer. Mitochondrial protein concentrations were determined using the Biuret reaction. Respiratory control indexes were on average 24 ± 7 , using 5 mM malate plus 5 mM glutamate as substrates. Under these conditions, average state 3 and 4 oxygen consumption rates were 181 ± 18 and 9.0 ± 2.5 $nmol\ min^{-1}\ mg^{-1}$.

2.3. Mitoplast preparation

Mitochondria (1 mg/mL) were incubated under gentle stirring for 10 min in ice-cold medium containing 11 mM KCl and 0.7 mM HEPES, pH 7.2, then centrifuged at $12,000\times g$ for 10 min. The pellet was resuspended in 20 mL of isolation buffer, centrifuged again at $12,000\times g$ for 10 min, and resuspended in a small volume of isolation buffer. Rupture of the outer mitochondrial membrane was confirmed by verifying the stimulatory effect of 0.5 μ M cytochrome *c* on respiratory rates.

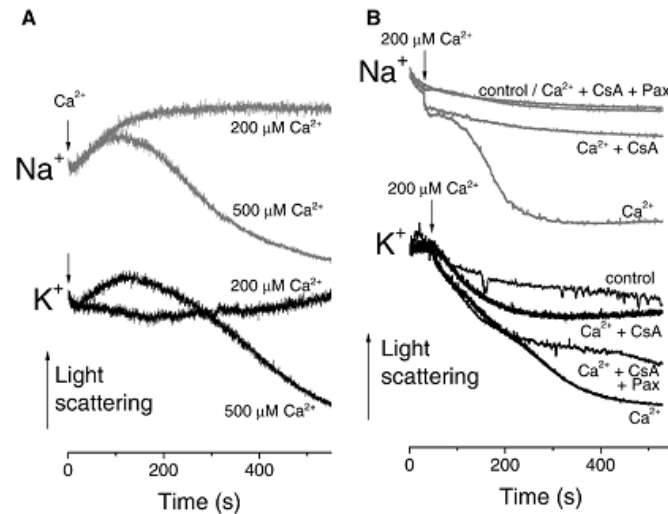


Fig. 6. Calcium and uncoupling do not promote selective K^+ transport in mitochondria. Mitochondria (0.25 mg protein/mL) were incubated in K^+ (black lines) or Na^+ (grey lines) working buffer in the presence of 1 $\mu g/mL$ oligomycin, 5 mM glutamate, 5 mM malate. Light scattering was followed over time, in the presence of the Ca^{2+} concentrations indicated (Panel A). In Panel B, 1 μM dinitrophenol and 200 μM EGTA were present in all traces, and the following additions were made: none (control), 200 μM Ca^{2+} (Ca^{2+}), 2 μM cyclosporin A (CsA) and/or 5 μM paxilline (Pax). Ca^{2+} concentrations are expressed as estimated free Ca^{2+} calculated using MaxChelator software. DNP produced an average depolarization of $41.9 mV \pm 3.3 mV$ in K^+ media and $36.0 \pm 2.2 mV$ in Na^+ media. Traces were offset for easier visibility and represent typical experiments reproduced using at least three different preparations.

by stimulating its activity with putative physiological channel activators. Two different activating strategies were used: treating mitochondria with Ca^{2+} ions and uncoupling mitochondria with low doses of the mild protonophore dinitrophenol to decrease the inner membrane potential. Under these conditions, effects in K^+ and Na^+ media were compared, in search of K^+ -specific transport. Fig. 6 shows representative data of a very large number of experiments conducted seeking a condition in which Ca^{2+} (with or without mitochondrial uncoupling, Panels B and A, respectively) lead to mitochondrial permeabilization exclusively in K^+ -rich media (black lines). We found no evidence for such a condition, measuring mitochondrial swelling and varying Ca^{2+} concentrations. In all cases, when membrane permeabilization was observed (as indicated by a decrease in light scattering), it occurred also in Na^+ -based media (grey lines), indicating it is attributable to non-selective permeabilization, as is typical of mitochondrial permeability transition. Indeed, the swelling observed was inhibited by mitochondrial permeability transition inhibitor cyclosporin A (CsA), but not mito K_{Ca} antagonist paxilline (Pax), which causes slight swelling itself. These results are expected, since permeability transition is stimulated by Ca^{2+} and inner membrane depolarization [28,29].

A further attempt to verify the effects of mito K_{Ca} in isolated mitochondria was to induce channel opening using β -estradiol [17], which has been reported to activate these channels at high concentrations (up to 10 μM ; physiological concentrations usually do not exceed 2 nM [30]). In isolated

mitochondria treated with 10 μM β -estradiol, light scattering measurements again indicated that increased cation permeability was not specific for K^+ (data not shown). Similar experiments were conducted using BK $_{Ca}$ agonists Evans blue (25–50 μM), flufenamic acid (50–100 μM), GABA (2–200 μM), resveratrol (60 μM), or phloretin (50 μM) [31,32] as possible mito K_{Ca} activators. In all cases, no specific K^+ transport was observed (data not shown).

4. Discussion

The data presented in this manuscript were obtained with the initial intent of identifying and quantifying effects of mito K_{Ca} activity in isolated rat heart mitochondria. Using isolated mitochondria as an experimental model may present certain limitations in relation to intact cell or tissue samples, such as loss of possible regulating factors or damage induced by the isolation process. On the other hand, the use of isolated mitochondria allows for more stringent controls (such as changing the main ions in which the organelles are incubated) and a closer evaluation of bioenergetic functions (by using different substrates and respiratory states, for example). Indeed, using this experimental setup, we were able to uncover a myriad of undesirable actions of NS-1619, the main agonist used in the literature to study the cellular and whole heart effects of mito K_{Ca} [13,15,16,33].

Interestingly, although NS-1619 has been widely used to uncover possible effects of mito K_{Ca} , there is little evidence that it is an activator of mito K_{Ca} , apart from the fact that this

drug activates other Ca^{2+} -activated K^+ channels (reviewed in [31,32]). Notably, in the most prominent publication related to this channel [13], the effects of NS-1619 were not tested in patch clamp experiments used to identify the activity of mitoK_{Ca} . Instead, NS-1619 was used in experiments measuring K^+ uptake into mitochondria using a fluorescent probe. The results obtained indicated that NS-1619 increased mitochondrial permeability to K^+ , but do not determine if this permeability is specific for K^+ . These findings are completely compatible with our data showing that NS-1619 increases mitochondrial permeability to K^+ , Na^+ and TEA^+ (Figs. 1, 2, 4 and 5). Although NS-1619 is not capable of generating such a permeabilization in artificial phospholipid bilayers [18], mitochondrial inner membranes are extremely rich in proteins and present unique lipid compositions (such as the presence of cardiolipin [34]), which may allow for non-specific effects of this drug in mitochondrial membranes, increasing ion permeability.

In addition to uncovering NS-1619-induced non-specific inner membrane permeabilization, we found that it also promotes significant inhibition of mitochondrial respiration supported by NADH-linked substrates or succinate (Fig. 3). These results are in line with the previous finding that NS-1619 causes respiratory inhibition in glioma cells [18] and heart [19,20] and decreases respiratory control ratios in a manner insensitive to paxilline [19].

Due to the extensive mitochondrial toxicity of NS-1619, we attempted to study the bioenergetic effects of mitoK_{Ca} by activating the channel physiologically. The strategies we adopted included adding Ca^{2+} , promoting inner membrane depolarization (Fig. 6), or testing the effects of a variety of signaling molecules previously described to activate these channels (as described in Results). Again, we found no evidence of selective K^+ transport in isolated mitochondrial preparations. Our inability to promote mitoK_{Ca} channel opening, however, can be conciliated with patch-clamp studies of mitoplasts (mitochondria devoid of outer membranes) that show changes in the probability of the individual mitoK_{Ca} channel opening promoted by depolarization and Ca^{2+} [12,13]. These studies were performed in patches at -60 to $+40$ mV potentials, while inner mitochondrial membranes commonly display electric potentials between -200 and -150 mV. Since polarization was found to decrease open probability, it is possible that physiological membrane potentials impair this channel's activity.

Thus, we were unable to observe pharmacological activation of mitoK_{Ca} due to non-specific effects of NS-1619, and could not obtain physiological conditions in isolated mitochondria in which the activity of this channel could be observed. Indeed, considering the very large measured conductance and abundance of mitoK_{Ca} [12,13], the effects of K^+ transport through this channel would be expected to lead to impaired oxidative phosphorylation, mitochondrial swelling, outer membrane rupture, release of intermembrane space proteins and, possibly, cell death. These undesirable effects are quite different from those

promoted by K^+ transport through $\text{mitoK}_{\text{ATP}}$ which is very limited due to low conductance and abundance and does not impair oxidative phosphorylation nor lead to outer mitochondrial membrane rupture [9].

Both inner membrane permeabilization and respiratory inhibition observed in the presence of NS-1619 were obtained in a concentration range ($3\text{--}50$ μM) similar to the concentrations in which this drug has been shown to protect the heart against ischemic damage ($3\text{--}30$ μM [13,15,16]). This observation, added to the fact that heart preparations do not appear to have plasma membrane calcium-activated potassium channels [35], leads us to the hypothesis that the cardioprotective effects of this drug may be related to its non-specific effects and not to pharmacological activation of a target channel. Indeed, many drugs and conditions that promote mitochondrial uncoupling [36–40] or respiratory inhibition [41,42] have previously been shown to be cardioprotective. It is possible that, in a manner similar to ischemic preconditioning, moderate exposures to potentially damaging conditions can lead to signaling events that promote a more adapted cellular state to resist the damaging effects of ischemia. Furthermore, mitochondrial uncouplers may be protective against ischemia because they often reduce reactive oxygen species production [38–40,43].

In conclusion, our results show that NS-1619 has many effects unrelated to the activity of a mitoK_{Ca} channel. This data uncovers the importance of careful controls when studying ion permeability of the inner mitochondrial membrane. Furthermore, our results suggest that alternative mechanisms for NS-1619-induced cardioprotection should be considered when studying the actions of this drug.

Acknowledgements

The authors thank Camille C. da Silva and Edson A. Gomes for excellent technical assistance and *Fundação de Amparo à Pesquisa do Estado de São Paulo* (FAPESP), *Conselho Nacional de Desenvolvimento Científico e Tecnológico* (CNPq), *Instituto do Milênio Redoxoma* and the John Simon Guggenheim Memorial Foundation for financial support. D.V.C. is a post-doctoral researcher supported by FAPESP and B.B.Q. is an undergraduate student supported by CNPq.

References

- [1] Murry CE, Jennings RB, Reimer KA. Preconditioning with ischemia: a delay of lethal cell injury in ischemic myocardium. *Circulation* 1986;74:1124–36.
- [2] Gross GJ, Peart JN. K_{ATP} channels and myocardial preconditioning: an update. *Am J Physiol* 2003;285:H921–30.
- [3] Yellon DM, Downey JM. Preconditioning the myocardium: from cellular physiology to clinical cardiology. *Physiol Rev* 2003;83:1113–51.
- [4] Auchampach JA, Grover GJ, Gross GJ. Blockade of ischaemic preconditioning in dogs by the novel ATP dependent potassium channel antagonist sodium 5-hydroxydecanoate. *Cardiovasc Res* 1992;26:1054–62.

- [5] Armstrong SC, Liu GS, Downey JM, Ganote CE. Potassium channels and preconditioning of isolated rabbit cardiomyocytes: effects of glyburide and pinacidil. *J Mol Cell Cardiol* 1995;27:1765–74.
- [6] Jaburek M, Yarov-Yarovoy V, Paucek P, Garlid KD. State-dependent inhibition of the mitochondrial K_{ATP} channel by glyburide and 5-hydroxydecanoate. *J Biol Chem* 1998;273(27):13578–82.
- [7] Garlid KD, Paucek P, Yarov-Yarovoy V, Murray HN, Darbenzio RB, D'Alonzo AJ, et al. Cardioprotective effect of diazoxide and its interaction with mitochondrial ATP-sensitive K^+ channels. Possible mechanism of cardioprotection. *Circ Res* 1997;81:1072–82.
- [8] Vanden Hoek T, Becker LB, Shao ZH, Li CQ, Schumacker PT. Preconditioning in cardiomyocytes protects by attenuating oxidant stress at reperfusion. *Circ Res* 2000;17(86):541–8.
- [9] Kowaltowski AJ, Seetharaman S, Paucek P, Garlid KD. Bioenergetic consequences of opening the ATP-sensitive K^+ channel of heart mitochondria. *Am J Physiol* 2001;280:H649–57.
- [10] Garlid KD, Dos Santos P, Xie ZJ, Costa AD, Paucek P. Mitochondrial potassium transport: the role of the mitochondrial ATP-sensitive K^+ channel in cardiac function and cardioprotection. *Biochim Biophys Acta* 2003;30(1606):1–21.
- [11] Facundo HT, Fomazari M, Kowaltowski AJ. Tissue protection mediated by mitochondrial K^+ channels. *Biochim Biophys Acta* 2006;1762:202–12.
- [12] Siemen D, Loupatatzis C, Borecky J, Gulbins E, Lang F. Ca^{2+} -activated K channel of the BK-type in the inner mitochondrial membrane of a human glioma cell line. *Biochem Biophys Res Commun* 1999;257:549–54.
- [13] Xu W, Liu Y, Wang S, McDonald T, Van Eyk JE, Sidor A, et al. Cytoprotective role of Ca^{2+} -activated K^+ channels in the cardiac inner mitochondrial membrane. *Science* 2002;298:1029–33.
- [14] Cao CM, Xia Q, Gao Q, Chen M, Wong TM. Calcium-activated potassium channel triggers cardioprotection of ischemic preconditioning. *J Pharmacol Exp Ther* 2005;312:644–50.
- [15] Stowe DF, Aldakkak M, Camara AK, Riess ML, Heinen A, Varadarajan SG, et al. Cardiac mitochondrial preconditioning by big Ca^{2+} -sensitive K^+ channel opening requires superoxide radical generation. *Am J Physiol* 2006;290:H434–40.
- [16] Wang X, Yin C, Xi L, Kukreja RC. Opening of Ca^{2+} -activated K^+ channels triggers early and delayed preconditioning against I/R injury independent of NOS in mice. *Am J Physiol* 2004;287:H2070–7.
- [17] Ohya S, Kuwata Y, Sakamoto K, Muraki K, Imaizumi Y. Cardioprotective effects of estradiol include the activation of large-conductance Ca^{2+} -activated K^+ channels in cardiac mitochondria. *Am J Physiol* 2005;289:H1635–42.
- [18] Debska G, Kicinska A, Dobrucki J, Dworakowska B, Nurowska E, Skalska J, et al. Large-conductance K^+ channel openers NS1619 and NS004 as inhibitors of mitochondrial function in glioma cells. *Biochem Pharmacol* 2003;65:1827–34.
- [19] Heinen A, Camara A, Aldakkak M, Rhodes S.S., Riess M.L., Stowe DF. Mitochondrial Ca^{2+} -induced K^+ influx increases respiration and enhances ROS production while maintaining membrane potential. *Am J Physiol* in press. [Electronic publication ahead of print, Jul 26].
- [20] Kicinska A, Szewczyk A. Large-conductance potassium cation channel opener NS1619 inhibits cardiac mitochondria respiratory chain. *Toxicol Mech Meth* 2004;14:59–61.
- [21] Beavis AD, Brannan RD, Garlid KD. Swelling and contraction of the mitochondrial matrix. I. A structural interpretation of the relationship between light scattering and matrix volume. *J Biol Chem* 1985;260:13424–33.
- [22] Akerman KE, Wikstrom MK. Safranin as a probe of the mitochondrial membrane potential. *FEBS Lett* 1976;68:191–7.
- [23] Kowaltowski AJ, Cosso RG, Campos CB, Fiskum G. Effect of Bcl-2 overexpression on mitochondrial structure and function. *J Biol Chem* 2002;277(42):42802–7.
- [24] Costa AD, Garlid KD, West IC, Lincoln TM, Downey JM, Cohen MV, et al. Protein kinase G transmits the cardioprotective signal from cytosol to mitochondria. *Circ Res* 2005;97:329–36.
- [25] Spurr AR. A low-viscosity epoxy resin embedding medium for electron microscopy. *J Ultrastruct Res* 1969;26:31–43.
- [26] Garlid KD, Paucek P. Mitochondrial potassium transport: the K^+ cycle. *Biochim Biophys Acta* 2003;30(1606):23–41.
- [27] Stanfield PR. Tetraethylammonium ions and the potassium permeability of excitable cells. *Rev Physiol Biochem Pharmacol* 1983;97:1–67.
- [28] Zoratti M, Szabo I. The mitochondrial permeability transition. *Biochim Biophys Acta* 1995;1241:139–76.
- [29] Kowaltowski AJ, Castillo RF, Vercesi AE. Mitochondrial permeability transition and oxidative stress. *FEBS Lett* 2001;20(495):12–5.
- [30] Stenchever MA, Droegemueller W, Herbst AL, Mishell Jr DR. *Comprehensive gynecology*. St. Louis, MO: Mosby; 2001.
- [31] Calderone V. Large-conductance, Ca^{2+} -activated K^+ channels: function, pharmacology and drugs. *Curr Med Chem* 2002;9:1385–95.
- [32] Wu SN. Large-conductance Ca^{2+} -activated K^+ channels: physiological role and pharmacology. *Curr Med Chem* 2003;10:649–61.
- [33] Sato T, Saito T, Saegusa N, Nakaya H. Mitochondrial Ca^{2+} -activated K^+ channels in cardiac myocytes: a mechanism of the cardioprotective effect and modulation by protein kinase A. *Circulation* 2005;111:198–203.
- [34] Daum G. Lipids of mitochondria. *Biochim Biophys Acta* 1985;822:1–42.
- [35] Kenyon JL, McKemy DD, Airey JA, Sutko JL. Interaction between ryanodine receptor function and sarcolemmal Ca^{2+} currents. *Am J Physiol* 1995;269:C334–40.
- [36] Minners J, van den Bos EJ, Yellon DM, Schwab H, Opie LH, Sack MN. Dinitrophenol, cyclosporin A, and trimetazidine modulate preconditioning in the isolated rat heart: support for a mitochondrial role in cardioprotection. *Cardiovasc Res* 2000;47:68–73.
- [37] Rodrigo GC, Lawrence CL, Standen NB. Dinitrophenol pretreatment of rat ventricular myocytes protects against damage by metabolic inhibition and reperfusion. *J Mol Cell Cardiol* 2002;34:555–5569.
- [38] Bienengraeber M, Ozcan C, Terzic A. Stable transfection of UCP1 confers resistance to hypoxia/reoxygenation in a heart-derived cell line. *J Mol Cell Cardiol* 2003;35:861–5.
- [39] Hoerter J, Gonzalez-Barroso MD, Couplan E, Mateo P, Gelly C, Cassard-Doulcier AM, et al. Mitochondrial uncoupling protein 1 expressed in the heart of transgenic mice protects against ischemic-reperfusion damage. *Circulation* 2004;110:528–33.
- [40] McLeod CJ, Aziz A, Hoyt Jr RF, McCoy Jr JP, Sack MN. Uncoupling proteins 2 and 3 function in concert to augment tolerance to cardiac ischemia. *J Biol Chem* 2005;280:33470–6.
- [41] Oekaili RA, Bhargava P, Kukreja RC. Chemical preconditioning with 3-nitropropionic acid in hearts: role of mitochondrial K_{ATP} channel. *Am J Physiol* 2001;280:H2406–11.
- [42] Riepe MW, Ludolph AC. Chemical preconditioning: a cytoprotective strategy. *Mol Cell Biochem* 1997;174:249–54.
- [43] Korshunov SS, Skulachev VP, Starkov AA. High protonic potential actuates a mechanism of production of reactive oxygen species in mitochondria. *FEBS Lett* 1997;416:15–8.

Ap.2. Mitochondrial Ion Transport Pathways: Role in Metabolic Diseases

Biochimica et Biophysica Acta 1797 (2010) 832–838



Contents lists available at ScienceDirect

Biochimica et Biophysica Acta

journal homepage: www.elsevier.com/locate/bbambio

Review

Mitochondrial ion transport pathways: Role in metabolic diseases

Ariel R. Cardoso, Bruno B. Queliconi, Alicia J. Kowaltowski *

Departamento de Bioquímica, Instituto de Química, Universidade de São Paulo, São Paulo, SP, Brazil

ARTICLE INFO

Article history:
Received 30 August 2009
Received in revised form 16 December 2009
Accepted 21 December 2009
Available online 5 January 2010

Keywords:
Uncoupling protein
Ca²⁺ uniporter
ATP-sensitive K⁺ channel
Reactive oxygen species

ABSTRACT

Mitochondria are the central coordinators of energy metabolism and alterations in their function and number have long been associated with metabolic disorders such as obesity, diabetes and hyperlipidemias. Since oxidative phosphorylation requires an electrochemical gradient across the inner mitochondrial membrane, ion channels in this membrane certainly must play an important role in the regulation of energy metabolism. However, in many experimental settings, the relationship between the activity of mitochondrial ion transport and metabolic disorders is still poorly understood. This review briefly summarizes some aspects of mitochondrial H⁺ transport (promoted by uncoupling proteins, UCPs), Ca²⁺ and K⁺ uniporters which may be determinant in metabolic disorders.

© 2009 Elsevier B.V. All rights reserved.

1. Introduction

Mitochondria are the central coordinators and the site of essential biochemical transformations involved in energy metabolism. As such, these organelles have always been focused on within studies involving metabolic diseases. Indeed, a vast array of findings link changes in mitochondrial functions with disorders associated with the metabolic syndrome. In some cases, mitochondrial alterations appear as causes of the metabolic changes observed. For example, enhancement of mitochondrial proliferation improves symptoms associated with the metabolic syndrome, indicating that defective mitochondrial biogenesis leads to these characteristics [1–3]. Indeed, mutations in mitochondrial tRNA promote maternally-inherited symptoms characteristic of the metabolic syndrome [4]. In other studies, the link between mitochondrial dysfunction and metabolic syndrome is correlative, but still highly interesting. As examples, the selection for low aerobic capacity produces animals with metabolic alterations typical of the metabolic syndrome and decreased mitochondrial biogenesis [5]. Insulin resistance induced by early introduction to animal fat in the diet is preceded by altered mitochondrial gene expression and reduced mitochondrial DNA content [6]. Non-alcoholic steatohepatitis and gains in visceral fat are associated with mitochondrial dysfunction [3,7,8]. Furthermore, mitochondria are the most quantitatively relevant intracellular source of reactive oxygen species (ROS) [9–11], and oxidative imbalance is strongly linked to the metabolic syndrome [12].

These studies mostly focus on changes in mitochondrial content, point mutations or changes of respiratory capacity as determinants for

alterations in metabolic control. On the other hand, recent results suggest mitochondrial ion carriers may also be important regulators of animal energy metabolism. In this review, we uncover some characteristics of mitochondrial ion transport which may be important in metabolic disorders.

2. Mitochondrial ion transport: general properties

Mitochondria must, at the same time, exchange metabolites and other compounds with the cytoplasm and maintain the high protonmotive force across the inner mitochondrial membrane necessary for oxidative phosphorylation. Most metabolites transported are anions, and are often symported with protons or antiported against hydroxyl anions in order to use protonmotive force to drive the accumulation of these metabolites. Cation exchangers are present in the mitochondrial inner membrane to remove specific ions from the matrix. A small group of cation uniporters allow the regulated entry of selected cations into the matrix. These uniporters must present limited transport rates in order to maintain protonmotive force and oxidative phosphorylation [13,14].

Most mitochondrial ion transporters have been characterized functionally and pharmacologically, but still remain uncharacterized structurally, due to their low abundance. This makes their link with metabolic diseases much harder to study than other properties and biomolecules in mitochondria.

3. Uncoupling proteins

A notable exception to the lack of structural knowledge regarding mitochondrial ion carriers are uncoupling proteins (UCPs), a family of inner membrane carriers that increase proton conductance and are

* Corresponding author. Av. Prof. Lineu Prestes, 748, São Paulo, SP, 05508-900, Brazil.
E-mail address: alicia@iq.usp.br (A.J. Kowaltowski).

the product of well-established genes [15–18]. Interestingly, UCPs are not proton channels, but anion transporters instead. They are believed to transport free fatty acid anions from the mitochondrial matrix to the intermembrane space (see Fig. 1). The fatty acids become protonated due to the electrochemical proton gradient, lose their charge and flip-flop through the inner membrane lipid bilayer, transporting a proton into the matrix (for reviews, see [19,20]). Another proposed mechanism for UCP function [21] suggests UCPs transport H^+ using fatty acids at their active site, in a process mediated by histidines. However, not all UCPs possess histidines in this site [20,22]. The following publications provide overviews of differing proposed mechanisms of uncoupling protein function: [15,23–26].

UCP1, the first such protein described, is present in high quantities in the brown adipose tissue, and promotes overt uncoupling, widely associated with thermogenesis [27–30]. The discovery of a family of proteins with high identities to UCP1 in the 1990s, widely distributed in many tissues, immediately attracted the attention of researchers in energy metabolism, and the idea that UCP content could regulate body weight by determining mitochondrial coupling surfaced [31,32]. Subsequently, a large body of work investigated the expression of UCPs in metabolic alterations, including obesity, diabetes and hyperlipidemias [33–35]. Many correlations were uncovered, including correlations of UCP polymorphisms with obesity and diabetes [35,36], but unfortunately results varied widely, and often showed unexpected correlations (such as increased UCP expression in obesity [37]). Furthermore, most studies quantified mRNA levels for UCP2 or UCP3 and investigated polymorphisms, while few measured protein levels in tissues or looked directly at the activity of these transporters, hampering precise conclusions. Indeed, Yu et al. [38] demonstrated experimentally that significant discrepancies exist between UCP mRNA levels, temperature and mitochondrial proton leak.

Clues regarding the functional activities of UCP family members were also expected to be uncovered using knockout animal models. Interestingly, knockouts of either UCP2 or UCP3 have little or no phenotype [34,39–41]. Overexpression of UCP3 generated leaner mice in one model [42], but the levels of overexpression required were very high, and can lead to uncoupling simply due to protein misfolding [43]. These results increasingly made it clear that the role of UCP family members in energy metabolism was more subtle and complex: The simplistic hypothesis for the function of these proteins did not completely account for their actions. Indeed, the degree of uncoupling promoted by these transporters varies largely with their abundance, and generalized uncoupling leading to whole body increases in energy

expenditure does not seem to be the primary function of UCP2 and UCP3 [43–45].

Since the metabolic syndrome involves a complex network of pathophysiological changes, tissue-specific activation of UCPs could be involved in the metabolic responses. Indeed, obesity and a pro-inflammatory state can induce the expression of UCP2 in the liver, where its expression is normally low [46–49]. UCP2 could be an adaptation to oxidize excessive lipids in mitochondria by increasing respiratory rates and the NAD^+ pool. However, UCP2 null mice submitted to hyperlipidemic diets do not exhibit any differences in non-alcoholic steatohepatitis development [34], possibly due to the compensatory effect of increasing other uncoupling pathways that mitigate the steatotic phenotype, such as K^+ channels (discussed below). Indeed, UCP2 overexpression measured in the livers of obese animals could be due to Kupffer cells (liver resident macrophages), without a relevant hepatocyte-related change in metabolic function [34].

A well-established function for UCP family members is the control of the intracellular redox state, by limiting mitochondrial production of ROS [19,45,50,51], a necessary byproduct of energy metabolism [10,11]. Indeed, mild mitochondrial uncoupling is often an effective manner to control the generation of mitochondrial oxidants in isolated mitochondria [10,11,22,52], and systemic mild uncoupling is associated with strong improvements in redox state [53,54]. In this general line, many publications have shown that UCP activation effectively prevents mitochondrial ROS release, under physiological and pathological conditions [19,45,50,51,55,56]. While ROS control contributes toward tissue protection under many conditions, mild uncoupling can be lethal for cerebellar cultures [57]. In these cells, mild uncoupling decreases ATP generation leading to a decreased capacity to exchange Na^+ for K^+ , resulting in cell death. Thus, the protection caused by mild uncoupling via ROS regulation is probably dependent on the ability of the cell to maintain levels of ATP despite the decrease in coupling.

Other results suggest UCPs may also have a role transporting ROS anion fatty acid hydroperoxides, thus further contributing toward redox control [58]. A strong indicator that the redox role of UCP proteins is indeed physiologically relevant is the finding that the activity of these proteins is increased by oxidants [59].

Another clear metabolic role for a specific member of the UCP family, UCP2, is the control of glucose-stimulated insulin release by pancreatic β -cells (for a review see [43]). UCP2 activity in these cells decreases the quantity of ATP produced in the presence of a set concentration of glucose, increasing the activity of ATP-sensitive K^+

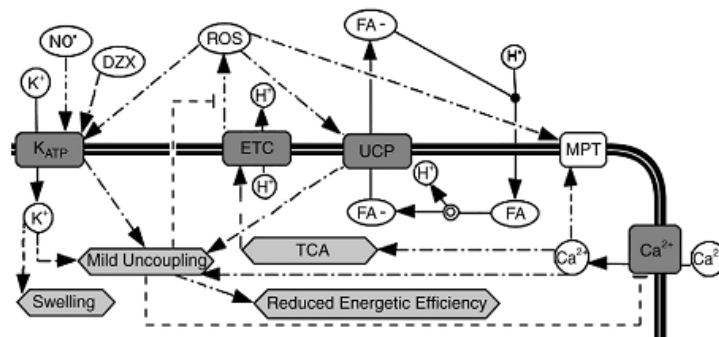


Fig. 1. K^+ , H^+ and Ca^{2+} transport in mitochondria – effects on ROS production and energy metabolism. K^+ transport (through $mitoK_{ATP}$ channels), H^+ transport (mediated by UCPs, and involving free fatty acids, FA) and Ca^{2+} transport (through Ca^{2+} uniporters) occurs down the electrochemical gradient generated by the electron transport chain (ETC), using electrons collected in the tricarboxylic acid cycle (TCA). The activity of these pathways promotes uncoupling, which prevents the formation of mitochondrial reactive oxygen species (ROS), which in turn, are activators of $mitoK_{ATP}$ and UCPs. $mitoK_{ATP}$ is also activated by agonists such as diazoxide (DZX) and the reactive nitrogen species NO . Uncoupling decreases energetic efficiency. Excessive ROS and Ca^{2+} uptake into mitochondria can lead to non-selective inner membrane permeabilization, due to the activation of the mitochondrial permeability transition (MPT).

channels on the plasma membrane, and leading to lower insulin release [60,61] (see Fig. 2). As a result, inhibition of UCP2 leads to more efficient insulin secretion in the presence of equal quantities of glucose. This helps explain why UCP2 expression levels were often paradoxically related to body weight, and may be the reason for correlations between UCP2 polymorphisms and type 2 diabetes [62,63].

A recent publication has suggested yet another role for tissue-specific effects of UCP2 in the regulation of energy metabolism: Andrews et al. [64] suggest that UCP2 in arcuate nucleus neurons controls the response to ghrelin and, hence, food intake. However, the UCP2 knockout preparations in this work appear to have lower mitochondrial membrane potentials and capacity to phosphorylate ADP, a point which requires further clarification. Another possible role for uncoupling proteins in energy metabolism has been suggested based on studies in plant mitochondria, which present significant plant uncoupling mitochondrial protein (PUMP) activity [65]: by increasing NADH oxidation, uncoupling allows NAD⁺-dependent reactions such as those within the citric acid cycle to occur even in the presence of high ATP levels, thus permitting biosynthesis reactions to occur in the presence of high energy states.

UCP1, the first UCP to be described, is highly abundant and overtly uncoupling in brown adipose tissue, and was for many years believed to be an adaptation to induce thermogenesis under specific conditions, such as arousal after hibernation and body heat maintenance in newborns. The finding that brown adipose tissue is closely related to muscular tissue [66–68] has shed new interest in this protein as a more general metabolic regulator. In a highly insightful study, Needegard's group demonstrated that UCP1 ablation induced obesity in mice housed at thermoneutrality [69]. Indeed, there is convincing, if preliminary, evidence that UCP1 and brown adipose tissue activity may be a factor in the regulation of human weight gain [70–72].

UCPs are not the only fatty acid anion transporters in mitochondria capable of promoting mild uncoupling. In fact, in many tissues, the adenine nucleotide translocator is the main protein responsible for this activity, and other mitochondrial carriers such as the aspartate/glutamate antiporter have also been shown to present this activity (for review, see [73]). Although difficult to evaluate, it would be very interesting to know if the uncoupling activity of these proteins can impact energy metabolism. The adenine nucleotide translocator has been shown to regulate ROS release through its uncoupling activity [74], and is involved in cardiac protection induced by ischemic preconditioning [75,76].

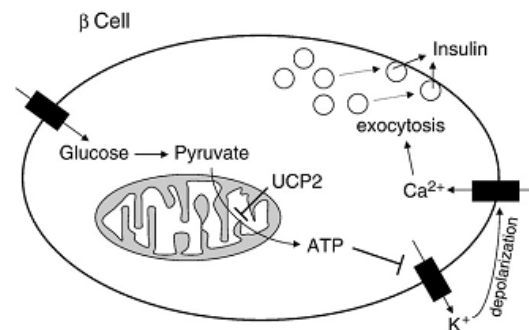


Fig. 2. Regulation of insulin release by UCP2 in pancreatic β cells. Glucose freely enters the cytosol, producing intracellular pyruvate, which is oxidized by mitochondria, generating ATP in a manner regulated by UCP2 activity. High ATP levels close plasma membrane ATP-sensitive K⁺ channels, leading to membrane depolarization and activation of voltage-gated Ca²⁺ channels. Increased intracellular Ca²⁺ stimulates both insulin synthesis (not shown) and release through exocytosis.

4. Ca²⁺ uniporters

One of the first characteristics noted in isolated mitochondria was the high capacity to take up Ca²⁺ ions. Indeed, mitochondrial inner membranes possess a highly selective Ca²⁺ uniporter [77]. As is often the case for inner membrane transporters, the identity of mitochondrial Ca²⁺ uniporters is yet undetermined. Trenker et al. [78] suggested the activity was mediated by UCPs, but this concept has been strongly rebuffed by most prominent researchers in the area [79]. Indeed, silencing UCP genes does not alter mitochondrial matrix calcium concentrations [80]. Furthermore, physiological characterizations suggest that more than one Ca²⁺ uptake pathway into mitochondria exists (reviewed in [81,82]).

The quantity and rate of Ca²⁺ uptake into mitochondria are determined not only by the activity of mitochondrial Ca²⁺ uptake pathways but also by the availability of this ion within the mitochondrial microenvironment, since the affinity of mitochondrial Ca²⁺ transporters is in general lower than those present in the endoplasmic reticulum. Indeed, Ca²⁺ signals are closely transmitted between the reticulum and mitochondria, which are functionally and spatially coupled [83].

Ca²⁺ in the matrix has strong effects on mitochondrial metabolism (see Fig. 1 and [82,84] for reviews). Pyruvate, isocitrate, α -glycerophosphate and α -ketoglutarate dehydrogenase are strongly activated by Ca²⁺ ions, leading to enhanced NAD⁺ reduction and increased protonmotive force. Ca²⁺ uptake by mitochondria also has an important role in regulating physiological Ca²⁺ transients [85].

Furthermore, Ca²⁺ ions can be determinant for the rates of mitochondrial ROS release (reviewed in [11,86]). Uptake of low concentrations of Ca²⁺ by mitochondria can decrease ROS release due to the temporary decrease in protonmotive force and, possibly, loss of pyrimidine nucleotides [87,88]. On the other hand, uptake of higher Ca²⁺ quantities can significantly increase ROS release from mitochondria [89–92], possibly due to interactions with inner mitochondrial membrane cardiolipin, leading to structural changes in the membrane-inserted electron transport chain [93].

When accumulated by mitochondria at high levels, and associated with conditions of oxidative stress, Ca²⁺ ions can lead to extensive changes in mitochondrial function, including a non-selective form of inner membrane permeabilization known as the mitochondrial permeability transition (see Fig. 1, reviewed in [82,86,94]). Ca²⁺-induced mitochondrial dysfunction has been associated with a wide variety of disorders, including dyslipidemias and diabetes [95–97]. On the other hand, although Ca²⁺ uniporters in the mitochondrial membrane have a large set of elements suggestive that they may be involved in dysfunctions associated with metabolic diseases, the lack of a molecular identity has hampered direct studies indicating if this is indeed the case.

5. K⁺ uniporters

K⁺ uniporters were first described in inner mitochondrial membranes in the early 1990s [98,99]. The presence of a regulated K⁺ entry pathway into mitochondria was surprising, since K⁺ is the main intracellular cation and leaks at small but significant rates through the mitochondrial lipid bilayer, reaching the matrix. Today, it is evident that there are many functional advantages in having a regulated K⁺ entry pathway in addition to a K⁺ leak (reviewed in [14,100–102]).

K⁺ uptake into mitochondria is inhibited by ATP and sulfonylureas, leading to the characterization of these K⁺ uniporters as ATP-sensitive K⁺ channels (mitoK_{ATP}, [99,103,104]). Other more recent findings suggest mitochondria may also have Ca²⁺ activated and/or voltage-gated Kv1.3 potassium channels and the twin-pore domain TASK-3 potassium channels (reviewed in [105]), but the roles of these are still poorly understood.

K^+ uptake is driven by the electrochemical potential and accompanied by phosphate and water, resulting in matrix swelling, which in turn dilutes matrix Mg^{2+} and activates the K^+/H^+ exchanger [14]. The net result is K^+ cycling and lower protonmotive force. The decrease in protonmotive force is, however, dependent on the transport efficiency of the K^+ channel. In keeping with the reality that mitochondria must be able to maintain oxidative phosphorylation, K^+ transport through $mitoK_{ATP}$ channels is very limited, and often undetectable by conventional measurement techniques [106]. $mitoK_{ATP}$ channels are thus a (very) mild uncoupling pathway (Fig. 1).

Over the years, many functions have been proposed for mitochondrial K^+ uniporters. Since their activity results in water uptake by the organelle, they play a role in the regulation of mitochondrial matrix volume, which may be important to maintain the structural relationship between the inner and outer membrane [14,106]. Another possible role for $mitoK_{ATP}$ may be to regulate mitochondrial ΔpH , since the activity of this channel may result in matrix alkalization [107].

Based on the fact that uncoupling, even to a very mild degree, can prevent mitochondrial ROS release [52,108–111], we proposed that K^+ cycling due to $mitoK_{ATP}$ activity could act as a regulating pathway to control rates of ROS release in mitochondria [100,112–115]. Although this hypothesis has met some resistance [116], the idea is supported by the finding that $mitoK_{ATP}$ channels are strongly activated by oxidants, and inhibited by thiol reductants [100,114,115,117–120]. Furthermore, the redox effects of this channel explain, at least in part, why $mitoK_{ATP}$ activation is protective against acute tissue damage [113,115] (see Fig. 3). Other protective activities of this channel include regulating mitochondrial volume, the physical relationship between the inner and outer membrane and, as a result, transport of metabolites into mitochondria (reviewed in [100]).

Although the strong protective effects of $mitoK_{ATP}$ in situations of acute tissue damage have attracted most of the attention in the area, it is most probable the main role of these channels is not related to acute

stimuli. In this sense, the first evidence that these channels could have a more general role regulating energy metabolism was uncovered by Vercesi's group [121], who found that $mitoK_{ATP}$ channel activity was higher in the livers of transgenic hypertriglyceridemic mice. Interestingly, the higher activity of $mitoK_{ATP}$ in these animals results in increased oxidative metabolism and a lower efficiency of energy conversion in these animals, preventing obesity. In view of these results, it is tempting to propose that $mitoK_{ATP}$ channels may act as modulators of animal energy metabolism and, as such, may play a central role in metabolic disorders [95,121]. Further studies have revealed that hypertriglyceridemic mice, while presenting indicators of oxidative stress in cytosolic extracts from their livers, present a protection against mitochondrial oxidation that is dependent on $mitoK_{ATP}$ activity [122]. Thus, the redox role of $mitoK_{ATP}$ channels is important also within metabolic alterations.

Since intracellular insulin responses involve Akt-dependent pathways (for a review see [123]), and $mitoK_{ATP}$ can be activated by Akt, at least in the ischemic heart [124,125], it is tempting to propose that $mitoK_{ATP}$ channels may have interesting functions under conditions of insulin resistance, although this possibility is largely unexplored. An indirect indication that $mitoK_{ATP}$ channels have changes in their activity in diabetes is the finding that protection against ischemic damage conferred by preconditioning, a process mediated by $mitoK_{ATP}$ (for reviews see [100,126]), is abrogated in models of this disease [127–130]. Another often overlooked point of relevance in diabetes is that treatment of the disorder with sulfonylureas such as glibenclamide (reviewed in [131]) not only increases insulin secretion due to the inhibition of β -cell K_{ATP} channels (see Fig. 2) but may also inhibit $mitoK_{ATP}$ channels, with yet unknown metabolic and redox consequences (see Fig. 3).

6. Final remarks

Altogether, many different approaches support the idea that ion transport rates across the inner mitochondrial membrane may be determinant in the regulation of energy metabolism. As a result, changes in activities of these transporters are certainly important as causes and response mechanisms in metabolic diseases. Unfortunately, studies in the field are limited by methodological difficulties regarding measuring the activities of ion channels *in vivo*. We believe the relationship between mitochondrial ion transport and metabolic disorders is an area that should be explored more intensely in the near future.

Acknowledgements

The authors are in debt to Professor Roger F. Castilho for critical reading of the manuscript. Supported by the Fundação de Amparo à Pesquisa no Estado de São Paulo (FAPESP), Conselho Nacional de Pesquisa e Desenvolvimento (CNPq), Coordenação de Aperfeiçoamento de Pessoal de Ensino Superior (CAPES) and the Instituto Nacional de Ciência e Tecnologia de Processos Redox em Biomedicina (Redoxoma).

References

- [1] Y. Nagai, Y. Nishio, T. Nakamura, H. Maegawa, R. Kikkawa, A. Kashiwagi, Amelioration of high fructose-induced metabolic derangements by activation of PPAR α , *Am. J. Physiol. Endocrinol. Metab.* 282 (2002) E1180–E1190.
- [2] T. Tanaka, J. Yamamoto, S. Iwasaki, H. Asaba, H. Hamura, Y. Ikeda, M. Watanabe, K. Magoori, R.X. Ioka, K. Tachibana, Y. Watanabe, Y. Uchiyama, K. Sumi, H. Iguchi, S. Ito, T. Doi, T. Hamakubo, M. Naito, J. Auwerx, M. Yanagisawa, T. Kodama, J. Sakai, Activation of peroxisome proliferator-activated receptor delta induces fatty acid beta-oxidation in skeletal muscle and attenuates metabolic syndrome, *Proc. Natl. Acad. Sci. USA* 100 (2003) 15924–15929.
- [3] E. Nisoli, E. Clementi, M.O. Carruba, S. Moncada, Defective mitochondrial biogenesis: a hallmark of the high cardiovascular risk in the metabolic syndrome? *Circ. Res.* 100 (2007) 795–806.

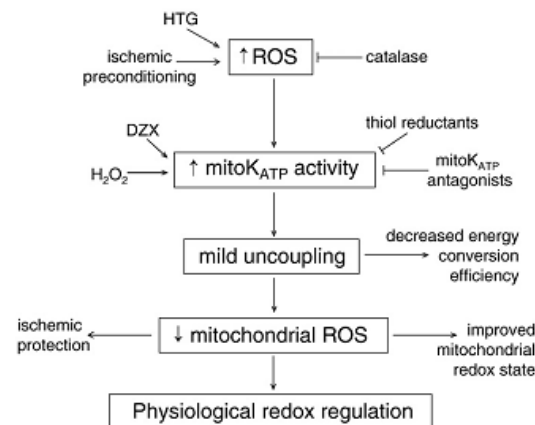


Fig. 3. $mitoK_{ATP}$ channels: redox-sensitive pathways that control physiological and pathological ROS release. Physiological increases in ROS levels in the mitochondrial microenvironment lead to the activation of $mitoK_{ATP}$ channels, resulting in mild uncoupling and controlling the production of oxidants in mitochondria. Specific pathological conditions also alter redox state, resulting in the activation of this pathway: ischemic preconditioning in the heart increases ROS release, resulting in $mitoK_{ATP}$ activation and ischemic protection associated with decreased ROS formation during reperfusion. Preconditioning is mimicked by oxidants such as H_2O_2 and $mitoK_{ATP}$ agonists (including diazoxide, DZX), and is inhibited by antioxidants and $mitoK_{ATP}$ antagonists. Hypertriglyceridemia (HTG) increases ROS and activates $mitoK_{ATP}$, resulting in decreased efficiency of energy conversion and an improvement in the mitochondrial redox state. Thiol reductants, which inhibit $mitoK_{ATP}$, prevent these effects.

- [4] F.H. Wilson, A. Hariri, A. Farhi, H. Zhao, K.F. Petersen, H.R. Toka, C. Nelson-Williams, K.M. Raja, M. Kashgarian, G.L. Shulman, S.J. Scheinman, R.P. Lifton, A cluster of metabolic defects caused by mutation in a mitochondrial tRNA, *Science* 306 (2004) 1190–1194.
- [5] U. Wisloff, S.M. Najjar, O. Ellingsen, P.M. Haram, S. Swoap, Q. Al-Share, M. Fernström, K. Rezaei, S.J. Lee, L.G. Koch, S.L. Britton, Cardiovascular risk factors emerge after artificial selection for low aerobic capacity, *Science* 307 (2005) 418–420.
- [6] P.D. Taylor, J. McConnell, I.Y. Khan, K. Holemans, K.M. Lawrence, H. Asare-Anane, S.J. Persaud, P.M. Jones, L. Petrie, M.A. Hanson, L. Poston, Impaired glucose homeostasis and mitochondrial abnormalities in offspring of rats fed a fat-rich diet in pregnancy, *Am. J. Physiol. Regul. Integr. Comp. Physiol.* 288 (2005) R134–R139.
- [7] D. Pessayre, B. Fromenty, NASH: a mitochondrial disease, *J. Hepatol.* 42 (2005) 928–940.
- [8] D. Pessayre, Role of mitochondria in non-alcoholic fatty liver disease, *J. Gastroenterol. Hepatol.* 22 (2007) 20–27.
- [9] A. Boveris, B. Chance, The mitochondrial generation of hydrogen peroxide. General properties and effect of hyperbaric oxygen, *Biochem. J.* 134 (1973) 707–716.
- [10] J.F. Turrens, Mitochondrial formation of reactive oxygen species, *J. Physiol.* 552 (2003) 335–344.
- [11] A.J. Kowaltowski, N.C. de Souza-Pinto, R.F. Castilho, A.E. Vercesi, Mitochondria and reactive oxygen species, *Free Radic. Biol. Med.* 47 (2009) 333–343.
- [12] S. Furukawa, T. Fujita, M. Shimabukuro, M. Iwaki, Y. Yamada, Y. Nakajima, O. Nakayama, M. Makishima, M. Matsuda, I. Shimomura, Increased oxidative stress in obesity and its impact on metabolic syndrome, *J. Clin. Invest.* 114 (2004) 1752–1761.
- [13] D.G. Nicholls, S. Fergusson, *Bioenergetics 3*, chapter 8, pages 219–248, Academic Press, London, 2002.
- [14] K.D. Garlid, P. Paucek, Mitochondrial potassium transport: the K⁺ cycle, *Biochim. Biophys. Acta* 1606 (2003) 23–41.
- [15] D. Ricquier, F. Bouillaud, The uncoupling protein homologues: UCP1, UCP2, UCP3, StUCP and AtUCP, *Biochem. J.* 345 (2000) 161–179.
- [16] P. Jezek, M. Zäcková, M. Růžicka, E. Skobisová, M. Jabůrek, Mitochondrial uncoupling proteins—facts and fantasies, *Physiol. Res.* 53 (2004) S199–S211.
- [17] P. Jezek, K.D. Garlid, Mammalian mitochondrial uncoupling proteins, *Int. J. Biochem. Cell Biol.* 30 (1998) 1163–1168.
- [18] C. Affourtit, P.G. Crichton, N. Parker, M.D. Brand, Novel uncoupling proteins, *Novartis Found. Symp.* 287 (2007) 70–80.
- [19] P. Jezek, H. Engstová, M. Zäcková, A.E. Vercesi, A.D. Costa, P. Arruda, K.D. Garlid, Fatty acid cycling mechanism and mitochondrial uncoupling proteins, *Biochim. Biophys. Acta* 1365 (1998) 319–327.
- [20] K.D. Garlid, M. Jabůrek, P. Jezek, Mechanism of uncoupling protein action, *Biochem. Soc. Trans.* 29 (2001) 803–806.
- [21] E. Winkler, M.J. Klingenberg, Effect of fatty acids on H⁺ transport activity of the reconstituted uncoupling protein, *Biol. Chem.* 269 (1994) 2508–2515.
- [22] V.P. Skulachev, Uncoupling: new approaches to an old problem of bioenergetics, *Biochim. Biophys. Acta* 1363 (1998) 100–124.
- [23] A. Ledesma, M.G. de Lacoza, E. Rial, The mitochondrial uncoupling proteins, *Genome Biol.* 3 (2002) 3015.
- [24] M. Klingenberg, K.S. Echtay, Uncoupling proteins: the issues from a biochemist point of view, *Biochim. Biophys. Acta* 1504 (2001) 128–143.
- [25] K.D. Garlid, D.E. Orosz, M. Modrianský, S. Vassanelli, P. Jezek, On the mechanism of fatty acid-induced proton transport by mitochondrial uncoupling protein, *J. Biol. Chem.* 271 (1996) 2615–2620.
- [26] D.G. Nicholls, The physiological regulation of uncoupling proteins, *Biochim. Biophys. Acta* 1757 (2006) 459–466.
- [27] D.G. Nicholls, E. Rial, A history of the first uncoupling protein, UCP1, *J. Bioenerg. Biomembr.* 31 (1999) 399–406.
- [28] V. Golozoubova, B. Cannon, J. Nedergaard, UCP1 is essential for adaptive adrenergic nonshivering thermogenesis, *Am. J. Physiol. Endocrinol. Metab.* 291 (2006) E350–E357.
- [29] E. Rial, M.M. González-Barroso, C. Fleury, F. Bouillaud, The structure and function of the brown fat uncoupling protein UCP1: current status, *Biofactors* 8 (1998) 209–219.
- [30] M. Klingenberg, S.G. Huang, Structure and function of the uncoupling protein from brown adipose tissue, *Biochim. Biophys. Acta* 1415 (1999) 271–296.
- [31] M.E. Harper, Obesity research continues to spring leaks, *Clin. Invest. Med.* 20 (1997) 239–244.
- [32] O. Boss, T. Hagen, B.B. Lowell, Uncoupling proteins 2 and 3: potential regulators of mitochondrial energy metabolism, *Diabetes* 49 (2000) 143–156.
- [33] C. Fleury, M. Neverova, S. Collins, S. Raimbault, O. Champigny, C. Levi-Meyrueis, F. Bouillaud, M.F. Seldin, R.S. Surwit, D. Ricquier, C.H. Warden, Uncoupling protein-2: a novel gene linked to obesity and hyperinsulinemia, *Nat. Genet.* 15 (1997) 269–272.
- [34] G. Baffy, C.Y. Zhang, J.N. Glickman, B.B. Lowell, Obesity-related fatty liver is unchanged in mice deficient for mitochondrial uncoupling protein 2, *Hepatology* (2002) 753–761.
- [35] J.J. Jia, X. Zhang, C.R. Ge, M. Jois, The polymorphisms of UCP2 and UCP3 genes associated with fat metabolism, obesity and diabetes, *Obes. Rev.* 10 (2009) 519–526.
- [36] A.L. Willig, K.R. Casazza, J. Divers, A.W. Bigham, B.A. Gower, G.R. Hunter, J.R. Fernandez, Uncoupling protein 2 Ala55Val polymorphism is associated with a higher acute insulin response to glucose, *Metabolism* 58 (2009) 877–881.
- [37] J.A. Simoneau, D.E. Kelley, M. Neverova, C.H. Warden, Overexpression of muscle uncoupling protein 2 content in human obesity associates with reduced skeletal muscle lipid utilization, *FASEB J.* 12 (1998) 1739–1745.
- [38] X.X. Yu, J.L. Barger, B.B. Boyer, M.D. Brand, G. Pan, S.H. Adams, Impact of endotoxin on UCP homolog mRNA abundance, thermoregulation, and mitochondrial proton leak kinetics, *Am. J. Physiol. Endocrinol. Metab.* 279 (2000) 433–446.
- [39] D.W. Gong, S. Monemdjou, O. Gavrilova, L.R. Leon, B. Marcus-Samuels, C.J. Chou, C. Everett, L.P. Kozak, C. Li, C. Deng, M.E. Harper, M.L. Reitman, Lack of obesity and normal response to fasting and thyroid hormone in mice lacking uncoupling protein-3, *J. Biol. Chem.* 275 (2000) 16251–16257.
- [40] A.J. Vidal-Puig, D. Grujic, C.Y. Zhang, T. Hagen, O. Boss, Y. Ido, A. Szczepanik, J. Wade, V. Mootha, R. Cortright, D.M. Muoio, B.B. Lowell, Energy metabolism in uncoupling protein 3 gene knockout mice, *J. Biol. Chem.* 275 (2000) 16258–16266.
- [41] D. Arsenijevic, H. Onuma, C. Pecqueur, S. Raimbault, B.S. Manning, B. Miroux, E. Couplan, M.C. Alves-Guerra, M. Goubern, R. Surwit, F. Bouillaud, D. Richard, S. Collins, D. Ricquier, Disruption of the uncoupling protein-2 gene in mice reveals a role in immunity and reactive oxygen species production, *Nat. Genet.* 26 (2000) 435–439.
- [42] J.C. Clapham, J.R. Arch, H. Chapman, A. Haynes, C. Lister, G.B. Moore, V. Piercy, S.A. Carter, I. Lehner, S.A. Smith, L.J. Beeley, R.J. Godden, N. Herrity, M. Skehel, K.K. Changani, P.D. Hockings, D.G. Reid, S.M. Squires, J. Hatcher, B. Trail, J. Latham, S. Rastan, A.J. Harper, S. Cadenas, J.A. Buckingham, M.D. Brand, A. Abuin, Mice overexpressing human uncoupling protein-3 in skeletal muscle are hyperphagic and lean, *Nature* 406 (2000) 415–418.
- [43] C. Affourtit, M.D. Brand, On the role of uncoupling protein-2 in pancreatic beta cells, *Biochim. Biophys. Acta* 1777 (2008) 973–979.
- [44] J. Nedergaard, B. Cannon, The ‘novel’ uncoupling proteins UCP2 and UCP3: what do they really do? Pros and cons for suggested functions, *Exp. Physiol.* 88 (2003) 65–84.
- [45] F. Bouillaud, UCP2, not a physiologically relevant uncoupler but a glucose sparing switch impacting ROS production and glucose sensing, *Biochim. Biophys. Acta* 1787 (2009) 377–383.
- [46] R. Faggioni, J. Shigenaga, A. Moser, K.R. Feingold, C. Grunfeld, Induction of UCP2 gene expression by LPS: a potential mechanism for increased thermogenesis during infection, *Biochem. Biophys. Res. Commun.* 244 (1998) 75–78.
- [47] A. Rashid, T.C. Wu, C.C. Huang, C.H. Chen, H.Z. Lin, S.Q. Yang, F.Y. Lee, A.M. Diehl, Mitochondrial proteins that regulate apoptosis and necrosis are induced in mouse fatty liver, *J. Hepatol.* 29 (1999) 1131–1138.
- [48] K. Kimura, B.D. Jung, K. Kanehira, Y. Irie, X. Cañas, M. Saito, Induction of uncoupling protein (UCP) 2 in primary cultured hepatocytes, *FEBS Lett.* 457 (1999) 75–79.
- [49] C. Pecqueur, M.C. Alves-Guerra, C. Gelly, C. Levi-Meyrueis, E. Couplan, S. Collins, D. Ricquier, F. Bouillaud, B. Miroux, Uncoupling protein 2, in vivo distribution, induction upon oxidative stress, and evidence for translational regulation, *J. Biol. Chem.* 276 (2001) 8705–8712.
- [50] A. Nègre-Salvayre, C. Hirtz, G. Carrera, R. Cazenave, M. Trolly, R. Salvayre, L. Pénicaud, L. Casteilla, A role for uncoupling protein-2 as a regulator of mitochondrial hydrogen peroxide generation, *FASEB J.* 11 (1997) 809–815.
- [51] A.J. Kowaltowski, A.D. Costa, A.E. Vercesi, Activation of the potato plant uncoupling mitochondrial protein inhibits reactive oxygen species generation by the respiratory chain, *FEBS Lett.* 425 (1998) 213–216.
- [52] P.S. Brookes, Mitochondrial H⁺ leak and ROS generation: an odd couple, *Free Radic. Biol. Med.* 38 (2005) 12–23.
- [53] C.C. Caldeira da Silva, F.M. Cerqueira, L.F. Barbosa, M.H. Medeiros, A.J. Kowaltowski, Mild mitochondrial uncoupling in mice affects energy metabolism, redox balance and longevity, *Aging Cell* 7 (2008) 552–560.
- [54] Z.B. Andrews, T.L. Horvath, Uncoupling protein-2 regulates lifespan in mice, *Am. J. Physiol. Endocrinol. Metab.* 296 (2009) E621–E627.
- [55] Y. Teshima, M. Akao, S.P. Jones, E. Marbán, Uncoupling protein-2 overexpression inhibits mitochondrial death pathway in cardiomyocytes, *Circ. Res.* 93 (2003) 192–200.
- [56] G. Mattiasson, M. Shamloo, G. Gido, K. Mathi, G. Tomasevic, S. Yi, C.H. Warden, R.F. Castilho, T. Melcher, M. Gonzalez-Zulueta, K. Nikolich, T. Wieloch, Uncoupling protein-2 prevents neuronal death and diminishes brain dysfunction after stroke and brain trauma, *Nat. Med.* 9 (2003) 1062–1068.
- [57] D.G. Nicholls, S. Vesce, L. Kirk, S. Chalmers, Interactions between mitochondrial bioenergetics and cytoplasmic calcium in cultured cerebellar granule cells, *Cell Calcium* 34 (2003) 407–424.
- [58] M. Jabůrek, S. Miyamoto, P. Di Mascio, K.D. Garlid, P. Jezek, Hydroperoxy fatty acid cycling mediated by mitochondrial uncoupling protein UCP2, *J. Biol. Chem.* 279 (2004) 53097–53102.
- [59] K.S. Echtay, D. Roussel, J. St-Pierre, M.B. Jakabsons, S. Cadenas, J.A. Stuart, J.A. Harper, S.J. Roebuck, A. Morrison, S. Pickering, J.C. Clapham, M.D. Brand, Superoxide activates mitochondrial uncoupling proteins, *Nature* 415 (2002) 96–99.
- [60] C.Y. Zhang, G. Baffy, P. Perret, S. Krauss, O. Peroni, D. Grujic, T. Hagen, A.J. Vidal-Puig, O. Boss, Y.B. Kim, X.X. Zheng, M.B. Wheeler, G.L. Shulman, C.B. Chan, B.B. Lowell, Uncoupling protein-2 negatively regulates insulin secretion and is a major link between obesity, beta cell dysfunction, and type 2 diabetes, *Cell* 105 (2001) 745–755.
- [61] C.T. De Souza, E.P. Araújo, L.F. Stoppiglia, J.R. Pauli, E. Ropelle, S.A. Rocco, R.M. Marin, K.G. Franchini, J.B. Carvalheira, M.J. Saad, A.C. Boschero, E.M. Carneiro, L.A. Velloso, Inhibition of UCP2 expression reverses diet-induced diabetes mellitus by effects on both insulin secretion and action, *FASEB J.* 21 (2007) 1153–1163.
- [62] S.A. Urhammer, L.T. Dalgaard, T.I. Sørensen, A.M. Møller, T. Andersen, A. Tybjaerg-Hansen, T. Hansen, J.O. Clausen, H. Vestergaard, O. Pedersen, Mutational analysis of the coding region of the uncoupling protein 2 gene in obese NIDDM patients:

- impact of a common amino acid polymorphism on juvenile and maturity onset forms of obesity and insulin resistance. *Diabetologia* 40 (1997) 1227–1230.
- [63] H. Wang, W.S. Chu, T. Lu, S.J. Hasstedt, P.A. Kern, S.C. Elbein, Uncoupling protein-2 polymorphisms in type 2 diabetes, obesity, and insulin secretion. *Am. J. Physiol. Endocrinol. Metab.* 286 (2004) E1–E7.
- [64] Z.B. Andrews, Z.W. Liu, N. Wallingford, D.M. Erion, E. Borok, J.M. Friedman, M.H. Tschöp, M. Shanabrough, G. Cline, G.I. Shulman, A. Coppola, X.B. Gao, T.L. Horvath, S. Diano, UCP2 mediates ghrelin's action on NPY/AgRP neurons by lowering free radicals. *Nature* 454 (2008) 846–851.
- [65] A.E. Vercesi, J. Borecky, L.G. Maia, P. Arruda, L.M. Cuccovia, H. Chaimovich, Plant uncoupling mitochondrial proteins. *Annu. Rev. Plant Biol.* 57 (2006) 383–404.
- [66] K. Almind, M. Manieri, W.I. Sivitz, S. Cinti, C.R. Kahn, Ectopic brown adipose tissue in muscle provides a mechanism for differences in risk of metabolic syndrome in mice. *Proc. Natl. Acad. Sci. USA* 104 (2007) 2366–2371.
- [67] M. Crisan, L. Casteilla, L. Lehr, M. Carmona, A. Paoloni-Giacobino, S. Yap, B. Sun, B. Léger, A. Logar, L. Pénicaud, P. Schrauwen, D. Cameron-Smith, A.P. Russell, B. Pédault, J.P. Giacobino, A reservoir of brown adipocyte progenitors in human skeletal muscle. *Stem Cells* 26 (2008) 2425–2433.
- [68] S. Kajimura, P. Seale, K. Kubota, E. Lunsford, J.V. Frangioni, S.P. Gygi, B.M. Spiegelman, Initiation of myoblast to brown fat switch by a PRDM16-C/EBP-beta transcriptional complex. *Nature* 460 (2009) 1154–1158.
- [69] H.M. Feldmann, V. Golozoubova, B. Cannon, J. Nedergaard, UCP1 ablation induces obesity and abolishes diet-induced thermogenesis in mice exempt from thermal stress by living at thermoneutrality. *Cell Metab.* 9 (2009) 203–209.
- [70] M.C. Zingaretti, F. Crosta, A. Vitelli, M. Guerrieri, A. Frontini, B. Cannon, J. Nedergaard, S. Cinti, The presence of UCP1 demonstrates that metabolically active adipose tissue in the neck of adult humans truly represents brown adipose tissue. *FASEB J.* 23 (2009) 3113–3120.
- [71] A.M. Cypess, S. Lehman, G. Williams, I. Tal, D. Rodman, A.B. Goldfine, F.C. Kuo, E.L. Palmer, Y.H. Tseng, A. Doria, G.M. Kolodny, C.R. Kahn, Identification and importance of brown adipose tissue in adult humans. *N. Engl. J. Med.* 360 (2009) 1509–1517.
- [72] W.D. van Marken Lichtenbelt, J.W. Vanhommerig, N.M. Smulders, J.M. Drossaerts, G.J. Kemerink, N.D. Bouvy, P. Schrauwen, G.J. Teule, Cold-activated brown adipose tissue in healthy men. *N. Engl. J. Med.* 360 (2009) 1500–1508.
- [73] V.P. Skulachev, Anion carriers in fatty acid-mediated physiological uncoupling. *J. Bioenerg. Biomembr.* 31 (1999) 431–445.
- [74] S.S. Korshunov, O.V. Korinkina, E.K. Runge, V.P. Skulachev, A.A. Starkov, Fatty acids as natural uncouplers preventing generation of O₂⁻ and H₂O₂ by mitochondria in the resting state. *FEBS Lett.* 435 (1998) 215–218.
- [75] S.M. Nadochiy, A.J. Tompkins, P.S. Brookes, Different mechanisms of mitochondrial proton leak in ischaemia/reperfusion injury and preconditioning: implications for pathology and cardioprotection. *Biochem. J.* 395 (2006) 611–618.
- [76] R.S. Carreira, S. Miyamoto, P. Di Mascio, L.M. Gonçalves, P. Monteiro, L.A. Providência, A.J. Kowaltowski, Ischemic preconditioning enhances fatty acid-dependent mitochondrial uncoupling. *J. Bioenerg. Biomembr.* 39 (2007) 313–320.
- [77] Y. Kirichok, G. Kravinsky, D.E. Clapham, The mitochondrial calcium uniporter is a highly selective ion channel. *Nature* 427 (2004) 360–364.
- [78] M. Trenker, R. Malli, I. Fertsch, S. Levak-Frank, W.F. Graier, Uncoupling proteins 2 and 3 are fundamental for mitochondrial Ca²⁺ uniporter. *Nat. Cell Biol.* 9 (2007) 445–452.
- [79] P.S. Brookes, N. Parker, J.A. Buckingham, A. Vidal-Puig, A.P. Halestrap, T.E. Gunter, D.G. Nicholls, P. Bernardi, J.J. Lemasters, M.D. Brand, UCPs—unlikely calcium porters. *Nat. Cell Biol.* 10 (2008) 1235–1237.
- [80] D. Jiang, L. Zhao, D.E. Clapham, Genome-wide RNAi screen identifies Letm1 as a mitochondrial Ca²⁺/H⁺ antiporter. *Science* 326 (2009) 144–147.
- [81] T.E. Gunter, L. Buntinas, G.C. Sparagna, K.K. Gunter, The Ca²⁺ transport mechanisms of mitochondria and Ca²⁺ uptake from physiological-type Ca²⁺ transients. *Biochim. Biophys. Acta* 1366 (1998) 5–15.
- [82] T.E. Gunter, D.J. Yule, K.K. Gunter, R.A. Eliseev, J.D. Salter, Calcium and mitochondria. *FEBS Lett.* 567 (2004) 96–102.
- [83] G. Csordás, A.P. Thomas, G. Hajnóczky, Quasi-synaptic calcium signal transmission between endoplasmic reticulum and mitochondria. *EMBO J.* 18 (1999) 96–108.
- [84] D.G. Nicholls, Mitochondria and calcium signaling. *Cell Calcium* 38 (2005) 311–317.
- [85] A.P. Thomas, G.S. Bird, G. Hajnóczky, L.D. Robb-Gaspers, J.W. Putney Jr., Spatial and temporal aspects of cellular calcium signaling. *FASEB J.* 10 (1996) 1505–1517.
- [86] P.S. Brookes, Y. Yoon, J.L. Robotham, M.W. Anders, S.S. Sheu, Calcium, ATP, and ROS: a mitochondrial love-hate triangle. *Am. J. Physiol. Cell Physiol.* 287 (2004) C817–C833.
- [87] A.A. Starkov, B.M. Polster, G. Fiskum, Regulation of hydrogen peroxide production by brain mitochondria by calcium and Bax. *J. Neurochem.* 83 (2002) 220–228.
- [88] Z. Komary, L. Tretter, V. Adam-Vizi, H₂O₂ generation is decreased by calcium in isolated brain mitochondria. *Biochim. Biophys. Acta* 1777 (2008) 800–807.
- [89] J.A. Dykens, Isolated cerebral and cerebellar mitochondria produce free radicals when exposed to elevated Ca²⁺ and Na⁺: implications for neurodegeneration. *J. Neurochem.* 63 (1994) 584–591.
- [90] A.J. Kowaltowski, R.F. Castilho, A.E. Vercesi, Ca²⁺-induced mitochondrial membrane permeabilization: role of coenzyme Q redox state. *Am. J. Physiol. Cell Physiol.* 269 (1995) C141–C147.
- [91] A.J. Kowaltowski, R.F. Castilho, A.E. Vercesi, Opening of the mitochondrial permeability transition pore by uncoupling or inorganic phosphate in the presence of Ca²⁺ is dependent on mitochondrial-generated reactive oxygen species. *FEBS Lett.* 378 (1996) 150–152.
- [92] T.V. Votyakova, I.J. Reynolds, Detection of hydrogen peroxide with Amplex Red: interference by NADH and reduced glutathione auto-oxidation. *Arch. Biochem. Biophys.* 431 (2004) 138–144.
- [93] M.T. Grijalba, A.E. Vercesi, S. Schreier, Ca²⁺-induced increased lipid packing and domain formation in submitochondrial particles. A possible early step in the mechanism of Ca²⁺-stimulated generation of reactive oxygen species by the respiratory chain. *Biochemistry* 38 (1999) 13279–13287.
- [94] A.J. Kowaltowski, R.F. Castilho, A.E. Vercesi, Mitochondrial permeability transition and oxidative stress. *FEBS Lett.* 495 (2001) 12–15.
- [95] A.E. Vercesi, A.J. Kowaltowski, H.C. Oliveira, R.F. Castilho, Mitochondrial Ca²⁺ transport, permeability transition and oxidative stress in cell death: implications in cardiotoxicity, neurodegeneration and dyslipidemias. *Front. Biosci.* 11 (2006) 2554–2564.
- [96] L.C. Alberici, H.C. Oliveira, E.J. Bighetti, E.C. De Faria, G.R. Degaspari, C.T. Souza, A.E. Vercesi, Hypertriglyceridemia increases mitochondrial resting respiration and susceptibility to permeability transition. *J. Bioenerg. Biomembr.* 35 (2003) 451–457.
- [97] P.J. Oliveira, T.C. Esteves, R. Seica, A.J. Moreno, M.S. Santos, Calcium-dependent mitochondrial permeability transition is augmented in the kidney of Goto-Kakizaki diabetic rat. *Diabetes Metab. Res. Rev.* 20 (2004) 131–136.
- [98] I. Inoue, H. Nagase, K. Kishi, T. Higuti, ATP-sensitive K⁺ channel in the mitochondrial inner membrane. *Nature* 352 (1991) 244–247.
- [99] P. Paucek, G. Mironova, F. Mahdi, A.D. Beavis, G. Woldegiorgis, K.D. Garlid, Reconstitution and partial purification of the glibenclamide-sensitive, ATP-dependent K⁺ channel from rat liver and beef heart mitochondria. *J. Biol. Chem.* 267 (1992) 26062–26069.
- [100] H.T. Facundo, M. Fornazari, A.J. Kowaltowski, Tissue protection mediated by mitochondrial K⁺ channels. *Biochim. Biophys. Acta* 1762 (2006) 202–212.
- [101] H. Ardehali, B. O'Rourke, Mitochondrial K(ATP) channels in cell survival and death. *J. Mol. Cell. Cardiol.* 39 (2005) 7–16.
- [102] A.D. Costa, K.D. Garlid, MitokATP activity in healthy and ischemic hearts. *J. Bioenerg. Biomembr.* 41 (2009) 123–126.
- [103] M. Jabůrek, V. Yarov-Yarovoy, P. Paucek, K.D. Garlid, State-dependent inhibition of the mitochondrial K_{ATP} channel by glyburide and 5-hydroxydecanoate. *J. Biol. Chem.* 273 (1998) 13578–13582.
- [104] E.A. Belyaeva, A. Szewczyk, B. Mikolajek, M.J. Nalecz, L. Wojtczak, Demonstration of glibenclamide-sensitive K⁺ fluxes in rat liver mitochondria. *Biochem. Mol. Biol. Int.* 31 (1993) 493–500.
- [105] A. Szewczyk, W. Jarmuszkievicz, W.S. Kunz, Mitochondrial potassium channels. *IUBMB Life* 61 (2009) 134–143.
- [106] A.J. Kowaltowski, S. Seetharaman, P. Paucek, K.D. Garlid, Bioenergetic consequences of opening the ATP-sensitive K⁺ channel of heart mitochondria. *Am. J. Physiol. Heart Circ. Physiol.* 280 (2001) H649–H657.
- [107] A.D. Costa, C.L. Quinlan, A. Andrukhiv, L.C. West, M. Jabůrek, K.D. Garlid, The direct physiological effects of mitoK_{ATP} opening on heart mitochondria. *Am. J. Physiol. Heart Circ. Physiol.* 290 (2006) H406–H415.
- [108] S. Miwa, M.D. Brand, Mitochondrial matrix reactive oxygen species production is very sensitive to mild uncoupling. *Biochem. Soc. Trans.* 31 (2003) 1300–1301.
- [109] A.A. Starkov, "Mild" uncoupling of mitochondria. *Biosci. Rep.* 17 (1997) 273–279.
- [110] V.P. Skulachev, Mitochondria, reactive oxygen species and longevity: some lessons from the Barja group. *Aging Cell* 3 (2004) 17–19.
- [111] E.B. Tahara, F.D. Navarete, A.J. Kowaltowski, Tissue-, substrate-, and site-specific characteristics of mitochondrial reactive oxygen species generation. *Free Radic. Biol. Med.* 46 (2009) 1283–1297.
- [112] R. Ferranti, M.M. da Silva, A.J. Kowaltowski, Mitochondrial ATP-sensitive K⁺ channel opening decreases reactive oxygen species generation. *FEBS Lett.* 536 (2003) 51–55.
- [113] H.T. Facundo, R.S. Carreira, J.G. de Paula, C.C. Santos, R. Ferranti, F.R. Laurindo, A.J. Kowaltowski, Ischemic preconditioning requires increases in reactive oxygen release independent of mitochondrial K⁺ channel activity. *Free Radic. Biol. Med.* 40 (2006) 469–479.
- [114] H.T. Facundo, J.G. de Paula, A.J. Kowaltowski, Mitochondrial ATP-sensitive K⁺ channels are redox-sensitive pathways that control reactive oxygen species production. *Free Radic. Biol. Med.* 42 (2007) 1039–1048.
- [115] M. Fornazari, J.G. de Paula, R.F. Castilho, A.J. Kowaltowski, Redox properties of the adenosine triphosphate-sensitive K⁺ channel in brain mitochondria. *J. Neurosci. Res.* 86 (2008) 1548–1556.
- [116] A. Andrukhiv, A.D. Costa, L.C. West, K.D. Garlid, Opening mitoK_{ATP} increases superoxide generation from complex I of the electron transport chain. *Am. J. Physiol. Heart Circ. Physiol.* 291 (2006) H2067–H2074.
- [117] D.X. Zhang, Y.F. Chen, W.B. Campbell, A.P. Zou, G.J. Gross, P.L. Li, Characteristics and superoxide-induced activation of reconstituted myocardial mitochondrial ATP-sensitive potassium channels. *Circ. Res.* 89 (2001) 1177–1183.
- [118] H.Y. Zhang, B.C. McPherson, H. Liu, T.S. Baman, P. Rock, Z. Yao, H₂O₂ opens mitochondrial K_{ATP} channels and inhibits GABA receptors via protein kinase C-epsilon in cardiomyocytes. *Am. J. Physiol. Heart Circ. Physiol.* 282 (2002) H1395–H1403.
- [119] A.D. Costa, K.D. Garlid, Intramitochondrial signaling: interactions among mitoK_{ATP}, PKCepsilon, ROS, and MPT. *Am. J. Physiol. Heart Circ. Physiol.* 295 (2008) H874–H882.
- [120] A.P. Wojtovich, P.S. Brookes, The endogenous mitochondrial complex II inhibitor malonate regulates mitochondrial ATP-sensitive potassium channels: implications for ischemic preconditioning. *Biochim. Biophys. Acta* 1777 (2008) 882–889.
- [121] L.C. Alberici, H.C. Oliveira, P.R. Patrício, A.J. Kowaltowski, A.E. Vercesi, Hyperlipidemic mice present enhanced catabolism and higher mitochondrial ATP-sensitive K⁺ channel activity. *Gastroenterology* 131 (2006) 1228–1234.
- [122] L.C. Alberici, H.C. Oliveira, B.A. Paim, C.C. Mantello, A.C. Augusto, K.G. Zecchin, S.A. Gurgueira, A.J. Kowaltowski, A.E. Vercesi, Mitochondrial ATP-sensitive K⁺

- channels as redox signaling to liver mitochondria in response to hypertriglyceridemia, *Free Radic. Biol. Med.* 47 (2009) 1432–1439.
- [123] E.L. Whiteman, H. Cho, M.J. Birnbaum, Role of Akt/protein kinase B in metabolism, *Trends Endocrinol. Metab.* 13 (2002) 444–451.
- [124] Y. Wang, N. Ahmad, M. Kudo, M. Ashraf, Contribution of Akt and endothelial nitric oxide synthase to diazoxide-induced late preconditioning, *Am. J. Physiol. Heart Circ. Physiol.* 287 (2004) H1125–H1131.
- [125] N. Ahmad, Y. Wang, K.H. Haider, B. Wang, Z. Pasha, O. Uzun, M. Ashraf, Cardiac protection by mitoK_{ATP} channels is dependent on Akt translocation from cytosol to mitochondria during late preconditioning, *Am. J. Physiol. Heart Circ. Physiol.* 290 (2006) H2402–H2408.
- [126] K.D. Garlid, P. Dos Santos, Z.J. Xie, A.D. Costa, P. Paucek, Mitochondrial potassium transport: the role of the mitochondrial ATP-sensitive K⁺ channel in cardiac function and cardioprotection, *Biochim. Biophys. Acta* 1606 (2003) 1–21.
- [127] S.P. Jones, W.G. Girod, D.N. Granger, A.J. Palazzo, D.J. Lefer, Reperfusion injury is not affected by blockade of P-selectin in the diabetic mouse heart, *Am. J. Physiol. Heart Circ. Physiol.* 277 (1999) H763–H769.
- [128] J.R. Kersten, M.W. Montgomery, T. Ghassemi, E.R. Gross, W.G. Toller, P.S. Pagel, D.C. Waritier, Diabetes and hyperglycemia impair activation of mitochondrial K_{ATP} channels, *Am. J. Physiol. Heart Circ. Physiol.* 280 (2001) H1744–H1750.
- [129] J.J. Greer, D.P. Ware, D.J. Lefer, Myocardial infarction and heart failure in the db/db diabetic mouse, *Am. J. Physiol. Heart Circ. Physiol.* 290 (2005) H146–H153.
- [130] A. Tsang, D.J. Hausenloy, M.M. Mocanu, R.D. Carr, D.M. Yellon, Preconditioning the diabetic heart: the importance of Akt phosphorylation, *Diabetes* 54 (2005) 2360–2364.
- [131] M. Rendell, The role of sulphonylureas in the management of type 2 diabetes mellitus, *Drugs* 64 (2004) 1339–1358.

Ap.3. Redox regulation of the mitochondrial K(ATP) channel in cardioprotection

Biochimica et Biophysica Acta 1813 (2011) 1309–1315



Contents lists available at ScienceDirect

Biochimica et Biophysica Acta

journal homepage: www.elsevier.com/locate/bbamcr

Redox regulation of the mitochondrial K_{ATP} channel in cardioprotection[☆]Bruno B. Queliconi^{a,1}, Andrew P. Wojtovich^{b,1}, Sergiy M. Nadtochiy^b,
Alicia J. Kowaltowski^a, Paul S. Brookes^{b,*}^a Departamento de Bioquímica, Instituto de Química, Universidade de São Paulo, São Paulo, SP, Brazil^b Department of Anesthesiology, University of Rochester Medical Center, Rochester, NY, USA

ARTICLE INFO

Article history:

Received 4 June 2010

Received in revised form 5 October 2010

Accepted 11 November 2010

Available online 20 November 2010

Keywords:

K⁺ channel

Ischemia

Preconditioning

Nitric oxide

Redox

ABSTRACT

The mitochondrial ATP-sensitive potassium channel (mK_{ATP}) is important in the protective mechanism of ischemic preconditioning (IPC). The channel is reportedly sensitive to reactive oxygen and nitrogen species, and the aim of this study was to compare such species in parallel, to build a more comprehensive picture of mK_{ATP} regulation. mK_{ATP} activity was measured by both osmotic swelling and Ti⁺ flux assays, in isolated rat heart mitochondria. An isolated adult rat cardiomyocyte model of ischemia–reperfusion (IR) injury was also used to determine the role of mK_{ATP} in cardioprotection by nitroxyl. Key findings were as follows: (i) mK_{ATP} was activated by O₂^{•−} and H₂O₂ but not other peroxides. (ii) mK_{ATP} was inhibited by NADPH. (iii) mK_{ATP} was activated by S-nitrosothiols, nitroxyl, and nitrolinoleate. The latter two species also inhibited mitochondrial complex II. (iv) Nitroxyl protected cardiomyocytes against IR injury in an mK_{ATP}-dependent manner. Overall, these results suggest that the mK_{ATP} channel is activated by specific reactive oxygen and nitrogen species, and inhibited by NADPH. The redox modulation of mK_{ATP} may be an underlying mechanism for its regulation in the context of IPC. This article is part of a Special Issue entitled: Mitochondria and Cardioprotection.

© 2010 Elsevier B.V. All rights reserved.

1. Introduction

The past 25 years has witnessed much investigation into the phenomenon of ischemic preconditioning (IPC), in which short non-lethal periods of ischemia and reperfusion (IR) can elicit protection against prolonged ischemia–reperfusion (IR) injury [1]. Despite this effort, the mechanism by which IPC protects organs such as the heart and brain from IR injury is still debated.

One proposed mechanism of IPC-induced cardioprotection is the opening of a mitochondrial ATP-sensitive potassium channel (mK_{ATP}), which elicits mild swelling of the mitochondrial matrix. This in turn is thought to impact on mitochondrial Ca²⁺ loading, reactive oxygen species (ROS) generation, metabolic efficiency, and assembly of the permeability transition pore [2], and these downstream events bring about protection via unclear mechanisms. Although the molecular identity of the mK_{ATP} channel remains unknown, several pharmacologic mK_{ATP} modulators mimic IPC, and many IPC signaling pathways are thought to converge on mK_{ATP} as an end effector [3].

Mitochondria are a quantitatively significant source of ROS, which contribute to tissue damage during ischemia, but are also mediators of IPC signaling [4]. Accumulating evidence suggests that redox signaling

pathways play an important role in IPC [5–9], and can promote mK_{ATP} activation [10–15]. The primary ROS generated by mitochondria is superoxide (O₂^{•−}) [16,17], while hydrogen peroxide (H₂O₂) or lipid peroxides can be formed secondarily [17]. Both O₂^{•−} and H₂O₂ are thought to activate mK_{ATP} [13,18–20], although conflicting reports exist regarding O₂^{•−} [18,20]. The effect of other peroxides on mK_{ATP} is not known. Furthermore, it is apparent that some but not all types of antioxidants can inhibit IPC and mK_{ATP} activity [6,13], warranting further investigation. Table 1 summarizes the disparate results to date regarding redox regulation of the mK_{ATP} channel.

Nitric oxide (NO[•]) is also implicated in IPC, and elicits a large variety of cardioprotective effects [21]. NO[•] has been detected in isolated mitochondrial preparations [22], and can secondarily generate many reactive nitrogen species (RNS) [23–25], which can serve either damaging or beneficial signaling roles [17,21,25,26]. mK_{ATP} is a potential target for such RNS, and while high doses (10 mM) of an S-nitrosothiol have been shown to activate the channel in intact mitochondria [20], evidence for more subtle physiologically relevant effects of NO[•] has mostly relied on indirect measures of channel activity [27] or study of the channel removed from its mitochondrial environment [28]. Thus, it is not clear whether the levels of NO[•] that would be experienced inside mitochondria are capable of modulating mK_{ATP} activity.

The one electron reduction product of NO[•], nitroxyl (HNO) may also modulate the mK_{ATP} channel. Nitroxyl is protective in IR injury [29], and while it shares some signaling pathways with NO[•], it also possesses distinct biochemistry from NO[•], such as a direct interaction

[☆] This article is part of a Special Issue entitled: Mitochondria and Cardioprotection.

* Corresponding author. Dept. of Anesthesiology, University of Rochester Medical Center, 601 Elmwood Avenue, Rochester, NY 14642, USA. Tel.: +1 585 273 1626.

E-mail address: paul_brookes@urmc.rochester.edu (P.S. Brookes).

¹ These authors contributed equally to this work.

Table 1
Previous studies on the effects of oxidants, reactive nitrogen species, antioxidants and reducing agents on mK_{ATP} channel activity.

Reagent	Conc.	Effects	Experimental conditions	References
Ascorbate	1 mM	No effect	Isolated mitochondria	[12]
DTE	10 mM	Inhibits glyburide binding	Submitochondrial particles	[46]
DTNB	500 μ M	Inhibits glyburide binding	Submitochondrial particles	[46]
DTT	100 μ M	Inhibits activation by DZX	Isolated mitochondria	[12,13]
	1 mM	Activates run-down channels Loss in selectivity	Reconstituted channels	[66]
	10 mM	Inhibits glyburide binding	Submitochondrial particles	[46]
Mersalyl	100 μ M	Inhibits glyburide binding	Submitochondrial particles	[46]
MPG	200 μ M	Inhibits activation by DZX	Isolated mitochondria	[12,13,31]
NAC	4 mM	Inhibits activation by DZX	Isolated mitochondria	[12,13]
NEM	2 mM	Inhibits activation by $O_2^{\cdot-}$	Reconstituted channels	[18]
		Inhibits glyburide binding	Submitochondrial particles	[46]
	60 nmol/mg	Decreases selectivity	Isolated mitochondria	[67]
Thimerosal	500 μ M	Inhibits glyburide binding	Submitochondrial particles	[46]
X/XO	0.038 U/mL	Activates	Reconstituted channels	[18]
	6 mU/mL	No Effect	Isolated mitochondria	[20]
H_2O_2	1 μ M	Activates	Isolated mitochondria	[13]
	1 μ M	Activates	Isolated mitochondria	[19]
	6 mU/mL X/XO + 30 U SOD	Activates	Isolated mitochondria	[20]
SNAP	10 mM	Activates	Isolated mitochondria	[20]

with thiols. In this regard, the nitroxyl donor Angeli's salt (AS) inhibits mitochondrial complex II in a manner sensitive to glutathione and independent of S-nitrosation [30]. mK_{ATP} activity is exquisitely sensitive to complex II modulation [31,32], and herein we explored the concept that nitroxyl may regulate mK_{ATP} via effects on complex II.

Despite a collection of studies to date examining the effect of single redox agents on mK_{ATP} , often at high doses, a comparative study across a wide range of doses is lacking. In addition, unique chemical properties of certain NO^* derived species have precluded their use to date in studying mK_{ATP} . The current study aimed to address such issues, and the collective results suggest that mitochondrial redox state is an important regulator of mK_{ATP} channel activity, mitochondrial function, and cardioprotection in the context of IPC.

2. Materials and methods

Full experimental details are in the online supplement.

2.1. Animals, chemicals and supplies

Male Sprague–Dawley rats, 200–300 g, were purchased from Harlan (Indianapolis, IN) or bred at the *Biotério do Conjunto das Químicas (Universidade de São Paulo)* housed on a 12 h light/dark cycle with food and water available *ad libitum*. All procedures were performed in accordance with the US National Institutes of Health "Guide for the care and use of laboratory animals" and the *Colégio Brasileiro de Experimentação Animal*, and were approved by the appropriate university animal ethics committees. Linoleic peroxide was a kind gift from Sayuri Miyamoto (São Paulo) and stored under argon in methanol [33]. Nitro-linoleate was synthesized and analyzed as previously described [34]. All other reagents used were analytical grade or higher, obtained from Sigma (St. Louis MO) or EMD (Gibbstown NJ).

2.2. Mitochondrial isolation, Cx-II, and mK_{ATP} assays

Heart mitochondria were rapidly isolated as previously described [31,35]. Cx-II activity was measured as previously described [31,32]. mK_{ATP} activity was measured by osmotic swelling as previously described [32,36]. All channel modulating agents (reactive oxygen and nitrogen species, antioxidants, etc.) were present in the assay buffer prior to mitochondrial addition. The nature of the mK_{ATP} osmotic swelling assay, requiring mitochondrial addition last of all,

precludes its use to study highly reactive species such as HNO [37]. In such cases a fluorescence-based Ca^{2+} flux assay for mK_{ATP} activity [38] was used, permitting incubation of mitochondria prior to assay initiation by Ca^{2+} addition.

2.3. Cardiomyocyte model of IR injury

Adult rat ventricular myocytes were isolated, and a model of simulated IR (SIR) injury was as previously described [32]. Cells were incubated in anoxic glucose-free Krebs Henseleit (KH) buffer at pH 6.5 for 30 min, followed by reoxygenation in glucose-replete KH at pH 7.4. Where indicated, compounds were present 20 min prior to the onset of simulated ischemia. At the end of all protocols, viability was determined by Trypan blue exclusion.

2.4. Statistics

All experiments were performed on at least 3 independent mitochondrial or cell preparations, and results are presented as mean \pm SEM. Statistical significance between groups was determined by ANOVA.

3. Results and discussion

3.1. mK_{ATP} is activated by some but not all peroxides

While the ability of ROS to modulate mK_{ATP} activity has been reported [13,18–20], the differential action of various classes of ROS is less well understood. In particular, ROS such as H_2O_2 may initiate chemistry that generates secondary peroxides such as lipid hydroperoxides (LOOH) [17]. We therefore hypothesized that peroxides may modulate mK_{ATP} activity. In Fig. 1A, the effects of H_2O_2 , *t*-butyl hydroperoxide (*t*-BuOOH), and linoleic hydroperoxide (LOOH) on mK_{ATP} were tested. Interestingly, while H_2O_2 robustly opened the channel at 1 μ M, higher concentrations of *t*-BuOOH and LOOH did not. The differential hydrophobicity of *t*-BuOOH, LOOH, and H_2O_2 suggests that the peroxide sensor of mK_{ATP} may be in a hydrophilic region of the molecule. Alternatively, it has been suggested that H_2O_2 activation of the mK_{ATP} may occur via a PKC ϵ dependent mechanism [20], although the location of the kinase in this particular mitochondrial preparation is unknown.

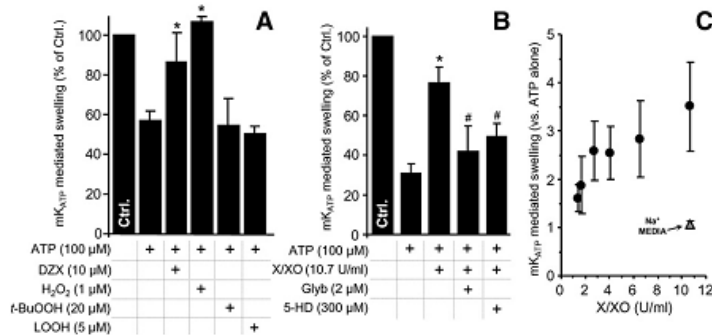


Fig. 1. Selective mK_{ATP} activation by ROS; mK_{ATP} activity was measured by osmotic swelling as detailed in *Materials and methods*. Controls (Na^+ based media) are in Fig. S1. (A): mK_{ATP} is activated by H_2O_2 but not by t -BuOOH or LOOH. Diazoxide (DZX) opening of mK_{ATP} was used as a positive control. (B): mK_{ATP} activation by $O_2^{\cdot-}$ generated by the X/XO system. Glyburide (Glyb) and 5-hydroxydecanoate (5-HD) are mK_{ATP} antagonists. (C): Dose response of mK_{ATP} activation by X/XO in K^+ (black circles) or Na^+ (gray triangles) based media. * $p < 0.05$ vs. ATP alone. # $p < 0.05$ vs. ATP + H_2O_2 or X/XO. Experimental conditions are listed below the X axis.

3.2. mK_{ATP} is activated by supra-physiological levels of superoxide

Activation of mK_{ATP} by $O_2^{\cdot-}$ has been reported previously [18], but at relatively high doses. It is unclear whether the amounts of $O_2^{\cdot-}$ made by mitochondria are capable of modulating mK_{ATP} activity. To investigate this, a xanthine/xanthine oxidase (X/XO) system was used to modulate ROS flux. Fig. 1B and C shows that XO levels as low as 1.4 U/ml (approximating to a $O_2^{\cdot-}$ flux of 1.2 $\mu M/min$) activated the channel. Reported maximal rates of $O_2^{\cdot-}$ generation by heart mitochondria range from 30 nM/min to 1 $\mu M/min$ [39,40]. Thus, it is unlikely that mitochondrial $O_2^{\cdot-}$ generation under normal conditions approaches levels required for mK_{ATP} channel activation. This finding suggests that the channel would only be activated in situ with ROS originated from non-mitochondrial sources or conditions that increase ROS production such as pre- and post-conditioning. Also under conditions of reverse electron flow, $O_2^{\cdot-}$ in the mitochondrial microenvironment may reach levels capable of activating the channel [13]. No effect of H_2O_2 or X/XO on mitochondrial swelling was observed in Na^+ based media (supplemental Fig. 1).

3.3. mK_{ATP} is inhibited by some but not all reductants/antioxidants

While IPC is inhibited by both thiol antioxidants and catalase (suggesting a role for H_2O_2 [12]), cardioprotection by mK_{ATP} agonists such as diazoxide is prevented only by thiol antioxidants [13], suggesting that antioxidant-sensitive proteins distinct from mK_{ATP} may be important in IPC (e.g. SERCA, [41]). Thus, a detailed understanding of the selective regulation of mK_{ATP} by reductants is a key step toward understanding its role in IPC.

The effect of several reducing agents on mK_{ATP} activity was tested under baseline conditions and conditions of maximal channel opening (presence of ATP and diazoxide). Fig. 2 shows that while most reducing agents had a mild inhibitory effect on mK_{ATP} activity, NADPH was a strong inhibitor, almost completely preventing channel activity. Compiling these data with those from our previous study [13], supplemental Fig. 2 shows the ability of reductants to inhibit mK_{ATP} channel activity correlated with redox potential ($r^2 = 0.73$). A notable outlier to this correlation was NADPH (inclusion of NADPH in the linear regression fit lowers r^2 to 0.43). The underlying mechanism for a difference in the effect of NADH vs. NADPH, despite their identical redox potentials, is elusive at this stage. Interestingly, while both surface K_{ATP} channels [42–45] and the mK_{ATP} [12,13,18,46,47] do have redox active thiols, NADPH does not directly reduce thiols, suggesting that its direct redox activity is not the mechanism of channel regulation.

Nevertheless, NADPH does play an important role in overall mitochondrial redox status; transhydrogenases reduce mitochondrial $NADP^+$ using electrons from NADH and the electrochemical proton gradient as an energy source [48]. The resulting NADPH is used as an electron source for thiol peroxidase removal systems, including glutathione and thioredoxin peroxidase/reductase [17]. Thus, the finding that NADPH can regulate mK_{ATP} activity suggests that this channel may play a role in sensing both energy metabolism and redox status [13,49].

Notably, surface K_{ATP} channel activity has been shown to be sensitive to pyridine nucleotides [50], possibly at the same site as adenine nucleotides modulate channel activity. Furthermore, insulin secretion in pancreatic β cells, which occurs secondarily to K_{ATP} closure, correlates with NADPH/NADP⁺ ratios [51]. Thus, a direct modulation of the mK_{ATP} channel by NADPH binding may occur. Another possibility might be that NADPH competes with DZX for a binding site on the mK_{ATP} channel. However, we consider this unlikely since NADPH was also able to inhibit channel opening by the structurally unrelated opener atpenin A5 [32] (supplemental Fig. 3).

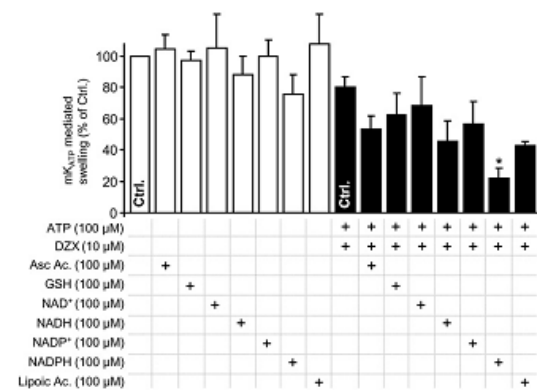


Fig. 2. Inhibition of DZX-activated mK_{ATP} by reductants; mK_{ATP} activity was measured by osmotic swelling as detailed in *Materials and methods*. Data are shown for the baseline condition (open bars) or maximal swelling in the presence of both ATP and DZX (filled bars). Reductants were present in the media before mitochondrial addition, at the concentrations indicated. * $p < 0.05$ vs. the appropriate control (bar marked Ctrl.) in the absence of reductant.

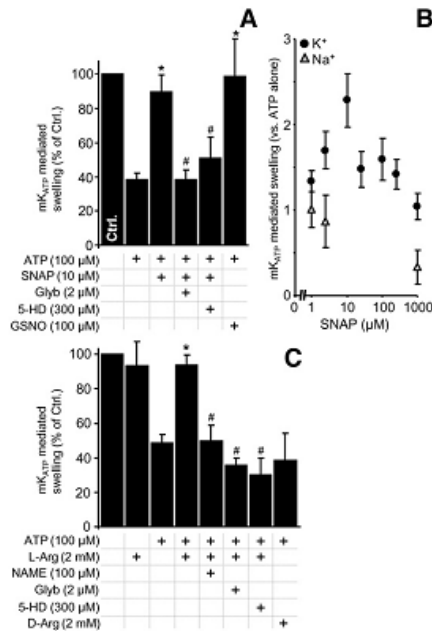


Fig. 3. mK_{ATP} activation by S-nitrosothiols and mitochondrial-associated NOS: mK_{ATP} activity was measured by osmotic swelling as detailed in *Materials and methods*. Controls (Na^+ based media) are in Fig. S2. (A): mK_{ATP} was activated by S-nitrosoacetylpenicillamine (SNAP) and S-nitrosoglutathione (GSNO), at the indicated doses. (B): Dose response of mK_{ATP} activation by SNAP in K^+ (black circles) or Na^+ (gray triangles) based media. * $p < 0.05$ vs. ATP alone. # $p < 0.05$ vs. ATP plus SNAP. (C): mK_{ATP} activation by NOS modulators. L- or D-Arginine, L-nitroarginine methyl ester (NAME), Glyb and 5-HD were present at the concentrations indicated. * $p < 0.05$ vs. ATP alone. # $p < 0.05$ vs. ATP plus L-arginine.

3.4. mK_{ATP} is activated by S-nitrosothiols and L-arginine

In addition to ROS, much recent interest has focused on mK_{ATP} as a possible target for NO^* or its redox congeners [20]. While NO^* effects on mK_{ATP} activity in intact cells are thought to be mediated via cGMP signaling [52,53], direct effects of NO^* on the purified channel have been measured in planar bilayer studies [28]. In addition NO^* was shown to activate mK_{ATP} in mitochondria by using flavoprotein fluorescence as a read-out [27]. However, the dose response of mK_{ATP} to NO^* in intact mitochondria is unknown. Fig. 3A and B shows that S-nitrosoacetylpenicillamine (SNAP) dose-dependently activated mK_{ATP} in a glybenclamide and 5-HD sensitive manner. Notably, $>10 \mu M$ SNAP led to mK_{ATP} inhibition, presumably due to NO^* inhibition of cytochrome c oxidase [54] leading to mitochondrial de-energization, removing the driving force for K^+ uptake. SNAP did not activate swelling in Na^+ based buffers (supplemental Fig. 4). Notably, the optimal SNAP concentration for mK_{ATP} channel opening in this study (10 μM) is 3 orders of magnitude lower than previously reported (Table 1). We are unsure as to the origin of this very large discrepancy [20].

There has been much interest in the possibility that mitochondria may contain a nitric oxide synthase, termed "mtNOS". Despite recent developments including retraction of some work [55–57], NOS is a common contaminant of isolated mitochondrial preparations [58]. This may be particularly applicable to mK_{ATP} studies, since a rapid and crude mitochondrial isolation is required to effectively measure channel activity (full experimental details are in the online supplement) [32,36]. The data in Fig. 3C show that the NOS substrate L-arginine stimulates mK_{ATP}

opening, in a manner sensitive to the NOS inhibitor L-NAME. No effect was seen with D-arginine, suggesting that the origin of this effect resides at the level of a mitochondrially associated NOS or L-NAME-sensitive enzyme. Unfortunately, further purification of mitochondria that would be required to assert a mitochondria-resident NOS in mediating these effects, also results in loss of mK_{ATP} channel activity, in a manner mechanically related to classical channel "run-down" [38].

3.5. Certain RNS can activate mK_{ATP} via a mechanism involving mitochondrial complex II

In addition to "classical" RNS such as NO^* , RNS such as nitro-lipids and nitroxyl may regulate mK_{ATP} . Nitro-lipids are an emerging class of anti-inflammatory signaling lipids which can mediate NO^* signaling [59,60] and are known to be generated during IPC [34,61]. One example of a nitro-lipid, nitrooleate ($LA-NO_2$), can elicit cardioprotection in a cGMP-independent manner [34,62]. Fig. 4A shows that, low doses (0.5 μM) of $LA-NO_2$ opened the mK_{ATP} channel in a 5-HD- and glyburide-sensitive manner, while native linoleic acid (LA) did not. Complex II of the mitochondrial respiratory chain has been proposed as an important regulator of mK_{ATP} activity [31,32,63], and in this regard Fig. 4B shows that $LA-NO_2$, but not LA, inhibited complex II in a dose-dependent manner. Notably however, the amount of $LA-NO_2$ required to open the channel was significantly lower than that required to inhibit complex II (see below for discussion).

The disparate effects of $LA-NO_2$ (stimulation mK_{ATP} activity), and lipid hydroperoxide (no effect on mK_{ATP} , see section 3.1) highlight the different chemical properties of these species. While both are hydrophobic reactive lipids, only $LA-NO_2$ possesses an electrophilic moiety that can adduct thiols by Michael addition [61]. Thus it is suggested that the mechanism of $LA-NO_2$ mediated mK_{ATP} opening may involve modification of thiols on the channel (c.f. section 3.3).

The levels of $LA-NO_2$ generated inside mitochondria during IPC may reach 1 μM [34], raising the possibility that $LA-NO_2$ is an important endogenous mK_{ATP} regulator. However, we previously showed that cardioprotection induced by exogenously added $LA-NO_2$ was insensitive to mK_{ATP} blockers [34], suggesting that other mechanisms of $LA-NO_2$ action (e.g. mild uncoupling) may account for its cardioprotective effects.

Similar to nitro-lipids, the importance of nitroxyl in cardiovascular signaling has also been the subject of recent attention [29,37]. In agreement with previous findings, we showed that the nitroxyl donor Angeli's salt (AS) dose-dependently inhibited complex II in rat heart mitochondria (Fig. 5A). Consistent with an interaction between complex II and the mK_{ATP} channel, we also found that Angeli's salt

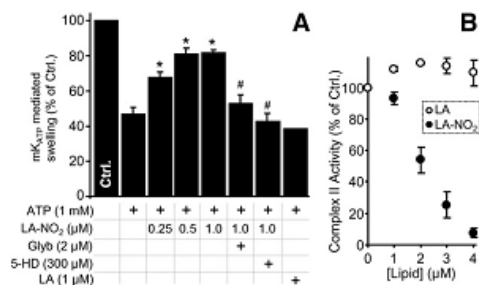


Fig. 4. $LA-NO_2$ opens mK_{ATP} and inhibits complex II: (A): mK_{ATP} activity was measured by osmotic swelling as detailed in *Materials and methods*. $LA-NO_2$, native linoleate (LA), Glyb, and 5-HD were present at the indicated concentrations. * $p < 0.05$ vs. ATP alone. # $p < 0.05$ vs. ATP plus $LA-NO_2$. (B): Complex II activity in the presence of $LA-NO_2$ was determined as detailed in *Materials and methods*. Values are expressed as percentage of control complex II rate ($128 \pm 26 \text{ nmol DCPIP min}^{-1} \text{ mg protein}^{-1}$).

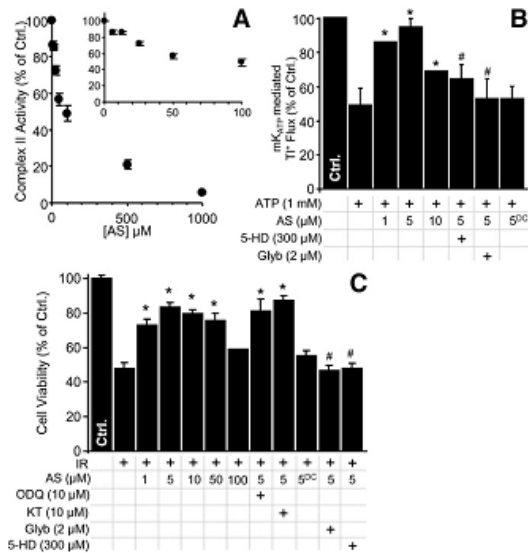


Fig. 5. Nitroxyl inhibits complex II, opens mK_{ATP} and is cardioprotective: (A): Complex II activity was measured, following nitroxyl exposure of mitochondria, as described in *Materials and methods*. Values are expressed as percentage of control complex II rate (108 ± 8 nmol DCPiP min^{-1} mg protein $^{-1}$). (B): Nitroxyl activation of mK_{ATP} was monitored using a novel Ti^+ flux assay as described in *Materials and methods*. Data show the magnitude of change in intra-mitochondrial Ti^+ based fluorescence following Ti^+ addition, relative to control. 5-HD, Glyb, the nitroxyl donor Angeli's salt (AS) and decomposed AS (AS^{PC}) were present at the indicated concentrations. * $p < 0.05$ vs. ATP alone. # $p < 0.05$ vs. ATP plus 5 μM AS. (C): Nitroxyl protects against cardiomyocyte IR injury. Cell viability was measured via Trypan blue exclusion at the end of reoxygenation, as described in *Materials and methods*, and expressed as percentage of control (normoxic) cell viability. 5-HD, Glyb, Angeli's salt (AS), decomposed AS (AS^{PC}), the PKG inhibitor KT-5823 (KT) or the soluble guanylate cyclase inhibitor ODQ were present at the indicated concentrations. * $p < 0.05$ vs. IR alone. # $p < 0.05$ vs. IR plus 5 μM AS.

opened mK_{ATP} in a manner sensitive to 5-HD and glyburide (Fig. 5B). Furthermore, in agreement with previous studies [29,64] Angeli's salt was protective in a cardiomyocyte model of IR injury. This protection was sensitive to 5-HD and glyburide, but insensitive to the guanylate cyclase inhibitor ODQ or the protein kinase G inhibitor KT-5823 (Fig. 5C). The role of other known components of the preconditioning signaling pathway (e.g. PKC, ERK, PI3 kinase) in mediating the effects of Angeli's salt is currently unknown, although none of these signals has previously been linked to nitroxyl. Together, these data suggest that Angeli's salt mediated cardioprotection proceeds via non-PKG mediated activation of mK_{ATP} , possibly involving an inhibition of complex II.

Both nitroxyl and LA- NO_2 inhibit mitochondrial complex II, activate mK_{ATP} , and are known to react with complex II thiols [30,34]. This suggests that modification of complex II thiols may underlie the mechanism of mK_{ATP} activation. However, the concentrations of nitroxyl and LA- NO_2 which activated mK_{ATP} did not significantly inhibit complex II enzymatic activity (Figs. 4 and 5). In this regard, nitroxyl and LA- NO_2 are similar to other species which activate the mK_{ATP} at doses far below those at which they inhibit complex II, including atpenin A5 [32], malonate [31] and diazoxide [65]. Thus, the regulation of mK_{ATP} activity appears to be mechanistically divorced from the bulk enzymatic activity of complex II itself. The fact that 5 unrelated compounds which inhibit complex II by distinct mechanisms all activate mK_{ATP} at lower concentrations, collectively suggests that a small sub-population of complex II may play an important role in regulating mK_{ATP} activity, while not impacting total complex II enzymatic activity.

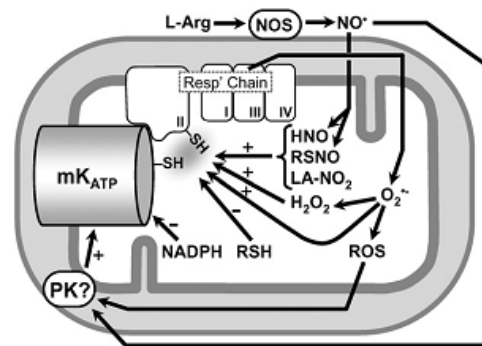


Fig. 6. Schematic showing redox regulation of mK_{ATP} . Nitroxyl (HNO), RSNO, and LA- NO_2 activate the channel, possibly via thiols on the channel itself or on complex II of the respiratory chain. The ability of low molecular weight thiols (RSH) to inhibit the channel may also be mediated via thiols on the channel or on complex II. In contrast, the effects of NADPH are likely no mediated via thiols. The ability of NO^+ to activate the channel may be mediated via the generation of secondary RNS (e.g. RSNO, LA- NO_2 , HNO), which can activate the channel via PKG-independent mechanisms, or via classical NO^+ protein kinase signaling. ROS (in particular H_2O_2) can also activate the channel, via mechanisms that may include thiol modification or protein kinase signaling. The nature of the interaction between complex II and the subunits of the mK_{ATP} channel itself remains to be elucidated.

4. Conclusions

In summary, a variety of redox active species, including ROS, RNS, antioxidants, and reductants, all act on the mK_{ATP} . While a broad conclusion of this work can be summarized as "oxidants activate, reductants inhibit", it is apparent that many species do not conform to this simple model. Key examples include NADPH, which may regulate the channel via direct binding, and LA- NO_2 and nitroxyl, which are thought to mediate their effects via complex II. A summary of the potential mechanisms of mK_{ATP} channel modulation by various species is shown in Fig. 6. Clearly, further work in this area, including the molecular identification of the mK_{ATP} itself, and the redox-sensitive residues within it, will facilitate a better understanding of the role that channel regulation by redox plays in events such as IPC.

Acknowledgements

We thank Camille C. Caldeira da Silva (São Paulo) and Emily Redman (Rochester) for technical support, and Sayuri Miyamoto (São Paulo) for providing linoleic hydroperoxide. This work was supported by the National Institutes of Health [HL-071158 and GM-087483 to PSB]; the John Simon Guggenheim Memorial Foundation [AJK]; the Fundação de Amparo à Pesquisa do Estado de São Paulo (FAPESP) [AJK]; the Instituto Nacional de Ciência e Tecnologia de Processos Redox em Biomedicina (Redoxoma) [AJK]; the American Heart Association Founders Affiliate [0815770D to APW]; and FAPESP Predoctoral Fellowship [BBQ].

Appendix A. Supplementary data

Supplementary data to this article can be found online at doi:10.1016/j.bbamcr.2010.11.005.

References

- C.E. Murry, R.B. Jennings, K.A. Reimer, Preconditioning with ischemia: a delay of lethal cell injury in ischemic myocardium, *Circulation* 74 (1986) 1124–1136.
- H.T. Facundo, M. Fornazari, A.J. Kowaltowski, Tissue protection mediated by mitochondrial K^+ channels, *Biochim. Biophys. Acta* 1762 (2006) 202–212.

- [3] K.D. Garlid, S.P. Dos, Z.J. Xie, A.D. Costa, P. Paucuk, Mitochondrial potassium transport: the role of the mitochondrial ATP-sensitive K(+) channel in cardiac function and cardioprotection, *Biochim. Biophys. Acta* 1606 (2003) 1–21.
- [4] E. Murphy, C. Steenbergen, Preconditioning: the mitochondrial connection, *Annu. Rev. Physiol.* 69 (2007) 51–67.
- [5] T.L. Vanden Hoek, L.B. Becker, Z. Shao, C. Li, P.T. Schumacker, Reactive oxygen species released from mitochondria during brief hypoxia induce preconditioning in cardiomyocytes, *J. Biol. Chem.* 273 (1998) 18092–18098.
- [6] W. Chen, S. Gabel, C. Steenbergen, E. Murphy, A redox-based mechanism for cardioprotection induced by ischemic preconditioning in perfused rat heart, *Circ. Res.* 77 (1995) 424–429.
- [7] L.B. Becker, T.L. Vanden Hoek, Z.H. Shao, C.Q. Li, P.T. Schumacker, Generation of superoxide in cardiomyocytes during ischemia before reperfusion, *Am. J. Physiol.* 277 (1999) H2240–H2246.
- [8] C. Penna, D. Mancardi, R. Rastaldo, P. Pagliaro, Cardioprotection: a radical view. Free radicals in pre and postconditioning, *Biochim. Biophys. Acta* 1787 (2009) 781–793.
- [9] C.P. Baines, M. Goto, J.M. Downey, Oxygen radicals released during ischemic preconditioning contribute to cardioprotection in the rabbit myocardium, *J. Mol. Cell. Cardiol.* 29 (1997) 207–216.
- [10] R.A. Forbes, C. Steenbergen, E. Murphy, Diazoxide-induced cardioprotection requires signaling through a redox-sensitive mechanism, *Circ. Res.* 88 (2001) 802–809.
- [11] T. Pain, X.M. Yang, S.D. Critz, Y. Yue, A. Nakano, G.S. Liu, G. Heusch, M.V. Cohen, J.M. Downey, Opening of mitochondrial K(ATP) channels triggers the preconditioned state by generating free radicals, *Circ. Res.* 87 (2000) 460–466.
- [12] H.T. Facundo, F.S. Carreira, J.G. de Paula, C.C. Santos, R. Ferranti, F.R. Laurindo, A.J. Kowaltowski, Ischemic preconditioning requires increases in reactive oxygen release independent of mitochondrial K⁺ channel activity, *Free Radic. Biol. Med.* 40 (2006) 469–479.
- [13] H.T. Facundo, J.G. de Paula, A.J. Kowaltowski, Mitochondrial ATP-sensitive K⁺ channels are redox-sensitive pathways that control reactive oxygen species production, *Free Radic. Biol. Med.* 42 (2007) 1039–1048.
- [14] Y. Yue, Q. Qin, M.V. Cohen, J.M. Downey, S.D. Critz, The relative order of mK(ATP) channels, free radicals and p38 MAPK in preconditioning's protective pathway in rat heart, *Cardiovasc. Res.* 55 (2002) 681–689.
- [15] P. Pasdois, C.L. Quinlan, A. Rissa, L. Tariosse, B. Vinassa, A.D. Costa, S.V. Pierre, S.P. Dos, K.D. Garlid, Ouabain protects rat hearts against ischemia–reperfusion injury via pathway involving src kinase, mitoKATP, and ROS, *Am. J. Physiol.* 292 (2007) H1470–H1478.
- [16] M.P. Murphy, How mitochondria produce reactive oxygen species, *Biochem. J.* 417 (2009) 1–13.
- [17] A.J. Kowaltowski, N.C. de Souza-Pinto, R.F. Castilho, A.E. Vercesi, Mitochondria and reactive oxygen species, *Free Radic. Biol. Med.* 47 (2009) 333–343.
- [18] D.X. Zhang, Y.F. Chen, W.B. Campbell, A.P. Zou, G.J. Gross, P.L. Li, Characteristics and superoxide-induced activation of reconstituted myocardial mitochondrial ATP-sensitive potassium channels, *Circ. Res.* 89 (2001) 1177–1183.
- [19] M. Fornazari, J.G. de Paula, R.F. Castilho, A.J. Kowaltowski, Redox properties of the adenosine triphosphate-sensitive K⁺ channel in brain mitochondria, *J. Neurosci. Res.* 86 (2008) 1548–1556.
- [20] A.D. Costa, K.D. Garlid, Intramitochondrial signaling: interactions among mitoKATP, PKCepsilon, ROS, and MPT, *Am. J. Physiol.* 295 (2008) H874–H882.
- [21] L.S. Burwell, P.S. Brookes, Mitochondria as a target for the cardioprotective effects of nitric oxide in ischemia–reperfusion injury, *Antioxid. Redox Signal.* 10 (2007) 579–600.
- [22] C. Giulivi, J.J. Poderoso, A. Boveris, Production of nitric oxide by mitochondria, *J. Biol. Chem.* 273 (1998) 11038–11043.
- [23] G. Ferrer-Sueta, R. Radi, Chemical biology of peroxynitrite: kinetics, diffusion, and radicals, *ACS Chem. Biol.* 4 (2009) 161–177.
- [24] A. Trostchansky, H. Rubbo, Nitrate fatty acids: mechanisms of formation, chemical characterization, and biological properties, *Free Radic. Biol. Med.* 44 (2008) 1887–1896.
- [25] Grisham M.B., Jourdain H., Wink D.A., Nitric oxide. I. Physiological chemistry of nitric oxide and its metabolites: implications in inflammation, *Am. J. Physiol.* 276 (1999) G315–G321.
- [26] V. Rudolph, B.A. Freeman, Cardiovascular consequences when nitric oxide and lipid signaling converge, *Circ. Res.* 105 (2009) 511–522.
- [27] N. Sasaki, T. Sato, A. Ohler, B. O'Rourke, E. Marban, Activation of mitochondrial ATP-dependent potassium channels by nitric oxide, *Circulation* 101 (2000) 439–445.
- [28] M. Ljubkovic, Y. Shi, Q. Cheng, Z. Bosnjak, M.T. Jiang, Cardiac mitochondrial ATP-sensitive potassium channel is activated by nitric oxide in vitro, *FEBS Lett.* 581 (2007) 4255–4259.
- [29] P. Pagliaro, D. Mancardi, R. Rastaldo, C. Penna, D. Gattullo, K.M. Miranda, M. Feelsch, D.A. Wink, D.A. Kass, N. Paolocci, Nitroxyl affords thiol-sensitive myocardial protective effects akin to early preconditioning, *Free Radic. Biol. Med.* 34 (2003) 33–43.
- [30] S. Shiva, J.H. Crawford, A. Ramachandran, E.K. Ceaser, T. Hillson, P.S. Brookes, R.P. Patel, V.M. Darley-Usmar, Mechanisms of the interaction of nitroxyl with mitochondria, *Biochem. J.* 379 (2004) 359–366.
- [31] A.P. Wojtovich, P.S. Brookes, The endogenous mitochondrial complex II inhibitor malonate regulates mitochondrial ATP-sensitive potassium channels: implications for ischemic preconditioning, *Biochim. Biophys. Acta* 1777 (2008) 882–889.
- [32] A.P. Wojtovich, P.S. Brookes, The complex II inhibitor atpenin A5 protects against cardiac ischemia–reperfusion injury via activation of mitochondrial KATP channels, *Basic Res. Cardiol.* 104 (2009) 121–129.
- [33] S. Miyamoto, G.R. Martinez, M.H. Medeiros, M.P. Di, Singlet molecular oxygen generated from lipid hydroperoxides by the russell mechanism: studies using 18 (O)-labeled linoleic acid hydroperoxide and monomol light emission measurements, *J. Am. Chem. Soc.* 125 (2003) 6172–6179.
- [34] S.M. Nadtochiy, P.R. Baker, B.A. Freeman, P.S. Brookes, Mitochondrial nitroalkene formation and mild uncoupling in ischaemic preconditioning: implications for cardioprotection, *Cardiovasc. Res.* 82 (2009) 333–340.
- [35] D.V. Cancherini, B.B. Queliconi, A.J. Kowaltowski, Pharmacological and physiological stimuli do not promote Ca(2+)-sensitive K⁺ channel activity in isolated heart mitochondria, *Cardiovasc. Res.* 73 (2007) 720–728.
- [36] A.J. Kowaltowski, S. Seetharaman, P. Paucuk, K.D. Garlid, Bioenergetic consequences of opening the ATP-sensitive K(+) channel of heart mitochondria, *Am. J. Physiol.* 280 (2001) H649–H657.
- [37] J.M. Fukuto, C.H. Switzer, K.M. Miranda, D.A. Wink, Nitroxyl (HNO): chemistry, biochemistry, and pharmacology, *Annu. Rev. Pharmacol. Toxicol.* 45 (2005) 335–355.
- [38] A.P. Wojtovich, D.M. Williams, M.K. Karcz, C.M. Lopes, D.A. Gray, K.W. Nehrke, P.S. Brookes, A novel mitochondrial KATP channel assay, *Circ. Res.* 106 (2010) 1190–1196.
- [39] Q. Chen, E.J. Vazquez, S. Moghaddas, C.L. Hoppel, E.J. Lesnfsky, Production of reactive oxygen species by mitochondria: central role of complex III, *J. Biol. Chem.* 278 (2003) 36027–36031.
- [40] E.B. Tahara, F.D. Navarete, A.J. Kowaltowski, Tissue-, substrate-, and site-specific characteristics of mitochondrial reactive oxygen species generation, *Free Radic. Biol. Med.* 46 (2009) 1283–1297.
- [41] X. Tong, A. Evangelista, R.A. Cohen, Targeting the redox regulation of SERCA in vascular physiology and disease, *Curr. Opin. Pharmacol.* 10 (2010) 133–138.
- [42] M.S. Islam, P.O. Berggren, O. Larsson, Sulfhydryl oxidation induces rapid and reversible closure of the ATP-regulated K⁺ channel in the pancreatic beta-cell, *FEBS Lett.* 319 (1993) 128–132.
- [43] S. Trapp, S.J. Tucker, F.M. Ashcroft, Mechanism of ATP-sensitive K channel inhibition by sulfhydryl modification, *J. Gen. Physiol.* 112 (1998) 325–332.
- [44] D. Tricarico, D.C. Camerino, ATP-sensitive K⁺ channels of skeletal muscle fibers from young adult and aged rats: possible involvement of thiol-dependent redox mechanisms in the age-related modifications of their biophysical and pharmacological properties, *Mol. Pharmacol.* 46 (1994) 754–761.
- [45] W.A. Coetzee, T.Y. Nakamura, J.F. Faivre, Effects of thiol-modifying agents on KATP channels in guinea pig ventricular cells, *Am. J. Physiol.* 269 (1995) H1625–H1633.
- [46] A. Szewczyk, G. Wojcik, N.A. Lobanov, M.J. Nalecz, Modification of the mitochondrial sulfonylurea receptor by thiol reagents, *Biochem. Biophys. Res. Commun.* 262 (1999) 255–258.
- [47] S.M. Grigoriev, Y.Y. Skarga, G.D. Mironova, B.S. Marinov, Regulation of mitochondrial KATP channel by redox agents, *Biochim. Biophys. Acta* 1410 (1999) 91–96.
- [48] A. Pedersen, G.B. Karlsson, J. Rydstrom, Proton-translocating transhydrogenase: an update of unsolved and controversial issues, *J. Bioenerg. Biomembr.* 40 (2008) 463–473.
- [49] Cardoso A.R., Queliconi B.B., Kowaltowski A.J., Mitochondrial ion transport pathways: role in metabolic diseases, *Biochim. Biophys. Acta* (2010).
- [50] Dabrowski M., Trapp S., Ashcroft F.M., Pyridine nucleotide regulation of the KATP channel Kir6.2/SUR1 expressed in Xenopus oocytes, *J. Physiol.* 550 (2003) 357–363.
- [51] S.M. Ronnebaum, O. Ilkayeva, S.C. Burgess, J.W. Joseph, D. Lu, R.D. Stevens, T.C. Becker, A.D. Sherry, C.B. Newgard, M.V. Jensen, A pyruvate cycling pathway involving cytosolic NADP-dependent isocitrate dehydrogenase regulates glucose-stimulated insulin secretion, *J. Biol. Chem.* 281 (2006) 30593–30602.
- [52] D.V. Cuong, N. Kim, J.B. Youm, H. Joo, M. Warda, J.W. Lee, W.S. Park, T. Kim, S. Kang, H. Kim, J. Han, Nitric oxide–cGMP–protein kinase G signaling pathway induces anoxic preconditioning through activation of ATP-sensitive K⁺ channels in rat hearts, *Am. J. Physiol.* 290 (2006) H1808–H1817.
- [53] A.D. Costa, K.D. Garlid, I.C. West, T.M. Lincoln, J.M. Downey, M.V. Cohen, S.D. Critz, Protein kinase G transmits the cardioprotective signal from cytosol to mitochondria, *Circ. Res.* 97 (2005) 329–336.
- [54] M. Brunori, A. Giuffrè, E. Forte, D. Mastronicola, M.C. Barone, P. Sarti, Control of cytochrome c oxidase activity by nitric oxide, *Biochim. Biophys. Acta* 1655 (2004) 365–371.
- [55] T. Zemojtel, A. Frohlich, M.C. Palmieri, M. Kolanczyk, I. Mikula, L.S. Wyrwicz, E.E. Wanker, S. Mundlos, M. Vingron, P. Martasek, J. Durner, Plant nitric oxide synthase: a never-ending story? *Trends Plant Sci.* 11 (2006) 524–525.
- [56] F. Guo, Response to Zemojtel et al.: plant nitric oxide synthase: AtNOS1 is just the beginning, *Trends Plant Sci.* 11 (2006) 527–528.
- [57] Crowford N., Gallim, Tischner R., Heimer Y.M., Okamoto M., Mack A., Response to Zemojtel et al.: plant nitric oxide synthase: back to square one, *Trends Plant Sci.* 11 (2006) 526–527.
- [58] P. Venkatakrishnan, E.S. Nakayasu, I.C. Almeida, R.T. Miller, Absence of nitric-oxide synthase in sequentially purified rat liver mitochondria, *J. Biol. Chem.* 284 (2009) 19843–19855.
- [59] P.R. Baker, Y. Lin, F.J. Schopfer, S.R. Woodcock, A.L. Groeger, C. Bathany, S. Sweeney, M.H. Long, K.E. Iles, L.M. Baker, B.P. Branchaud, Y.E. Chen, B.A. Freeman, Fatty acid transduction of nitric oxide signaling: multiple nitrated unsaturated fatty acid derivatives exist in human blood and urine and serve as endogenous peroxisome proliferator-activated receptor ligands, *J. Biol. Chem.* 280 (2005) 42464–42475.
- [60] F.J. Schopfer, P.R. Baker, G. Giles, P. Chumley, C. Bathany, J. Crawford, R.P. Patel, N. Hogg, B.P. Branchaud, J.R. Lancaster Jr., B.A. Freeman, Fatty acid transduction of

- nitric oxide signaling. Nitrolinoleic acid is a hydrophobically stabilized nitric oxide donor. *J. Biol. Chem.* 280 (2005) 19289–19297.
- [61] F.J. Schopfer, C. Batthyany, P.R. Baker, G. Bonacci, M.P. Cole, V. Rudolph, A.L. Groeger, T.K. Rudolph, S. Nadochiy, P.S. Brookes, B.A. Freeman, Detection and quantification of protein adduction by electrophilic fatty acids: mitochondrial generation of fatty acid nitroalkene derivatives, *Free Radic. Biol. Med.* 46 (2009) 1250–1259.
- [62] V. Rudolph, T.K. Rudolph, F.J. Schopfer, G. Bonacci, S.R. Woodcock, M.P. Cole, P.R. Baker, R. Ramani, B.A. Freeman, Endogenous generation and protective effects of nitro-fatty acids in a murine model of focal cardiac ischaemia and reperfusion, *Cardiovasc. Res.* 85 (2010) 155–166.
- [63] H. Ardehali, Z. Chen, Y. Ko, R. Mejia-Alvarez, E. Marban, Multiprotein complex containing succinate dehydrogenase confers mitochondrial ATP-sensitive K⁺ channel activity, *Proc. Natl Acad. Sci.* 101 (2004) 11880–11885.
- [64] C.G. Tocchetti, W. Wang, J.P. Froehlich, S. Huke, M.A. Aon, G.M. Wilson, B.G. Di, B. O'Rourke, W.D. Gao, D.A. Wink, J.P. Toscano, M. Zaccolo, D.M. Bers, H.H. Valdivia, H. Cheng, D.A. Kass, N. Paolocci, Nitroxyl improves cellular heart function by directly enhancing cardiac sarcoplasmic reticulum Ca²⁺ cycling, *Circ. Res.* 100 (2007) 96–104.
- [65] P.P. Dzeja, P. Bast, C. Ozcan, A. Valverde, E.L. Holmuhamedov, D.G. Van Weylen, A. Terzic, Targeting nucleotide-requiring enzymes: implications for diazoxide-induced cardioprotection, *Am. J. Physiol.* 284 (2003) H1048–H1056.
- [66] G.D. Mironova, Y.Y. Skarga, S.M. Grigoriev, A.E. Negoda, O.V. Kolomytkin, B.S. Marinov, Reconstitution of the mitochondrial ATP-dependent potassium channel into bilayer lipid membrane, *J. Bioenerg. Biomembr.* 31 (1999) 159–163.
- [67] A.D. Beavis, Y. Lu, K.D. Garlid, On the regulation of K⁺ uniport in intact mitochondria by adenine nucleotides and nucleotide analogs, *J. Biol. Chem.* 268 (1993) 997–1004.

Ap.4. Mitochondrial compartmentalization of redox processes

Free Radical Biology and Medicine 52 (2012) 2201–2208



Contents lists available at SciVerse ScienceDirect

Free Radical Biology and Medicine

journal homepage: www.elsevier.com/locate/freeradbiomed

Review Article

Mitochondrial compartmentalization of redox processes

Ariel R. Cardoso^{a,1}, Bruno Chausse^{a,1}, Fernanda M. da Cunha^{b,1}, Luis A. Luévano-Martínez^{a,1},
Thire B.M. Marazzi^{a,1}, Phillipe S. Pessoa^{a,1}, Bruno B. Queliconi^{a,1}, Alicia J. Kowaltowski^{a,*}

^a Departamento de Bioquímica, Instituto de Química, Brazil^b Escola de Artes, Ciências e Humanidades, Universidade de São Paulo, 05508-900 São Paulo, SP, Brazil

ARTICLE INFO

Article history:

Received 16 January 2012

Received in revised form

5 March 2012

Accepted 6 March 2012

Available online 26 April 2012

Keywords:

Mitochondria

Compartments

Antioxidants

Mitochondrially-targeted probes

Mitochondrially-targeted antioxidants

ABSTRACT

Knowledge of location and intracellular subcompartmentalization is essential for the understanding of redox processes, because oxidants, owing to their reactive nature, must be generated close to the molecules modified in both signaling and damaging processes. Here we discuss known redox characteristics of various mitochondrial microenvironments. Points covered are the locations of mitochondrial oxidant generation, characteristics of antioxidant systems in various mitochondrial compartments, and diffusion characteristics of oxidants in mitochondria. We also review techniques used to measure redox state in mitochondrial subcompartments, antioxidants targeted to mitochondrial subcompartments, and methodological concerns that must be addressed when using these tools.

© 2012 Elsevier Inc. All rights reserved.

Contents

Introduction	2201
Where are mitochondrial oxidants generated?	2201
Mitochondrial antioxidant compartmentalization	2202
Diffusion of oxidants and mitochondrial subcompartments	2203
Subcompartmentalized measurements of mitochondrial redox state and oxidants	2204
Mitochondrial probes: a few words of caution	2205
Targeted antioxidants and other "antioxidant strategies"	2206
Conclusions	2206
References	2206

Introduction

Isolated mitochondria were first reported to release hydrogen peroxide in the late 1960s, and this oxidant was subsequently demonstrated to be a product of superoxide radical dismutation [8,19,37,53]. Since then, it has become clear that these organelles are a quantitatively relevant source of intracellular oxidants, produced mostly as by-products of electron transfer reactions.

The electron transfer reactions that generate oxidants are diverse in nature and occur in submitochondrial locations. This, added to specific characteristics of removal systems and differences in

reactivity (and thus diffusion), may result in very distinct redox status in mitochondrial compartments. Because redox processes are highly dependent on local intracellular characteristics and targets, it is important to understand these environmental properties. This review focuses on current knowledge regarding the compartmentalization of mitochondrial redox processes.

Where are mitochondrial oxidants generated?

The electron transport chain is the most studied source of mitochondrial superoxide radicals ($O_2^{\cdot-}$), formed through one-electron reduction of molecular oxygen [1,66,108]. NADH-ubiquinone oxidoreductase (complex I) releases $O_2^{\cdot-}$ to the matrix, possibly through the flavin and iron-sulfur clusters into the hydrophilic arm [9,51,114]. Complex III (ubiquinone:cytochrome

* Corresponding author. Fax: +55 11 38155579.

E-mail address: alicia@iq.usp.br (A.J. Kowaltowski).¹ These authors contributed equally to this work.

c reductase), on the other hand, releases O_2^- to both the intermembrane space and the matrix [9,114]. Although isolated succinate dehydrogenase (complex II) has been shown to release O_2^- in the absence of added coenzyme Q [125], this complex seems to be of lesser importance considering total oxidant release in intact organelles and cells, perhaps because of structural characteristics of this enzyme [124]. Complex IV is not usually considered a quantitatively relevant source of mitochondrial O_2^- , because of its ability to bind tightly to partially reduced intermediates [9,48,60,114].

In addition to the electron transport chain, the importance of other mitochondrial enzymes, in particular flavoproteins, as O_2^- sources has increasingly been recognized [1]. Two of these enzymes, pyruvate and α -ketoglutarate dehydrogenase, are located in the matrix and possess the same flavin subunit (dihydropyrimidine dehydrogenase or dihydrolipoyl dehydrogenase), which is the source of O_2^- [102,106,111]. For reasons that are still unclear, O_2^- generation is more pronounced in α -ketoglutarate dehydrogenase compared to pyruvate dehydrogenase [102]. Interestingly, α -ketoglutarate dehydrogenase is tightly associated with the matrix surface of the inner mitochondrial membrane [55] and, in yeast, is a component of the mitochondrial nucleoid [43,86]. This close proximity between an important source of mitochondrial oxidants and mitochondrial DNA (mtDNA) may explain why this enzyme is involved in mtDNA dysfunction [107] and is an oxidant source involved in aging in yeast [106].

Other sources of matrix O_2^- include the electron-transferring flavoprotein Q oxidoreductase and possibly acyl-CoA dehydrogenases, although these sources still remain poorly explored [9,101,108]. Other mitochondrial flavoenzymes such as the branched-chain α -ketoacid dehydrogenase complex are possible and yet unstudied mitochondrial reactive oxygen species (ROS) sources.

Aconitase is a matrix enzyme commonly used as a marker for mitochondrial oxidant levels, because O_2^- can oxidize its iron-sulfur clusters. Vasquez-Vivar and colleagues [117] reported that oxidized aconitase can produce hydroxyl radicals by the Fenton mechanism. Interestingly, aconitase is also a component of the nucleoid involved in the maintenance of mtDNA [107].

Enzymes on the outer surface of the inner mitochondrial membrane can contribute to oxidant release in the intermembrane space. Dihydroorotate dehydrogenase participates in the synthesis of pyrimidine nucleotides and donates electrons to coenzyme Q. In the absence of this electron acceptor, this enzyme has been shown to generate H_2O_2 , although this remains to be further investigated [1,19]. α -Glycerophosphate dehydrogenase is an enzyme located on the outer surface of the inner mitochondrial membrane that has a clear role as a source of intermembrane space O_2^- [9,60,108,112,129]. Moreover, topological measurements of O_2^- generation originating from α -glycerophosphate dehydrogenase suggest radicals may be produced at both sides of the membrane [60], although the location of the flavin, far from the membrane, does not support this possibility [123]. Superoxide radical production within the mitochondrial matrix originating from glycerol phosphate may also be the result of reverse electron transfer to complex I [1,9,60,112,113,108].

Monoamino oxidase is an enzyme located on the outer face of the mitochondrial outer membrane. It can generate H_2O_2 at higher rates than the electron transfer chain, thus resulting in mtDNA damage [30,49,91].

Mitochondrial antioxidant compartmentalization

Considering the diverse and quantitatively significant sources of oxidants in the mitochondrial microenvironment described above, effective antioxidant mechanisms are necessary to maintain

mitochondrial and cell function. Antioxidant systems vary greatly in each mitochondrial compartment and include many different strategies: (i) catalytic removal of free radicals and other ROS, (ii) reduction of free radicals by electron donors, (iii) chelating mechanisms for pro-oxidant metal ions, and (iv) repair mechanisms [25,48,50,114,116]. The antioxidant characteristics of the various mitochondrial subcompartments are described next.

O_2^- in the matrix is dismutated into H_2O_2 either spontaneously or catalyzed by the MnSOD (SOD2). The high concentration and reaction rate of SOD2 suggest that the steady-state levels of mitochondrial O_2^- are low, in keeping with the perceived importance of removing this oxidant [20,21,46,66,120].

H_2O_2 generated in the matrix can diffuse to other cellular compartments because of its high stability and membrane permeability (as will be discussed below). Alternatively, H_2O_2 generated in the mitochondrial matrix will be removed by enzymatic systems in this compartment. These systems include glutathione peroxidases (GPx), thioredoxin peroxidases (TPx), and, in some tissues, catalase [18,48]. GPx and TPx convert hydrogen peroxide to H_2O at the expense of oxidizing glutathione (GSH) and thioredoxin (Trx), respectively. The ubiquity of both systems suggests the central importance of peroxide removal within cells, although simulations based on rate constants and concentrations suggest TPx is the premier enzyme responsible for H_2O_2 removal in mitochondria, mostly because of its relative abundance [15]. On the other hand, the rate constant of GPx and the concentrations of glutathione are higher. Differences also exist regarding substrate specificity: TPx also removes organic hydroperoxides [67]. Both TPx and GPx H_2O_2 -removal systems use electrons from NADPH to regenerate reduced GSH and Trx [3,35,80]. NADPH in the mitochondrial matrix is regenerated from electrons donated by NADH, through the activity of the proton-translocating transhydrogenase [73], linking the presence of the inner membrane proton gradient to an effective removal of H_2O_2 . Catalase has been found in heart and liver mitochondria [77,85], although it is probably not as effective as GPx and TPx in removing mitochondrial H_2O_2 at physiological levels [121]. Despite this, overexpression of catalase specifically in mitochondria significantly extends murine life span [90], indicating it is functionally relevant in this compartment.

Important nonenzymatic antioxidant systems also exist within the mitochondrial matrix: GSH is a powerful antioxidant itself. It is synthesized in the cytoplasm and imported into mitochondria by two electroneutral antiport carrier proteins, reaching concentrations as high as 11 mM in the matrix [22,34,38,57,116]. GSH scavenges hydroxyl radicals and singlet oxygen directly and can regenerate vitamins C and E to their reduced forms. The oxidized-to-reduced glutathione ratio is widely used as an indicator of the mitochondrial or cellular redox state. Ascorbate (vitamin C) is also an important electron donor in the mitochondrial matrix. It participates in the regeneration of oxidized vitamin E and is a radical scavenger. Ascorbate can also be a cofactor for one-Cys peroxiredoxins, which are located in yeast mitochondria, removing H_2O_2 [56,61,116].

Metal chelation is an essential antioxidant defense in the mitochondrial matrix, because the mitochondrion is a metal-rich organelle. Indeed, iron chelation prevents mitochondrial damage under conditions of oxidative stress [12,39]. Finally, mtDNA-repairing systems are essential for mtDNA integrity, ensuring efficient electron transport chain assembly that prevents further oxidant generation in mitochondria [29,48,114].

Hydrophobic antioxidant systems are located within the mitochondrial inner membrane, protecting both membrane integrity and inner membrane proteins. Phospholipid hydroperoxide glutathione peroxidase is a membrane-associated GPx that reacts with both hydrogen peroxide and lipid hydroperoxides. This enzyme protects against membrane-damaging lipid oxidation

and has been reported to be antiapoptotic, preventing the formation of cardiolipin hydroperoxide and cytochrome *c* release [70,109,115]. Vitamin E (α -tocopherol) is a relevant lipid-soluble antioxidant in the mitochondrial inner membrane, preventing the propagation of free radical-mediated chain reactions by trapping lipid peroxyl radicals [26,110]. Coenzyme Q is a recognized $O_2^{\cdot-}$ source when partially reduced but also represents an important inner membrane antioxidant when fully reduced. Ubiquinol inhibits lipid and protein oxidation by reducing perferyl radicals or eliminating lipid peroxyl radicals. Ubiquinol can also regenerate vitamin E from the α -tocopheroxyl radical [5,62].

In the mitochondrial intermembrane space, $O_2^{\cdot-}$ is dismutated to H_2O_2 by CuZnSOD (SOD1), the cytosolic isoform of SOD, also present in the intermembrane space [44,71]. Interestingly, targeting SOD1 specifically to the mitochondrial intermembrane space rescues the motor phenotype of SOD1 knockout animals, indicating that the mitochondrial location of this enzyme is essential for the maintenance of motor neuron integrity [17]. Cytochrome *c* is also an important mitochondrial antioxidant, oxidizing $O_2^{\cdot-}$ to O_2 and then transferring the electron to complex IV [74,93]. Finally, GSH is abundant in the intermembrane space; it is transported by voltage-dependent anion-selective channels located in the outer membrane [44].

Overall, mitochondrial antioxidant systems are so effective that it has been proposed that release of oxidants from mitochondria within cells under physiological conditions may not be significant [10,69,100].

Diffusion of oxidants and mitochondrial subcompartments

The presence of oxidants in various mitochondrial subcompartments depends not only on their generation properties, but also on their reactivity and diffusibility (see Fig. 1). Diffusion distance can be estimated by the Einstein–Schomulochowski equation,

$$\bar{x} = \sqrt{(6Dt)}, \quad (1)$$

where \bar{x} is the quadratic mean of the diffusion distance in three-dimensional space, D is the diffusion coefficient, and t is the time, usually taken as the molecule half-life time. A half-life time is the time for a decrease in concentration of $1/e$, or 37%. The diffusion

coefficient can be calculated using the Stokes–Einstein equation,

$$D = kT/6\pi\eta r, \quad (2)$$

where k represents the Boltzman constant, T is the absolute temperature, η is the viscosity of the biological matrix, and r is the hydrodynamic radius of the solute species. The diffusion coefficient was assumed to be $1 \times 10^{-9} \text{ s}^{-1}$. Molecule half-life times are estimated considering all the rates at which a molecule reacts in the cell or tissue and reactant concentrations:

$$\tau = \ln 2 / (k_d + k_1[M_1] + k_2[M_2] + \dots + k_n[M_n]). \quad (3)$$

Chemical reactions in the condensed phase are limited by the solvent surrounding the reactants, which is usually water within cells. Encounters between reactants last about 10^{-8} to 10^{-10} s. If the probability of a reaction is high enough, the overall reaction rate will depend only on solvent diffusion, restricted by the diffusion limit (10^9 – $10^{10} \text{ mol L}^{-1} \text{ s}^{-1}$).

Considering both the predicted short diffusion distances for $O_2^{\cdot-}$ and the limitations in measuring intracellular concentrations of this radical, the rates/concentrations of $O_2^{\cdot-}$ that leave or enter mitochondria remain a largely open question. Fig. 1 shows a schematic drawing of a $16 \mu\text{m}$ diameter cell and its mitochondria, with predicted diffusion distances of some ROS brought to scale. Fig. 2 shows ROS concentration evolutions based on their estimated lifetimes.

Superoxide diffusion distances and lifetimes are strongly dependent on the presence of superoxide dismutase and free metal ions. The high rate constant for the SOD reaction (about $5 \times 10^9 \text{ L mol}^{-1} \text{ s}^{-1}$) reduces $O_2^{\cdot-}$ lifetime from 100 ms (in the absence of SOD) to $35 \mu\text{s}$ [59,84], whereas the diffusion distance changes from about $50 \mu\text{m}$ to 400 nm . Thus, in mitochondria, matrix and membrane SOD isoforms will remove most $O_2^{\cdot-}$ produced under physiological conditions [10]. Because superoxide is negatively charged, its diffusion through the lipid bilayer is unfavorable, and it is thus highly improbable that the radical generated in the mitochondrial matrix could leave this subcompartment. However, the protonated form of $O_2^{\cdot-}$, the perhydroxyl radical (HOO^{\cdot} ; $\text{p}K_a=4.7$), is potentially membrane-diffusible. Superoxide production occurring in the proton-rich intermembrane space could lead to the production of HOO^{\cdot} , which may diffuse into mitochondria (stimulated by the pH gradient) or to the immediate extramitochondrial space [23,52,84]. Intermembrane-space $O_2^{\cdot-}$ diffuses out

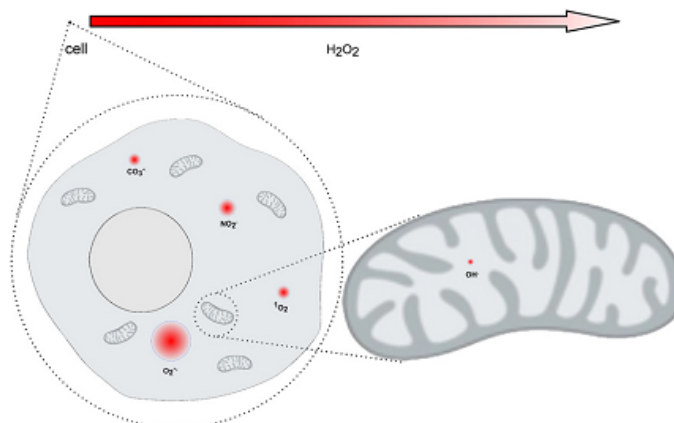


Fig. 1. Schematic representation of selected oxidant diffusion distances based on Einstein–Schomulochowski relations and $t=3\tau_{1/2}$ accounting for $\sim 95\%$ decay of the initial concentration. Cell dimensions adopted were approximately $16 \times 16 \mu\text{m}$; mitochondrial dimensions were $2 \times 1 \mu\text{m}$; hydrogen peroxide diffusion radius (represented by the arrow) is $\sim 3 \text{ mm}$. Half-life times: CO_3^- $3.5 \mu\text{s}$, NO_2 $7 \mu\text{s}$, $^1\text{O}_2$ $4 \mu\text{s}$, $\text{O}_2^{\cdot-}$ $35 \mu\text{s}$, OH^{\cdot} 10 ns , H_2O_2 500 s .

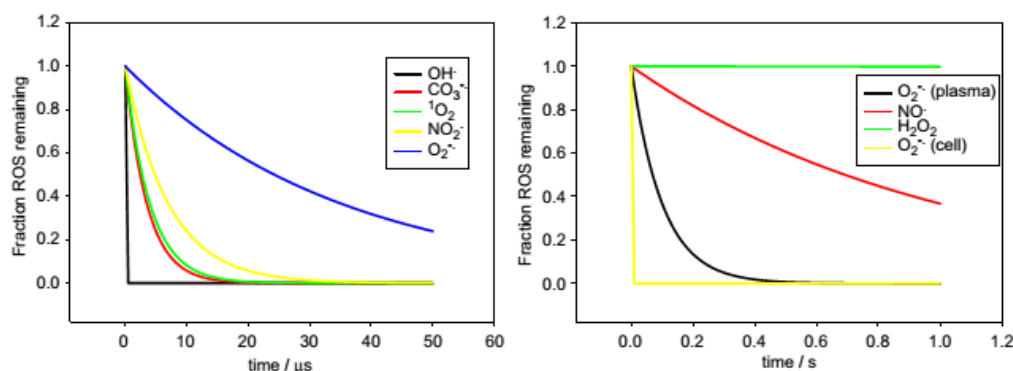


Fig. 2. Time evolution of selected oxidant species based on their estimated half-life times: OH• 10 ns, CO₃•⁻ 3.5 μs, ¹O₂ 4 μs, NO₂• 7 μs, O₂•⁻ 35 μs (in the presence of SOD), O₂•⁻ 100 ms (in absence of SOD), NO• 1 s, H₂O₂ 500 s.

of the organelle through the outer membrane voltage-dependent anion channel [27].

Hydrogen peroxide is a relatively stable molecule in solution, with long lifetimes and large diffusion distances, mostly eliminated by thiol peroxidase and catalase activities, as described above. H₂O₂ is often believed to diffuse through membranes because of its lack of charge, small size, and physical properties similar to water [7]. However, biomembranes constitute a barrier to peroxide diffusion and lead to the formation of gradients. This was investigated experimentally in Jurkat cells by measuring H₂O₂ consumption rates by scavenging enzymes [2]. The magnitude of the H₂O₂ gradient is proportional to consumption rates in each compartment. Furthermore, the formation of the H₂O₂ gradient is determined by the size of the cell or organelle (smaller compartments are more permeable to H₂O₂) and expression levels of aquaporins known to transport H₂O₂ [6]. Membrane and/or cell wall composition also determines H₂O₂ permeability [98].

Hydroxyl radical lifetimes and diffusion distances in water are 10 ns and 5 nm, respectively [24,76]. Inside the cell, however, the lifetime may be much lower because of high reactivity toward cell components, and the diffusion distance in water should be considered an upper limit for diffusion in the cell. Singlet oxygen (¹O₂), which can be generated in various cellular locations by photosensitization, also has limited lifetime and diffusion (4 μs and 100 nm) in water and within cells [79].

Subcompartmentalized measurements of mitochondrial redox state and oxidants

Because the outcome of mitochondrial oxidant generation varies largely with the type, quantity, and location of ROS, gaining access to technologies that provide specific, localized, and quantitative measurements of these species is essential. Unfortunately, although considerable progress has been made, precise forms to measure mitochondrial redox state are still lacking, and all techniques should be used critically, include appropriate controls, and be associated with other mechanistically distinct techniques to confirm the findings [64]. We will first present techniques available and then discuss their shortcomings. Table 1 lists some commonly used mitochondrial redox probes, their strengths, and their weaknesses.

Probes available for measurements of mitochondrial redox state or oxidant levels can be separated into two main groups: protein and nonprotein probes. The majority of nonprotein probes

are targeted to mitochondria through their coupling to the lipophilic triphenylphosphonium cation (TPP⁺), a group that favors the accumulation of the probe (several hundreds of times) within mitochondria, driven by the membrane potential [65]. Mitochondrially targeted probes in this category include those designed for the detection of highly reactive oxygen/nitrogen species (MitoAR [45]), hydrogen peroxide/peroxynitrite (MitoPY1 [16]; MitoB [14]), superoxide (MitoSOX [41]), and lipid peroxides (MitoDPPP [89]; MitoFOX green, a diphenyl-1-pyrenylphosphine derivative available from Molecular Probes, Eugene, OR, USA, although a report describing its use could not be located).

Dichlorofluorescein (DCF) is another nonprotein probe that is not targeted to mitochondria, but we find important to mention because it is the most widely used fluorescent probe for ROS measurements, including mitochondrially derived oxidants. DCF has numerous artifacts and limitations [13,40,41], as discussed in the next section.

Recently, a hybrid probe, SPG2, was described by Srikun et al. [99]. This probe was designed to detect peroxynitrite/hydrogen peroxide and consists of a derivatized boronate bioconjugated to SNAP-tag fusion protein. This strategy allows the targeting of nonprotein compounds to various subcellular locations, a fact feasible only for protein probes so far.

Genetically encoded proteinaceous probes have been developed with a number of targeting sequences that promote their localization to specific mitochondrial compartments [28,32,54,83,118,119]. cpYFP, a circularly permuted yellow fluorescent protein that shifts its fluorescence emission under strong oxidizing conditions [118], was targeted to mitochondria through its fusion to the targeting sequence of subunit IV of cytochrome c oxidase [118]. HyPer, a genetically encoded biosensor for hydrogen peroxide based on cpYFP and the OxyR bacterial transcription factor [4], was targeted to the mitochondrial matrix or the intermembrane space through the use of the targeting sequence of subunit VIII of cytochrome c oxidase or a partial sequence of mouse mitochondrial glycerol phosphate dehydrogenase 2, respectively [54,83]. Finally, rxYFP [72] and roGFP [28], two fluorescent protein probes for measurement of thiol/disulfide intracellular redox state, were targeted to the mitochondrial matrix or the intermembrane space through the use of different leading sequences [32,119]. Quantitative measurements using rxYFP in yeast grown in high-glucose cultures (a condition that increases their H₂O₂ release [106]) suggest that GSH:GSSG ratios are in the range of 900:1 in the matrix and 250:1 in the intermembrane space. Both environments are thus distinct in redox state and more oxidized than the cytosol, in which the ratio is in the range of 3000:1 [32].

Table 1
Commonly used mitochondrial redox probes.

Probe	Characteristics	Cautionary notes	Refs.
<i>Nonprotein probes</i>			
MitoAR	High fluorescence intensity pH-independent fluorescence	Nonspecific Mitochondrial accumulation depends on membrane potential	[45]
MitoB1	Tolerance to photobleaching Tolerance to autoxidation More specific for mitochondrial H ₂ O ₂	Mitochondrial accumulation depends on membrane potential	[14]
MitoDPPP	May be analyzed by mass spectrometry Does not react with O ₂ ^{•-} or OH [•]	Oxidized by various lipid peroxides, including those from other cellular sites	[89]
MitoPY	More specific for mitochondrial H ₂ O ₂ than other nonprotein probes	Mitochondrial accumulation depends on membrane potential	[16]
MitoSOX	Reacts with O ₂ ^{•-} to form a specific product (2-OH-Mito-E ⁺)	Reacts with other oxidants (OH [•] , ONOO ⁻) to form Mito-E ⁺ and dimers, which have similar spectral parameters Irreversible reaction—not suitable for transient measurements	[40,41,128]
DCFH ₂	Easy manipulation Cheap Easily obtained	Nonspecific Dependent on pH, concentration of transition metals, and phenotype Modified by many biological molecules including GSH, NADH, and Ascorbate Autoxidation, photo-oxidation, autocatalysis, respiratory inhibition	[13,41,42,127]
<i>Protein-based probes</i>			
cpYFP	Can be targeted to specific mitochondrial compartments	Requires transfection and appropriate expression Very pH sensitive Suitability as a O ₂ ^{•-} probe is under debate	[33,58,63,87,118]
HyPer	Ratiometric Specific for H ₂ O ₂ Presents high sensitivity	Requires transfection and appropriate expression pH sensitive	[4,54,83]
rxYFP	Targeted	Not ratiometric High background noise	[32,58,72]
roGFP	Ratiometric Allows dynamic measurement of mitochondrial redox state Can be targeted to specific mitochondrial compartments	Sensitive to pH and chloride Limited sensitivity Biosynthesis of one mature molecule of GFP implies the release of one H ₂ O ₂	[28,81,119]
<i>Hybrid probe</i>			
SPG2	Specific for H ₂ O ₂ Can be targeted to specific mitochondrial compartments	Requires transfection Reaction with H ₂ O ₂ is irreversible—not suitable for transient measurements Rate constant with H ₂ O ₂ is lower than that of catalase, glutathione peroxidase, or peroxiredoxin	[81,99]

Mitochondrial probes: a few words of caution

Redox measurements in themselves are tricky, because of the reactive nature of oxidants, and localized measurements are even more so. Although most probes are designed to react preferentially with specific oxidants, they certainly react with other species, too [41,45,128], making specificity a rare quality. Furthermore, several important artifacts of these probes are particularly relevant to mitochondrial microenvironments.

Probes linked to TPP⁺ [14,16,82] or any other lipophilic cation will accumulate in mitochondria in a manner related to the magnitude of the inner membrane potential. Thus, the first obvious point to be taken into account is that probe fluorescence both in the whole cell and in the mitochondria within the cell will vary with changes in the cellular and mitochondrial membrane potentials, independent of variations in oxidant levels. Because most changes in mitochondrial oxidant generation involve alterations of mitochondrial oxidative phosphorylation and energy metabolism, this is a central point that must always be considered and that precludes the use of these probes as sole measurements of mitochondrial oxidant levels. Furthermore, the accumulation of probes in the mitochondrial microenvironment does not increase proportionally

to its localized fluorescence. Because the quantity of these probes in a small environment can be significant, both quenching [65,68] and mitochondrial uncoupling due to the accumulation of the indicator may occur. Uncoupling is a highly effective antioxidant strategy [11,95], so uptake of the probe is a possible mechanism in which the technique used to measure oxidants changes oxidant production. Finally, the presence of very high quantities of these chemicals in the mitochondrial microenvironment can lead to changes in mitochondrial function. It is worth noting that DCF, which can accumulate in mitochondria under some conditions, promotes mitochondrial respiratory inhibition when added to the extramitochondrial medium at micromolar concentrations [104]. Because these effects are certainly variable with cell type and loading conditions, it is recommended that mitochondrial functionality be verified as a control for the use of these indicators.

Protein-based probes [28,99,118] can be directed to specific compartments with low risk of quenching or interference with other proteins. Nonetheless, overexpression of any protein can change the normal physiology and morphology of the organelle. In addition, proteinaceous probes are based on cysteine redox chemistry [28,118] and are therefore limited to processes that affect thiols.

An issue that affects both protein and nonprotein probes is changes in mitochondrial quantity and morphology, which can affect probe signal [47]. Another central point for all probes is pH sensitivity. Mitochondria present substantial ΔpH across the inner mitochondrial membrane [78], and the pH in different mitochondrial environments is influenced by metabolic activity. Changes in pH can notably change the signal obtained with different probes [87,88,122], within the physiological range. For example, cpYFP fluorescence increases five times by shifting the pH from 7 to 8 [118], and clamping cytosolic pH has led to questions regarding O_2^- measurements using this probe [87]. DCF presents at least threefold changes in fluorescence, with pH shifts between 7 and 8, and doubles its fluorescence emission with shifts of pH between 6 and 7 [122].

Targeted antioxidants and other “antioxidant strategies”

An effective way to demonstrate the participation of mitochondrial oxidants in pathophysiological processes is by verifying the effects of antioxidants designed to selectively remove ROS from mitochondrial microenvironments.

Lipophilic cationic antioxidants make use of the mitochondrial inner membrane potential, similar to TPP^+ -bound probes, to promote the accumulation of antioxidants in the matrix. TPP^+ -associated vitamin E (MitoVitE) and, especially, coenzyme Q (MitoQ) have been widely used and provide protection against many different oxidant-related forms of cell and organismal damage (reviewed by Smith and Murphy [96]). Both accumulate by more than 2 orders of magnitude in mitochondria, in a membrane-potential-dependent manner. The downfall of these probes is that they can cause uncoupling themselves [103], possibly preventing mitochondrial O_2^- formation. These probes also undergo redox cycling that can generate O_2^- and may be poor inhibitors of thiol oxidation [36]. Furthermore, MitoQ has been demonstrated to accept electrons before the rotenone-inhibitory site in complex I and to have its reduced form recycled by complex II, allowing it to act as an intracellular pro-oxidant under conditions under which electron flow through complex I is high [75].

SkQ_n compounds are similar to MitoQ in mitochondrial accumulation and protective properties, but are less prone to redox cycling because of the use of plastoquinones instead of the ubiquinone moiety present in MitoQ. The main pharmacological advantage of SkQ_n compounds over MitoQ is a larger window between their antioxidant and pro-oxidant effects (for review see [92,94]). Plastoquinones in vivo are located in thylakoid membranes, a highly oxidant environment, and present distinct redox properties: whereas the plastoquinone redox potential is around +110 mV, that of ubiquinone is +70 mV [97]. Moreover, SkQ_n compounds are reduced by mitochondrial cytochrome b_h , and the reduced form of SkQ_n compounds promptly reacts with superoxide produced in mitochondria. In addition, the SkQH_2 structure, especially SkQH_2 , favors a direct interaction with cardiolipin molecules, hence avoiding oxidation of this lipid.

Cell-permeative mitochondrially targeted peptides have also been developed [105,126], and they mostly accumulate (by 3 or 4 orders of magnitude) in the inner mitochondrial membrane, without reaching the matrix, in a manner that is not highly dependent on the membrane potential. The differential location and accumulation properties of these mitochondrial antioxidants are interesting in terms of studying mitochondrial redox compartmentalization, but this possibility has not yet been fully explored. Membrane-potential-sensitive polycationic peptides that penetrate into the matrix have also been developed [31].

Conclusions

Because of the reactive nature of oxidants, their intracellular targets for both damaging and signaling effects must be within very specific constraints regarding the separation from their source. Given the importance of mitochondria as generators and targets of these oxidants, understanding the subcompartmentalization of mitochondrial redox processes is essential. In the past few years, a lot of knowledge has been gained regarding the characteristics and locations of mitochondrial oxidant generation, as well as more quantitative measurements of the antioxidant capacity and redox state of various mitochondrial subcompartments. A challenge for the area in the future will be the development of more trustworthy and specific mitochondrially targeted antioxidants, as well as mechanisms to conduct real-time, localized, specific, and quantitative measurements of oxidants in mitochondrial microenvironments in vivo.

References

- Andreyev, A. Y.; Kushnareva, Y. E.; Starkov, A. A. Mitochondrial metabolism of reactive oxygen species. *Biochemistry* 2:200–214; 2005.
- Antunes, F.; Cadenas, E. Estimation of H_2O_2 gradients across biomembranes. *FEBS Lett.* 475:121–126; 2000.
- Armér, E. S. J.; Holmgren, A. Physiological functions of thioredoxin and thioredoxin reductase. *Eur. J. Biochem.* 267:6102–6109; 2000.
- Belousov, V. V.; Fradkov, A. F.; Lukyanov, K. A.; Staroverov, D. B.; Shakhbuzov, K. S.; Tersikh, A. V.; Lukyanov, S. Genetically encoded fluorescent indicator for intracellular hydrogen peroxide. *Nat. Methods* 3:281–286; 2006.
- Bentinger, M.; Brismar, K.; Dallner, G. The antioxidant role of coenzyme Q. *Mitochondrion* 7:41–50; 2007.
- Bienert, G. P.; Møller, A. L. B.; Kristiansen, K. A.; Schulz, A.; Møller, I. M.; Schjoerring, J. K.; Jahn, T. P. Specific aquaporins facilitate the diffusion of hydrogen peroxide across membranes. *J. Biol. Chem.* 282:1183–1192; 2007.
- Bienert, G. P.; Schjoerring, J. K.; Jahn, T. P. Membrane transport of hydrogen peroxide. *Biochim. Biophys. Acta* 1758:994–1003; 2006.
- Boveris, A.; Chance, B. The mitochondrial generation of hydrogen peroxide: general properties and effect of hyperbaric oxygen. *Biochem. J.* 134:707–716; 1973.
- Brand, M. D. The sites and topology of mitochondrial superoxide production. *Exp. Gerontol.* 45:466–472; 2010.
- Brown, G. C.; Borutaite, V. There is no evidence that mitochondria are the main source of reactive oxygen species in mammalian cells. *Mitochondrion* 12:1–4; 2012.
- Caldeira da Silva, C. C.; Cerqueira, F. M.; Barbosa, L. F.; Medeiros, M. H. G.; Kowaltowski, A. J. Mild mitochondrial uncoupling in mice affects energy metabolism, redox balance and longevity. *Aging Cell* 7:552–560; 2008.
- Castilho, R. F.; Kowaltowski, A. J.; Meinicke, A. R.; Bechara, E. J.; Vercesi, A. E. Permeabilization of the inner mitochondrial membrane by Ca^{2+} ions is stimulated by t-butyl hydroperoxide and mediated by reactive oxygen species generated by mitochondria. *Free Radic. Biol. Med.* 18:479–486; 1995.
- Chen, X.; Zhong, Z.; Xu, Z.; Chen, L.; Wang, Y. 2',7'-Dichlorodihydrofluorescein as a fluorescent probe for reactive oxygen species measurement: forty years of application and controversy. *Free Radic. Res.* 44:587–604; 2010.
- Cochemé, H. M.; Quin, C.; McQuaker, S. J.; Cabreiro, F.; Logan, A.; Prime, T. A.; Abakumova, I.; Patel, J. V.; Fearnley, I. M.; James, A. M.; Porteous, C. M.; Smith, R. A.; Saeed, S.; Carré, J. E.; Singer, M.; Gems, D.; Hartley, R. C.; Partridge, L.; Murphy, M. P. Measurement of H_2O_2 within living *Drosophila* during aging using a ratiometric mass spectrometry probe targeted to the mitochondrial matrix. *Cell Metab.* 13:340–350; 2011.
- Cox, A. G.; Winterbourn, C. C.; Hampton, M. B. Mitochondrial peroxiredoxin involvement in antioxidant defence and redox signalling. *Biochem. J.* 425:313–325; 2009.
- Dickinson, B. C.; Chang, C. J. A targetable fluorescent probe for imaging hydrogen peroxide in the mitochondria of living cells. *J. Am. Chem. Soc.* 130:9638–9639; 2008.
- Fischer, L. R.; Igoudjil, A.; Magrané, J.; Li, Y.; Hansen, J. M.; Manfredi, G.; Glass, J. D. SOD1 targeted to the mitochondrial intermembrane space prevents motor neuropathy in the Sod1 knockout mouse. *Brain* 134:196–209; 2011.
- Forkink, M.; Smeitink, J. A. M.; Brock, R.; Willems, P. H. G. M.; Koopman, W. J. H. Detection and manipulation of mitochondrial reactive oxygen species in mammalian cells. *Biochim. Biophys. Acta* 1797:1034–1044; 2010.
- Forman, H. J.; Kennedy, J. A. Role of superoxide radical in mitochondrial dehydrogenase reactions. *Biochem. Biophys. Res. Commun.* 60:1044–1050; 1974.

- [20] Forman, H. J.; Azzi, A. On the virtual existence of superoxide anions in mitochondria: thoughts regarding its role in pathophysiology. *FASEB J.* **11**:374–375; 1997.
- [21] Fridovich, I. Superoxide radical and superoxide dismutases. *Annu. Rev. Biochem.* **64**:97–112; 1995.
- [22] Griffith, O. W.; Meister, A. Origin and turnover of mitochondrial glutathione. *Proc. Nat. Acad. Sci. U.S.A.* **82**:4668–4672; 1985.
- [23] Guidot, D. M.; Repine, J. E.; Kitlowski, A. D.; Flores, S. C.; Nelson, S. K.; Wright, R. M.; McCord, J. M. Mitochondrial respiration scavenges extramitochondrial superoxide anion via a nonenzymatic mechanism. *J. Clin. Invest.* **96**:1131–1136; 1995.
- [24] Guo, Q. Q.; Yue, Q. L.; Zhao, J. J.; Wang, L.; Wang, H. S.; Wei, X. L.; Liu, J.; Jia, J. How far can hydroxyl radicals travel? An electrochemical study based on a DNA mediated electron transfer process. *Chem. Commun.* **47**:11906–11908; 2011.
- [25] Halliwell, B. Antioxidants: the basics—what they are and how to evaluate them. *Adv. Pharmacol.* **38**:3–20; 1997.
- [26] Ham, A. J.; Liebler, D. C. Vitamin E oxidation in rat liver mitochondria. *Biochemistry* **34**:5754–5761; 1995.
- [27] Han, D.; Antunes, F.; Canali, R.; Rettori, D.; Cadenas, E. Voltage-dependent anion channels control the release of the superoxide anion from mitochondria to cytosol. *J. Biol. Chem.* **278**:5557–5563; 2003.
- [28] Hanson, G. T.; Aggeler, R.; Oglesbee, D.; Cannon, M.; Capaldi, R. A.; Tsien, R. Y.; Remington, S. J. Investigating mitochondrial redox potential with redox-sensitive green fluorescent protein indicators. *J. Biol. Chem.* **279**:13044–13053; 2004.
- [29] Hashiguchi, K.; Bohr, V. A.; Souza-Pinto, N. C. Oxidative stress and mitochondrial DNA repair: implications for NRTIs induced DNA damage. *Mitochondrion* **4**:215–222; 2004.
- [30] Hauptmann, N.; Grimsby, J.; Shih, J. C.; Cadenas, E. The metabolism of tyramine by monoamine oxidase A/B causes oxidative damage to mitochondrial DNA. *Arch. Biochem. Biophys.* **335**:295–304; 1996.
- [31] Horton, K. L.; Stewart, K. M.; Fonseca, S. B.; Guo, Q.; Kelley, S. O. Mitochondria-penetrating peptides. *Chem. Biol.* **15**:375–382; 2008.
- [32] Hu, J.; Dong, L.; Outten, C. E. The redox environment in the mitochondrial intermembrane space is maintained separately from the cytosol and matrix. *J. Biol. Chem.* **283**:29126–29134; 2008.
- [33] Huang, Z.; Zhang, W.; Fang, H.; Zheng, M.; Wang, X.; Xu, J.; Cheng, H.; Gong, G.; Wang, W.; Dirksen, R. T.; Sheu, S. S. Response to “A critical evaluation of cpYFP as a probe for superoxide”. *Free Radic. Biol. Med.* **51**:1937–1940; 2011.
- [34] Hurd, T. R.; Costa, N. J.; Dahm, C. C.; Beer, S. M.; Brown, S. E.; Filipovska, A.; Murphy, M. P. Glutathionylation of mitochondrial proteins. *Antioxid. Redox Signal* **8**:999–1010; 2005.
- [35] Imai, H.; Nakagawa, Y. Biological significance of phospholipid hydroperoxide glutathione peroxidase (PHPGx, GPx4) in mammalian cells. *Free Radic. Biol. Med.* **34**:145–169; 2003.
- [36] James, A. M.; Cochemé, H. M.; Smith, R. A.; Murphy, M. P. Interactions of mitochondria-targeted and untargeted ubiquinones with the mitochondrial respiratory chain and reactive oxygen species: implications for the use of exogenous ubiquinones as therapies and experimental tools. *J. Biol. Chem.* **280**:21295–21312; 2005.
- [37] Jensen, P. K. Antimycin-insensitive oxidation of succinate and reduced nicotinamide-adenine dinucleotide in electron-transport particles. I. pH dependency and hydrogen peroxide formation. *Biochim. Biophys. Acta* **122**:157–166; 1966.
- [38] Jocelyn, P. C. Some properties of mitochondrial glutathione. *Biochim. Biophys. Acta* **369**:427–436; 1975.
- [39] Kakhlon, O.; Manning, H.; Breuer, W.; Melamed-Book, N.; Lu, C.; Cortopassi, G.; Munnich, A.; Cabantchik, Z. I. Cell functions impaired by frataxin deficiency are restored by drug-mediated iron relocation. *Blood* **112**:5219–5227; 2008.
- [40] Kalyanaram, B.; Darley-Usmar, V.; Davies, K. J.; Dennery, P. A.; Forman, H. J.; Grisham, M. B.; Mann, G. E.; Moore, K.; Roberts, L. J. 2nd; Ischiropoulos, H. Measuring reactive oxygen and nitrogen species with fluorescent probes: challenges and limitations. *Free Radic. Biol. Med.* **52**:1–6; 2012.
- [41] Kalyanaram, B. Oxidative chemistry of fluorescent dyes: implications in the detection of reactive oxygen and nitrogen species. *Biochem. Soc. Trans.* **39**:1221–1225; 2011.
- [42] Karlsson, M.; Kurz, T.; Brunk, U. T.; Nilsson, S. E.; Frennesson, C. I. What does the commonly used DCF test for oxidative stress really show? *Biochem. J.* **428**:183–190; 2010.
- [43] Kaufman, B. A.; Newman, S. M.; Hallberg, R. L.; Slaughter, C. A.; Perlman, P. S.; Butow, R. A. In organello formaldehyde crosslinking of proteins to mtDNA: identification of bifunctional proteins. *Proc. Nat. Acad. Sci. U.S.A.* **97**:7772–7777; 2000.
- [44] Koehler, C. M.; Beverly, K. N.; Leverich, E. P. Redox pathways of the mitochondrion. *Antioxid. Redox Signal* **6**:813–822; 2006.
- [45] Koide, Y.; Urano, Y.; Kenmoku, S.; Kojima, H.; Nagano, T. Design and synthesis of fluorescent probes for selective detection of highly reactive oxygen species in mitochondria of living cells. *J. Am. Chem. Soc.* **129**:10324–10325; 2007.
- [46] Koopman, W. J.; Nijtmans, L. G.; Dieteren, C. E.; Roestenberg, P.; Valsecchi, F.; Smeitink, J. A.; Willems, P. H. Mammalian mitochondrial complex I: biogenesis, regulation and reactive oxygen species generation. *Antioxid. Redox Signal* **12**:1431–1470; 2010.
- [47] Kowaltowski, A. J.; Cosso, R. G.; Campos, C. B.; Fiskum, G. Effect of Bcl-2 overexpression on mitochondrial structure and function. *J. Biol. Chem.* **277**:42802–42807; 2002.
- [48] Kowaltowski, A. J.; Souza-Pinto, N. C.; Castilho, R. F.; Vercesi, A. E. Mitochondria and reactive oxygen species. *Free Radic. Biol. Med.* **47**:333–343; 2009.
- [49] Kunduzova, O. R.; Bianchi, P.; Parini, A.; Cambon, C. Hydrogen peroxide production by monoamine oxidase during ischemia/reperfusion. *Eur. J. Pharmacol.* **448**:225–230; 2002.
- [50] Limon-Pacheco, J.; Gensebatt, M. E. The role of antioxidants and antioxidant-related enzymes in protective responses to environmentally induced oxidative stress. *Mutat. Res.* **674**:137–147; 2009.
- [51] Liu, Y.; Fiskum, G.; Schubert, D. Generation of reactive oxygen species by the mitochondrial electron transport chain. *J. Neurochem.* **80**:780–787; 2002.
- [52] Liu, S. S. Cooperation of a “reactive oxygen cycle” with the Q cycle and the proton cycle in the respiratory chain—superoxide generating and cycling mechanisms in mitochondria. *J. Bioenerg. Biomembr.* **31**:367–376; 1999.
- [53] Loschen, G.; Azzi, A.; Richter, C.; Flohe, L. Superoxide radicals as precursors of mitochondrial hydrogen peroxide. *FEBS Lett.* **42**:68–72; 1974.
- [54] Malinouski, M.; Zhou, Y.; Belousov, V. V.; Hatfield, D. L.; Gladyshev, V. N. Hydrogen peroxide probes directed to different cellular compartments. *PLoS One* **6**:e14564; 2011.
- [55] Maas, E.; Bisswanger, H. Localization of the α -oxoacid dehydrogenase multi-enzyme complexes within the mitochondrion. *FEBS Lett.* **277**:189–190; 1990.
- [56] Matés, J. M.; Pérez-Gómez, C.; Castro, I. N. Antioxidant enzymes and human diseases. *Clin. Biochem.* **32**:595–603; 1999.
- [57] Meredith, M. J.; Reed, D. J. Status of the mitochondrial pool of glutathione in the isolated hepatocyte. *J. Biol. Chem.* **257**:3747–3753; 1982.
- [58] Meyer, A. J.; Dick, T. P. Fluorescent protein-based redox probes. *Antioxid. Redox Signal* **13**:621–650; 2010.
- [59] Mikkelsen, R. B.; Wardman, P. Biological chemistry of reactive oxygen and nitrogen and radiation-induced signal transduction mechanisms. *Oncogene* **22**:5734–5754; 2003.
- [60] Miwa, S.; St-Pierre, J.; Partridge, L.; Brand, M. D. Superoxide and hydrogen peroxide production by *Drosophila* mitochondria. *Free Radic. Biol. Med.* **8**:938–948; 2003.
- [61] Monteiro, G.; Horta, B. B.; Pimenta, D. C.; Augusto, O.; Netto, L. E. S. Reduction of 1-Cys peroxiredoxins by ascorbate changes the thiol-specific antioxidant paradigm, revealing another function of vitamin C. *Proc. Nat. Acad. Sci. U.S.A.* **104**:4886–4891; 2007.
- [62] Mukai, K.; Kikuchi, S.; Urano, S. Stopped-flow kinetic study of the regeneration reaction of tocopheroxyl radical by reduced ubiquinone-10 in solution. *Biochim. Biophys. Acta* **1035**:77–82; 1990.
- [63] Muller, F. L. A critical evaluation of cpYFP as a probe for superoxide. *Free Radic. Biol. Med.* **47**:1779–1780; 2009.
- [64] Murphy, M. P.; Holmgren, A.; Larsson, N. G.; Halliwell, B.; Chang, C. J.; Kalyanaram, B.; Rhee, S. G.; Thornalley, P. J.; Partridge, L.; Gems, D.; Nyström, T.; Belousov, V.; Schumacker, P. T.; Winterbourn, C. C. Unraveling the biological roles of reactive oxygen species. *Cell Metab.* **13**:361–366; 2011.
- [65] Murphy, M. P.; Smith, R. A. Targeting antioxidants to mitochondria by conjugation to lipophilic cations. *Annu. Rev. Pharmacol. Toxicol.* **47**:629–656; 2007.
- [66] Murphy, M. How mitochondria produce reactive oxygen species. *Biochem. J.* **417**:1–13; 2009.
- [67] Netto, L. E.; de Oliveira, M. A.; Monteiro, G.; Demasi, A. P.; Cussiol, J. R.; Discola, K. F.; Demasi, M.; Silva, G. M.; Alves, S. V.; Faria, V. G.; Horta, B. B. Reactive cysteine in proteins: protein folding, antioxidant defense, redox signaling and more. *Comp. Biochem. Physiol. C Toxicol. Pharmacol.* **146**:180–193; 2007.
- [68] Nicholls, D. G.; Ward, M. W. Mitochondrial membrane potential and neuronal glutamate excitotoxicity: mortality and millivolts. *Trends Neurosci.* **23**:166–174; 2000.
- [69] Nohl, H.; Gille, L.; Kozlov, A.; Staniek, K. Are mitochondria a spontaneous and permanent source of reactive oxygen species? *Redox Rep.* **8**:135–141; 2003.
- [70] Nomura, K.; Imai, H.; Koumura, T.; Kobayashi, T.; Nakagawa, Y. Mitochondrial phospholipid hydroperoxide glutathione peroxidase inhibits the release of cytochrome c from mitochondria by suppressing the peroxidation of cardiolipin in hypoglycaemia-induced apoptosis. *Biochem. J.* **351**:183–193; 2000.
- [71] Okado-Matsumoto, A.; Fridovich, I. Subcellular distribution of superoxide dismutases (SOD) in rat liver: Cu,Zn-SOD in mitochondria. *J. Biol. Chem.* **276**:38388–38393; 2001.
- [72] Ostergaard, H.; Henriksen, A.; Hansen, F. G.; Winther, J. R. Shedding light on disulfide bond formation: engineering a redox switch in green fluorescent protein. *EMBO J.* **20**:5853–5862; 2001.
- [73] Pedersen, A.; Karlsson, G. B.; Rydström, J. Proton-translocating transhydrogenase: an update of unsolved and controversial issues. *J. Bioenerg. Biomembr.* **40**:463–473; 2008.
- [74] Pereverzev, M. O.; Vygodina, T. V.; Konstantinov, A. A.; Skulachev, V. P. Cytochrome c, an ideal antioxidant. *Biochem. Soc. Trans.* **31**:1312–1315; 2003.
- [75] Plectić-Hlavatá, L.; Jezek, J.; Jezek, P. Pro-oxidant mitochondrial matrix-targeted ubiquinone MitoQ10 acts as anti-oxidant at retarded electron transport or proton pumping within Complex I. *Int. J. Biochem. Cell Biol.* **41**:1697–1707; 2009.
- [76] Pryor, W. A. Oxy-radicals and related species: their formation, lifetimes, and reactions. *Annu. Rev. Physiol.* **48**:657–667; 1986.

- [77] Radi, R.; Turrens, J. F.; Chang, L. Y.; Bush, K. M.; Crapoll, J. D.; Freeman, B. A. Detection of catalase in rat heart mitochondria. *J. Biol. Chem.* **266**:22028–22034; 1991.
- [78] Ramshesh, V. K.; Lemasters, J. J. Imaging of mitochondrial pH using SNARF-1. *Methods Mol. Biol.* **810**:243–248; 2012.
- [79] Redmond, R. W.; Kochevar, I. E. Spatially resolved cellular responses to singlet oxygen. *Photochem. Photobiol.* **82**:1178–1186; 2006.
- [80] Rhee, S. G.; Kang, S. W.; Chang, T.; Jeong, W.; Kim, K. Peroxiredoxin, a novel family of peroxidases. *IUBMB Life.* **52**:35–41; 2001.
- [81] Rhee, S. G.; Chang, T. S.; Jeong, W.; Kang, D. Methods for detection and measurement of hydrogen peroxide inside and outside of cells. *Mol. Cells* **29**:539–549; 2010.
- [82] Robinson, K. M.; James, M. S.; Pehar, M.; Monette, J. S.; Ross, M. F.; Hagen, T. M.; Murphy, M. P.; Beckman, J. S. Selective fluorescent imaging of superoxide in vivo using ethidium-based probes. *Proc. Nat. Acad. Sci. U.S.A.* **103**:15038–15043; 2006.
- [83] Roma, L. P.; Duprez, J.; Takahashi, H. K.; Gilon, P.; Wiederkehr, A.; Jonas, J. C. Dynamic measurements of mitochondrial hydrogen peroxide concentration and glutathione redox state in rat pancreatic β -cells using ratiometric fluorescent proteins: confounding effects of pH with HyPer but not roGFP1. *Biochem. J.* **441**:971–978; 2012.
- [84] Salvador, A.; Sousa, J.; Pinto, R. E. Hydroperoxyl, superoxide and pH gradients in the mitochondrial matrix: a theoretical assessment. *Free Radic. Biol. Med.* **31**:1208–1215; 2001.
- [85] Salvi, M.; Battaglia, V.; Brunati, A. M.; La Rocca, N.; Tibaldi, E.; Pietrangeli, P.; Marocci, L.; Mondovi, B.; Rossi, C. A.; Toninello, A. Catalase takes part in rat liver mitochondrial oxidative stress defense. *J. Biol. Chem.* **282**:24407–24415; 2007.
- [86] Sato, H.; Tachifuji, A.; Tamura, M.; Miyakawa, I. Identification of the YMN-1 antigen protein and biochemical analyses of protein components in the mitochondrial nucleoid fraction of the yeast *Saccharomyces cerevisiae*. *Protoplasma* **219**:51–58; 2002.
- [87] Schwarzländer, M.; Logan, D. C.; Fricker, M. D.; Sweetlove, L. J. The circularly permuted yellow fluorescent protein cpYFP that has been used as a superoxide probe is highly responsive to pH but not superoxide in mitochondria: implications for the existence of superoxide "flashes". *Biochem. J.* **437**:381–387; 2011.
- [88] Selivanov, V. A.; Zeak, J. A.; Roca, J.; Cascante, M.; Trucco, M.; Votyakova, T. V. The role of external and matrix pH in mitochondrial reactive oxygen species generation. *J. Biol. Chem.* **283**:29292–29300; 2008.
- [89] Shioji, K.; Oyama, Y.; Okuma, K.; Nakagawa, H. Synthesis and properties of fluorescence probe for detection of peroxides in mitochondria. *Bioorg. Med. Chem. Lett.* **20**:3911–3915; 2010.
- [90] Schriener, S. E.; Linford, N. J.; Martin, G. M.; Treuting, P.; Ogburn, C. E.; Emond, M.; Coskun, P. E.; Ladiges, W.; Wolf, N.; Van Remmen, H.; Wallace, D. C.; Rabinovitch, P. S. Extension of murine life span by overexpression of catalase targeted to mitochondria. *Science* **308**:1909–1911; 2005.
- [91] Simonson, S. G.; Zhang, J.; Canada Jr. A. T.; Su, Y. F.; Benveniste, H.; Piantadosi, C. A. Hydrogen peroxide production by monoamine oxidase during ischemia-reperfusion in the rat brain. *J. Cereb. Blood Flow Metab.* **13**:125–134; 1993.
- [92] Skulachev, M. V.; Antonenko, Y. N.; Anisimov, V. N.; Chernyak, B. V.; Cherepanov, D. A.; Chistyakov, V. A.; Egorov, M. V.; Kolosova, N. G.; Korshunova, G. A.; Lyamzaev, K. G.; Plotnikov, E. Y.; Roginsky, V. A.; Savchenko, A. Y.; Severina, I. I.; Severin, F. F.; Shkurat, T. P.; Tashlitsky, V. N.; Shidlovsky, K. M.; Vyssokikh, M. Y.; Zamyatin Jr. A. A.; Zorov, D. B.; Skulachev, V. P. Mitochondrial-targeted plastoquinone derivatives: effect on senescence and acute age-related pathologies. *Curr. Drug Targets* **12**:800–826; 2011.
- [93] Skulachev, V. P. Cytochrome c in the apoptotic and antioxidant cascades. *FEBS Lett.* **423**:275–280; 1998.
- [94] Skulachev, V. P.; Antonenko, Y. N.; Cherepanov, D. A.; Chernyak, B. V.; Izyumov, D. S.; Khailova, L. S.; Klislin, S. S.; Korshunova, G. A.; Lyamzaev; Pletjushkina, O. Y.; Roginsky, V. A.; Rokitskaya, T. I.; Severin, F. F.; Severina, I. I.; Simonyan, R. A.; Skulachev, M. V.; Sumbatyan, N. V.; Sukhanova, E. I.; Tashlitsky, V. N.; Trendeleva, T. A.; Vyssokikh, M. Y.; Zvyagilskaya, R. A. Prevention of cardioplipin oxidation and fatty acid cycling as two antioxidant mechanisms of cationic derivatives of plastoquinone (SkQs). *Biochim. Biophys. Acta* **1797**:878–889; 2010.
- [95] Skulachev, V. P. Uncoupling: new approaches to an old problem of bioenergetics. *Biochim. Biophys. Acta* **1363**:100–124; 1998.
- [96] Smith, R. A.; Murphy, M. P. Animal and human studies with the mitochondria-targeted antioxidant MitoQ. *Ann. N. Y. Acad. Sci.* **1201**:96–103; 2010.
- [97] Song, Y.; Garry, R. B. Thermodynamic and kinetic considerations for the reaction of semiquinone radicals to form superoxide and hydrogen peroxide. *Free Radic. Biol. Med.* **49**:919–962; 2010.
- [98] Sousa-Lopes, A.; Antunes, F.; Cyrne, L.; Marinho, H. S. Decreased cellular permeability to H₂O₂ protects *Saccharomyces cerevisiae* cells in stationary phase against oxidative stress. *FEBS Lett.* **578**:152–156; 2004.
- [99] Srikun, D.; Albers, A. E.; Nam, C. I.; Iavarone, A. T.; Chang, C. J. Organelle-targetable fluorescent probes for imaging hydrogen peroxide in living cells via SNAP-Tag protein labeling. *J. Am. Chem. Soc.* **132**:4455–4465; 2010.
- [100] Staniek, K.; Nohl, H. Are mitochondria a permanent source of reactive oxygen species? *Biochem. Biophys. Acta* **1460**:268–275; 2000.
- [101] St-Pierre, J.; Buckingham, J. A.; Roebuck, S. J.; Brand, M. D. Topology of superoxide production from different sites in the mitochondrial electron transport chain. *J. Biol. Chem.* **277**:44784–44790; 2002.
- [102] Starkov, A. A.; Fiskum, G.; Chinopoulos, C.; Lorenzo, B. J.; Browne, S. E.; Patel, M. S.; Beal, M. F. Mitochondrial α -ketoglutarate dehydrogenase complex generates reactive oxygen species. *J. Neurosci.* **24**:7779–7788; 2004.
- [103] Sukhanova, E. I.; Trendeleva, T. A.; Zvyagilskaya, R. A. Interaction of yeast mitochondria with fatty acids and mitochondria-targeted lipophilic cations. *Biochem. (Moscow)* **75**:139–144; 2010.
- [104] Swift, L. M.; Sarvazyan, N. Localization of dichlorofluorescein in cardiac myocytes: implications for assessment of oxidative stress. *Am. J. Phys.* **278**:H982–H990; 2000.
- [105] Szteto, H. H. Mitochondria-targeted peptide antioxidants: novel neuroprotective agents. *AAAPS J.* **8**:E521–E531; 2006.
- [106] Tahara, E. B.; Barros, M. H.; Oliveira, G. A.; Netto, L. E. S.; Kowaltowski, A. J. Dihydropyridyl dehydrogenase as a source of reactive oxygen species inhibited by caloric restriction and involved in *Saccharomyces cerevisiae* aging. *FASEB J.* **21**:274–283; 2007.
- [107] Tahara, E. B.; Cezário, K.; Souza-Pinto, N. C.; Barros, M. H.; Kowaltowski, A. J. Respiratory and TCA cycle activities affect *S. cerevisiae* lifespan, response to caloric restriction and mtDNA stability. *J. Bioenerg. Biomembr.* **43**:483–491; 2011.
- [108] Tahara, E. B.; Navarete, F. D.; Kowaltowski, A. J. Tissue-, substrate-, and site-specific characteristics of mitochondrial reactive oxygen species generation. *Free Radic. Biol. Med.* **9**:1283–1297; 2009.
- [109] Thomas, J. P.; Maiorino, M.; Ursini, F.; Girotti, A. W. Protective action of phospholipid hydroperoxide glutathione peroxidase against membrane-damaging lipid peroxidation. *J. Biol. Chem.* **265**:454–461; 1990.
- [110] Thomas, S. M.; Gebicki, J. M.; Dean, R. T. Radical initiated α -tocopherol depletion and lipid peroxidation in mitochondrial membranes. *Biochim. Biophys. Acta* **1002**:189–197; 1989.
- [111] Tretter, L.; Adam-Vizi, V. Generation of reactive oxygen species in the reaction catalyzed by α -ketoglutarate dehydrogenase. *J. Neurosci.* **24**:7771–7778; 2004.
- [112] Tretter, L.; Takacs, K.; Kővér, K.; Adam-Vizi, V. Stimulation of H₂O₂ generation by calcium in brain mitochondria respiring on α -glycerophosphate. *J. Neurosci. Res.* **15**:3471–3479; 2007.
- [113] Tretter, L.; Takacs, K.; Hegedus, V.; Adam-Vizi, V. Characteristics of α -glycerophosphate-evoked H₂O₂ generation in brain mitochondria. *J. Neurochem.* **3**:650–663; 2007.
- [114] Turrens, J. F. Mitochondrial formation of reactive oxygen species. *J. Physiol.* **552**:335–344; 2003.
- [115] Ursini, F.; Maiorino, M.; Gregolin, C. The selenoenzyme phospholipid hydroperoxide glutathione peroxidase. *Biochim. Biophys. Acta* **839**:62–70; 1985.
- [116] Valko, M.; Leibfriz, D.; Moncol, J.; Cronin, M. T. D.; Mazur, M.; Telser, J. Free radicals and antioxidants in normal physiological functions and human disease. *Int. J. Biochem. Cell Biol.* **39**:44–84; 2007.
- [117] Vasquez-Vivar, J.; Kalyanaram, B.; Kennedy, M. C. Mitochondrial aconitase is a source of hydroxyl radical: an electron spin resonance investigation. *J. Biol. Chem.* **19**:14064–14069; 2000.
- [118] Wang, W.; Fang, H.; Groom, L.; Cheng, A.; Zhang, W.; Liu, J.; Wang, X.; Li, K.; Han, P.; Zheng, M.; Yin, J.; Wang, W.; Mattson, M. P.; Kao, J. P.; Lakatta, E. G.; Sheu, S. S.; Ouyang, K.; Chen, J.; Dirksen, R. T.; Cheng, H. Superoxide flashes in single mitochondria. *Cell* **134**:279–290; 2008.
- [119] Waypa, G. B.; Marks, J. D.; Guzy, R.; Mungai, P. T.; Schriever, J.; Dokic, D.; Schumacker, P. T. Hypoxia triggers subcellular compartmental redox signaling in vascular smooth muscle cells. *Circ. Res.* **106**:526–535; 2010.
- [120] Weisiger, R. A.; Fridovich, I. Superoxide dismutase: organelle specificity. *J. Biol. Chem.* **248**:3582–3592; 1973.
- [121] Winterbourn, C. C.; Hampton, M. B. Thiol chemistry and specificity in redox signaling. *Free Radic. Biol. Med.* **45**:549–561; 2008.
- [122] Wrona, M.; Wardman, P. Properties of the radical intermediate obtained on oxidation of 2',7'-dichlorodihydrofluorescein, a probe for oxidative stress. *Free Radic. Biol. Med.* **41**:657–667; 2006.
- [123] Yeh, J. I.; Chinte, U.; Du, S. Structure of glycerol-3-phosphate dehydrogenase, an essential monotopic membrane enzyme involved in respiration and metabolism. *Proc. Nat. Acad. Sci. U.S.A.* **105**:3280–3285; 2008.
- [124] Yankovskaya, V.; Horsefield, R.; Trnroth, S.; Luna-Chavez, C.; Miyoshi, H.; Léger, C.; Byrne, B.; Cecchini, G.; Iwata, S. Architecture of succinate dehydrogenase and reactive oxygen species generation. *Science* **299**:700–704; 2003.
- [125] Zhang, L.; Yu, L.; Yu, C. A. Generation of superoxide anion by succinate-cytochrome c reductase from bovine heart mitochondria. *J. Biol. Chem.* **273**:33972–33976; 1998.
- [126] Zhao, K.; Zhao, G. M.; Wu, D.; Soong, Y.; Birk, A. V.; Schiller, P. W.; Szteto, H. H. Cell-permeable peptide antioxidants targeted to inner mitochondrial membrane inhibit mitochondrial swelling, oxidative cell death, and reperfusion injury. *J. Biol. Chem.* **279**:34682–34690; 2004.
- [127] Zhou, M.; Diwu, Z.; Panchuk-Voloshina, N.; Haugland, R. P. A stable nonfluorescent derivative of resorufin for the fluorometric determination of trace hydrogen peroxide: applications in detecting the activity of phagocyte NADPH oxidase and other oxidases. *Anal. Biochem.* **253**:162–168; 1997.
- [128] Zielonka, J.; Kalyanaram, B. Hydroethidine- and MitoSOX-derived red fluorescence is not a reliable indicator of intracellular superoxide formation: another inconvenient truth. *Free Radic. Biol. Med.* **48**:983–1001; 2010.
- [129] Zoccarato, F.; Cavallini, L.; Deana, R.; Alexandre, A. Pathways of hydrogen peroxide generation in guinea pig cerebral cortex mitochondria. *Biochem. Biophys. Res. Commun.* **2**:727–734; 1988.

Ap.5 Bicarbonate modulates oxidative and functional damage in ischemia-reperfusion

Free Radical Biology and Medicine 55 (2013) 46–53



ELSEVIER

Contents lists available at SciVerse ScienceDirect

Free Radical Biology and Medicine

journal homepage: www.elsevier.com/locate/freeradbiomed

Original Contribution

Bicarbonate modulates oxidative and functional damage in ischemia–reperfusion

Bruno B. Queliconi^a, Thire B.M. Marazzi^a, Sandra M. Vaz^a, Paul S. Brookes^b, Keith Nehrke^b, Ohara Augusto^a, Alicia J. Kowaltowski^{a,*}^a Departamento de Bioquímica, Instituto de Química, Universidade de São Paulo, 05508–900 São Paulo, SP, Brazil^b University of Rochester Medical Center, Rochester, NY 14642, USA

ARTICLE INFO

Article history:

Received 25 May 2012

Received in revised form

1 November 2012

Accepted 13 November 2012

Available online 27 November 2012

Keywords:

Carbonate radical

Ischemic damage

Heart

Caenorhabditis elegans

Free radicals

ABSTRACT

The carbon dioxide/bicarbonate ($\text{CO}_2/\text{HCO}_3^-$) pair is the main biological pH buffer. However, its influence on biological processes, and in particular redox processes, is still poorly explored. Here we study the effect of $\text{CO}_2/\text{HCO}_3^-$ on ischemic injury in three distinct models (cardiac HL-1 cells, perfused rat heart, and *Caenorhabditis elegans*). We found that, although various concentrations of $\text{CO}_2/\text{HCO}_3^-$ do not affect function under basal conditions, ischemia–reperfusion or similar insults in the presence of higher $\text{CO}_2/\text{HCO}_3^-$ resulted in greater functional loss associated with higher oxidative damage in all models. Because the effect of $\text{CO}_2/\text{HCO}_3^-$ was observed in all models tested, we believe this buffer is an important determinant of oxidative damage after ischemia–reperfusion.

© 2012 Elsevier Inc. All rights reserved.

Introduction

CO_2 , formed in a multitude of intracellular reactions, is hydrated in a reaction catalyzed by carbonic anhydrase to carbonic acid (H_2CO_3), which deprotonates, generating bicarbonate (HCO_3^-). The $\text{CO}_2/\text{HCO}_3^-$ pair, with a pK_a of 6.4, is the main physiological buffer, due mostly to its high concentration in biological compartments (extracellular fluid pH is ~ 7.2 [10,14]).

Interestingly, despite its ubiquity and abundance, biological activities of the $\text{CO}_2/\text{HCO}_3^-$ pair have received very little attention, probably because there is little ability to control concentrations in vivo. Bicarbonate buffer, which is composed of ~ 1.3 mM CO_2 in equilibrium with 25 mM HCO_3^- in serum and 14 mM HCO_3^- intracellularly, has well-demonstrated redox effects (see [23] for a review). The first suggestion in this sense came from Hodgson and Fridovich in 1976 [15], who reported that xanthine oxidase-catalyzed luminescence was dependent on the presence of carbonate. After that, a series of studies demonstrated that the presence of $\text{CO}_2/\text{HCO}_3^-$ stimulates the oxidation, peroxidation,

and nitration of various biomolecules [2,3,21,24,27,34,42,43]. The mechanism through which $\text{CO}_2/\text{HCO}_3^-$ stimulates these oxidations has been elucidated for peroxynitrite-mediated processes but remains uncovered in most cases because of methodological difficulties involving the detection of highly reactive intermediates, such as the carbonate radical (see [23] for a review).

Most studies addressing the role of $\text{CO}_2/\text{HCO}_3^-$ in biological oxidations have been exclusively conducted in vitro or, less commonly, in vivo systems to which oxidants were added exogenously, promoting overt oxidative stress followed by an evaluation of the effects of HCO_3^- [10]. This still leaves open the question if $\text{CO}_2/\text{HCO}_3^-$ levels are relevant for oxidative injury resulting from reactive oxygen species (ROS)¹ generated endogenously in vivo under physiological or pathological conditions. The question is highly relevant because, owing to their reactive and diverse nature, ROS effects mostly result from localized intracellular reactions [6,39]. In addition, quantities of added oxidants may differ very significantly from those produced intracellularly, even under pathological conditions. The demonstration that $\text{CO}_2/\text{HCO}_3^-$ levels affect tissues under physiologically relevant conditions would provide evidence, albeit indirect, of the participation of carbonate radicals in biologically relevant processes [23].

To address this point, we chose to study the effects of $\text{CO}_2/\text{HCO}_3^-$ in ischemia–reperfusion (IR). IR occurs in important pathological conditions such as heart attack and stroke and involves a burst in ROS production and oxidative damage, mainly during

Abbreviations: DNPH, 2,4-dinitrophenylhydrazine; BCECF, 2',7'-bis(carboxyethyl)-5(6)-carboxyfluorescein; BPM, beats per minute; DTT, dithiothreitol; IR, ischemia–reperfusion; AS, anoxia–starvation; NGM, normal growth medium; PLML, posterior lateral microtubule cell left; PLMR, posterior lateral microtubule cell right; ROS, reactive oxygen species; SDS, sodium dodecyl sulfate

* Corresponding author. Fax: +55 11 38155579.

E-mail address: alicia@iq.usp.br (A.J. Kowaltowski).

reperfusion, that is a determinant of the final outcome of tissue damage [12,22,35]. Furthermore, because of the nature of these pathologies, which involve changes in local tensions of diluted gasses and modifications from oxidative to fermentative metabolism, $\text{CO}_2/\text{HCO}_3^-$ levels are expected to change during IR and may, thus, have an important role in determining the extent of posts ischemic lesions.

The effects of $\text{CO}_2/\text{HCO}_3^-$ levels on functional and oxidative damage after IR were tested in three distinct models, under conditions in which external pH was clamped despite the changes in $\text{CO}_2/\text{HCO}_3^-$ concentrations. Our results show that $\text{CO}_2/\text{HCO}_3^-$ levels contribute strongly toward posts ischemic functional loss and oxidative damage.

Materials and methods

Materials

All chemicals were of the highest purity available from Sigma (St. Louis, MO, USA), unless otherwise specified. BCECF was purchased from Molecular Probes (Eugene, OR, USA). Antibody sources are provided under Western blots.

Isolated heart perfusion

Heart perfusion was conducted as described previously [12]. Briefly, hearts were rapidly removed from male Sprague–Dawley rats (~300 g, 2–3 months of age) and Langendorff-perfused with oxygenated Krebs–Henseleit buffer (described below). Hearts were eliminated from the study if the time between rat death and the beginning of perfusion was longer than 3 min. All studies were conducted in accordance with guidelines for animal care and use established by the *Colégio Brasileiro de Experimentação Animal* and approved by the local animal ethics committee.

After isolation, the hearts were stabilized for 50 min and then subjected to 30 min ischemia and 60 min reperfusion. The reperfusion was conducted with buffers containing 0, 5, and 10% CO_2 . The buffer for 0% CO_2 contained (in mmol/L) 118 NaCl, 1.2 KH_2PO_4 , 4.7 KCl, 1.2 MgSO_4 , 1.25 CaCl_2 , 10 glucose, and 20 Na^+ -Hepes, pH 7.4, gassed with pure O_2 , at 37°C; that for 5% (in mmol/L) 118 NaCl, 17 NaHCO_3 , 1.2 KH_2PO_4 , 4.7 KCl, 1.2 MgSO_4 , 1.25 CaCl_2 , 10 glucose, and 20 Na^+ -Hepes, pH 7.4, at 37°C gassed with 95% O_2 + 5% CO_2 ; and that for 10% (in mmol/L) 118 NaCl, 25 NaHCO_3 , 1.2 KH_2PO_4 , 4.7 KCl, 1.2 MgSO_4 , 1.25 CaCl_2 , 10 glucose, and 20 Na^+ -Hepes, pH 7.4, at 37°C gassed with 90% O_2 + 10% CO_2 . L-NAME (200 μM), when present, was added 10 min before ischemia and remained in the perfusate until the end of the reperfusion time.

Hemodynamic data were obtained using an electrode connected to a Powerlab Langendorff apparatus from ADInstruments. The pressure transducer was connected to a latex balloon and placed inside the left ventricle, as described previously [12].

Infarcted area

Quantification of the infarcted area was conducted as previously described [5,13]. Briefly, after reperfusion the heart was sliced and incubated in 1% triphenyltetrazolium chloride for 15 min. The infarcted area was quantified using ImageJ and is presented as a percentage of the total area of the slice. Each heart was sliced in three places and the areas from both sides were quantified by an unblinded scorer and averaged.

Cardiac HL-1 cell cultures and simulated cellular IR

Cardiac HL-1 cells were kindly donated by Professor William C. Claycomb. These cells maintain their cardiac phenotype during

extended passages and present ordered myofibrils, cardiac-specific junctions, and voltage-dependent currents that are characteristic of a cardiac myocyte phenotype [7]. For routine growth, HL-1 cells were maintained in T-75 flasks at 37°C in an atmosphere of 5% CO_2 in Claycomb medium (Sigma) supplemented with 0.1 mM norepinephrine, 100 U/ml penicillin, 100 U/ml streptomycin, 2 mM glutamine, and 10% fetal bovine serum. Experiments were conducted at 100% confluence, after trypsinization and resuspension in a standard buffer (pH 7.4) containing (in mmol/L) 137 NaCl, 20 Na-Hepes, 22 glucose, 5 Na-pyruvate, 20 taurine, 5 creatine, 5.4 KCl, 1 MgCl_2 , and 1 CaCl_2 .

Cell IR was simulated as previously described [11,12]. Briefly, 10^6 cells/ml were subjected to simulated ischemia by metabolic inhibition using 50 mM KCN and 2 mM 2-deoxyglucose added to standard cell buffer devoid of glucose and pyruvate for 90 min, followed by 5 min centrifugation and resuspension of the cell pellet in experiment buffer for simulated reperfusion. Control HL-1 cardiomyocytes were incubated with standard buffer solution during the entire experimental period and subjected only to centrifugations and washes. The standard buffer was gassed with 100% O_2 for the 0% CO_2 condition, and 25 mM NaHCO_3 was added to a buffer gassed with a mixture of 90% O_2 + 10% CO_2 for 10% CO_2 condition.

Cell viability

Cell viability was assessed by relative fluorescence of 50 μM ethidium bromide (Sigma–Aldrich) using a Hitachi F4500 spectrofluorimeter at excitation and emission wavelengths of 365 and 580 nm, respectively [11,12,17]. Cells were permeabilized with 0.1% Triton at the end of the each experiment to promote 100% cell death. The autofluorescence of ethidium bromide was subtracted from total fluorescence in the presence of cells, ethidium bromide, and Triton. Data are expressed as the percentage of total cells.

Intracellular pH measurements

pH measurements were conducted using the highly sensitive intracellular probe BCECF, with a modification of a described method [16,30]. Cells were trypsinized, washed, and resuspended in experimental buffer (described in the cell IR protocol) twice. Cells ($10^6/\text{ml}$) were incubated with 5 μM BCECF for 90 min, pelleted, and resuspended in experimental buffer. The readings were conducted using a Hitachi F4500 spectrofluorimeter with fixed emission at 535 nm. The excitation was scanned from 400 to 550 nm. After the measurement of the baseline fluorescence, calibration was conducted adding 10 mg/ml nigericin to allow from proton exchange across the plasma membrane and adding NaOH and HCl to promote maximal alkalization and acidification. The intracellular pH was calculated as described by the maker. Briefly, the formula used was $[\text{H}^+] = K_a((R - R_A)/(R_B - R))(F_{A(\lambda_2)}/F_{B(\lambda_2)})$, where R is the $F_{(\lambda_1)}/F_{(\lambda_2)}$ ratio of fluorescence intensities (F) measured at two wavelengths, λ_1 , 490 nm, and λ_2 , 440 nm, and the subscripts A and B represent the limiting values at the acidic and basic endpoints of the titration, respectively.

Caenorhabditis elegans culture and strains

C. elegans were cultured using standard techniques at 20°C on normal growth medium (NGM) agar plates [4]. Synchronized young adults were used in the experiments. The strains used were Bristol N2 (wild type) and KWN85 (*him-5(e1490)V*, *uls22(Pmec-18::GFP)V*).

C. elegans anoxia–starvation (AS)

IR in *C. elegans* was simulated by promoting AS followed by reoxygenation and feeding, as previously described [32,40,41].

C. elegans young adults were collected from NGM plates, washed three times, and resuspended in M9 medium (22 mM KH_2PO_4 , 42 mM Na_2HPO_4 , 86 mM NaCl, 1 mM MgSO_4 , pH 7.0) supplemented with 20 mM Hepes. The animals were incubated in 100 μl of M9 in an open Eppendorf tube at 26 °C for 20 h under either 100 or 90% N_2 and 10% CO_2 . After AS, *C. elegans* were moved to a seeded plate with a minimal amount of M9 and left to recover for another 24 h and then scored by an unblinded observer for viability and sensitivity to touch.

C. elegans neuron imaging

Animals were transferred to a 2% M9 agarose pad containing 0.1% tetramisole and 0.1% tricaine (EMS, Hatfield, PA, USA) and were imaged within 20 min of being placed under a coverslip. A Nikon Eclipse TE2000-U microscope (Nikon USA, Melville, NY, USA), Polychrome V monochromator (TILL Photonics, Gräfelfing, Germany), and Cooke Sencicam CCD (PCO-TECH, Romulus, MI, USA) were coordinated using TILLvisION software to obtain fluorescence images (470 nm excitation/535 nm emission) under a 100 \times oil objective.

Western blots

Western blots used 12% denaturing gels. Gels were transferred (4 h, 400 mV) onto polyvinylidene difluoride membranes. Protein was quantified by the Bradford technique. For carbonylation detection, 5 μg of protein was used per lane. Detection of 3-nitrotyrosine and methionine sulfoxide residues used 10 μg of protein.

The samples from hearts and cells were prepared by homogenizing the tissue or the cells in the presence of a RIPA buffer (135 mM NaCl, 50 mM Tris-HCl, 1% Nonidet P-40, 0.5% sodium deoxycholate, 0.1% SDS, and 1:10 Sigma proteinase inhibitor cocktail, pH 8) and frozen at -80°C until use. For *C. elegans* samples, the live worms were selected after reperfusion and resuspended in buffer previously described in [5] (0.2 M Tris-HCl, 100 mM DTT, 20% glycerol, 10% SDS, and 1:10 Sigma proteinase inhibitor cocktail, pH 8), subjected to three freeze/thaw cycles (liquid nitrogen/boiling water), and frozen at -80°C until use.

For the carbonylation Western blots, samples were treated as described before [8,26], or the OxyBlot kit from Millipore was used and the reactions were done as described by the manufacturer. Briefly, we added SDS to the samples to reach a final concentration of 12% and then subjected the proteins to

a reaction with 2,4-dinitrophenylhydrazine (DNPH) for 30 min followed by the addition of a neutralization buffer. For detection, we used 1:5000 anti-DNP antibody from Sigma and 1:7000 anti-rabbit from Calbiochem. For other Western blots, we added the protein with sample buffer (20 μg). Antibody concentrations were anti-nitrotyrosine from Upstate, 1:5000; anti-mouse from Calbiochem, 1:5000; anti-methionine sulfoxide from Upstate, 1:5000; and anti-rabbit from Calbiochem and anti-phospho-Akt(Ser473) from Cell Signaling, 1:5000.

The blots were scanned and analyzed using ImageJ. Images were converted to 8 bits color and intensities of the whole lane were included. Blots were compared to the 0% CO_2 control or to the 0% CO_2 ischemic group. In the 3-nitrotyrosine blot, we ran a standard amount of nitrated protein to quantify modified tyrosine.

Statistics

All experiments presented were replicated at least three times, and statistical analysis was conducted using GraphPad Prism 5. Fig. 2A, B, D, and E were analyzed using two-way ANOVA followed by Bonferroni correction, and all other data were analyzed using Student *t* tests. Correlations were analyzed using linear fits. Differences were considered significant if $p < 0.05$.

Results

Our aim in this work was to evaluate the impact of $\text{CO}_2/\text{HCO}_3^-$ on oxidative and functional tissue damage under the pathologically relevant condition of IR. Because $\text{CO}_2/\text{HCO}_3^-$ is a vital buffer, and we wished to focus on the effects of $\text{CO}_2/\text{HCO}_3^-$ itself, and not changes in pH, all extracellular solutions used in this study were buffered using Hepes, and the pH was carefully adjusted after gassing. Additionally, we questioned if, despite the clamped pH, changes in extracellular $\text{CO}_2/\text{HCO}_3^-$ concentrations could result in alterations in intracellular pH. To address this question, we used cardiac HL-1 cells, a cell line that maintains the cardiac phenotype and has been extensively used to study cardiac IR (Fig. 1) [7,12,38]. Cells were loaded with the intracellular pH probe BCECF, and intracellular pH was measured in the absence or presence of $\text{CO}_2/\text{HCO}_3^-$ (indicated as the percentage of gassed CO_2 , 0 or 10%). We found that intracellular pH was indistinguishable under both incubation conditions (Fig. 1A). Thus, the conditions established allow for the evaluation of the biological role of $\text{CO}_2/\text{HCO}_3^-$ independent of changes in physiological intracellular pH.

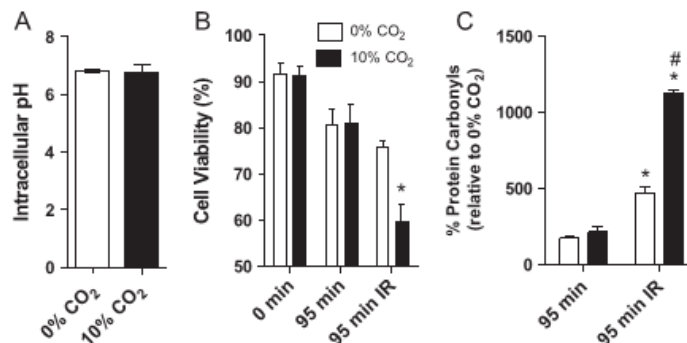


Fig. 1. Cardiac HL-1 cells present increased oxidative damage and loss of viability when subjected to IR in the presence of CO_2 . (A) Intracellular pH was measured as described under Materials and methods, in the presence or absence of CO_2 , after 95 min stabilization. (B) Cell viability was measured in the absence (open bars) or presence (filled bars) of 10% $\text{H}_2\text{CO}_3/\text{HCO}_3^-$. Cell viability was measured as described under Materials and methods, at 0 and 95 min, in the absence or presence of IR, as indicated and (C) Protein carbonyl levels were detected as described under Materials and methods and are shown as percentage of 0% CO_2 levels at 0 min. * $p < 0.05$ relative to nonischemic, 95 min; # $p < 0.05$ relative to 95 min IR in 0% CO_2 .

We then subjected the cells to simulated IR (see Materials and methods) in the presence of 0 and 10% CO₂ (Fig. 1B). We found that after IR, cells incubated in buffer containing CO₂/HCO₃⁻ (filled bars, 95 min IR) had significantly lower viability compared to cells incubated in the absence of CO₂/HCO₃⁻ (open bars). Indeed, cell viability in the absence of CO₂ was similar to that of cells subjected to 95 min incubation and centrifugations, but not IR. Cell viability before the ischemic intervention (0 min) and under nonischemic conditions (95 min) was similar in both CO₂/HCO₃⁻-containing and 0% CO₂ groups, indicating that changes in CO₂/HCO₃⁻ levels do not affect cell viability under physiological conditions, but exacerbate cell death after IR.

To verify if the loss of cell survival was associated with oxidative damage, we measured protein carbonyls in cell lysates. We found that incubation and centrifugation of samples for 95 min in the absence of IR increased carbonyl levels slightly relative to baseline in both 0 and 10% CO₂ (Fig. 1C, 95 min). However, after 95 min IR, very significant increments in protein carbonyl levels were observed, and this increase was substantially larger in 10% CO₂ samples. Together, these results demonstrate that the presence of CO₂/HCO₃⁻ substantially affects cell survival and oxidative damage after IR in cardiac cells.

Given the striking results of changes in CO₂/HCO₃⁻ concentrations in cells subjected to IR, we sought next to evaluate the effects of these on ischemic hearts. Langendorff-perfused rat

hearts were either maintained for 150 min without any intervention (nonischemic) or subjected to IR as described under Materials and methods (Fig. 2). We found that the various gassed CO₂ concentrations (0, 5, or 10%) did not affect nonischemic heart beat rates (BPM; Fig. 2A) or left-ventricular developed pressure (Fig. 2B), a measure of cardiac function. Furthermore, the various CO₂ concentrations did not affect activating Akt phosphorylation, a known determinant of infarct injury (results not shown). On the other hand, ischemic hearts perfused with 10% CO₂ presented severely decreased BPM (Fig. 2D) and change in developed pressure (Fig. 2E) during reperfusion; the difference was significant both comparing the curves point by point (as shown in the figures) and integrating the area under the curve at reperfusion ($p < 0.05$ comparing 0 and 10% CO₂ using a *t* test, for both BPM and developed pressure). Indeed, 10% CO₂ hearts displayed an infarcted area that was double that observed in 0% CO₂ IR hearts (Fig. 2F). Overall, these results confirm, in a whole-heart model, that CO₂/HCO₃⁻ levels are a determinant of functional cardiac recovery after IR.

To evaluate if the changes in cardiac function observed were associated with oxidative damage, we measured protein carbonyl levels. Whereas carbonyls were unaltered under various incubation conditions in nonischemic hearts (results not shown), in IR hearts, protein carbonyl levels increased in proportion to the percentage of gassed CO₂ (Fig. 3A) and were more than 50% higher in 10% CO₂

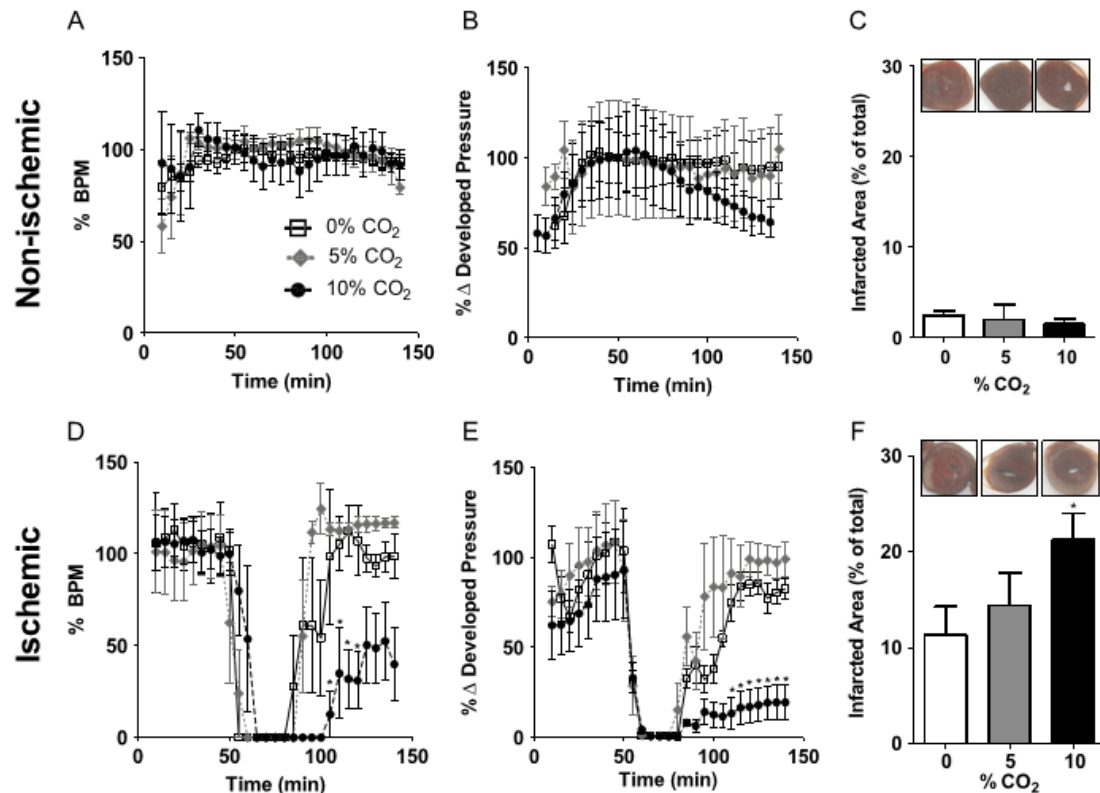


Fig. 2. Perfused rat hearts present increased functional loss when subjected to IR in the presence of 10% CO₂. (A and D) Beats per minute (BPM), (B and E) left-ventricular developed pressure, and (C and F) infarct areas were measured as described under Materials and methods for nonischemic (A–C) or IR (D–F) hearts perfused with 0, 5, or 10% CO₂. * $p < 0.05$ relative to IR with 0% CO₂.

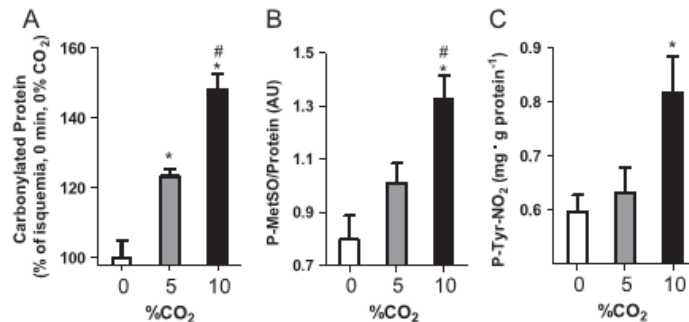


Fig. 3. Increases in CO₂ are accompanied by enhanced oxidative damage in IR hearts. The amounts of (A) carbonylated proteins, (B) methionine sulfoxide and (C) nitrotyrosine were quantified as described under Materials and methods after IR conducted under the conditions of Fig. 2. **p* < 0.05 relative to 0% CO₂; #*p* < 0.05 relative to 5% CO₂.

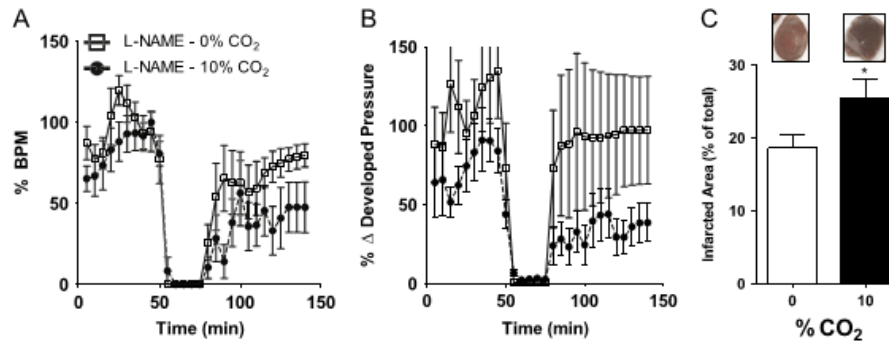


Fig. 4. L-NAME does not inhibit functional loss promoted by CO₂ in IR hearts. (A) Beats per minute (BPM), (B) left-ventricular developed pressure and (C) infarct areas were measured as for Fig. 2, with the addition of 200 μM L-NAME to the perfusion medium. **p* < 0.05 relative to 0% CO₂.

relative to the absence of this gas. Similar increases in methionine sulfoxide (Fig. 3B) and nitrotyrosine (Fig. 3C) residue levels were also observed in 10% CO₂ tissues. These protein modifications were undetectable in nonischemic heart samples perfused with any concentration of CO₂. Again, our results suggest that, although CO₂/HCO₃⁻ does not overtly affect hearts under physiological conditions, it is a determinant in functional and oxidative damage after IR.

The detection of increased nitrotyrosine radicals in hearts perfused with CO₂ indicates the participation of nitric oxide-derived species in cardiac damage enhanced by CO₂. Indeed, peroxynitrite in the presence of CO₂ is very efficient at promoting tyrosine nitration due to the production of nitrogen dioxide and the carbonate radical anion (reviewed in [23]). To investigate a potential role for nitric oxide-derived oxidants in this process, we measured the effects of L-NAME, an inhibitor of nitric oxide synthases, on CO₂-enhanced cardiac damage after IR (Fig. 4). We found that cardiac damage increases promoted by CO₂ persisted in the presence of L-NAME. Whereas this result suggests nitric oxide synthases are not involved in the effects of CO₂, a role for nitric oxide cannot be excluded because it can be produced through nitrite reduction during ischemia [36,44].

We next evaluated the effect of CO₂/HCO₃⁻ on protein carbonyl formation in *C. elegans* during anoxia-starvation as a model for worm IR. Behavior and cell morphology were also assessed in the surviving worms. We found that CO₂ had little apparent effect in the absence of AS (results not shown), whereas survival after AS was not altered by 0 or 10% CO₂ either (Fig. 5A). Protein carbonyls under

AS conditions tended, nonsignificantly, to increase in 10% CO₂ (Fig. 5B). Interestingly, however, surviving animals exhibited subtle but significant differences in behavior, manifested as an increased defective response to light body wall touch as a function of CO₂ during hypoxia (Fig. 5C). The behavioral response to body wall touch is mediated by six mechanosensory neurons whose processes run just under the hypodermis of the animal. To investigate if the decrease in function in these animals was accompanied by damage to these neurons, an integrated transgene was used to label the touch cells with green fluorescent protein (GFP), and two of these neurons (PLML and PLMR) were examined in detail, as described (Materials and methods). Neuronal abnormalities that were scored included the appearance of GFP inclusions in the processes, tortuous processes, and breaks, all of which have been shown to accumulate as a result of hypoxia [9]. The incidence of such abnormalities was significantly increased by AS in 10% CO₂ compared to 0% CO₂ (Fig. 6) demonstrating that, in a whole organism model, higher CO₂/HCO₃⁻ promoted more significant tissue and functional damage after AS.

Discussion

Considering its role as the main biological buffer, it is surprising so little recent attention has been given to the biological activity of CO₂/HCO₃⁻ [14,23]. In particular, metabolic and redox effects of this buffer are expected. In this work, we evaluated the results of various tensions of CO₂, incurring at different CO₂/HCO₃⁻ levels.

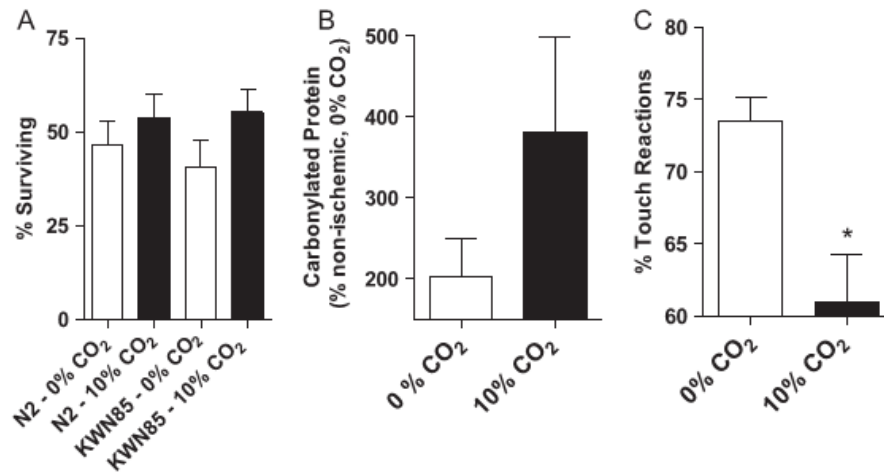


Fig. 5. 10% CO₂ decreases touch responses in *C. elegans* after IR, without affecting survival. (A) The percentage of worms that exhibit 24-h post-AS survival in the presence or absence of CO₂ was measured as described under Materials and methods. The N2 strain is the canonical wild-type genetic background, and KWN85 contains an integrated transgene that labels mechanosensory neurons with green fluorescent protein. (B) Proteins were extracted from living *C. elegans* after AS in the presence or absence of CO₂, and protein carbonyls were detected using an OxyBlot and (C) The response to touch stimuli of living *C. elegans* after AS in the presence or absence of CO₂ was measured as described under Materials and methods. **p* < 0.01 relative to 0% CO₂.

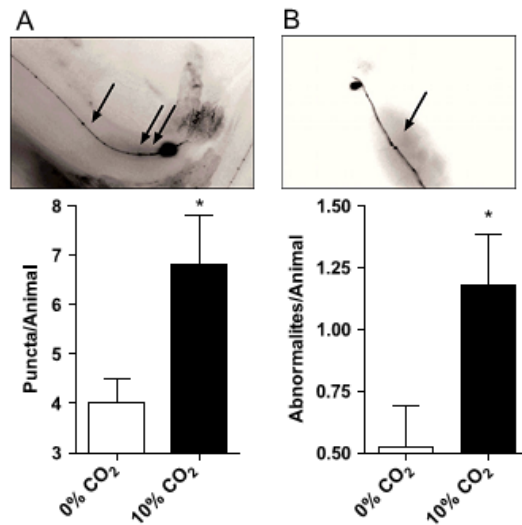


Fig. 6. 10% CO₂ increases touch neuron modifications. (A) The accumulation of GFP aggregates in the touch neuron (PLML and PLMR) processes or (B) abnormalities such as tortuous processes and breaks were monitored in surviving anesthetized *C. elegans* after IR in the presence or absence of CO₂, as described under Materials and methods. **p* < 0.05 relative to 0% CO₂.

Using cardiac cells, perfused rat hearts, and *C. elegans*, we found that increased CO₂/HCO₃⁻ heightened the injury associated with IR (Figs. 1–3) [18]. Previous studies have determined that increased levels of CO₂ result in increased heart beat rates [33], but no change in pumping function [37]. However, these changes were completely reversed by normalizing pH, indicating that they are related to pH and not to other possible biological activities of CO₂/HCO₃⁻. These data, in fact, correlate well with our finding that changes in CO₂/HCO₃⁻ in the presence of clamped perfusion pH do not alter the basal function of perfused rat hearts (Fig. 2). On the other hand, Lavani et al.

[20] found that reperfusion in the presence of high CO₂ tension resulted in protection against cardiac damage. This result differs from ours, in that we found higher cardiac damage in the presence of high CO₂ tension. Because Lavani et al. [20] did not correct for pH changes, and acidic pH is strongly protective in cardiac ischemia [19,31], it seems reasonable to propose that their effects also are attributable to pH changes promoted by altered CO₂ tension. Our work separated the pH effect of CO₂ from other biological effects by clamping pH with high concentrations of other buffers. Although we could not ascertain that this extracellular pH clamping maintained intracellular pH in perfused hearts and *C. elegans*, measured intracellular pH was identical in cells incubated in the presence and absence of CO₂/HCO₃⁻ (Fig. 1A), indicating that changes in pH are not necessary for the detrimental effects of CO₂.

Under these conditions, it was possible to focus on the redox effects of CO₂/HCO₃⁻ under basal conditions and IR. The presence of CO₂ in solution allows for the generation of the highly reactive carbonate radical from the reaction of CO₂ with peroxynitrite. CO₂ also reacts with H₂O₂, producing peroxydicarbonate, which is a better two-electron oxidant than H₂O₂ and decomposes to the carbonate radical in the presence of biologically ubiquitous metal ions [25,29]. The carbonate radical does not produce any known stable target adducts and is therefore difficult to detect in vivo and even in vitro [23]. Peroxydicarbonate and other oxidants may also be derived from bicarbonate. Thus, we investigated if changing CO₂/HCO₃⁻ altered markers of tissue redox state.

Levels of protein carbonyls, the only modification detected in the absence of IR, were not altered by CO₂/HCO₃⁻ under nonischemic conditions in any of the models studied. This result is not unexpected, because bicarbonate-derived oxidants are produced secondarily to reactions promoted by other reactive oxygen and nitrogen species, which are much more abundant after IR. Indeed, we found that in both cardiac cells and perfused hearts (Figs. 1 and 3), levels of oxidized proteins after IR increase markedly with the presence and increasing levels of CO₂/HCO₃⁻. In fact, a linear correlation was detected between carbonylated protein (*r*² = 0.995, *p* = 0.01) and methionine sulfoxide (*r*² = 0.9881, *p* = 0.06) and CO₂ levels. Changes in protein modifications were not significantly increased in *C. elegans*, although they tended to be higher; it should be pointed out that AS

in *C. elegans* requires 20 h after reoxygenation to produce notable functional effects, and the long reperfusion time may result in the removal of many modified proteins. Despite the lack of strong evidence for changes in redox state in the *C. elegans* system, $\text{CO}_2/\text{HCO}_3^-$ affected the functional recovery of the worms after AS (Figs. 5 and 6), once again demonstrating the importance of bicarbonate in ischemic damage.

Overall, our results show that over a wide range of experimental models (cells, organs, and whole organisms), the presence of $\text{CO}_2/\text{HCO}_3^-$ promotes a strong decrease in function after IR, in a manner correlated with tissue oxidative damage. This demonstrates that $\text{CO}_2/\text{HCO}_3^-$ levels are a determinant of the outcome of pathologically relevant conditions of oxidative imbalance and may explain the protective effect of modulating carbonic anhydrases [1,28]. Although $\text{CO}_2/\text{HCO}_3^-$ are unavoidable in biological systems, our data provide a gain in the understanding of the mechanisms involved in tissue damage after ischemic insults, which we hope will be important for future development of therapeutic interventions. Furthermore, our results provide evidence, albeit indirect, for the participation of bicarbonate radicals in pathologically relevant biological processes and indicate that more attention should be focused on the redox biology of the $\text{CO}_2/\text{HCO}_3^-$ buffer.

Acknowledgments

This work was supported by the Fundação de Amparo à Pesquisa do Estado de São Paulo (FAPESP), the Instituto Nacional de Ciência e Tecnologia de Processos Redox em Biomedicina, the Núcleo de Apoio à Pesquisa Redoxoma, USPHS NS064945 (K.N.), and USPHS GM087483 (P.S.B. and K.N.). B.B.Q. is a doctoral student supported by a FAPESP grant and an American Society for Biochemistry and Molecular Biology PROLAB award. We gratefully acknowledge Camille Caldeira da Silva, Edson Alves Gomes, and Doris Araújo for their technical support and Silvana Neves and the staff of the animal facilities for excellent animal care.

References

- Ahmad, S. Acetazolamide and enalapril combination offers complete protection from nitric oxide-deficient stroke in stroke-prone spontaneously hypertensive rats. *Pharmacol. Res.* **41**:649–656; 2000.
- Arai, H.; Berlett, B. S.; Chock, P. B.; Stadtman, E. R. Effect of bicarbonate on iron-mediated oxidation of low-density lipoprotein. *Proc. Natl. Acad. Sci. USA* **102**:10472–10477; 2005.
- Bonini, M. G.; Miyamoto, S.; Di Mascio, P.; Augusto, O. Production of the carbonate radical anion during xanthine oxidase turnover in the presence of bicarbonate. *J. Biol. Chem.* **279**:51836–51843; 2004.
- Brenner, S. The genetics of *Caenorhabditis elegans*. *Genetics* **77**:71–94; 1974.
- Budas, G. R.; Disatnik, M. H.; Chen, C. H.; Mochly-Rosen, D. Activation of aldehyde dehydrogenase 2 (ALDH2) confers cardioprotection in protein kinase C epsilon (PKC ϵ) knockout mice. *J. Mol. Cell. Cardiol.* **48**:757–764; 2010.
- Cardoso, A. R.; Chausse, B.; da Cunha, F. M.; Luévano-Marín, L. A.; Marazzi, T. B. M.; Pessoa, P. S.; Queliconi, B. B.; Kowaltowski, A. J. Mitochondrial compartmentalization of redox processes. *Free Radic. Biol. Med.* **52**:2201–2208; 2012.
- Claycomb, W. C.; Lanson Jr N. A.; Stallworth, B. S.; Egeland, D. B.; Delcarpio, J. B.; Bahinski, A.; Izzo Jr. N. J. HL-1 cells: a cardiac muscle cell line that contracts and retains phenotypic characteristics of the adult cardiomyocyte. *Proc. Natl. Acad. Sci. USA* **95**:2979–2984; 1998.
- da Cunha, F. M.; Demasi, M.; Kowaltowski, A. J. Aging and calorie restriction modulate yeast redox state, oxidized protein removal, and the ubiquitin-proteasome system. *Free Radic. Biol. Med.* **51**:664–670; 2011.
- Dasgupta, N.; Patel, A. M.; Scott, B. A.; Crowder, C. M. Hypoxic preconditioning requires the apoptosis protein CED-4 in *C. elegans*. *Curr. Biol.* **17**:1954–1959; 2007.
- Ezraty, B.; Chaballier, M.; Ducret, A.; Maisonneuve, E.; Dukan, S. CO_2 exacerbates oxygen toxicity. *EMBO Rep.* **12**:321–326; 2011.
- Facundo, H. T.; de Paula, J. G.; Kowaltowski, A. J. Mitochondrial ATP-sensitive K channels prevent oxidative stress, permeability transition and cell death. *J. Bioenerg. Biomembr.* **37**:75–82; 2005.
- Facundo, H. T.; Carreira, R. S.; de Paula, J. G.; Santos, C. C.; Ferranti, R.; Laurindo, F. R.; Kowaltowski, A. J. Ischemic preconditioning requires increases in reactive oxygen release independent of mitochondrial K^+ channel activity. *Free Radic. Biol. Med.* **40**:469–479; 2006.
- Fishbein, M. C.; Meerbaum, S.; Rit, J.; Lando, U.; Kanmatsuse, K.; Mercier, J. C.; Corday, E.; Ganz, W. Early phase acute myocardial infarct size quantification: validation of the triphenyl tetrazolium chloride tissue enzyme staining technique. *Am. Heart J.* **101**:593–600; 1981.
- Guais, A.; Brand, G.; Jacquot, L.; Karrer, M.; Dukan, S.; Grévillet, G.; Molina, T. J.; Bonte, J.; Regnier, M.; Schwartz, L. Toxicity of carbon dioxide: a review. *Chem. Res. Toxicol.* **24**:2061–2070; 2011.
- Hodgson, E. K.; Fridovich, I. The mechanism of the activity-dependent luminescence of xanthine oxidase. *Arch. Biochem. Biophys.* **172**:202–205; 1976.
- Johnson, D.; Nehrke, K. Mitochondrial fragmentation leads to intracellular acidification in *Caenorhabditis elegans* and mammalian cells. *Mol. Biol. Cell* **21**:2191–2201; 2010.
- Karsten, U. Fluorometric estimation of dead cells in cell suspensions. *Experientia* **36**:263–264; 1980.
- Khandoudi, N.; Bernard, M.; Cozzone, P.; Feuvray, D. Mechanisms of intracellular pH regulation during postischemic reperfusion of diabetic rat hearts. *Diabetes* **44**:196–202; 1995.
- Kitakaze, M.; Weisfeldt, M. L.; Marban, E. Acidosis during early reperfusion prevents myocardial stunning in perfused ferret hearts. *J. Clin. Invest.* **82**:920–927; 1988.
- Lavani, R.; Chang, W. T.; Anderson, T.; Shao, Z. H.; Wojcik, K. R.; Li, C. Q.; Pietrowski, R.; Beiser, D. G.; Idris, A. H.; Hamann, K. J.; Becker, L. B.; Vanden Hoek, T. L. Altering CO_2 during reperfusion of ischemic cardiomyocytes modifies mitochondrial oxidant injury. *Crit. Care Med.* **35**:1709–1716; 2007.
- Liochev, S. I.; Fridovich, I. CO_2 , not HCO_3^- facilitates oxidations by Cu,Zn superoxide dismutase plus H_2O_2 . *Proc. Natl. Acad. Sci. USA* **101**:743–744; 2004.
- Martin, A.; Zulueta, J.; Hassoun, P.; Blumberg, J. B.; Meydani, M. Effect of vitamin E on hydrogen peroxide production by human vascular endothelial cells after hypoxia/reoxygenation. *Free Radic. Biol. Med.* **20**:99–105; 1996.
- Medinas, D. B.; Cerchiaro, G.; Trindade, D. F.; Augusto, O. The carbonate radical and related oxidants derived from bicarbonate buffer. *IUBMB Life* **59**:255–262; 2007.
- Medinas, D. B.; Toledo Jr J. C.; Cerchiaro, G.; do-Amaral, A. T.; de-Rezende, L.; Malvezzi, A.; Augusto, O. Peroxymonocarbonate and carbonate radical displace the hydroxyl-like oxidant in the Sod1 peroxidase activity under physiological conditions. *Chem. Res. Toxicol.* **22**:639–648; 2009.
- Medinas, D. B.; Augusto, O. Mechanism of the peroxidase activity of superoxide dismutase. *Free Radic. Biol. Med.* **49**:682; 2010.
- Nakamura, A.; Goto, S. Analysis of protein carbonyls with 2,4-dinitrophenylhydrazine and its antibodies by immunoblot in two-dimensional gel electrophoresis. *J. Biochem.* **119**:768–774; 1996.
- Radi, R. Nitric oxide, oxidants, and protein tyrosine nitration. *Proc. Natl. Acad. Sci. USA* **101**:4003–4008; 2004.
- Räsänen, S. R.; Lehenkari, P.; Tasanen, M.; Rähkila, P.; Härkönen, P. L.; Väänänen, H. K. Carbonic anhydrase III protects cells from hydrogen peroxide-induced apoptosis. *FASEB J.* **13**:513–522; 1999.
- Ramirez, D. C.; Mejiba, S. E.; Mason, R. P. Copper-catalyzed protein oxidation and its modulation by carbon dioxide: enhancement of protein radicals in cells. *J. Biol. Chem.* **280**:27402–27411; 2005.
- Rink, T. J.; Tsien, R. Y.; Pozzan, T. Cytoplasmic pH and free Mg^{2+} in lymphocytes. *J. Cell Biol.* **95**:189–196; 1982.
- Schäfer, C.; Ladilov, Y. V.; Siegmund, B.; Piper, H. M. Importance of bicarbonate transport for protection of cardiomyocytes against reoxygenation injury. *Am. J. Physiol. Heart Circ. Physiol.* **278**:H1457–H1463; 2000.
- Scott, B. A.; Avidan, M. S.; Crowder, C. M. Regulation of hypoxic death in *C. elegans* by the insulin/IGF receptor homolog DAF-2. *Science* **296**:2388–2391; 2002.
- Stinson, J. M.; Mattsson, J. L. Tolerance of rhesus monkeys to graded increase in environmental CO_2 : serial changes in heart rate and cardiac rhythm. *Aerosol Med.* **41**:415–418; 1970.
- Surmeli, N. B.; Litterman, N. K.; Miller, A. F.; Groves, J. T. Peroxynitrite mediates active site tyrosine nitration in manganese superoxide dismutase: evidence of a role for the carbonate radical anion. *J. Am. Chem. Soc.* **132**:17174–17185; 2010.
- Vanden Hoek, T. L.; Shao, Z.; Li, C.; Zak, R.; Schumacker, P. T.; Becker, L. B. Reperfusion injury on cardiac myocytes after simulated ischemia. *Am. J. Physiol.* **270**:H1334–H1341; 1996.
- Webb, A.; Bond, R.; McLean, P.; Uppal, R.; Benjamin, N.; Ahluwalia, A. Reduction of nitrite to nitric oxide during ischemia protects against myocardial ischemia-reperfusion damage. *Proc. Natl. Acad. Sci. USA* **101**:13683–13688; 2004.
- Wexels, J. C.; Mjøs, O. D. Effects of carbon dioxide and pH on myocardial function in dogs with acute left ventricular failure. *Crit. Care Med.* **15**:1116–1120; 1987.
- White, S. M.; Constantin, P. E.; Claycomb, W. C. Cardiac physiology at the cellular level: use of cultured HL-1 cardiomyocytes for studies of cardiac muscle cell structure and function. *Am. J. Physiol. Heart Circ. Physiol.* **286**:H823–H829; 2004.
- Winterbourn, C. C. Reconciling the chemistry and biology of reactive oxygen species. *Nat. Chem. Biol.* **4**:278–286; 2008.
- Wojtovich, A. P.; Sherman, T. A.; Nadochchiy, S. M.; Urciuoli, W. R.; Brookes, P. S.; Nehrke, K. SLO-2 is cytoprotective and contributes to mitochondrial potassium transport. *PLoS One* **6**: 2011e28287 6; 2011.

- [41] Wojtovich, A. P.; DiStefano, P.; Sherman, T.; Brookes, P. S.; Nehrke, K. Mitochondrial ATP-sensitive potassium channel activity and hypoxic preconditioning are independent of an inwardly rectifying potassium channel subunit in *Caenorhabditis elegans*. *FEBS Lett* **586**:428–434; 2012.
- [42] Zhang, H.; Andreopoulos, C.; Joseph, J.; Chandran, K.; Karoui, H.; Crow, J. P.; Kalyanaraman, B. Bicarbonate-dependent peroxidase activity of human Cu,Zn-superoxide dismutase induces covalent aggregation of protein: intermediacy of tryptophan-derived oxidation products. *J. Biol. Chem.* **278**:24078–24089; 2003.
- [43] Zhou, H.; Singh, H.; Parsons, Z. D.; Lewis, S. M.; Bhattacharya, S.; Seiner, D. R.; LaButti, J. N.; Reilly, T. J.; Tanner, J. J.; Gates, K. S. The biological buffer bicarbonate/CO₂ potentiates H₂O₂-mediated inactivation of protein tyrosine phosphatases. *J. Am. Chem. Soc.* **133**:15803–15805; 2011.
- [44] Zweier, J. L.; Wang, P.; Samouilov, A.; Kuppusamy, P. Enzyme-independent formation of nitric oxide in biological tissues. *Nat. Med* **1**:804–809; 1995.

Ap.6 Exercise training restores cardiac protein quality control in heart failure

OPEN ACCESS Freely available online



Exercise Training Restores Cardiac Protein Quality Control in Heart Failure

Juliane C. Campos¹, Bruno B. Queliconi², Paulo M. M. Dourado³, Telma F. Cunha⁴, Vanessa O. Zambelli⁵, Luiz R. G. Bechara⁴, Alicia J. Kowaltowski², Patricia C. Brum⁴, Daria Mochly-Rosen⁶, Julio C. B. Ferreira^{1,6*}

1 Department of Anatomy, Institute of Biomedical Sciences, University of Sao Paulo, Sao Paulo, Brazil, **2** Departamento de Bioquímica, Instituto de Química, Universidade de São Paulo, Sao Paulo, Brazil, **3** Heart Institute, University of Sao Paulo, Sao Paulo, Brazil, **4** School of Physical Education and Sport, University of Sao Paulo, Sao Paulo, Brazil, **5** Butantan Institute, Sao Paulo, Brazil, **6** Department of Chemical and Systems Biology, Stanford University School of Medicine, Stanford, California, United States of America

Abstract

Exercise training is a well-known adjuvant in heart failure treatment; however, the molecular mechanisms underlying its beneficial effects remain elusive. Despite the primary cause, heart failure is often preceded by two distinct phenomena: mitochondria dysfunction and cytosolic protein quality control disruption. The objective of the study was to determine the contribution of exercise training in regulating cardiac mitochondria metabolism and cytosolic protein quality control in a post-myocardial infarction-induced heart failure (MI-HF) animal model. Our data demonstrated that isolated cardiac mitochondria from MI-HF rats displayed decreased oxygen consumption, reduced maximum calcium uptake and elevated H₂O₂ release. These changes were accompanied by exacerbated cardiac oxidative stress and proteasomal insufficiency. Declined proteasomal activity contributes to cardiac protein quality control disruption in our MI-HF model. Using cultured neonatal cardiomyocytes, we showed that either antimycin A or H₂O₂ resulted in inactivation of proteasomal peptidase activity, accumulation of oxidized proteins and cell death, recapitulating our *in vivo* model. Of interest, eight weeks of exercise training improved cardiac function, peak oxygen uptake and exercise tolerance in MI-HF rats. Moreover, exercise training restored mitochondrial oxygen consumption, increased Ca²⁺-induced permeability transition and reduced H₂O₂ release in MI-HF rats. These changes were followed by reduced oxidative stress and better cardiac protein quality control. Taken together, our findings uncover the potential contribution of mitochondrial dysfunction and cytosolic protein quality control disruption to heart failure and highlight the positive effects of exercise training in re-establishing cardiac mitochondrial physiology and protein quality control, reinforcing the importance of this intervention as a non-pharmacological tool for heart failure therapy.

Citation: Campos JC, Queliconi BB, Dourado PMM, Cunha TF, Zambelli VO, et al. (2012) Exercise Training Restores Cardiac Protein Quality Control in Heart Failure. PLoS ONE 7(12): e52764. doi:10.1371/journal.pone.0052764

Editor: Maria Moran, Instituto de Investigación Hospital 12 de Octubre, Spain

Received: May 7, 2012; **Accepted:** November 22, 2012; **Published:** December 27, 2012

Copyright: © 2012 Campos et al. This is an open-access article distributed under the terms of the Creative Commons Attribution License, which permits unrestricted use, distribution, and reproduction in any medium, provided the original author and source are credited.

Funding: This study was supported by Fundação de Amparo à Pesquisa do Estado de São Paulo, São Paulo - SP (FAPESP #2009/18546-4, #2010/00028-4 and #2012/05765-2), Conselho Nacional de Pesquisa e Desenvolvimento - Brasil (CNPq, 479407/2010-0), Instituto Nacional de Ciência e Tecnologia and Núcleo de Apoio à Pesquisa de Processos Redox em Biomedicina. J.C.C. held a master's fellowship from Fundação de Amparo a Pesquisa do Estado de São Paulo (FAPESP #2009/12349-2). The funders had no role in study design, data collection and analysis, decision to publish, or preparation of the manuscript.

Competing Interests: The authors have declared that no competing interests exist.

* E-mail: jcesarfb@usp.br

Introduction

Heart failure is a common endpoint of most cardiovascular diseases and a leading cause of morbidity and mortality worldwide. There is a consensus that adjuvant therapies for cardiovascular disease are able to increase patients' quality of life and survival rates [1]. Acting as a non-pharmacological therapy, exercise training reduces a number of cardiovascular risk factors [2,3] and has been recognized as an important and safe strategy for preventing and treating heart failure [4,5,6]. However, the underlying cellular mechanisms by which exercise training improves heart failure patients' clinical outcome are still under investigation.

Mitochondrial dysfunction has been widely recognized as key player in the progression of cardiovascular diseases [7]. Exacerbated generation of reactive oxygen species (ROS) due to impaired mitochondrial bioenergetics is believed to underlie intra- and extra-mitochondrial signal transduction during cardiac remodeling

and heart failure [8]. Evidences indicate that 4-hydroxy-2-nonenal (4-HNE), a long-lived lipid peroxidation product that accumulates during oxidative stress, irreversibly interacts with and inactivates mitochondrial, cytosolic and membrane proteins [9,10,11]. However, the contribution of 4-HNE protein adduction to heart failure pathophysiology remains elusive.

Over the last years, *in vitro* studies have demonstrated that specific subunits of the 20S proteasome are targeted for modification by 4-HNE, which results in reduced proteasomal peptidase activities [9,10]. Recent findings showing that the ubiquitin-proteasome system is negatively regulated by oxidative stress during cardiac ischemia-reperfusion injury generated the hypothesis that mitochondrial dysfunction-mediated redox imbalance may negatively affect ubiquitin-proteasome activity in an ATP-independent manner.

Over the past decades, the ubiquitin-proteasome system has emerged as an important player on essential cellular processes such as cellular proliferation, differentiation and apoptosis

[12,13,14]. The ubiquitin-proteasome system is the primary effector of the protein quality control process, protecting long-lived cells, such as neurons and cardiomyocytes, through selective removal of polypeptides that are terminally misfolded and toxic to the cell [15]. Perturbations in the ubiquitin-proteasome system have been shown to disturb protein turnover and thereby affect cell function. Recent studies have highlighted the role of the ubiquitin-proteasome system in stressed cardiac phenotypes including cardiac remodelling and heart failure [16]. Accumulation of ubiquitinated and damaged proteins is a common feature of human failing hearts and indicates the relevance of the ubiquitin-proteasome system in maintaining cardiac homeostasis [16,17]. However, it remains to be determined whether dysfunction of specific protein quality control components, such as the ubiquitin-proteasome system, contributes to the development of heart failure, and which signaling events regulate them.

Despite the increased knowledge regarding the molecular basis of mitochondrial ROS generation and redox balance in cardiovascular diseases, there is still uncertainty in the literature regarding the contribution of the long-lived lipid peroxidation product 4-HNE in protein modification and intracellular system disruption in cardiovascular diseases. Some evidence indicates that 4-HNE modification of proteins is triggered by mitochondrial dysfunction and provides an operational criterion for inactivation of mitochondrial and cytosolic systems related to cell survival [18,19]. Therefore, the objectives of the study were: 1) to test the hypothesis that mitochondrial dysfunction disrupts cardiac protein quality control through specific 4-HNE modification/inhibition of proteasome and 2) to verify whether exercise training prevents impairment of mitochondrial metabolism, 4-HNE adduct formation and protein quality control disruption in heart failure.

Materials and Methods

Study design

The present investigation was carried out in male Wistar rats assigned into three experimental groups: sham (control, $n = 9$), myocardial infarction-induced heart failure (MI-HF, $n = 10$) and exercised-trained MI-HF (MI-HFtr, $n = 8$). Heart failure was induced by myocardial infarction surgery. Four weeks later, physiological parameters were determined and animals with heart failure were randomly assigned into sedentary (MI-HF) and exercise-trained (MI-HFtr) groups (Figure 1A). MI-HFtr rats performed a moderate-intensity running training on a motor treadmill over eight weeks (from 4th–6th month of age). At the end of the protocol, physiological parameters were re-analysed. Forty-eight hours later, all rats were killed by decapitation and cardiac structure, bioenergetics and protein quality control measurements were performed.

Animals and procedures

A cohort of male Wistar rats (250–300 g) was selected for the study. Rats were maintained in a 12:12 h light-dark cycle and temperature-controlled environment (22°C) with free access to standard laboratory chow (Nuvital Nutrientes, Curitiba, PR Brazil) and tap water. This study was conducted in accordance with the ethical principles in animal research adopted by the Brazilian College of Animal Experimentation (www.cobea.org.br). The animal care and protocols in this study were reviewed and approved by the Ethical Committee of Medical School of University of São Paulo (2008/40).

Myocardial infarction-induced heart failure model

Myocardial infarction was induced by ligation of the left anterior descending coronary artery (LAD), as previously described [20]. We have chosen this model since myocardial infarction is the underlying etiology of heart failure in nearly 70% of patients [21]. Male Wistar rats were anesthetized with ketamine (50 mg kg⁻¹ IP) and xylazine (10 mg kg⁻¹ IP), endotracheally intubated, and mechanically ventilated with room air (respiratory rate of 60–70 breaths/min and tidal volume of 2.5 mL). Left thoracotomy between the fourth and fifth ribs was performed and the LAD was ligated. After the surgery, animals were monitored daily. Heart failure was observed four weeks after coronary artery ligation and was defined when animal presented pathological cardiac remodeling accompanied by left ventricle dysfunction, cardiac dilation and exercise intolerance (Tables 1 and 2), according to the Guidelines of American Heart Association [22]. Left thoracotomy with equal procedure duration to that of heart failure group, but without LAD ligation, was undertaken in the sham group (control).

Graded treadmill exercise test and oxygen uptake measurement

After being adapted to treadmill exercises and the test environment for over one week (10 minutes each session), rats were placed on the exercise streak inside a metabolic chamber equipped with plastic tubes that allowed air into the chamber and out to a high-resolution oxygen analyzer (FC-10, Sable Systems International, Las Vegas, USA). Ambient air was pumped into the chamber (3500 mL min⁻¹), continuously extracted at the same rate and directed to the oxygen analyzer. Oxygen fraction in effluent air was registered every second. The analyzer was calibrated with known gas mixtures every day of tests. Each rat had a twenty-minute rest period and a ten-minute warm-up at 3 m min⁻¹ before the test protocol. Treadmill speed was increased by 3 m min⁻¹ every 3 minutes until the animal was unable to run [23]. We considered the VO₂ reached at the highest workload during the treadmill test as peak VO₂. It is worth mentioning that peak VO₂ has been described to the best predictor of mortality in humans with cardiovascular diseases [24]. VO₂ (mL O₂ kg⁻¹ min⁻¹) was calculated using the measured flow through the metabolic chamber (3500 mL min⁻¹), expired fraction of effluent oxygen (E), fraction of oxygen in room air (A) and rat body mass (M [kg]), as described by the formula: $VO_2 = [3500 \times (A - E)] / M$. Peak VO₂ was measured both before (week 16) and after experimental protocol (week 24) (Figure 1).

Running training protocol

Heart failure rats performed moderated-intensity running training on a motor treadmill, 5 days/wk, 60 min/day. Running speed and duration of exercise were progressively increased to elicit 60% of maximal speed at the second week of training, corresponding to the maximal lactate steady state workload [25]. At the fourth week of training, run capacity was evaluated in order to readjust exercise training intensity. Treadmill running skills were maintained in sedentary HF and sham rats by treadmill running for 5 min, twice a week. This procedure was performed in order to avoid any interference of treadmill stress on the variables studied. This latter activity did not seem to alter maximal exercise capacity (Table 1).

Cardiovascular measurements

Heart rate and blood pressure were determined noninvasively using a computerized tail-cuff system (BP 2000 Visitech Systems)

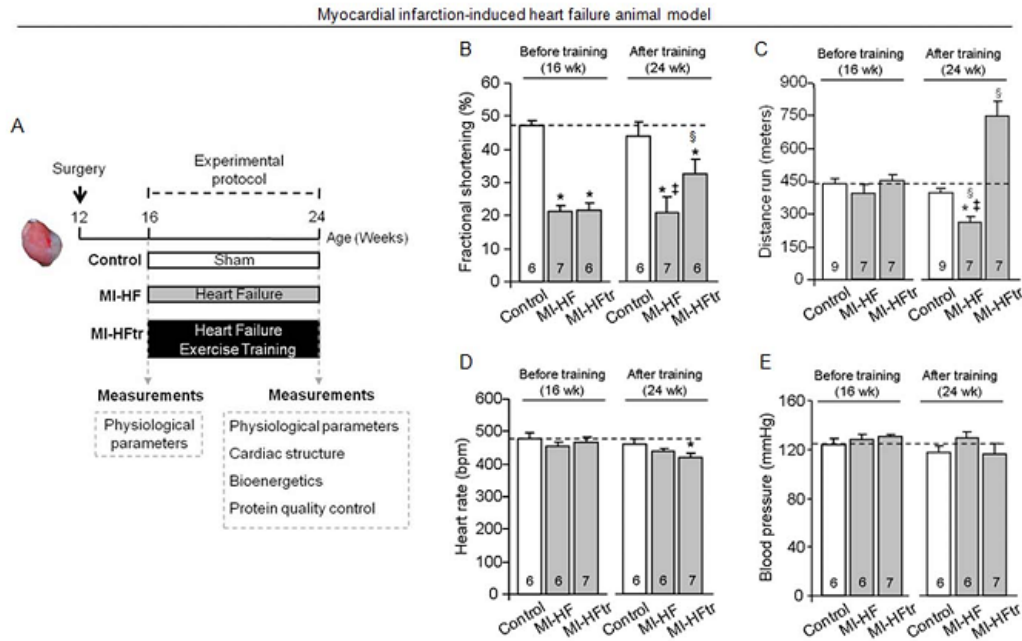


Figure 1. Exercise training improves cardiac function and exercise tolerance in myocardial infarction-induced heart failure. Schematic panel (A). Fractional shortening (B), distance run (C), heart rate (D) and blood pressure (E) in control (sham, white bars), MI-HF (gray bars) and MI-HF exercise trained (MI-HFtr, gray bars) rats before and after 8 wks of either sedentary or exercise training protocol. Error bars indicate SEM. Interaction between main effects: fractional shortening [F (2, 15) = 5.28, p = 0.0183]; distance run [F (2, 31) = 48.97, p < 0.0001]; heart rate [F (2, 13) = 4.06, p = 0.0425] and blood pressure [F (2, 13) = 1.05, p = 0.3764]. §, p < 0.05 vs. before experimental protocol. *, p < 0.05 vs. control (sham) rats. ‡, p < 0.05 vs. MI-HFtr rats.

doi:10.1371/journal.pone.0052764.g001

described elsewhere [26]. Rats were acclimatized to the apparatus during daily sessions over 4 days, one week before starting the experimental period.

Non-invasive cardiac function evaluation was performed by M-mode echocardiography in anesthetized (isoflurane 3%) sham and HF rats, four and twelve weeks after surgery. Briefly, rats were

Table 1. Physiological parameters.

Parameter	Before experimental protocol (16 wk)			After experimental protocol (24 wk) ^e		
	Control (9)	MI-HF (7)	MI-HFtr (7)	Control (9)	MI-HF (7)	MI-HFtr (7)
Peak VO ₂ , mL O ₂ ·kg ⁻¹ ·min ⁻¹	65.6 ± 1.8	67.5 ± 2.4	68.4 ± 3.2	58.7 ± 2.5	47.8 ± 2.4	66.3 ± 3.1
BW, g	418 ± 12	390 ± 11	391 ± 11	432 ± 22	429 ± 14	415 ± 12
CS activity, μmol·mg ⁻¹ ·min ⁻¹	-	-	-	4476 ± 718	3200 ± 677*‡	6386 ± 1007*
HW/BW, mg·g ⁻¹	-	-	-	2.0 ± 0.1	2.4 ± 0.1*	2.4 ± 0.1*
MI area, %	-	-	-	-	31 ± 3	35 ± 4
Cardiomyocyte width, μm	-	-	-	14.33 ± 0.17	14.90 ± 0.17*	14.42 ± 0.22
Cardiac collagen content, %	-	-	-	5.45 ± 0.33	6.77 ± 0.44*‡	5.66 ± 0.32

Peak VO₂ (in mL O₂·kg⁻¹·min⁻¹), body weight (BW in grams), soleus muscle citrate synthase activity (CS in μmol·mg⁻¹·min⁻¹), heart weight/body weight ratio (HW/BW), myocardial infarction (MI) area, cardiomyocyte width (μm) and cardiac collagen content (%) data in control (sham), MI-HF and MI-HF exercise trained (MI-HFtr) rats (Mean ± SEM).

^eMain time effect: peak VO₂ [F (1, 18) = 9.75, p = 0.0058] pre-training values > post-training values and BW [F (1, 16) = 10.73, p = 0.0047]. CS activity [F (2, 21) = 29.80, p < 0.0001] *MI-HF < control (p = 0.0047) and ‡MI-HFtr (p < 0.0001), *MI-HFtr > control (p = 0.0002); HW/BW [F (2, 16) = 8.55, p = 0.0029] *control < MI-HF (p = 0.0044) and MI-HFtr (p = 0.0036); cardiomyocyte width [F (2, 14) = 11.42, p < 0.0001] *MI-HF > control (p < 0.0001) and cardiac collagen content [F (2, 23) = 3.76, p = 0.0245] *MI-HF > control (p = 0.0189) and ‡MI-HFtr (p = 0.0311).

doi:10.1371/journal.pone.0052764.t001

Table 2. Echocardiographic measurements.

Parameter	Before experimental protocol (16 wk)			After experimental protocol (24 wk) ^c		
	Control (9)	MI-HF (7)	MI-HFtr (7)	Control (9)	MI-HF (7)	MI-HFtr (7)
EF, %	83.2±1.22	47.2±3.89*	48.0±4.43*	79.2±3.45	47.0±5.04*‡	64.3±6.16 [§]
IVSd, mm	1.4±0.02	1.2±0.08	1.2±0.06	1.5±0.05	1.2±0.05	1.4±0.11
IVSs, mm	2.5±0.10	1.3±0.10	1.3±0.09	2.6±0.13	1.5±0.13	2.0±0.29
LVEDd, mm	7.0±0.14	9.1±0.27	8.7±0.21	7.9±0.29	9.1±0.13	8.7±0.4
LVESd, mm	3.7±0.14	7.2±0.24	6.8±0.23	4.5±0.37	7.2±0.51	6.0±0.63
LVPWd, mm	1.4±0.03	1.6±0.09	1.5±0.13	1.6±0.08	1.3±0.06 [§]	1.5±0.12
LVPWs, mm	2.6±0.14	2.6±0.17	2.7±0.20	2.7±0.18	2.2±0.13	2.7±0.24

Left ventricular ejection fraction (EF), interventricular septum in diastole (IVSd), interventricular septum in systole (IVSs), left ventricular end-diastolic diameter (LVEDd), left ventricular end-systolic diameter (LVESd), left ventricular posterior wall in diastole (LVPWd) and left ventricular posterior wall in systole (LVPWs) were obtained before and after 8 wks of the experimental protocol in control (sham), MI-HF and MI-HF exercise trained (MI-HFtr) rats (Mean ± SEM). Interaction between main effects: EF [F (2, 15) = 6.84, p = 0.0077] *control>MI-HF (p<0.0001) and MI-HFtr (p<0.0001) before and after experimental protocol, †MI-HFtr>MIHF after experimental protocol (p = 0.0136) and §MI-HFtr before<after experimental protocol (p = 0.0167); and LVPWd [F (2, 15) = 4.52, p = 0.0289] §MI-HF before>after experimental protocol (p = 0.0401).

^aMain time effect: IVSs [F (1, 15) = 5.98, p = 0.0272] pre-training values<post-training values.
doi:10.1371/journal.pone.0052764.t002

positioned in the supine position with front paws wide open and ultrasound transmission gel was applied to the precordium. Transthoracic echocardiography was performed using an Acuson Sequoia model 512 echocardiographer equipped with a 14-MHz linear transducer. Left ventricle systolic function was estimated by fractional shortening (FS) as follows: $FS(\%) = [(LVEDD - LVESD)/LVEDD] \times 100$, where LVEDD is the left ventricular end-diastolic diameter, and LVESD is the left ventricular end-systolic diameter.

Cardiac structural analysis

Forty-eight hours after the end of protocol, all rats were killed by decapitation and their tissues were harvested. Cardiac chambers were then fixed by immersion in 4% buffered formalin and embedded in paraffin for routine histological processing. Sections (4 μm) were stained with Hematoxylin-eosin, Picrosirius red or Masson's trichrome for the quantification of the cardiomyocyte width, cardiac collagen content and myocardial infarct area, respectively. These measurements were performed in the left ventricle free wall with a computer-assisted morphometric system (Leica Quantimet 500, Cambridge, UK, England), as described previously [27]. The myocardial infarcted area was expressed as a percentage of total surface area of the left ventricle [28].

Citrate synthase activity

Soleus muscles were homogenized in phosphate buffer (50 mM sodium phosphate, 1 mM EDTA and protease inhibitor cocktail (Sigma-Aldrich), pH 7.4) and centrifuged for 15 minutes at 12000 g and 4°C, pellet was discarded and supernatant was used for the assay. Assay mixture contained 100 mM Tris, 1 mM EDTA, 0.2 mM DTNB, 0.1 mM acetyl-CoA, 1% (v:v) Triton X-100, sample (130 μg of soluble proteins per mL of total assay) and 0.5 mM oxaloacetate (added latest), as originally described [29]. Sample absorbance was monitored at 412 nm in 96-well plate during 10 minutes at 25°C and maximal citrate synthase activity was measured within the linear range of the assay.

Mitochondrial isolation

Heart mitochondria were isolated as described elsewhere [30]. Briefly, cardiac samples from a remote area were minced and homogenized in isolation buffer (300 mM sucrose, 10 mM Hepes,

2 mM EGTA, pH 7.2, 4°C) containing 0.1 mg mL⁻¹ of type I protease (bovine pancreas) to release mitochondria from within muscle fibers and later washed in the same buffer in the presence of 1 mg mL⁻¹ bovine serum albumin. The suspension was homogenized in a 40 mL tissue grinder and centrifuged at 950 g for 5 min. The resulting supernatant was centrifuged at 9500 g for 10 min. The mitochondrial pellet was washed, resuspended in isolation buffer and submitted to a new centrifugation (9500 g for 10 min). The mitochondrial pellet was washed and the final pellet was resuspended in a minimal volume of isolation buffer.

Mitochondrial H₂O₂ release

Mitochondrial H₂O₂ release was measured as described elsewhere [31]. Briefly, mitochondrial H₂O₂ release was measured in a 0.125 mg protein mL⁻¹ mitochondrial suspensions in buffer containing 125 mM sucrose, 65 mM KCl, 10 mM Hepes, 2 mM inorganic phosphate, 2 mM MgCl₂, 100 μM EGTA and 0.01% bovine serum albumin, pH 7.2, at 30°C, with continuous stirring. Amplex Red (25 μM) oxidation was followed in the presence of 0.5 U mL⁻¹ horseradish peroxidase and using succinate, malate and glutamate (2 mM of each) as substrates. Amplex Red is oxidized in the presence of extramitochondrial horseradish peroxidase bound to H₂O₂, generating resorufin, which can be detected using a fluorescence spectrophotometer. Excitation/emission wavelengths were 563/587 nm. Calibration was conducted by adding H₂O₂ at known concentrations (A₂₄₀ = 43.6 M⁻¹ cm⁻¹) to the experimental buffer.

Mitochondrial O₂ consumption

Mitochondrial O₂ consumption was monitored in a 0.25 mg protein mL⁻¹ mitochondrial suspension under the same conditions as H₂O₂ release measurements using a computer-interfaced Clark-type electrode (OROBOROS Oxygraph-2k) operating with continuous stirring at 37°C [31]. Succinate, malate and glutamate (2 mM of each) were used as substrates and ADP (1 mM) was added to induce State 3 respiratory rate. A subsequent addition of oligomycin (1 μg mL⁻¹) was used to determine State 4 rate. Respiratory control ratio (RCR) was calculated by dividing State 3 by State 4 oxygen consumption rates, which demonstrates the tightness of the coupling between mitochondrial respiration and phosphorylation.

Maximal mitochondrial calcium uptake

Extramitochondrial Ca^{2+} concentrations were measured in a $0.125 \text{ mg protein mL}^{-1}$ mitochondrial suspensions using the fluorescent probe Calcium Green (100 nM) as described [32]. The reactions were carried out under the same conditions as H_2O_2 release measurements with continuous stirring at 37°C . For each experiment, consecutive additions of $50 \mu\text{M CaCl}_2$ were made until the mitochondria failed to reduce extramitochondrial Ca^{2+} . We therefore plotted a calibration curve that correlates fluorescence and Ca^{2+} concentration. Succinate, malate and glutamate (2 mM of each) were used as substrates and $100 \mu\text{M EGTA}$ was used to establish the baseline. Excitation/emission wavelengths were 506/532 nm.

In vitro 4-hydroxy-2-nonenal modification of proteasome

Either $50 \mu\text{g}$ of heart lysate from control (*sham*) animals or $2 \mu\text{g}$ of purified 20S proteasome (PW8720, Enzo Lif Sci, PA) were incubated with different concentrations of 4-HNE (10 or $100 \mu\text{M}$) in assay buffer containing 25 mM Tris-HCl, 1 mM CaCl_2 , 20 mM MgCl_2 , pH 7.5 at 37°C for 60 minutes. Dithiothreitol (DTT, 1 μM) was added to the reaction either 30 minutes prior or after 4-HNE incubation to assess the reversibility of 4-HNE modification of proteasome. Measurement of proteasome activity was carried out after finishing the *in vitro* assay.

Proteasome activity

ATP-dependent chymotrypsin-like activity of the proteasome was assayed in the total lysate from heart, isolated cardiomyocyte or purified proteasome using the fluorogenic peptide Suc-Leu-Leu-Val-Tyr-7-amido-4-methylcoumarin (LLVY-AMC, 25 μM). The assay was performed in a microtiter plate (FlexStation II 384, Molecular Device Inc, CA), in assay buffer containing 25 mM Tris-HCl, 5.0 mM MgCl_2 , 25 μM ATP, pH 7.5. Kinetic analyses were carried out using $50 \mu\text{g}$ of protein for 30 min at 37°C in the presence and absence of 1 μM epoxomicin (a selective proteasome inhibitor), with the difference attributed to ATP-dependent proteasomal activity. Excitation/emission wavelengths were 350/440 nm. Proteasome activity was linear for 30 min under the conditions of the assays.

Cell culture

Cardiac myocytes were isolated from 1-day-old Sprague-Dawley rat litters, as described [33].

Cell death

Cell death was measured using the cytotoxicity detection kit (Roche), which measures LDH released in the medium. Percentage cytotoxicity was calculated according to the manufacturer's instructions.

Immunoprecipitation

Total lysate of rat heart (500 μg protein) was incubated with the indicated antibodies for 3 h at 4°C , followed by incubation with protein A/G agarose beads (Santa Cruz Biotechnology) for 1 h at 4°C . The immunoprecipitates were separated on SDS-PAGE and transferred onto nitrocellulose membranes. The membranes were then probed with the indicated antibodies.

Western blot

20S proteasome ($\alpha 5/\alpha 7$, $\beta 1$, $\beta 5$, $\beta 7$ subunits), polyubiquitinated proteins, soluble oligomers, HSP25, $\alpha\beta$ -crystallin and 4-HNE expression levels were evaluated by western blotting in total extracts from the ventricular remote area. Briefly, samples were

subjected to SDS-PAGE in polyacrylamide gels (6–15%) depending upon protein molecular weight. Cardiac soluble oligomers levels were evaluated in non-denaturing gel electrophoresis according to Glabe et al. (2004) [34]. After electrophoresis, proteins were electrotransferred to nitrocellulose membranes (BioRad Biosciences; Piscataway, NJ, USA). Equal gel loading and transfer efficiency were monitored using 0.5% Ponceau S staining of blot membrane. Blotted membrane was then blocked (5% nonfat dry milk, 10 mM Tris-HCl (pH = 7.6), 150 mM NaCl, and 0.1% Tween 20) for 2 h at room temperature and then incubated overnight at 4°C with specific antibodies against 20S proteasome ($\alpha 5/\alpha 7$, $\beta 1$, $\beta 5$, $\beta 7$ subunits) and polyubiquitinated proteins (Biomol Int., PA, USA), HSP25 and $\alpha\beta$ -crystallin (Stressgen, MI, USA), 4-HNE (Calbiochem, HE, Germany), GAPDH (Advanced Immunochemical Inc. CA, USA) and soluble oligomers A11 (Invitrogen, CA, USA). Binding of the primary antibody was detected with the use of peroxidase-conjugated secondary antibodies (rabbit or mouse, depending on the protein, for 2 h at room temperature) and developed using enhanced chemiluminescence (Amersham Biosciences, NJ, USA) detected by autoradiography. Quantification analysis of blots was performed with the use of Scion Image software (Scion based on NIH image). Samples were normalized to relative changes in GAPDH and expressed as percent of control.

Cellular oxidized proteins

Protein oxidation was determined as previously described [35]. The carbonyl groups in the protein side chains were derivatized to 2,4-dinitrophenylhydrazone (DNPhydrazone) by reaction with 2,4-dinitrophenylhydrazine (DNPH). The DNP-derivatized protein samples were separated by polyacrylamide gel electrophoresis followed by Western blotting.

Statistical analysis

Data are presented as means \pm standard error of the mean (SEM). Data normality was assessed through Shapiro-Wilk's test and those not presenting normal distribution were log transformed (i.e. distance run and peak VO_2 before experimental protocol, and interventricular septum in diastole before and after experimental protocol). One-way analysis of variance (ANOVA) was used to analyze data presented in Figures 2, 3, 4, 5A–C and 6. Two-way ANOVA for repeated measures was used to analyze data depicted in Figure 1 and Tables 1 and 2. Whenever significant F-values were obtained, Tukey's adjustment was used for multiple comparison purposes (p-values displayed on Tables 1 and 2 legends). Statistical significance was considered achieved when the value of P was <0.05 . Linear regression was used to assess the association between variables in Figure 5D.

Results

Exercise training improves cardiac function and oxygen uptake in heart failure animals

At four weeks after myocardial infarction surgery (Figure 1A), heart failure rats displayed reduced cardiac function and exercise intolerance (Figures 1B–C). These changes were accompanied by a pathological cardiac remodeling, depicted by increased heart weight/body weight ratio (HW/BW), left ventricular dilation, cardiomyocyte hypertrophy and elevated cardiac fibrosis compared to control animals (Tables 1 and 2). No changes in heart rate and blood pressure were observed (Figures 1D and E).

Eight weeks of aerobic exercise training (Figure 1A) significantly increased cardiac function, depicted by elevated ventricular fractional shortening and ejection fraction in heart failure animals

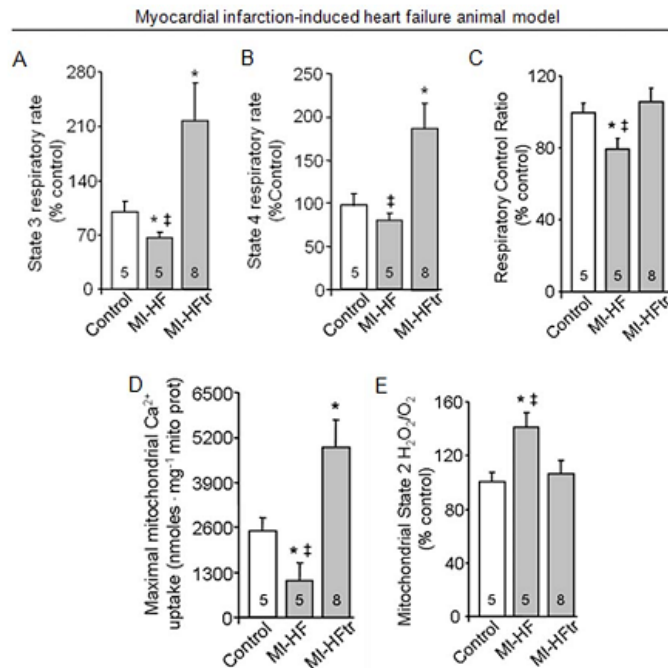


Figure 2. Exercise training improves oxygen consumption and reduces H₂O₂ release in cardiac isolated mitochondria from myocardial infarction-induced heart failure animal. Mitochondrial state 3 (A) and state 4 (B) respiratory rates; respiratory control ratio (C); maximum calcium uptake (D) and H₂O₂ release (E) in heart samples from 24 week-old control (sham, white bars), MI-HF (gray bars) and MI-HF exercise trained (MI-HFtr, gray bars) rats. All measurements were performed in the ventricular remote area. Error bars indicate SEM. Mitochondrial state 3 [F (2, 41) = 8.62, p = 0.0007] and state 4 [F (2, 41) = 8.86, p = 0.0006] respiratory rates; respiratory control ratio [F (2, 45) = 3.26, p = 0.0475]; maximum calcium uptake [F (2, 14) = 5.72, p = 0.0152] and H₂O₂ release [F (2, 37) = 5.28, p = 0.0095]. *, p < 0.05 vs. control (sham) rats. ‡, p < 0.05 vs. MI-HFtr rats. doi:10.1371/journal.pone.0052764.g002

(Figure 1B and Table 2). These findings were accompanied by a cardiac anti-remodeling effect, characterized by reduction of both cardiac collagen deposition and left ventricular dilation (Tables 1 and 2). Exercise training had no effect on HW/BW ratio and myocardial infarction area (Table 1). Cardiomyocyte width was normalized in trained heart failure animals towards control group (Table 1). Based on the data described above, we demonstrate a switch from pathological to physiological cardiac remodeling in trained heart failure animals, since exercise training improved cardiac function along with a prominent morphological change. These findings corroborate our previous work showing that aerobic exercise training promotes a cardiac anti-remodelling effect in a sympathetic hyperactivity-induced heart failure animal model [36]. Finally, the effectiveness of exercise training was demonstrated by increased exercise capacity, peak VO₂, citrate synthase activity and resting bradycardia in the trained heart failure animals (Figure 1C–D and Table 1).

Failing hearts display reduced mitochondrial function and exacerbated ROS release

Impaired mitochondrial metabolism associated with increased ROS release has been shown to contribute to a number of cardiovascular diseases [7,37]. In order to assess mitochondrial function in failing hearts, we measured oxygen consumption and

maximum calcium uptake in isolated mitochondria from 24 week-old myocardial infarction-induced heart failure rats and age-matched controls (Figure 2A–D). Our results indicate that heart failure rats displayed reduced state 3 respiratory rate along with a significant decrease in the efficiency of mitochondrial oxidative phosphorylation compared to control (sham) animals, as measured by respiratory control ratio (State 3/State 4) (Figure 2A–C). Of interest, reduced mitochondrial efficiency was paralleled by the inability of heart failure animals to perform prolonged physical activity (Table 1). Isolated mitochondria from failing hearts also displayed impaired maximum calcium uptake (Figure 2D). Strikingly, a moderate exercise training protocol (over 8 weeks) increased both state 3 and state 4 respiratory rates as well as re-established the efficiency of mitochondrial oxidative phosphorylation (Figures 2A–C). Moreover, exercise training improved maximum calcium uptake and exercise tolerance in heart failure animals (Figures 2D and Table 1).

Considering that ROS release has been strongly associated with changes in oxygen consumption and heart failure [7], we decided to measure H₂O₂ release in isolated mitochondria from 24 week-old failing hearts. Our results demonstrated that H₂O₂ release was significantly increased in mitochondria from heart failure animals compared to age-matched control group (Figure 2E). Interestingly, exercise training decreased mitochondrial H₂O₂ release to control group values.

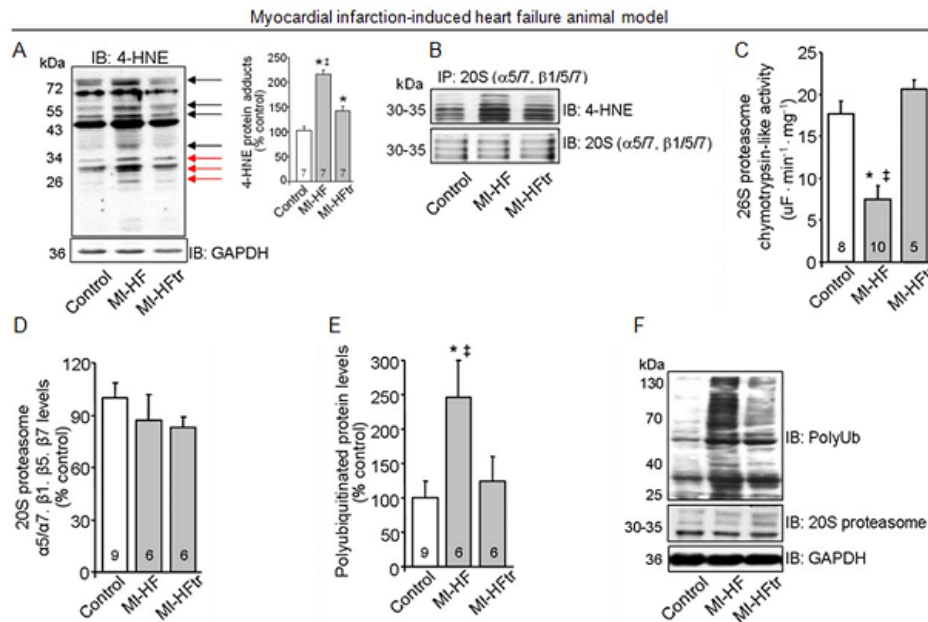


Figure 3. Exercise training decreases 4-HNE modification of proteasome and re-establishes cardiac ubiquitin-proteasome system function in myocardial infarction-induced heart failure. (A) 4-HNE protein adducts in heart samples from 24 week-old control (sham), MI-HF and MI-HF exercise trained (MI-HFtr) rats. Protein expression was normalized by GAPDH. Inset: Representative blot of 4-HNE protein adducts. Black arrows indicate changes in the adduct formation in MI-HF and MI-HFtr samples, red arrows indicate changes in the adduct formation of proteins at the molecular weight of proteasomal subunits. (B) 20S proteasome subunits ($\alpha 5/\alpha 7$, $\beta 1$, $\beta 5$, $\beta 7$) were precipitated from left ventricle tissue from 24-week-old control, MI-HF and MI-HFtr rats (B, n = 3 per group), and then probed with 4-HNE-modified proteins antibody. Equal sample loading was verified using $\alpha 5/\alpha 7$, $\beta 1$, $\beta 5$ and $\beta 7$ proteasome subunits antibody. (C) Chymotrypsin-like activity of 26S proteasome, (D) 20S proteasome $\alpha 5/\alpha 7$, $\beta 1$, $\beta 5$, $\beta 7$ protein levels and (E) polyubiquitinated proteins levels in heart samples from 24 week-old control, MI-HF and MI-HFtr rats. Protein expression was normalized by GAPDH. (F) Representative blots of polyubiquitinated proteins, 20S proteasome and GAPDH. All measurements were performed in the ventricular remote area. Error bars indicate SEM. 4-HNE protein adducts [F (2, 15) = 42.58, $p < 0.0001$]; chymotrypsin-like activity of 26S proteasome [F (2, 25) = 12.90, $p = 0.0001$]; 20S proteasome $\alpha 5/\alpha 7$, $\beta 1$, $\beta 5$, $\beta 7$ [F (2, 18) = 0.81, $p = 0.4595$] and polyubiquitinated proteins levels [F (2, 18) = 4.19, $p = 0.0318$]. *, $p < 0.05$ vs. control (sham) rats. †, $p < 0.05$ vs. MI-HFtr rats. doi:10.1371/journal.pone.0052764.g003

4-HNE modification inhibits proteasomal peptidase activity in heart failure

Elevated ROS release has been generally implicated in cellular damage during pathological processes. The introduction of carbonyl functional groups into proteins by 4-HNE, a major product of ROS-mediated lipid oxidation, has been reported to induce protein inactivation during ischemia-reperfusion injury [38]. Here, we found that non-infarcted cardiac zone from 24 week-old heart failure rats displayed exacerbated accumulation of 4-HNE-protein adducts compared to control animals (Figure 3A). Moreover, immunoprecipitation experiments showed that 4-HNE modifications of the 20S proteasome were elevated in failing hearts compared to controls (Figure 3B). Interestingly, exercise training was able to reduce the formation of adducts between 4-HNE and 20S proteasome in heart failure animals (Figure 3A–B).

Because oxidative modifications of the proteasome have been reported to reduce its proteolytic activity during ischemia-reperfusion injury [9], we decided to evaluate the efficacy of the proteasome chymotrypsin-like site (the main proteolytic site involved in peptide degradation) to cleave the artificial substrate LLVY-AMC *in vitro*. These experiments were performed in the

non-infarcted cardiac zone from 24 week-old heart failure rats and their age-matched controls. As shown in Figure 3C, proteasomal activity was strikingly reduced in failing hearts compared to controls, with no changes in protein expression of 20S proteasome subunits ($\alpha 5/\alpha 7$, $\beta 1/\beta 5/\beta 7$) (Figure 3D and F). Reduction of proteasomal activity was accompanied by accumulation of polyubiquitinated proteins in failing hearts (Figures 3E and F). Interestingly, exercise training re-established proteasomal activity and decreased polyubiquitinated protein levels in failing hearts. Therefore, our results suggest that exercise training prevents 20S proteasome dysfunction in heart failure, likely due to formation of 4-HNE adducts.

In vitro 4-HNE modification inhibits proteasomal activity in an irreversible manner

To directly test the effect of 4-HNE modification on proteasome function, purified 20S proteasome was incubated with 4-HNE for 60 min at 37°C (Figure 4A). *In vitro* incubation of purified 20S proteasome with different concentrations of 4-HNE (10 and 100 μ M) resulted in a significant reduction of proteasomal activity (Figure 4B). In order to test whether proteasome inhibition was

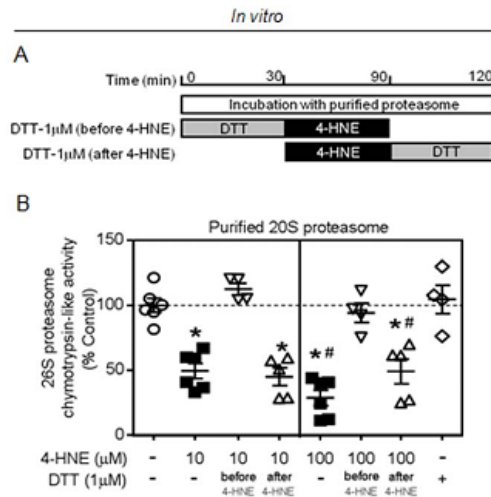


Figure 4. 4-HNE irreversibly inactivates 20S proteasome *in vitro*. (A) Schematic panel of *in vitro* incubations. (B) Purified 20S proteasome (1 μ g) was incubated for 30 min at 37°C with 4-HNE (10 or 100 μ M) and proteasomal activity was measured at the end of incubation. DTT (1 μ M) was added to the reaction either previous or after 4-HNE incubations. Of interest, prior, but no later, incubation with DTT protected 4-hydroxy-2-nonenal inhibition of proteasomal activity. Error bars indicate SEM. Proteasomal activity [F (7, 32) = 21.37, $p < 0.0001$]. *, $p < 0.05$ vs. control, 4-HNE (10 μ M)+DTT (before). #, $p < 0.05$ vs. 4-HNE (10 μ M). doi:10.1371/journal.pone.0052764.g004

mediated by oxidative modifications, purified 20S proteasome was pre-treated with DTT (1 μ M). Indeed, reduction of free sulphhydryl groups prior to incubation with either 10 μ M or 100 μ M of 4-HNE was effective to protect the proteasome against oxidative modification-mediated inhibition. Another explanation for the benefits of DTT pre-treatment might be related to a direct neutralization of 4-HNE oxidative capacity. Interestingly, DTT post-treatment of purified 20S proteasome did not rescue the proteasomal inactivation mediated by 4-HNE modifications. These results demonstrate that 4-HNE modification induces inactivation of proteolytic 20S proteasome activity *in vitro* in an irreversible manner.

Oxidative stress contributes to proteasomal inactivation, accumulation of damaged proteins and cell death in cultured neonatal cardiomyocytes

In order to validate our *in vivo* and *in vitro* findings showing that mitochondrial dysfunction-mediated oxidative modification inactivates proteasome and results in accumulation of damaged proteins, we challenged cultured neonatal cardiomyocytes isolated from rats with either antimycin A (a mitochondrial complex III inhibitor) or H_2O_2 . Antimycin A (100 μ M) resulted in a significant reduction of *in vitro* proteolytic proteasomal activity in an ATP-independent manner, since ATP was added during *in vitro* measurements (Figure 5A). Antimycin A-mediated proteasomal inhibition was accompanied by accumulation of oxidized proteins and elevated cardiomyocytes death (Figures 5B–C). These findings demonstrate that mitochondrial dysfunction-mediated ROS release inactivates proteasome and impairs removal of damaged

proteins. Indeed, treatment of cardiomyocytes with either H_2O_2 (100 μ M) or Epoxomicin (1 μ M, a selective proteasome inhibitor) drastically reduced proteasomal activity along with accumulation of oxidized proteins and cell death (Figures 5A–C). Finally, we found a tight correlation between proteasomal inactivation, accumulation of oxidized proteins and cell death in cultured neonatal cardiomyocytes treated with antimycin A, H_2O_2 or Epoxomicin (Figure 5D).

Proteasomal inhibition disrupts cardiac protein quality control in heart failure rats

The ubiquitin proteasome system is the primary effector of the protein quality control process in cardiomyocytes [39]. Considering our *in vivo* and cell cultured findings demonstrating that mitochondrial dysfunction mediates inactivation of proteasome and accumulation of damaged proteins, we evaluated the cardiac protein quality control profile in 24 week-old myocardial infarction-induced heart failure rats.

Heart failure animals displayed significant accumulation of oxidized proteins compared to age-matched controls (Figure 6A and E). In order to test whether decreased proteasomal activity would contribute to misfolded proteins accumulation, we evaluated cardiac soluble pre-amyloid oligomers levels in heart failure rats. In fact, myocardial infarction-induced heart failure rats presented a significant increase of misfolded proteins levels compared with control hearts (Figure 6B and E). Moreover, heart failure rats presented a significant increase in HSP25 protein levels compared to controls (Figure 6C and E). Our findings showing inhibition of the proteasome along with accumulation of damaged proteins and increased expression of small chaperones demonstrate a clear disruption of protein quality control in failing hearts. Interestingly, exercise training reduced cardiac oxidized and misfolded proteins levels in heart failure rats compared with age-matched non-trained heart failure animals (Figure 6A–B and E). This profile was accompanied by a reduction of small chaperone levels in trained animals (Figure 6C and E), suggesting that improved proteasomal activity mediated by aerobic exercise training contributes, at least in part, to better cardiac protein quality control in heart failure.

Discussion

Over the past decades, significant progression has been made in understanding the cellular processes involved in heart failure, which has positively contributed to drug development in this field. However, in spite of new therapies able to improve patient's quality of life and survival [1], heart failure remains the main cause of death worldwide. Thus, there is a compelling need for new pharmacological and non-pharmacological therapies that could improve clinical outcomes. To fulfill this issue, a number of studies have focused on identifying intracellular distal strategic nodes where signals converge and/or serve as multi-effector brakes to suppress or reverse heart failure, which would become attractive targets for heart failure therapy.

Due to its pivotal role in bioenergetics, calcium homeostasis, redox regulation and cell death, mitochondria have been considered an intracellular organelle capable of orchestrating biochemical processes across the cell [40]. Indeed, much of the current research focuses on understanding the crosstalk between mitochondrial and the rest of the cell. In the present study, we found that mitochondrial dysfunction-associated 4-HNE accumulation, a highly reactive α,β -unsaturated aldehyde and a major secondary product of lipid peroxidation, contributes to protein quality control disruption by directly targeting the proteasome in

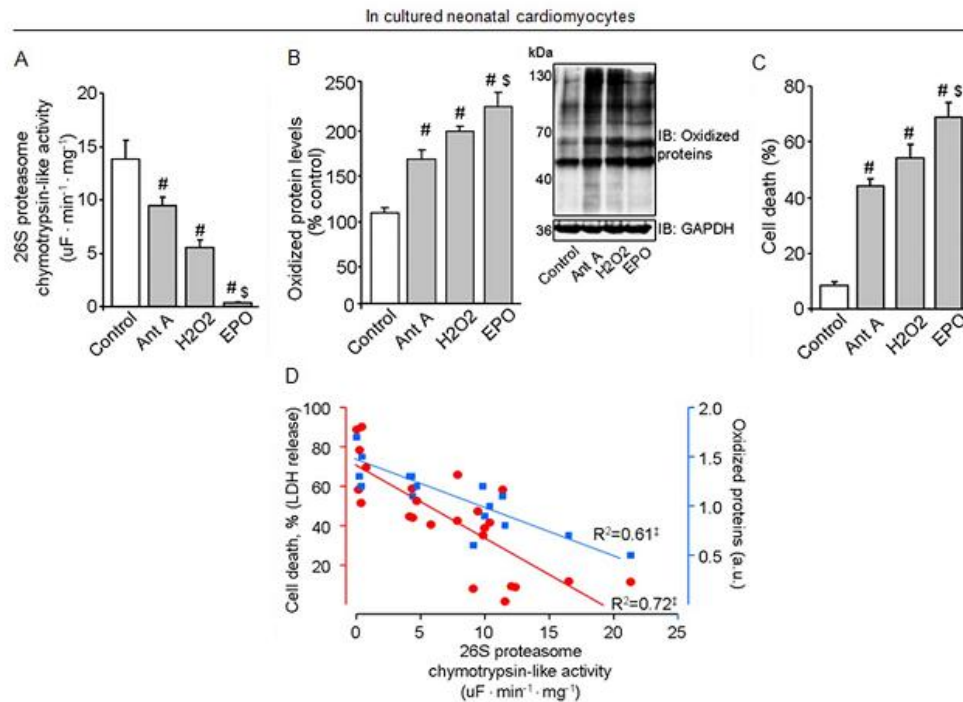


Figure 5. Oxidative stress contributes to proteasomal inactivation, accumulation of damaged proteins and cell death in cultured neonatal cardiomyocytes. Proteasomal activity (A), oxidized protein levels and representative blots (B) and cell death (C) in cultured neonatal cardiomyocytes. Concordance between proteasomal activity, oxidized protein levels and cell death in cultured neonatal cardiomyocytes (D). Cells were stimulated with antimycin A (100 μ M, Ant A, gray bars) or H₂O₂ (100 μ M, H₂O₂, gray bars) or Epoxomicin (1 μ M, EPO, gray bars) for 2 hours. Measurements were performed 24 hrs after treatments. Experiments were repeated at least 5 times. Protein expression was normalized by GAPDH. Error bars indicate SEM. Proteasomal activity [F (3, 20) = 30.85, $p < 0.0001$]; oxidized protein levels [F (2, 9) = 21.84, $p = 0.0003$] and cell death [F (3, 14) = 27.53, $p < 0.0001$]. #, $p < 0.05$ vs. non-treated cells (control). S, $p < 0.05$ vs. antimycin A- and Epoxomicin-treated cells. doi:10.1371/journal.pone.0052764.g005

failing hearts. Moreover, we demonstrated that *in vitro* 4-HNE-modification/inactivation of proteasome occurs in an irreversible manner, while reduction of free sulphhydryl groups prior to 4-HNE incubation abolished the inhibition of proteasomal chymotrypsin-like activity. Our study has shown for the first time that modification/inactivation of the cardiac proteasome by the lipid peroxidation product 4-HNE occurs in heart failure. Others have observed the same phenomenon during acute coronary occlusion/reperfusion, cerebral ischemia and aging [9,18].

The proteasome has been implicated in the removal of polyubiquitinated and oxidatively modified proteins [41,42,43,44]. Therefore, impairment of proteasomal proteolytic activity by 4-HNE may negatively affect cellular protein quality control and further contributes to cell death. In agreement with these findings, we observed a striking inactivation of proteasomal chymotrypsin-like activity paralleled by accumulation of oxidatively modified, misfolded and polyubiquitinated proteins in failing hearts. These responses were accompanied by increased expression of small chaperones. Over-expression of small chaperones such as HSP25 and $\alpha\beta$ crystallin is related to cellular protection against misfolded protein accumulation [45] and cell death [46] under acute insults (i.e. acute cardiac ischemia-reperfusion injury).

However, during chronic degenerative diseases such as heart failure, increased chaperones expression does not overcome the deleterious effects generated by accumulation of misfolded proteins.

Considering that maintenance of protein quality control is crucial to protect long-lived cells, such as cardiomyocytes and neurons, we evaluated whether mitochondrial dysfunction-mediated oxidative stress could affect proteasomal activity and overall protein quality control in cultured isolated cardiomyocytes. Either Antimycin A or H₂O₂ resulted in proteasomal inactivation, accumulation of oxidatively modified proteins and cell death in cultured cardiomyocytes. These findings demonstrate that oxidative stress-mediated chymotrypsin-like proteasomal inhibition (the main proteasomal proteolytic site involved in protein degradation and the most sensitive to 4-HNE modification) [10] decreases cardiomyocyte viability and contributes, at least in part, to the disruption of cardiac protein quality control in cardiomyocytes. We have previously shown that improvement of proteasomal activity using pharmacological tools protects neonatal cardiomyocytes against H₂O₂-induced cell death [42].

Emerging studies have revealed that disruption of cardiac mitochondrial metabolism and/or proteasomal insufficiency are

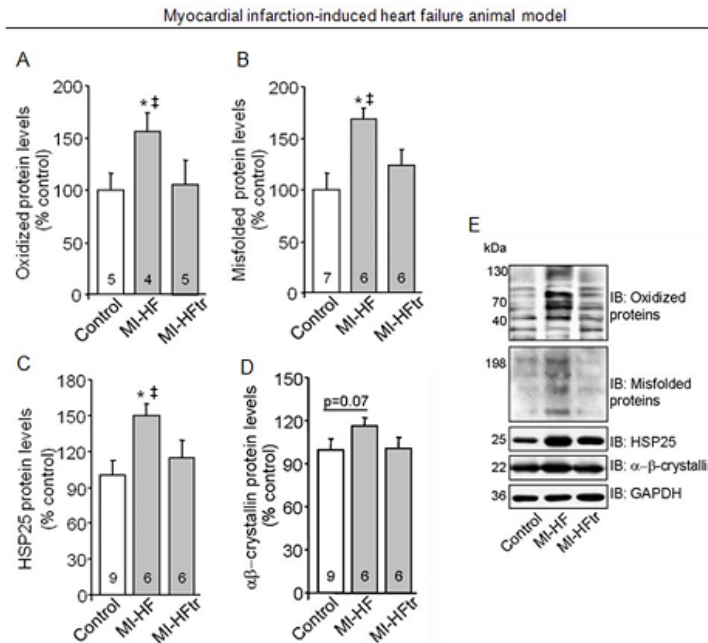


Figure 6. Exercise training improves protein quality control in myocardial infarction-induced heart failure. Oxidized protein levels (A), soluble oligomers accumulation (B), HSP25 (C) $\alpha\beta$ -crystallin (D) protein levels in heart samples from 24 week-old control (sham, white bars), MI-HF (gray bars) and MI-HF exercise trained (MI-HFtr, gray bars) rats. Representative blots of oxidized protein, soluble oligomers, HSP25, $\alpha\beta$ -crystallin and GAPDH (E). All measurements were performed in the ventricular remote area. Protein expression was normalized by GAPDH. Error bars indicate SEM. Oxidized protein levels [F (2, 19) = 5.25, $p = 0.0312$]; soluble oligomers accumulation [F (2, 15) = 3.97, $p = 0.0412$]; HSP25 [F (2, 19) = 4.21, $p = 0.0306$] and $\alpha\beta$ -crystallin proteins levels [F (2, 17) = 1.49, $p = 0.0252$]. *, $p < 0.05$ vs. control (sham) rats. †, $p < 0.05$ vs. MI-HFtr rats. doi:10.1371/journal.pone.0052764.g006

not only implicated but also play an important role in cardiac pathogenesis. In fact, selective pharmacological and genetic therapies capable to rescue either mitochondrial metabolism or proteasomal activity improve cardiac function in different heart disease animal models [39,42,47,48]. However, considering that both mitochondrial metabolism and proteasomal function are highly regulated by different cellular processes, we cannot exclude the possibility that these changes are secondary to the compromised cardiac function. Therefore, further studies investigating both direct and indirect proteasomal regulation by oxidative stress during heart failure progression are required. Also, the contribution of oxidative stress to other proteolytic systems such as autophagic/lysosomal pathways, and its effect on cardiac protein quality control in HF should be considered.

The possible mechanisms involved in 4-HNE-mediated proteasomal inhibition have been previously described in different cell lines and systems, including the heart. Analysis of two-dimension gel electrophoresis from purified proteasomes followed by mass spectrometry demonstrated that 4-HNE modification is not a random process and that specific proteasomal subunits, mainly α -subunits, are targeted by 4-HNE in the heart [9,10,49]. However, since the proteasomal catalytic sites are located in the β subunits ($\beta 1$, $\beta 2$ and $\beta 5$), it has been suggested that an indirect mechanism, probably mediated by protein-protein interactions between regulatory and catalytic subunits, drives the inhibition of

proteasomal peptidase activity mediated by 4-HNE. Indeed, further studies are required to better clarify this issue.

Another important finding of this study is the efficacy of exercise training in restoring cardiac mitochondrial function, proteasomal activity and protein quality control in heart failure animals. Exercise capacity has been widely recognized an independent predictor of mortality in patients with cardiovascular diseases [24]. Moreover, exercise training is considered an important adjuvant in the treatment of heart failure since it increases both peak VO_2 and exercise tolerance, resulting in improved patient outcome and quality of life [4,5,6]. However, the mechanisms underlying exercise-induced beneficial effect on heart failure are not completely understood.

Over the last decades, several studies have demonstrated the contribution of exercise training to improve expression of mitochondrial markers of biogenesis and metabolism in heart failure. However, the contribution of exercise training to mitochondrial physiology and its extension to cytosolic systems related to cell survival during heart failure remains unclear. A recent study has demonstrated that low-intensity interval exercise training decreases calcium-induced mitochondrial permeability transition in aortic-banded miniature swine [2], which may positively affect cytosolic systems. In addition, exercise training has been shown to improve cardiac redox balance in young and old healthy animals [23,50]. We extended these findings by showing that 8 weeks of aerobic exercise training restored

oxidative phosphorylation efficiency along with a reduction in H₂O₂ release and increased maximum calcium uptake in isolated mitochondria from myocardial infarction-induced heart failure rats. Interestingly, exercise training had a positive impact on cytosolic protein quality control machinery by re-establishing the proteasomal activity in failing hearts. These findings suggest that reduced cardiac oxidative stress along with better protein quality control are associated with the benefits promoted by exercise training in heart failure rats. However, considering the complexity of mitochondrial metabolism and protein quality control machinery, further investigations need to be conducted in order to establish a cause-and-effect relationship as well as clarify other possible regulatory mechanisms regulated by exercise training in heart failure.

In summary, we provide evidence that myocardial-infarction induced heart failure rats display a prominent cardiac mitochondrial dysfunction, 4-HNE accumulation and cytosolic protein

quality control disruption. In addition, the ability of exercise training to rescue mitochondrial function, decrease 4-HNE accumulation and improve cardiac protein quality control in heart failure highlights an important molecular mechanism underlying the benefits of exercise training in failing hearts.

Acknowledgments

We thank Katt C. Mattos, Marcelle C. Coelho and Camille C. Caldeira-da-Silva for technical assistance.

Author Contributions

Conceived and designed the experiments: JCC AJK PCB DMR JCBF. Performed the experiments: JCC BBQ PMMD VOZ TFC LRGB. Analyzed the data: JCC BBQ VOZ. Contributed reagents/materials/analysis tools: AJK PCB DMR. Wrote the paper: JCC JCBF.

References

- Guyatt GH, Devereaux PJ (2004) A review of heart failure treatment. *Mt Sinai J Med* 71: 47–54.
- Emter CA, McCune SA, Sparagna GC, Radin MJ, Moore RL (2005) Low-intensity exercise training delays onset of decompensated heart failure in spontaneously hypertensive heart failure rats. *Am J Physiol Heart Circ Physiol* 289: H2030–2038.
- Powers SK, Lennon SL, Quindry J, Mehta JL (2002) Exercise and cardioprotection. *Curr Opin Cardiol* 17: 495–502.
- Jonsdottir S, Andersen KK, Sigursson AF, Sigursson SB (2006) The effect of physical training in chronic heart failure. *Eur J Heart Fail* 8: 97–101.
- Roveda F, Middlekauff HR, Rondon MU, Reis SF, Souza M, et al. (2003) The effects of exercise training on sympathetic neural activation in advanced heart failure: a randomized controlled trial. *J Am Coll Cardiol* 42: 854–860.
- Wisloff U, Stoylen A, Loennechen JP, Bruvold M, Rognum O, et al. (2007) Superior cardiovascular effect of aerobic interval training versus moderate continuous training in heart failure patients: a randomized study. *Circulation* 115: 3086–3094.
- Rosca MG, Hoppel CL (2010) Mitochondria in heart failure. *Cardiovasc Res* 88: 40–50.
- Roede JR, Jones DP (2010) Reactive species and mitochondrial dysfunction: mechanistic significance of 4-hydroxynonenal. *Environ Mol Mutagen* 51: 380–390.
- Balteau AL, Lundberg KC, Humphries KM, Sadek HA, Szewda PA, et al. (2001) Oxidative modification and inactivation of the proteasome during coronary occlusion/reperfusion. *J Biol Chem* 276: 30057–30063.
- Farout L, Mary J, Vinh J, Szewda LI, Friguet B (2006) Inactivation of the proteasome by 4-hydroxy-2-nonenal is site specific and dependant on 20S proteasome subtypes. *Arch Biochem Biophys* 453: 135–142.
- Isom AL, Barnes S, Wilson L, Kirk M, Coward L, et al. (2004) Modification of Cysteine 6 by 4-hydroxy-2-nonenal: evidence for histidine, lysine, and arginine-aldehyde adducts. *J Am Soc Mass Spectrom* 15: 1136–1147.
- Maki CG, Huijbreghse JM, Howley PM (1996) In vivo ubiquitination and proteasome-mediated degradation of p53(1). *Cancer Res* 56: 2649–2654.
- Salghetti SE, Kim SY, Tansey WP (1999) Destruction of Myc by ubiquitin-mediated proteolysis: cancer-associated and transforming mutations stabilize Myc. *Embo J* 18: 717–726.
- Dimmeler S, Breitschopf K, Haendeler J, Zeiher AM (1999) Dephosphorylation targets Bcl-2 for ubiquitin-dependent degradation: a link between the apoptosome and the proteasome pathway. *J Exp Med* 189: 1815–1822.
- Patterson C, Ike C, Willis PW, Stouffer GA, Willis MS (2007) The bitter end: the ubiquitin-proteasome system and cardiac dysfunction. *Circulation* 115: 1456–1463.
- Tsukamoto O, Minamoto T, Okada K, Shintani Y, Takashima S, et al. (2006) Depression of proteasome activities during the progression of cardiac dysfunction in pressure-overloaded heart of mice. *Biochem Biophys Res Commun* 340: 1125–1133.
- Hein S, Arnon E, Kostin S, Schonburg M, Elsasser A, et al. (2003) Progression from compensated hypertrophy to failure in the pressure-overloaded human heart: structural deterioration and compensatory mechanisms. *Circulation* 107: 984–991.
- Grune T, Davies KJ (2003) The proteasomal system and HNE-modified proteins. *Mol Aspects Med* 24: 195–204.
- Reinheckel T, Site N, Ullrich O, Kuckelkorn U, Davies KJ, et al. (1998) Comparative resistance of the 20S and 26S proteasome to oxidative stress. *Biochem J* 335 (Pt 3): 637–642.
- Johns TN, Olson BJ (1954) Experimental myocardial infarction. I. A method of coronary occlusion in small animals. *Ann Surg* 140: 675–682.
- Gheorghide M, Bonow RO (1998) Chronic heart failure in the United States: a manifestation of coronary artery disease. *Circulation* 97: 282–289.
- Hunt SA, Abraham WT, Chin MH, Feldman AM, Francis GS, et al. (2009) 2009 focused update incorporated into the ACC/AHA 2005 Guidelines for the Diagnosis and Management of Heart Failure in Adults: a report of the American College of Cardiology Foundation/American Heart Association Task Force on Practice Guidelines: developed in collaboration with the International Society for Heart and Lung Transplantation. *Circulation* 119: e391–479.
- Ferreira JC, Bacurau AV, Bueno CR Jr, Cunha TC, Tanaka LY, et al. (2010) Aerobic exercise training improves Ca²⁺ handling and redox status of skeletal muscle in mice. *Exp Biol Med* (Maywood) 235: 497–505.
- Myers J, Prakash M, Froelicher V, Do D, Partington S, et al. (2002) Exercise capacity and mortality among men referred for exercise testing. *N Engl J Med* 346: 795–801.
- Ferreira JC, Rolim NP, Bartholomeu JB, Gobatto CA, Kokubun E, et al. (2007) Maximal lactate steady state in running mice: effect of exercise training. *Clin Exp Pharmacol Physiol* 34: 760–765.
- Ferreira JC, Moreira JB, Campos JC, Pereira MG, Mattos KC, et al. (2011) Angiotensin receptor blockade improves the net balance of cardiac Ca²⁺ handling-related proteins in sympathetic hyperactivity-induced heart failure. *Life Sci* 88: 578–583.
- Ferreira JC, Bacurau AV, Evangelista FS, Coelho MA, Oliveira EM, et al. (2008) The role of local and systemic renin-angiotensin system activation in a genetic model of sympathetic hyperactivity-induced heart failure in mice. *Am J Physiol Regul Integr Comp Physiol* 294: R26–32.
- Kido M, Du L, Sullivan CC, Li X, Deutsch R, et al. (2003) Hypoxia-inducible factor 1- α reduces infarction and attenuates progression of cardiac dysfunction after myocardial infarction in the mouse. *J Am Coll Cardiol* 46: 2116–2124.
- Alp PR, Newsholme EA, Zammit VA (1976) Activities of citrate synthase and NAD⁺-linked and NADP⁺-linked isocitrate dehydrogenase in muscle from vertebrates and invertebrates. *Biochem J* 154: 689–700.
- Cancherini DV, Quelicini BB, Kowaltowski AJ (2007) Pharmacological and physiological stimuli do not promote Ca²⁺-sensitive K⁺ channel activity in isolated heart mitochondria. *Cardiovasc Res* 73: 720–728.
- Tahara EB, Navarete FD, Kowaltowski AJ (2009) Tissue-, substrate-, and site-specific characteristics of mitochondrial reactive oxygen species generation. *Free Radic Biol Med* 46: 1283–1297.
- Murphy AN, Bredesen DE, Cortopassi G, Wang E, Fiskum G (1996) Bcl-2 potentiates the maximal calcium uptake capacity of neural cell mitochondria. *Proc Natl Acad Sci U S A* 93: 9893–9898.
- Valentin A, Mochly-Rosen D (2007) RBCK1, a protein kinase Cheta1 (PKC β)-interacting protein, regulates PKC β -dependent function. *J Biol Chem* 282: 1650–1657.
- Glabbe CG (2004) Conformation-dependent antibodies target diseases of protein misfolding. *Trends Biochem Sci* 29: 542–547.
- Antony JM, van Marle G, Opii W, Butterfield DA, Mallet F, et al. (2004) Human endogenous retrovirus glycoprotein-mediated induction of redox reactants causes oligodendrocyte death and demyelination. *Nat Neurosci* 7: 1088–1095.
- Oliveira RS, Ferreira JC, Gomes ER, Paixao NA, Rolim NP, et al. (2009) Cardiac anti-remodelling effect of aerobic training is associated with a reduction in the calcineurin/NFAT signalling pathway in heart failure mice. *J Physiol* 587: 3899–3910.
- Chen CH, Sun L, Mochly-Rosen D (2010) Mitochondrial aldehyde dehydrogenase and cardiac diseases. *Cardiovasc Res* 88: 51–57.

38. Chen CH, Budas GR, Churchill EN, Disatnik MH, Hurley TD, et al. (2008) Activation of aldehyde dehydrogenase-2 reduces ischemic damage to the heart. *Science* 321: 1493–1495.
39. Wang X, Robbins J (2006) Heart failure and protein quality control. *Circ Res* 99: 1315–1328.
40. Schatz G (2007) The magic garden. *Annu Rev Biochem* 76: 673–678.
41. Churchill EN, Ferreira JC, Brum PC, Sawada LI, Mochly-Rosen D (2010) Ischaemic preconditioning improves proteasomal activity and increases the degradation of deltaPKC during reperfusion. *Cardiovasc Res* 85: 385–394.
42. Ferreira JC, Boer BN, Grinberg M, Brum PC, Mochly-Rosen D (2012) Protein quality control disruption by PKC β II in heart failure; rescue by the selective PKC β II inhibitor, β HIV5-3. *PLoS ONE* 7: e33175.
43. Powell SR, Wang P, Katzell H, Shringarpure R, Teoh C, et al. (2005) Oxidized and ubiquitinated proteins may predict recovery of postischemic cardiac function: essential role of the proteasome. *Antioxid Redox Signal* 7: 530–546.
44. da Cunha FM, Demasi M, Kowaltowski AJ (2011) Aging and calorie restriction modulate yeast redox state, oxidized protein removal, and the ubiquitin-proteasome system. *Free Radic Biol Med* 51: 664–670.
45. Liberek K, Lewandowska A, Zietkiewicz S (2008) Chaperones in control of protein disaggregation. *Embo J* 27: 328–335.
46. Shin JH, Kim SW, Lim CM, Jeong JY, Piao CS, et al. (2009) B-crystallin suppresses oxidative stress-induced astrocyte apoptosis by inhibiting caspase 3 activation. *Neurosci Res*.
47. Chen Y, Liu Y, Dorn GW 2nd (2011) Mitochondrial fusion is essential for organelle function and cardiac homeostasis. *Circ Res* 109: 1327–1331.
48. Li J, Horak KM, Su H, Sanbe A, Robbins J, et al. (2011) Enhancement of proteasomal function protects against cardiac proteinopathy and ischemia/reperfusion injury in mice. *J Clin Invest* 121: 3689–3700.
49. Ferrington DA, Kappahn RJ (2004) Catalytic site-specific inhibition of the 20S proteasome by 4-hydroxynonenal. *FEBS Lett* 578: 217–223.
50. Qj Z, He J, Su Y, He Q, Liu J, et al. (2011) Physical exercise regulates p53 activity targeting SCO2 and increases mitochondrial COX biogenesis in cardiac muscle with age. *PLoS ONE* 6: e21140.

Ap.7 An anoxia-starvation model for ischemia/reperfusion in *C. elegans*

Video Article

An Anoxia-starvation Model for Ischemia/Reperfusion in *C. elegans*

Bruno B. Queliconi¹, Alicia J. Kowaltowski¹, Keith Nehrke²

¹Departamento de Bioquímica, Instituto de Química, Universidade de São Paulo

²Department of Medicine, Nephrology Division, University of Rochester Medical Center, School of Medicine and Dentistry

Correspondence to: Bruno B. Queliconi at queliconi@gmail.com

URL: <http://www.jove.com/video/51231>

DOI: [doi:10.3791/51231](https://doi.org/10.3791/51231)

Keywords: Neuroscience, Issue 85, *C. elegans*, ischemia/reperfusion, anoxia/starvation, neuronal damage, touch assay

Date Published: 3/11/2014

Citation: Queliconi, B.B., Kowaltowski, A.J., Nehrke, K. An Anoxia-starvation Model for Ischemia/Reperfusion in *C. elegans*. *J. Vis. Exp.* (85), e51231, doi:10.3791/51231 (2014).

Abstract

Protocols for anoxia/starvation in the genetic model organism *C. elegans* simulate ischemia/reperfusion. Worms are separated from bacterial food and placed under anoxia for 20 hr (simulated ischemia), and subsequently moved to a normal atmosphere with food (simulated reperfusion). This experimental paradigm results in increased death and neuronal damage, and techniques are presented to assess organism viability, alterations to the morphology of touch neuron processes, as well as touch sensitivity, which represents the behavioral output of neuronal function. Finally, a method for constructing hypoxic incubators using common kitchen storage containers is described. The addition of a mass flow control unit allows for alterations to be made to the gas mixture in the custom incubators, and a circulating water bath allows for both temperature control and makes it easy to identify leaks. This method provides a low cost alternative to commercially available units.

Video Link

The video component of this article can be found at <http://www.jove.com/video/51231/>

Introduction

C. elegans is a nematode that has been widely adopted as a multicellular eukaryotic model organism since its introduction by Brenner¹. It is a cheap, simple, and versatile model, which allows easy links between genetic alterations and phenotypic changes².

Ischemia is characterized by a lack of nutrients and oxygen supply to a tissue, followed by reperfusion, when a burst of reactive oxygen species is produced³ and most of the damage occurs. In 2002, a model of ischemia/reperfusion (IR) in *C. elegans* was developed⁴ involving submitting the whole worm to anoxia, nutrient deprivation and heat stress for approximately 20 hr followed by 24 hr under normal conditions. Although this model is technically an anoxia-starvation (AS) condition, cell death occurs through mechanisms that are conserved in mammals, including damage induced by oxidants during reperfusion⁵. Furthermore, similar to mammalian IR, damage induced by AS in *C. elegans* can be prevented by ischemic preconditioning^{6,7} or anesthetic preconditioning^{8,9}.

The protocols below demonstrate how to mimic IR in *C. elegans* using the AS model, how to score morphological and behavioral abnormalities that result from AS, and how to adapt the protocol in a way that allows the experiment to be conducted with a lower initial investment using a custom-made, easily-constructed chamber alternative.

Protocol

1. *C. elegans* Growth

1. Prepare 35 mm Nematode Growth Media (NGM) agar plates seeded with OP50 bacteria, as per standard cultivation methods¹.
2. Synchronize *C. elegans* by placing 6 gravid adults onto a seeded NGM plate. Remove the adults after ~100 eggs have been laid (~3 hr).
3. Incubate the plates for 3 days at 20 °C, at which point the worms will have developed to young adult stage and are optimal for this experiment. Alternative protocols to synchronize *C. elegans* are described elsewhere¹⁰.

2. Materials for AS

1. M9 buffer (22 mM KH₂PO₄, 42 mM Na₂HPO₄, 86 mM NaCl, 1 mM MgSO₄) should be purged of oxygen by equilibrating with N₂ (argon can also be used) during 30 min prior to the experiment and kept surrounded by ice.
2. Make a small hole (3 mm wide) in the lid of 1.5 ml microcentrifuge tubes in which the worms will be placed during AS. The hole allows for gas exchange without keeping the lid open, as this can lead to excessive media evaporation.

3. Anoxia/Starvation

1. Conduct all experiments at least in triplicate.
2. Add 1 ml of RT, oxygenated M9 buffer to each 35 mm plate containing young adult worms grown as described above. Be careful to avoid removing bacteria from the plate (add M9 to the edges where bacteria weren't seeded). After ~1 min the worms should be swimming in the M9.
3. Coat a 1 ml pipette tip with BSA by pipetting and expelling a sterile 1% BSA solution.
4. Carefully incline the plate containing the worms in M9 buffer, remove the M9 from the same place where it was added, and place the suspension in the prepared microcentrifuge tubes. Let rest in ice until the worms have dropped to the bottom of the tubes (~1-2 min).
5. Remove the maximum amount of M9 possible without disturbing the worms from the tube (leaving around 100 μ l), add 1 ml of the oxygen-purged and iced M9 and place the tube over ice until the worms settle to the bottom again. Repeat the last step 3x. In the last wash, remove the M9 until ~100 μ l remains in the tube.
6. Place the tubes with the worms in deoxygenated M9 inside an anoxic/hypoxic chamber (see instructions below, Section 3.6.1) or, alternatively, into a custom sealed container (see instructions below, Section 3.6.2).
 1. If a commercial anoxic/hypoxic chamber is to be used, leave some purged M9 inside the chamber before starting step 3.5 and repeat step 3.5 once the worms are inside the chamber.
 2. If a custom chamber is to be used, a detailed description of how to create a low-cost apparatus is presented at the end of this protocol and has been described by another group previously¹¹. Briefly:
 1. Make two holes in a 250 ml Tupperware-type container lid and add tube connectors to them. One will be used to inject the gas mixture while the other will be the gas exit into a water bath.
 2. Place the worms into the chamber and seal the chamber using the lid.
 3. Gas with a constant N₂ flux (100 ml/min).
 4. Place the container inside a water bath at 26 °C. Ensure that the exit tube is well immersed in water so no air returns and that there are no leaks in the system (apparent by bubbles arising from the chamber itself).
7. Incubate the worms at 26 °C for 20 hr.

4. Simulated Reperfusion

1. After 20 hr under AS conditions, remove the tubes from the incubation chamber into room air.
2. Pipette *C. elegans* with a BSA-coated tip (as in step 3.3) onto an OP50 seeded 35 mm NGM plate. Incubate the plates at 20 °C for 24 hr. After this, the worms will be ready to be scored.

5. Identifying Dead Versus Live Worms

1. Using a platinum pick, lightly touch the top of the head of the worm. Live worms will move backwards after being touched. If the worms are nonresponsive, score as dead. Occasionally, a worm will not move backwards, but may exhibit a slight side-to-side head movement. Although not technically dead, these worms are almost certain to expire within hours, and should be scored as dead. If one waits too long to score the worms, internal hatching of progeny can occur and these "bags-of-worms" can rupture, making detecting the carcasses very difficult.
2. Remove both live and dead worms from the plate as they are counted to avoid duplicate counts. The live worms can be moved to a separate plate to perform behavioral assays. The amount of living worms relative to the total is represented as the % of surviving worms (**Figure 1A**).

6. Touch Response Assay

1. A detailed description of this protocol has been presented in Hart, Anne C., ed. Behavior (July 3, 2006), WormBook, ed. The *C. elegans* Research Community, WormBook, doi/10.1895/wormbook.1.87.1, http://www.wormbook.org.
 1. To score for touch response, identify worms that are moving and lightly touch the side of the worm's head (near the middle part of the pharynx) with an eyelash pick (**Figure 3**).
 2. If the worm moves backward, score as responsive, if not, score as nonresponsive (**Figure 1B**). Repeat this step 10-15x for each worm with 10 sec intervals. Probe at least 10 worms in each group to have accurate data. The same assay can be used to assess forward locomotory changes following light touch to the posterior body wall. Be sure not to touch the head or tail of the worm, since this stimulates a distinct behavior.
 3. Finally, incorporate genetic control strains [N2 Bristol wild-type for positive, mec (mechanosensory) mutant for negative - e.g. CB1338 *mec-3* (*e1338*)/IV] to calibrate the force with which to touch the worms. Too harsh of a stimulation will elicit a behavioral response in mec mutants, too little will not elicit an effect in wildtype N2 controls.

7. Neuronal Modifications

1. To visualize post AS neuronal modifications, use a strain which expresses GFP in the touch-responding mec neurons^{4,5}. These neurons have long processes that run along the body wall and are easily scored for morphological abnormalities. In addition, the morphologic information can be integrated with behavioral measures of neuronal function, as described above. One strain that can be used for this purpose is TU2583, which is available from the *C. elegans* Genetics Center and contains the *uls25* integrated transgene expressing GFP from the *mec-18* promoter, or alternatively TU2562, which contains an integrated *mec-3::GFP* fusion.
2. Prepare an agarose pad.
 1. Melt 2% agarose in water, bring to 1x M9 with a 10x stock, and maintain the solution at 70 °C.

2. Place a drop (~20 μ l) of this solution on a glass slide (25 mm x 75 mm) that has been placed between two other slides, each of which have a single piece of tape on their bottom side.
 3. Place a final glass slide perpendicular to the first on top of the 2% agarose solution, and let it cool at RT. This should form a pad that is the thickness of the tape.
 4. Remove the top slide and add 10 μ l of M9 containing 0.1% tetramisole, which will immobilize the worms.
3. Move some (~10) live worms onto the 2% agarose slide. Place a coverslip over them and visualize GFP using a fluorescence microscope under a 100X objective with the appropriate illumination.
 4. Damaged neurons will show a cytosolic membrane string of pearls pattern in the processes, comprised of multiple punctum (**Figure 2A**), and/or abnormalities where the processes appear to be broken (**Figure 2B**). Count punctum and abnormalities in both neurons for each worm, using a total of at least 10 worms.

8. Lab-made Hypoxic Chamber

1. A Tupperware-style, sealable, airtight container can be retrofit as an anoxic chamber. Take care to select a container that is as small as feasible. A small container creates a hypoxic environment faster and is easier to fit in the water bath (**Figure 4**).
2. Make two holes on the lid (can be done with a screwdriver or by heating forceps and forcing into the lid) and insert a plastic or metal connector that fits the tubing (**Figure 5A**). Use glue that can be placed under water, and also gets hard after drying, avoiding movement of the connector and hence reducing the possibility of leakage (**Figure 5B**).
3. The container should be placed into the water bath so that it is submerged completely (**Figure 4**). To immerse the container, use a bottle weight or a diving weight.
4. One of the tube connections will be used to introduce a gas mixture and the other tube will act as a pressure relief, hence it should be left under the water so that the container is sealed off from the external environment (**Figure 4**).
5. The air composition can be modulated by using custom made gas, mass flow controllers or any apparatus that mixes the desired gases. The gas flow should be controlled, as high flow can create excessive evaporation. For example, in a 250 ml container, 100 ml/min of gas will provide good space for the worms and a suitable flux.
6. The length of the tubing should be kept to a minimum, as they can be permeable to gas, allowing the entrance of O₂. It is important to avoid using silicone, Tygon tubes as these materials are permeable to gas exchange. We prefer polypropylene or nylon tubes. Glass or metal tubing maintain the gasses well, but are also harder to work with.

Representative Results

Subjecting *C. elegans* to 20 hr of AS at 26 °C in a custom lab-made incubation chamber as described (Section 3.6.2) resulted in significant mortality (**Figure 1A**)⁵. Subsequent fluorescent imaging of punctum and breaks in the GFP labeled neuronal processes of survivors confirmed the presence of morphological abnormalities (**Figure 2**). The survivors also responded poorly to light body wall touch (**Figure 1B**). This model has been used by multiple groups to study how genetic predisposition, pharmaceutical intervention, and metabolic plasticity affects AS dependent outcomes^{4,6,8,9,12,13}.

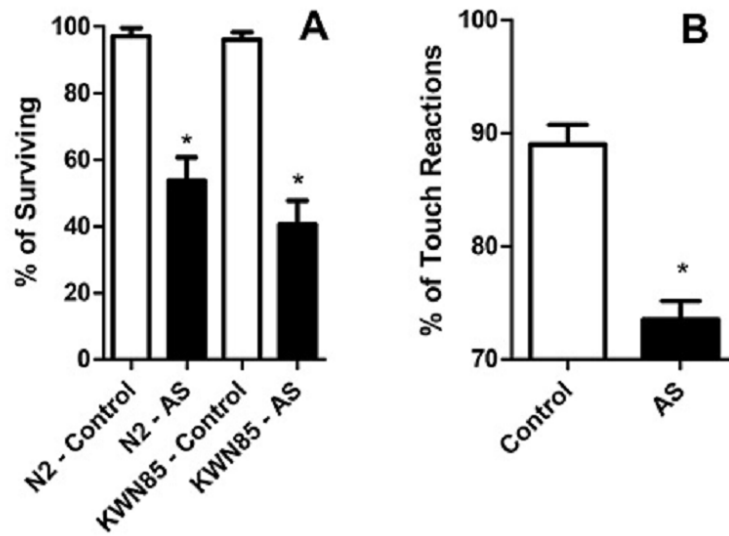


Figure 1. *C. elegans* survival and touch response after AS. **A)** Percentage of worms that exhibit 24 hr post-AS survival. The N2 strain is the wild type genetic background, and KWN85 contains an integrated transgene that labels mec neurons with GFP. **B)** Response to touch stimuli of living *C. elegans* (N2 Strain) after AS. [Please click here to view a larger version of this figure.](#)

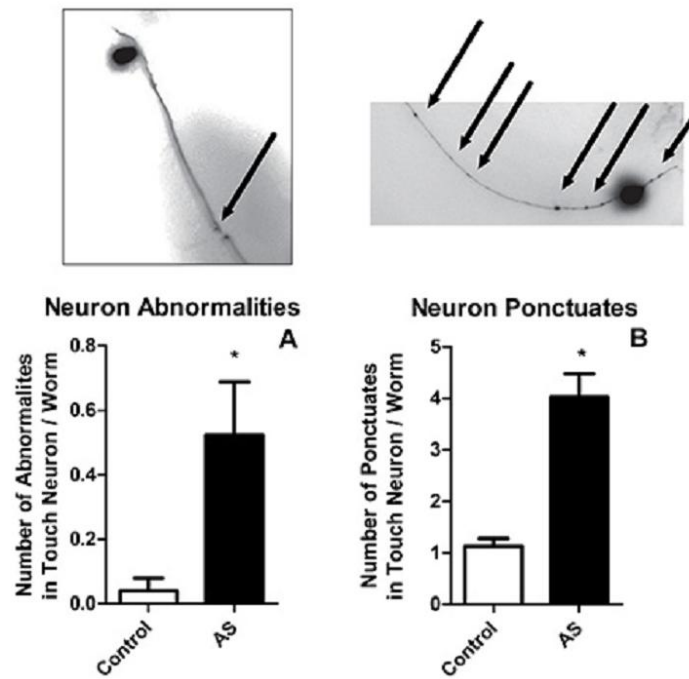


Figure 2. Touch neuron modifications after AS. Touch neuron (PLML and PLMR) abnormalities such as tortuous processes and breaks (A) or the accumulation of GFP aggregates in the processes (B) were monitored in surviving anesthetized *C. elegans* after AS.

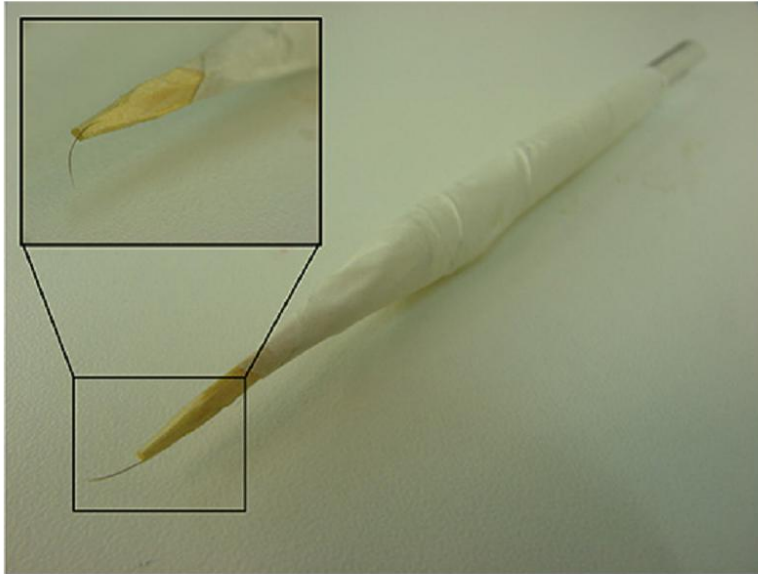


Figure 3. Eyelash pick. An assembled eyelash pick. In the inset, a detail of the eyelash glued to the toothpick wood.

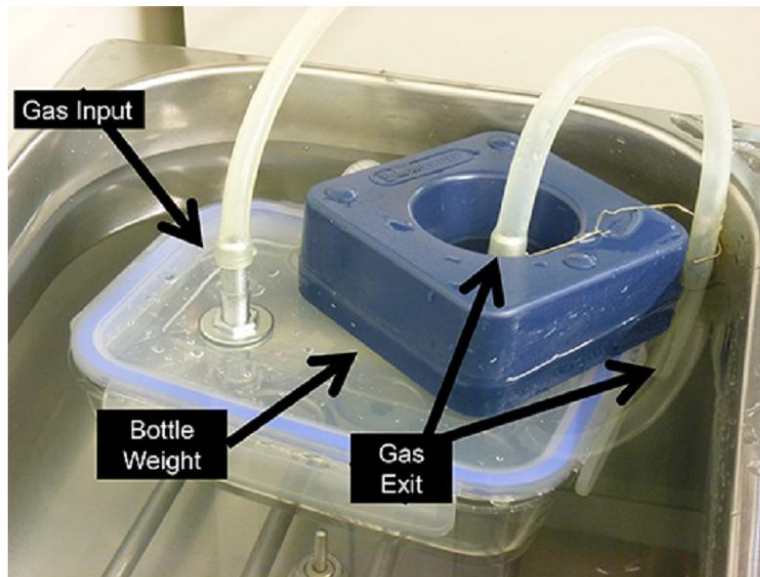


Figure 4. Lab-made hypoxic chamber inside the water bath. A closed container ready to start the experiment. Arrows indicate the gas entrance and exit and the bottle weight used to keep it from floating.

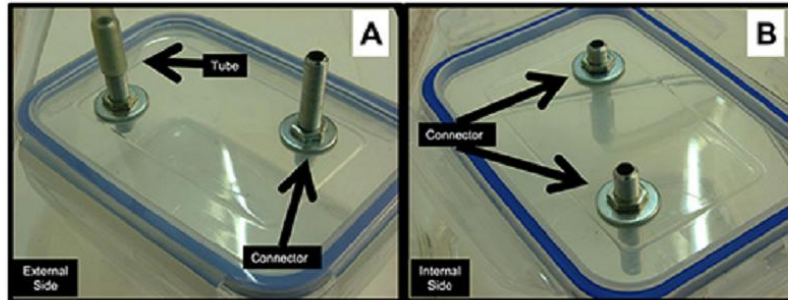


Figure 5. Details of the internal and external side of the container lid. **A)** External side of the container lid, indicating the tube and its connector attached to the previously made hole. **B)** Internal side of the container lid, indicating the tube connector attached to the previously made hole.

Discussion

AS has been widely used in *C. elegans* to model IR injury. Some key points should be highlighted for this protocol: *C. elegans* are resistant to a wide array of injuries, justifying the need for 3 concomitant insults (heat, starvation and anoxia) to achieve death using this system. Anoxia alone does not kill the worms in this window of time¹⁴. Furthermore, temperature increase is an additional stress, so it is important to monitor closely. Strictly speaking, starvation does not contribute significantly to the degree of mortality observed⁷, *per se*, but it appears to reduce variability among experimental replicates. Given that there can be significant variability from day-to-day, it is extremely important to compare samples run directly in parallel, and to repeat experiments over multiple days. In general, outcomes are measured for three separate plates of 50-100 worms/ experimental condition and these are then averaged and considered as a single experimental replicate. Generally, between seven and nine replicates appear to be sufficient to achieve or rule out statistical significance.

The developmental stage of the worms used in the experiment also needs to be carefully monitored as the susceptibility of different stages to AS damage varies significantly^{15,16}. The use of young adults is standard, and larval stage (L3 and L4) worms appear to be more resistant to the damaging effects of AS (unpublished data).

This protocol presents two ways to perform the experiments, one using a lab-made apparatus (using Tupperware-type containers and gas input¹¹) and other using a commercial hypoxic chamber^{4,6}. Anoxia can be achieved by other means that consume the oxygen, as described elsewhere^{13,17}. The use of alternate techniques to create a hypoxic environment may change the AS incubation time necessary to create the desired amount of death. Targeting ~20% survival is an ideal starting point for studying protective interventions, while 80% is similarly ideal for interventions that exacerbate the detrimental effects of AS. Another important caveat is the time at which the observer scores dead/alive worms. If the time for analysis is extended beyond 24 hr, the data may be misleading since dead worms become increasingly difficult to identify. This may be due to worm carcasses becoming relatively transparent over time, but also to the fact that fertilized embryos can develop into progeny post-mortem inside of the carcasses and disrupt them as they emerge.

The analysis of neuronal morphology can be modified to look at protein expression patterns¹⁸, nuclear fragmentation⁴ and other parameters¹⁹ by substituting a worm strain that expresses the appropriate genetically encoded marker. One final caveat is that the visualization of the neuronal processes should be done less than 30 min after placing the worms on the slide. Animals kept under anesthesia on slides for longer periods can exhibit AS-independent damage. Adjust the amount of animals per slide according to the time needed to track and analyze them.

Disclosures

The authors have nothing to disclose.

Acknowledgements

Figures 1 and 2 were previously published in *Free Radical Biology & Medicine* (Queliconi *et al.*⁵) and have copyright held by Elsevier. This work was supported by the Fundação de Amparo à Pesquisa do Estado de São Paulo (FAPESP), the Instituto Nacional de Ciência e Tecnologia de Processos Redox em Biomedicina, the Núcleo de Apoio à Pesquisa de Processos Redox em Biomedicina, USPHS NS064945 (K.N.), and USPHS GM087483 (K.N.). B.B.Q. is a doctoral student supported by a FAPESP fellowship.

References

- Brenner, S. The genetics of *Caenorhabditis elegans*. *Genetics*. **77** (1), 71-94 (1974).
- Maine, E. M. Studying gene function in *Caenorhabditis elegans* using RNA-mediated interference. *Briefings Funct. Genom. Proteom.* **7** (3), 184-194. doi:10.1093/bfpgp/eln019 (2008).
- Vanden Hoek, T. L., Shao, Z., Li, C., Zak, R., Schumacker, P. T. & Becker, L. B. Reperfusion injury on cardiac myocytes after simulated ischemia. *Am. J. Physiol.* **270** (4), H1334-1341 (1996).

4. Scott, B. a, Avidan, M. S. & Crowder, C. M. Regulation of hypoxic death in *C. elegans* by the insulin/IGF receptor homolog DAF-2. *Science*. **296** (5577), 2388-2391, doi:10.1126/science.1072302 (2002).
5. Queliconi, B. B., Marazzi, T. B. M., *et al.* Bicarbonate modulates oxidative and functional damage in ischemia-reperfusion. *Free Rad. Biol. Med.* **55**, 46-53, doi:10.1016/j.freeradbiomed.2012.11.007 (2013).
6. Wojtovich, A. P., DiStefano, P., Sherman, T., Brookes, P. S. & Nehrke, K. Mitochondrial ATP-sensitive potassium channel activity and hypoxic preconditioning are independent of an inwardly rectifying potassium channel subunit in *Caenorhabditis elegans*. *FEBS Lett.* **586** (4), 428-434, doi:10.1016/j.febslet.2012.01.021 (2012).
7. Dasgupta, N., Patel, A. M., Scott B. A. & Crowder C. M. Hypoxic Preconditioning Requires the Apoptosis Protein CED-4 in *C. elegans*. *Curr. Biol.* **17** (22), 1954-1959 doi: 10.1016/j.cub.2007.10.017 (2007).
8. Jia, B. & Crowder, C. M. Volatile anesthetic preconditioning present in the invertebrate *Caenorhabditis elegans*. *Anesthesiology*. **108** (3), 426-433, doi:10.1097/ALN.0b013e318164d013 (2008).
9. Wojtovich, A. P., Sherman, T. A., Nadtochiy, S. M., Urciuoli, W. R., Brookes, P. S. & Nehrke, K. SLO-2 is cytoprotective and contributes to mitochondrial potassium transport. *PLoS One*. **6** (12), e28287, doi:10.1371/journal.pone.0028287 (2011).
10. Porta-de-la-Riva, M., Fontrudona, L., Villanueva, A. & Cerón, J. Basic *Caenorhabditis elegans* methods: synchronization and observation. *J. Vis. Exp.* (64), e4019, doi:10.3791/4019 (2012).
11. Fawcett, E. M., Horsman, J. W. & Miller, D. L. Creating defined gaseous environments to study the effects of hypoxia on *C. elegans*. *J. Vis. Exp.* (65), e4088, doi:10.3791/4088 (2012).
12. Butler, J.A., Mishur, R.J., Bokov, A.F., Hakala, K.W., Weintraub, S.T., Rea, S.L. Profiling the anaerobic response of *C. elegans* using GC-MS. *PLoS One*. **7** (9), e46140. doi: 10.1371/journal.pone.0046140 (2012).
13. Padilla, P. A., Nystul, T. G., Zager, R. A., Johnson, A. C. & Roth, M. B. Dephosphorylation of cell cycle-regulated proteins correlates with anoxia-induced suspended animation in *Caenorhabditis elegans*. *Mol. Biol. Cell.* **13** (5), 1473-1483, doi: 10.1091/mbc.01-12-0594 (2002).
14. Jiang, H., Guo, R. & Powell-Coffman, J. The *Caenorhabditis elegans* hif-1 gene encodes a bHLH-PAS protein that is required for adaptation to hypoxia. *Proc. Natl. Acad. Sci. U.S.A.* **98** (14), 7916-7921, doi:10.1073/pnas.141234698 (2001).
15. Twumasi-Boateng, K., Wang, T. W., *et al.* An age-dependent reversal in the protective capacities of JNK signaling shortens *Caenorhabditis elegans* lifespan. *Aging Cell.* **11** (4), 659-667, doi:10.1111/j.1474-9726.2012.00829.x (2012).
16. Wang, Y., Chen, J., Wei, G., He, H., Zhu, X., Xiao, T., Yuan, J., Dong, B., He, S. Skogerbø G, Chen R. The *Caenorhabditis elegans* intermediate-size transcriptome shows high degree of stage-specific expression. *Nucleic Acids Res.* **39** (12), 5203-5214, doi: 10.1093/nar/gkr102 (2011).
17. Perry, C. N., Huang, C., Liu, W., Magee, N., Carreira, R. S. & Gottlieb, R. Xenotransplantation of mitochondrial electron transfer enzyme, Ndi1, in myocardial reperfusion injury. *PLoS One*. **6** (2), e16288, doi:10.1371/journal.pone.0016288 (2011).
18. Chai, Y., Li, W., Feng, G., Yang, Y., Wang, X. & Ou, G. Live Imaging of Cellular Dynamics During *Caenorhabditis elegans* Postembryonic Development. *Nature Protoc.* **7** (12), 2090-2102, doi:10.1038/nprot.2012.128 (2012).
19. Nehrke, K. A reduction in intestinal cell pH_i due to loss of the *Caenorhabditis elegans* Na⁺/H⁺ exchanger NHX-2 increases life span. *J. Biol. Chem.* **278** (45), 44657-44666, doi:10.1074/jbc.M307351200 (2003).

Ap.8 Aldehyde dehydrogenase 2 activation in heart failure restores mitochondrial function and improves ventricular function and remodeling



Cardiovascular Research (2014) 103, 498–508
doi:10.1093/cvr/cvu125

Aldehyde dehydrogenase 2 activation in heart failure restores mitochondrial function and improves ventricular function and remodelling

Katia M.S. Gomes¹, Juliane C. Campos¹, Luiz R.G. Bechara¹, Bruno Queliconi²,
Vanessa M. Lima¹, Marie-Helene Disatnik³, Paulo Magno⁴, Che-Hong Chen³,
Patricia C. Brum⁵, Alicia J. Kowaltowski², Daria Mochly-Rosen³, and Julio C.B. Ferreira^{1,3*}

¹Department of Anatomy, Institute of Biomedical Sciences, Paulo, Brazil; ²Departamento de Bioquímica, Instituto de Química, Paulo, Brazil; ³Department of Chemical and Systems Biology, Stanford University School of Medicine, Stanford, CA, USA; ⁴Heart Institute, Paulo, Brazil; and ⁵School of Physical Education and Sports, University of Sao Paulo, Paulo, Brazil

Received 9 September 2013; revised 14 March 2014; accepted 15 April 2014; online publish-ahead-of-print 9 May 2014

Time for primary review: 27 days

Aims

We previously demonstrated that pharmacological activation of mitochondrial aldehyde dehydrogenase 2 (ALDH2) protects the heart against acute ischaemia/reperfusion injury. Here, we determined the benefits of chronic activation of ALDH2 on the progression of heart failure (HF) using a post-myocardial infarction model.

Methods and results

We showed that a 6-week treatment of myocardial infarction-induced HF rats with a selective ALDH2 activator (Alda-1), starting 4 weeks after myocardial infarction at a time when ventricular remodelling and cardiac dysfunction were present, improved cardiomyocyte shortening, cardiac function, left ventricular compliance and diastolic function under basal conditions, and after isoproterenol stimulation. Importantly, sustained Alda-1 treatment showed no toxicity and promoted a cardiac anti-remodelling effect by suppressing myocardial hypertrophy and fibrosis. Moreover, accumulation of 4-hydroxynonenal (4-HNE)-protein adducts and protein carbonyls seen in HF was not observed in Alda-1-treated rats, suggesting that increasing the activity of ALDH2 contributes to the reduction of aldehydic load in failing hearts. ALDH2 activation was associated with improved mitochondrial function, including elevated mitochondrial respiratory control ratios and reduced H₂O₂ release. Importantly, selective ALDH2 activation decreased mitochondrial Ca²⁺-induced permeability transition and cytochrome c release in failing hearts. Further supporting a mitochondrial mechanism for ALDH2, Alda-1 treatment preserved mitochondrial function upon *in vitro* aldehydic load.

Conclusions

Selective activation of mitochondrial ALDH2 is sufficient to improve the HF outcome by reducing the toxic effects of aldehydic overload on mitochondrial bioenergetics and reactive oxygen species generation, suggesting that ALDH2 activators, such as Alda-1, have a potential therapeutic value for treating HF patients.

Keywords

Oxidant stress • Heart disease • Mitochondria • Pharmacological therapy • Bioenergetics

1. Introduction

Despite advances in clinical and pharmacological interventions, acute myocardial infarction with subsequent left ventricular dysfunction and heart failure (HF) continues to be a major cause of morbidity and mortality worldwide.^{1,2} Therefore, the identification of novel therapeutic targets that improve cardiac function in patients with myocardial infarction-induced HF remains a major priority. We recently found that mitochondrial aldehyde dehydrogenase 2 (ALDH2) plays a key

role in mediating cardioprotection against acute ischaemic injury.^{3,4} Acute ALDH2 activation using Alda-1, a small molecule allosteric activator of this enzyme,⁵ is sufficient to protect heart against ischaemia/reperfusion injury.⁶

Considering the pivotal role of ALDH2 in detoxifying mitochondrial reactive aldehydes that accumulate upon oxidative stress during chronic cardiac degenerative diseases,⁷ including the lipid peroxidation by-product (4-hydroxynonenal),⁸ we set out to determine the role of ALDH2 in HF. We tested here the possibility that selective

* Corresponding author: Departamento de Anatomia, Instituto de Ciências Biomédicas da Universidade de São Paulo, Av. Professor Lineu Prestes, 2415, CEP 05508-000, São Paulo, SP, Brazil. Tel: +55 11 3091 3136; fax: +55 11 3813 5921, Email: jcesarbf@usp.br

Published on behalf of the European Society of Cardiology. All rights reserved. © The Author 2014. For permissions please email: journals.permissions@oup.com.

pharmacological activation of mitochondrial ALDH2 in failed hearts counteracts the aldehydic load, preserves mitochondrial function, and inhibits the progression of cardiac dysfunction in myocardial infarction-induced HF in rats.

2. Methods

2.1 Animals and study design

This study was conducted in accordance with the ethical principles in animal research adopted by the Brazilian College of Animal Experimentation (www.cobea.org.br). The animal protocols were reviewed and approved by the Ethical Committee of Biomedical Sciences Institute of University of São Paulo (20012/36). A cohort of male Wistar rats (250–300 g) was selected for the study and maintained in a 12:12 h light–dark cycle and temperature-controlled environment (22°C) with free access to standard laboratory chow (Nuvital Nutrientes, Curitiba, PR, Brazil) and tap water.

2.2 Myocardial infarction-induced HF model

Myocardial infarction was induced by ligation of the left anterior descending coronary artery (LAD), as previously described.⁹ We have chosen this model since myocardial infarction is the underlying aetiology of HF in nearly 70% of patients.⁹ Male Wistar rats were anaesthetized with 3% isoflurane, endotracheally intubated, and mechanically ventilated with room air (respiratory rate of 60–70 breaths/min and tidal volume of 2.5 mL). Left thoracotomy between the fourth and fifth ribs was performed and the LAD was ligated. After the surgery, animals were monitored daily. HF was observed 4 weeks after coronary artery ligation and was defined when animal presented pathological cardiac remodelling accompanied by left ventricle dysfunction and cardiac dilation, according to the Guidelines of American Heart Association.^{2,10} A left thoracotomy with equal procedure duration to that of HF group, but without LAD ligation, was undertaken in the sham group (control).

2.3 In vivo treatment with Alda-1 (ALDH2 activator)

Four weeks after myocardial infarction surgery, physiological parameters were determined and animals were randomly assigned into three experimental groups: sham group (control, $n = 22$), placebo-treated myocardial infarction-induced HF group ($n = 14$), and Alda-1-treated HF group (HF + Alda-1, $n = 16$) (Figure 1A). Continuous infusion of Alda-1 (10 mg/kg per day) was achieved using Alzet osmotic pumps (2ML4 and 2ML2) and began 4 weeks after myocardial infarction and ended 10 weeks later (Figure 1A). A group of rats implanted with pumps containing the vehicle alone (50% polyethylene glycol and 50% dimethyl sulfoxide by volume) served as the control. Another group of healthy animals was treated with Alda-1 in order to check drug toxicity. Subcutaneous pump implantation was performed in 3% vaporized isoflurane-anaesthetized rats. This concentration provided deep anaesthesia, allowing mini-pump implantation without any clinical sign of pain, such as withdrawal reflex. The pumps were inserted in the back of animals after making a sub-scapular incision.

At the end of the protocol, physiological parameters were re-analysed. Forty-eight hours later, all rats were anaesthetized with sodium pentobarbital (100 mg/kg ip) and euthanized by decapitation.

2.4 Cardiovascular measurements

Systolic blood pressure was determined non-invasively, using a computerized tail-cuff system (BP-2000, Visitech System, Apex, NC, USA). Evaluation of non-invasive cardiac function was performed by echocardiography using a Vevo 770 rodent ultrasound system (VisualSonics, Canada), equipped with a high-resolution mechanical transducer (17-MHz scanhead RMV716). Echocardiography measurements were performed in anaesthetized (isoflurane 3%) sham and HF rats, 4 and 10 weeks after surgery. Myocardial images

were recorded using 2D-guided M-mode from the parasternal long axis. Mitral inflow pattern was recorded from the apical four-chamber view using pulsed-wave Doppler. Left ventricle systolic function was estimated by fractional shortening (FS) as follows: $FS(\%) = [(LVEDD - LVESD) / LVEDD] \times 100$, where LVEDD is the left ventricular end-diastolic diameter, and LVESD is the left ventricular end-systolic diameter. The observer was blinded to the treatment groups.

2.5 Isolated perfused rat heart model

Ten weeks after MI surgery, control, vehicle-treated HF, and Alda1-treated HF rats were injected with heparin (2000 U/kg ip), anaesthetized with sodium pentobarbital (100 mg/kg ip), and euthanized by decapitation. The hearts were rapidly excised and then perfused with an oxygenated Krebs–Henseleit solution containing (in mM) NaCl 120, KCl 5.8, NaHCO₃ 25, NaH₂PO₄ 1.2, MgSO₄ 1.2, CaCl₂ 1.0, and dextrose 10, pH 7.4, at 37°C in a Langendorff coronary perfusion system at a constant flow rate of 10 mL/min. The left atrium was then removed and a thin latex balloon was inserted into the left ventricle (LV) and connected to a pressure transducer (Utah Medical Deltran) for measurement of the isovolumic LV pressure. The balloon within the LV was initially inflated with water to a volume of 100 μ L, and LV developed pressure (LVDP) was measured. The balloon was then deflated in 20 μ L decrements to determine the relationship between LVDP and balloon volume. LVDP was determined under basal conditions and during the peak response of isoproterenol (10 μ M).

2.6 Isolation of adult rat cardiomyocytes

Ten weeks after MI surgery, control, vehicle-treated HF, and Alda1-treated HF rats were injected with heparin (2000 U/kg IP), anaesthetized with sodium pentobarbital (100 mg/kg IP), and euthanized by decapitation. The hearts were rapidly excised and then perfused with low-Ca²⁺ solution 1 (100 mM NaCl, 10 mM KCl, 1.2 mM KH₂PO₄, 5 mM MgSO₄, 20 mM glucose, 50 mM taurine, 10 mM HEPES, and 100 μ M CaCl₂), then with digestion solution containing low-Ca²⁺ solution 1, collagenase (0.5 mg mL⁻¹, Worthington Type 1A), and protease type XIV (0.04 mg mL⁻¹; Sigma). Following perfusion, the ventricles were cut into fragments (2–5 mm³) in digestion solution. The cell suspension was then filtered through a nylon sieve and centrifuged for 1 min (at 300–400 g) at room temperature. Cell pellets were resuspended in solution 1 containing 125 mg BSA and 500 μ M CaCl₂.

2.7 Cardiomyocyte shortening and relengthening

Cell contraction properties of cardiomyocytes were evaluated with a video-based sarcomere-spacing acquisition system (SarLen, IonOptix, Milton, MA, USA), as previously described.¹¹ Changes in sarcomere length were recorded and analysed using the IonWizard software (IonOptix, Milton, MA, USA). Sarcomeric shortening was determined under basal conditions and during the peak response of isoproterenol (10 μ M).

2.8 Cardiac structural analysis

Forty-eight hours after the end of the protocol, all rats were killed and their tissues were harvested. Cardiac chambers were then fixed by immersion in 4% buffered formalin and embedded in paraffin for routine histological processing. Sections (4 μ m) were stained with Picrosirius red or Masson's trichrome for the quantification of cardiac collagen content and myocardial infarct area, respectively. Cardiac collagen deposition was measured by scanning at least 15 fields per heart after serial sections at 1 mm intervals from apex to base. The analysis covered the whole LV viable area. For that we used a computer-assisted morphometric system (Leica Quantimet 500, Cambridge, UK), as previously described.¹² The myocardial infarcted area was expressed as a percentage of total surface area of the LV. The observer was blinded to the treatment groups.

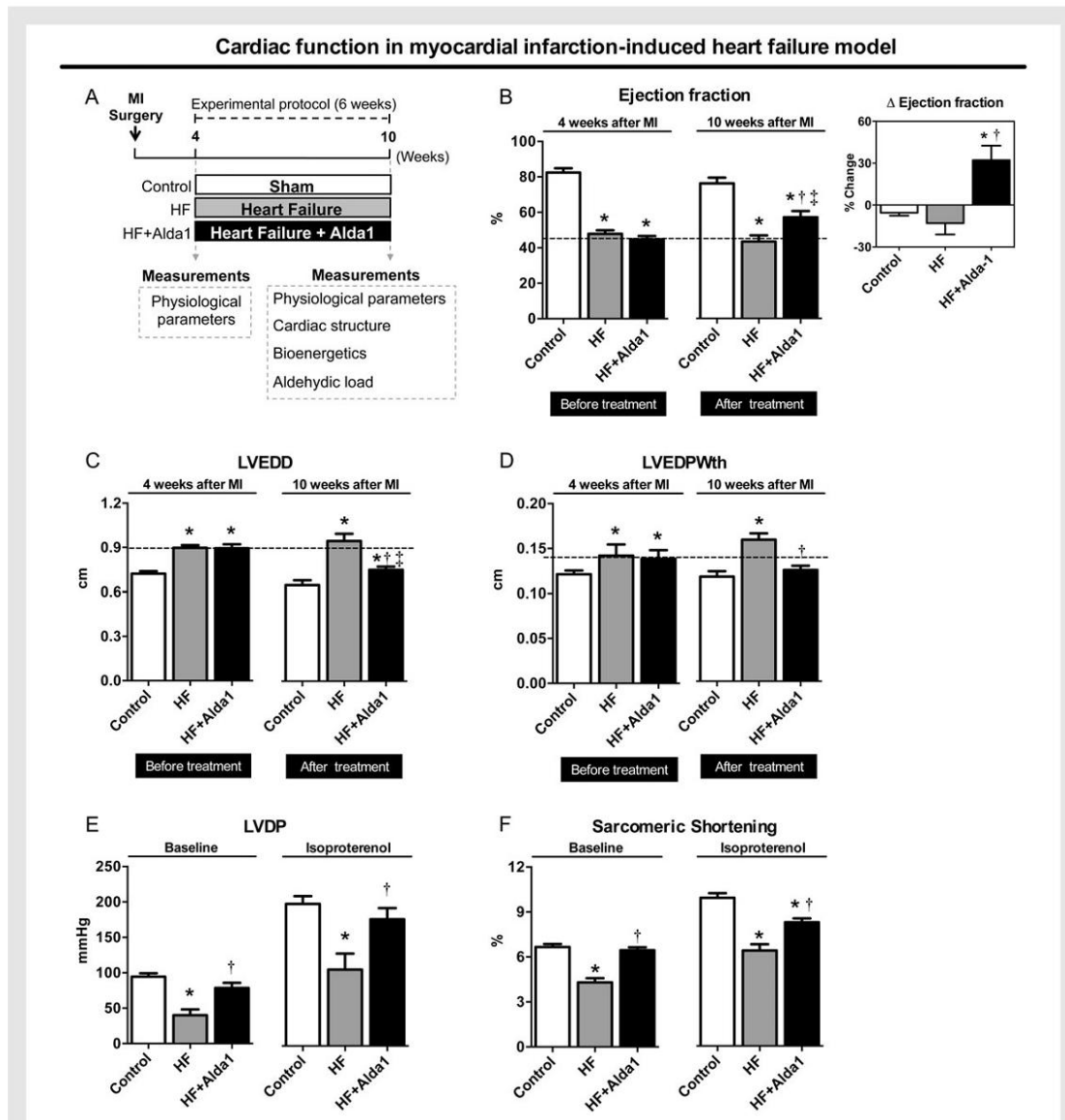


Figure 1 Mitochondrial ALDH2 activation improves cardiac function in a rat model of post-myocardial infarction-induced HF. (A) Schematic panel. HF induction and treatment protocol. Twelve-week-old rats were subjected to myocardial infarction by LAD ligation. Four weeks after myocardial infarction induction, the rats were treated with Alda-1 (selective ALDH2 activator) or with vehicle solution (50% polyethylene glycol and 50% dimethyl sulfoxide by volume). Alda-1 treatment was continuous (for 6 weeks) using subcutaneous Alzet pump delivery at 10 mg/kg/day. (B) Ejection fraction, input: delta ejection fraction; (C) LVEDD and (D) left ventricle end-diastolic posterior wall thickness (LVEDPWth) before and after treatment periods in control (sham, white bars, $n = 12$), vehicle-treated HF (HF, grey bars, $n = 12$), and Alda-1-treated HF (HF + Alda-1, black bars, $n = 14$). (E) LVDP in isolated *ex vivo* perfused heart and (F) sarcomeric shortening in isolated ventricular cardiomyocytes from control (sham, white bars, $n = 6$), vehicle-treated HF (HF, grey bars, $n = 6$), and Alda-1-treated HF (HF + Alda-1, grey bars, $n = 6$). Both LVDP and sarcomeric shortening were determined under basal conditions and during the peak response of isoproterenol (10 μ M) at 10 weeks after MI surgery. Data are means \pm SEM. * $P < 0.05$ vs. control (sham) rats. † $P < 0.05$ vs. vehicle-treated HF rats. ‡ $P < 0.05$ vs. before the experimental protocol. The observer was blinded to the treatment groups.

2.9 Mitochondrial isolation

Cardiac mitochondria were isolated as described elsewhere.¹³ Briefly, heart samples were minced and homogenized in isolation buffer (300 mM sucrose, 10 mM HEPES, 2 mM EGTA, pH 7.2, 4°C) containing 0.1 mg mL⁻¹ of Type I protease (bovine pancreas) to release mitochondria from within muscle fibres, and later washed in the same buffer in the presence of 1 mg mL⁻¹ of bovine serum albumin. The suspension was homogenized in a 40 mL tissue grinder and centrifuged at 950 g for 5 min. The resulting supernatant was centrifuged at 9500 g for 10 min. The mitochondrial pellet was washed, resuspended in isolation buffer, and submitted to a new centrifugation (9500 g for 10 min). The mitochondrial pellet was washed and the final pellet was resuspended in a minimal volume of isolation buffer.

2.10 Mitochondrial H₂O₂ release and O₂ consumption

Mitochondrial H₂O₂ release was determined by measuring the oxidation of Amplex Red in the presence of horseradish peroxidase using a spectrophotometer with 563 nm of excitation and 587 nm of emission.¹⁰ Mitochondrial O₂ consumption was monitored using a computer-interfaced Clark-type electrode (Hansatech Instruments) operating with continuous stirring at 37°C.¹⁰ Succinate, malate, and glutamate (2 mmol/L of each) were used as substrates, and ADP (1 mmol/L) was added to induce State 3 respiratory rate. A subsequent addition of oligomycin (1 µg mL⁻¹) was used to determine State 4 rate. Respiratory control ratio (RCR) was calculated by dividing State 3 by State 4 oxygen consumption rates.

2.11 Maximal mitochondrial calcium uptake

Extramitochondrial Ca²⁺ concentrations were measured in 0.125 mg protein mL⁻¹ of mitochondrial suspensions using the fluorescent probe Calcium Green (100 nM), as described elsewhere.¹⁴ The reactions were carried out under the same conditions as oxygen consumption measurements with continuous stirring at 37°C. For each experiment, consecutive additions of 50 µM CaCl₂ were made until the mitochondria failed to take up extramitochondrial Ca²⁺. We plotted a calibration curve that correlates fluorescence and Ca²⁺ concentration. Succinate, malate, and glutamate (2 mM of each) were used as substrates, and 100 µM EGTA was used to establish the baseline. Excitation/emission wavelength was 506/532 nm, respectively.

2.12 Enzymatic activity of ALDH2

Enzymatic activity of ALDH2 was determined by measuring the conversion of NAD⁺ to NADH, as described elsewhere.⁶ The assays were carried out at 25°C in 50 mM sodium pyrophosphate buffer (pH 9.5) in the presence of 10 mM acetaldehyde. Measurement of mitochondrial ALDH2 activity in the rat myocardium was determined by directly adding 400 mg of the mitochondrial fraction of the myocardium to the reaction mix and reading absorbance at 340 nm for 10 min.

2.13 Immunoblotting

Protein levels were evaluated by immunoblotting in cytosolic and mitochondrial extracts from the ventricular remote area.¹⁵ Briefly, samples were subjected to SDS-PAGE in polyacrylamide gels (6–15%) depending on protein molecular weight. After electrophoresis, proteins were electrotransferred onto nitrocellulose membranes (BioRad Biosciences, Piscataway, NJ, USA). Equal gel loading and transfer efficiency were monitored using 0.5% Ponceau S staining of blot membrane. A blotted membrane was then blocked [5% non-fat dry milk, 10 mM Tris-HCl (pH 7.6), 150 mM NaCl, and 0.1% Tween 20] for 2 h at room temperature and then incubated overnight at 4°C with specific antibodies. Binding of the primary antibody was detected with the use of peroxidase-conjugated secondary antibodies (rabbit or mouse, depending on the protein, for 2 h at room temperature) and developed using enhanced chemiluminescence (Amersham Biosciences, NJ, USA) detected by autoradiography. Quantification analysis of blots was

performed with the use of Scion Image software (Scion based on NIH image). Samples were normalized to relative changes in housekeeping proteins and expressed as the percent of control.

2.14 Protein carbonyl levels

Protein carbonyl levels were determined as previously described.¹⁶ The carbonyl groups in the protein side chains were derivatized to 2,4-dinitrophenylhydrazone (DNPhydrazone) by reaction with 2,4-dinitrophenylhydrazine (DNPH). The DNP-derivatized protein samples were separated by polyacrylamide gel electrophoresis followed by immunoblotting.

2.15 Cell culture

Cardiac fibroblasts were isolated from 1-day-old Sprague-Dawley rat litters, as described elsewhere.¹⁶ All rat litters were euthanized by decapitation.

2.16 Statistical analysis

Data are presented as means ± standard error of the mean (SEM). Data normality was assessed through Shapiro-Wilk's test. One-way analysis of variance (ANOVA) was used to analyse data presented in Figures 1B (input), 2C–J, and 3–5. Two-way ANOVA for repeated measures was used to analyse data depicted in Figure 1B–D and Table 1. Two-way ANOVA was also used to analyse data depicted in Figure 1E and F. Whenever significant *F*-values were obtained, Duncan's adjustment was used for multiple comparison purposes. Unpaired Student's *t*-test was used to analyse data presented in Figure 2B. GraphPad Prism Statistics was used for the analysis, and statistical significance was considered achieved when the value of *P* was <0.05.

3. Results

3.1 ALDH2 activation improves cardiac function and reverses pathological ventricular remodelling in HF animals

ALDH2 plays a key role in protecting the heart against oxidative stress during acute ischaemic injuries, mainly through detoxification of reactive aldehydes, such as 4-hydroxynonenal (4-HNE).^{17,18} We therefore determined the effects of selective ALDH2 activation on the progression of myocardial infarction-induced HF in rats. Ten weeks after myocardial infarction surgery (Figure 1A), the rats exhibited signs of HF as demonstrated by left ventricular dysfunction and pathological cardiac remodelling (Figures 1 and 2, Table 1, as well as see Supplementary material online, Table S1). These rats displayed decreased cardiac ejection fraction, FS and LVDP, as well as increased diastolic dilation compared with control animals under basal conditions (Figure 1B–E and Table 1). To determine whether the ventricular dysfunction observed *in vivo* was cardiomyocyte-specific, shortening parameters were characterized in isolated adult cardiomyocytes. Intrasarcomeric shortening was significantly decreased in the HF group (Figure 1F). These differences seen at baseline in both isolated *ex vivo* perfused heart and isolated cardiomyocytes were exacerbated upon isoproterenol challenge (Figure 1E and F). Moreover, these rats had an increased heart weight/body weight (HW/BW) ratio (see Supplementary material online, Table S1), increased both cardiomyocyte width and length (Figure 2A and G–I), and cardiac fibrosis (Figure 2A–F) compared with control rats. Cardiomyocyte width and length were measured in isolated cells using the Image J software (NIH, USA). Cardiac fibrosis was measured in the non-infarcted (remote) area. No changes in heart rate and blood pressure were observed in rats with HF (see Supplementary material online, Table S1).

Table 1 Echocardiographic measurements

Parameter	Four weeks after MI surgery (before drug treatment begins)			Ten weeks after MI surgery (6 weeks of treatment)		
	Control	HF	HF + Alda1	Control	HF	HF + Alda1
FS (%)	43.1 ± 1.2	24.6 ± 1.5*	20.3 ± 1.1*	42.8 ± 1.4	18.5 ± 1.1*	24.8 ± 1.5* ^{†‡}
LVEDD (mm)	7.23 ± 0.13	8.97 ± 0.14*	8.95 ± 0.25*	6.46 ± 0.26	9.45 ± 0.32*	8.01 ± 0.23* ^{†‡}
LVESD (mm)	4.09 ± 0.14	7.06 ± 0.11*	7.19 ± 0.24*	4.18 ± 0.29	7.65 ± 0.34*	5.99 ± 0.32* ^{†‡}
PWth (mm)	1.21 ± 0.03	1.41 ± 0.06	1.41 ± 0.05	1.17 ± 0.05	1.59 ± 0.05*	1.25 ± 0.04 [†]
IVSth (mm)	0.95 ± 0.03	0.87 ± 0.03	0.96 ± 0.03	0.89 ± 0.05	0.92 ± 0.04	0.96 ± 0.05
ET (ms)	78.5 ± 0.6	68.0 ± 2.3	64.9 ± 3.9	81.7 ± 2.4	66.3 ± 2.6*	79.2 ± 4.4
E (cm/s)	70.7 ± 1.0	80.8 ± 1.7*	79.9 ± 2.6*	70.5 ± 1.8	93.0 ± 2.7*	74.4 ± 3.7 [†]
A (cm/s)	43.5 ± 1.0	43.8 ± 1.8	41.5 ± 2.1	41.9 ± 1.5	31.0 ± 2.1*	39.1 ± 1.5
E/A	1.6 ± 0.1	1.9 ± 0.1	2.0 ± 0.1	1.7 ± 0.1	3.1 ± 0.3 [‡]	1.9 ± 0.1 [†]
IVRT (ms)	24.2 ± 1.7	25.9 ± 1.6	28.2 ± 1.4	26.0 ± 1.8	32.3 ± 3.0*	27.2 ± 2.2
MPI	0.40 ± 0.02	0.54 ± 0.03*	0.58 ± 0.06*	0.41 ± 0.03	0.63 ± 0.03*	0.43 ± 0.04 ^{†‡}
HR (bpm)	295 ± 12	272 ± 6	285 ± 7	296 ± 5	266 ± 14	274 ± 9

Data are means ± SEM.

The observer was blinded to the treatment groups.

Echocardiographic measurements. FS, fractional shortening; LVEDD, left ventricular end-diastolic diameter; LVESD, left ventricular end-systolic diameter; PWth, posterior wall thickness; IVSth, interventricular septum thickness; ET, ejection time; E, mitral inflow E velocity; A, mitral inflow A velocity; IVRT, isovolumic relaxation time; MPI, myocardial performance index; HR, heart rate in control (sham, n = 8–12), vehicle-treated HF (HF, n = 8–12), and Alda-1-treated HF (HF + Alda-1, n = 8–12) under basal conditions.

*P < 0.05 vs. control.

[†]P < 0.05 vs. HF.

[‡]P < 0.05 vs. pre-treatment.

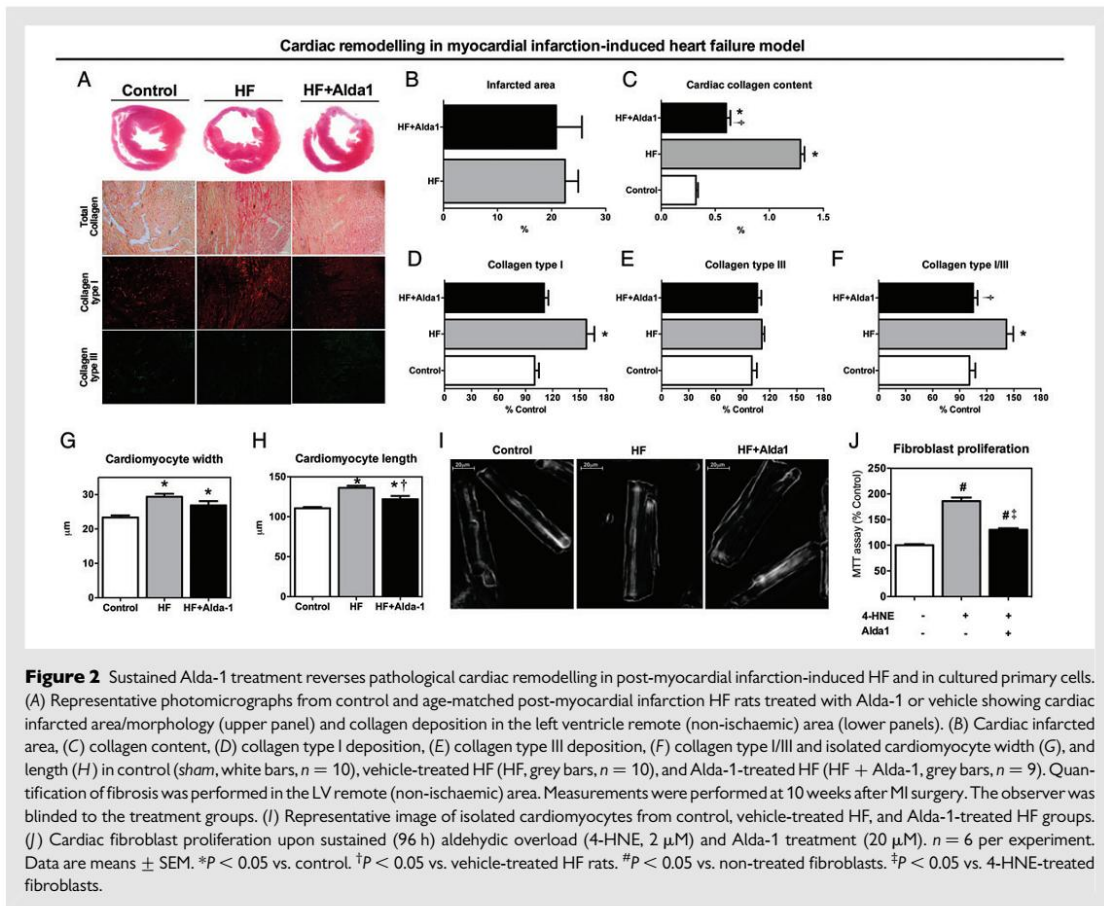
Using subcutaneously implanted Alzet pumps, we delivered Alda-1 in a sustained fashion at 10 mg/kg/day.⁶ Delivery of Alda-1 from Weeks 4 to 10 after inducing myocardial infarction (Figure 1A) not only prevented the development of cardiac dysfunction, but also increased left ventricular ejection fraction by 34% (Figure 1B, input). Indeed, Alda-1 treatment improved sarcomeric shortening, cardiac FS, and LVDP under basal conditions (Figure 1C–F and Table 1). Moreover, isolated hearts and cardiomyocytes from Alda-1-treated HF rats became more sensitive to isoproterenol-induced increased inotropism (Figure 1E and F). Finally, sustained Alda-1 treatment promoted a cardiac anti-remodelling effect by reducing LVEDD (Figure 1C, Table 1, and see Supplementary material online, Figure S1), posterior wall thickness (Figure 1D and Table 1), HW/BW (see Supplementary material online, Table S1), cardiac fibrosis (Figure 2A–F), and cardiomyocyte length (Figure 2H and I) relative to untreated HF rats. Of interest, prolonged ALDH2 activation by Alda-1 affected cardiac fibrosis by decreasing the extent of collagen type I deposition and collagen type I/III ratio (Figure 2A and D–F), further contributing, at least in part, to a better myocardial compliance (Table 1). In order to evaluate the direct contribution of aldehydic load to fibrosis, we treated cardiac fibroblast with 4-HNE (2 μM) over 96 h and observed that sustained aldehydic load increases fibroblast proliferation. Interestingly, co-administration of Alda-1 reduced fibroblast proliferation upon aldehydic load stress (Figure 2J). Finally, Alda-1 treatment did not significantly affect systolic blood pressure, heart rate, and myocardial infarct size in HF animals (see Supplementary material online, Table S1, and Figure 2A and B).

Since this is the first study evaluating the long-term effect of Alda-1 treatment, we performed some toxicity measurements in healthy (naïve) rats treated with Alda-1 for 6 weeks (10 mg/kg per day). No changes in haemodynamic parameters, BW, organ weight, cardiac

function, circulating aspartate aminotransferase and alanine aminotransferase activities, as well as serum uric acid and creatinine levels were observed in Alda-1-treated rats compared with untreated animals (see Supplementary material online, Tables S2 and S3), suggesting that sustained Alda-1 treatment is safe.

3.2 Increased detoxification activity of ALDH2 contributes to preventing 4-HNE accumulation in failing hearts

Excessive 4-HNE-protein adducts contribute towards cardiac ischaemic injuries.¹⁹ We have suggested that ALDH2 activation-mediated cardioprotection upon ischaemia/reperfusion injury occurs through preservation of protein function by reduction of the aldehydic load in the heart.³ ALDH2 metabolizes reactive aldehydes that accumulate under redox imbalance, and prevents the production of aldehydic adducts that inactivate key metabolic enzymes.²⁰ HF rats already presented increased aldehydic overload at 4 weeks after myocardial infarction surgery. We therefore measured 4-HNE-protein adducts and total protein carbonyls in the heart (non-infarcted area) 10 weeks after myocardial infarction surgery. Placebo-treated rats with HF displayed a significant increase of cardiac 4-HNE-protein adducts (Figure 3A and E) and protein carbonyls (Figure 3B and E) compared with relative controls. Sustained Alda-1 treatment increased cardiac ALDH2 activity by 2.7-fold (Figure 3C) and significantly reduced 4-HNE-protein adducts and protein carbonyls compared with untreated failing hearts (Figure 3A–B and E, 4-HNE-protein adducts: 98 ± 4 vs. 129 ± 11; protein carbonyls: 111 ± 11 vs. 157 ± 18 for the HF + Alda-1 and the HF + vehicle groups, respectively, P < 0.05). No changes in protein levels of mitochondrial ALDH2 (Figure 3D–E) were observed in either HF or Alda-1 treatment.



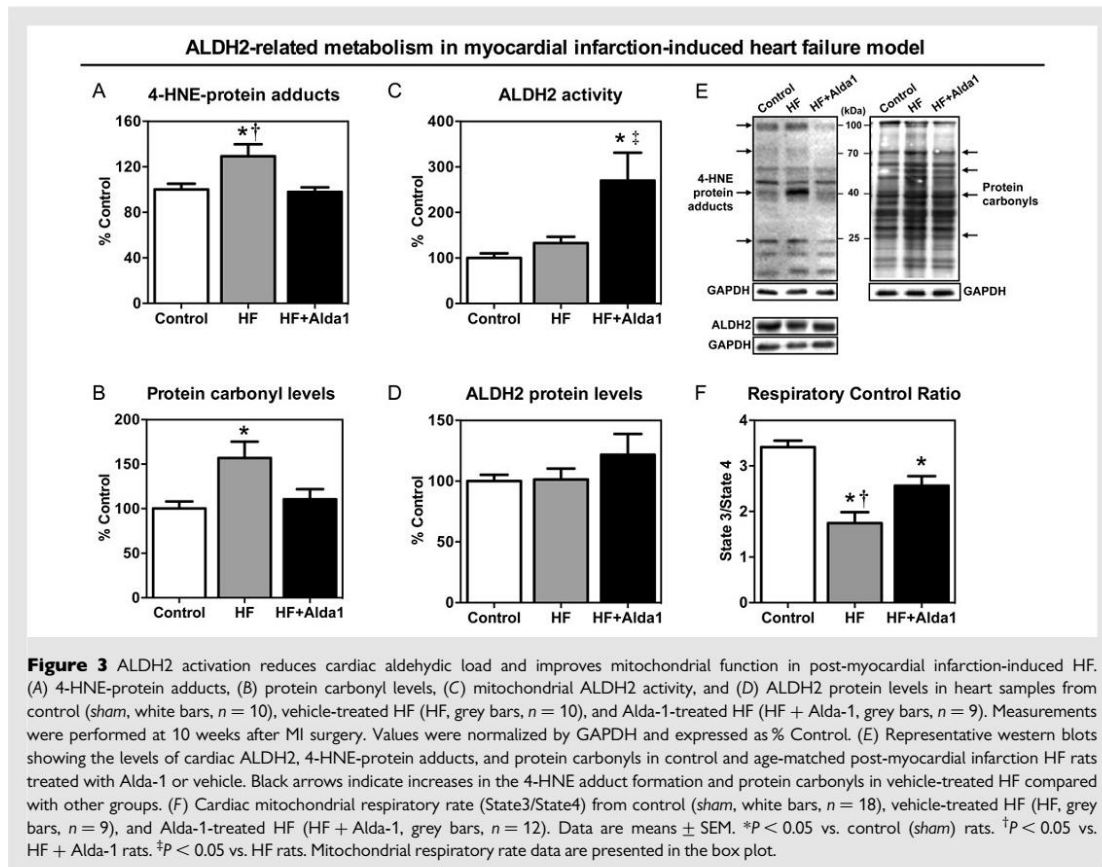
3.3 Alda-1 treatment protects mitochondrial function and prevents increases in reactive oxygen species release

Since accumulation of aldehydic adducts inhibits mitochondrial respiration by reacting with and inactivating metabolic enzymes during acute ischaemic injuries,¹⁹ we set out to determine mitochondrial function in a scenario of chronic aldehydic overload in HF. To assess mitochondrial function, we measured oxygen consumption, absolute (H_2O_2) and relative (H_2O_2/O_2) reactive oxygen species (ROS) release in isolated mitochondria from myocardial infarction-induced HF rats, and age-matched control rats, 10 weeks after myocardial infarction.

Our results indicate that vehicle-treated HF rats displayed a significant decrease in the efficiency of mitochondrial oxidative phosphorylation compared with control (*sham*) rats, as measured by the RCR (State 3/State 4; Figure 3F). This response was mainly due to a reduction of State 3 respiratory rate (the oxygen consumption rate maximized by the addition of ADP) in failing hearts (Figure 4B), while respiration in the absence of oxidative phosphorylation (State 4) was not affected (Figure 4C). Of interest, sustained ALDH2 activation by treating with Alda-1 improved the efficiency of mitochondrial oxidative phosphorylation (Figure 3F,

RCR: 2.6 ± 0.2 vs. 1.6 ± 0.2 for HF + Alda-1 and HF, respectively) by preserving State 3 respiratory rates. Moreover, oxygen consumption enhancement induced by the mitochondrial uncoupler, carbonyl cyanide *m*-chlorophenyl hydrazone, was attenuated in the placebo-treated HF rat, whereas sustained ALDH2 activation normalized it towards control (*sham*) values (data not shown). These results demonstrate that sustained pharmacological activation of mitochondrial ALDH2 with Alda-1 attenuates the prominent disruption of mitochondrial oxygen consumption rates observed in failing hearts.

Mitochondrial ROS release has been associated with reduction of oxygen consumption in HF,²¹ so we hypothesized that Alda-1 treatment-mediated improvements in mitochondrial oxygen consumption could be attributed to the prevention of excessive mitochondrial ROS release in failing hearts. Placebo-treated HF animals presented increased mitochondrial State 2 (basal), State 3, and State 4 H_2O_2 release when compared with control rats (Figure 4D–F). These changes were more pronounced when H_2O_2 release was normalized by oxygen consumption rates for each state (Figure 4G–I), demonstrating the tight interdependence between mitochondrial oxygen consumption and ROS release in HF. Mitochondria isolated from Alda-1-treated rats with HF did not present the increases in H_2O_2 and



H_2O_2/O_2 release observed in vehicle-treated HF rat mitochondria (Figure 4D–I). These data demonstrate that activating ALDH2 in failing hearts using Alda-1 is sufficient to prevent excessive mitochondrial ROS release during HF.

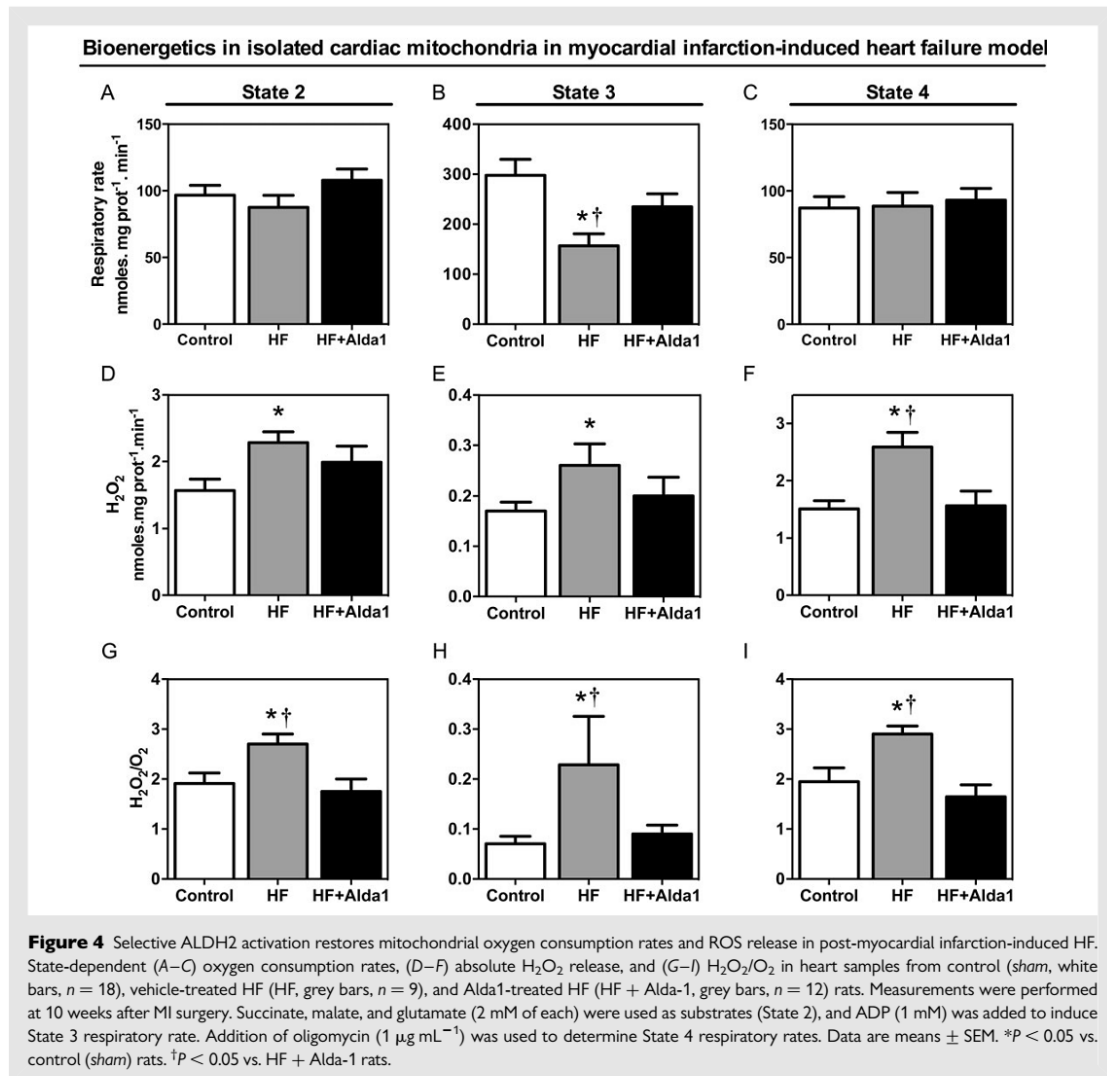
Excessive mitochondrial ROS and aldehydes in the presence of Ca^{2+} lead to non-selective inner mitochondrial membrane permeabilization known as mitochondrial permeability transition, a cause of cell death in the heart.^{22,23} To test the contribution of chronic aldehydic overload towards the occurrence of mitochondrial transition permeability in HF, we measured maximal Ca^{2+} uptake in isolated mitochondria from vehicle- and Alda-1-treated failing hearts. Control rats presented significantly higher ability to accumulate Ca^{2+} ions before undergoing mitochondrial permeability transition relative to vehicle-treated rats with HF (Figure 5A). Of interest, selective activation of mitochondrial ALDH2 corrected HF-induced susceptibility to mitochondrial permeability transition. Moreover, the observed alterations in mitochondrial permeability transition were blocked by cyclosporin A (Figure 5A).

Mitochondrial permeability transition has been implicated in cell death through release of cytochrome c into the cytosol.²⁴ Our results indicate that increased sensitivity to Ca^{2+} -induced mitochondrial permeability transition was associated with an exacerbated release of

mitochondrial cytochrome c (Figure 5B and C). Alda1 treatment significantly reduced cytochrome c release in failing hearts.

3.4 Alda-1 attenuates *in vitro* 4-HNE-mediated mitochondrial dysfunction

Elevated ROS release has generally been implicated in cellular damage during pathological processes. The introduction of carbonyl functional groups into proteins by 4-HNE, a major product of ROS-mediated lipid oxidation, has been reported to induce protein inactivation during ischaemia/reperfusion injury.³ We thus tested whether excessive aldehydic load directly affects mitochondrial function. *In vitro* incubation of cardiac mitochondria with different concentrations of 4-HNE (0.5–10 μ M)²⁵ resulted in a dose-dependent reduction in the efficiency of mitochondrial oxidative phosphorylation (Figure 5D). Of interest, similar to our *in vivo* results, 4-HNE incubation affected mainly mitochondrial State 3 oxygen consumption rates *in vitro*, without changing State 4 oxygen consumption rates (Figure 5E and F). To confirm the benefits of Alda-1 on 4-HNE-induced mitochondrial dysfunction, isolated mitochondria were incubated with Alda-1 prior to 4-HNE (10 μ M) treatment. Activation of ALDH2 protected against 4-HNE-mediated mitochondrial dysfunction, resulting in an improvement of RCRs and



State 3 oxygen consumption rates by 55 and 172%, respectively, when compared with 4-HNE-treated mitochondria (Figure 5D–E). Alda-1 treatment *per se* did not affect mitochondrial bioenergetics.

4. Discussion

Over the past decades, rapid and substantial advances have been made in the understanding of intracellular processes involved in HF, positively contributing to drug development in this field.¹ However, in spite of new therapies to improve clinical outcomes,²⁶ myocardial infarction-induced HF remains the main cause of death worldwide.² Thus, there is a compelling need for new pharmacological therapies that improve patient quality of life and survival once cardiac dysfunction occurs.

Due to its pivotal role in bioenergetics, redox homeostasis, ion handling, and cell death, mitochondrial dysfunction is considered a critical

factor in the progression of HF.^{27,28} Mitochondrial ALDH2 has emerged as a key enzyme in cardioprotection, since it efficiently eliminates toxic aldehydes by catalyzing their oxidation to non-reactive acids.⁴ Experimental approaches using either pharmacological activation or genetic overexpression of ALDH2 have shown that improved detoxification of reactive aldehydes, such as 4-HNE, is protective against acute ischaemia/reperfusion injury,³ nitroglycerine tolerance,²⁹ and alcoholic cardiomyopathy.³⁰ More recently, mitochondrial ALDH2 has been associated with remote preconditioning in humans³¹ and metabolic remodelling-related cardioprotection in patients with congenital heart disease.³² However, the role of mitochondrial ALDH2 in HF has not been determined yet.

Using an unconscious *in vivo* model of post-myocardial infarction-induced HF, we demonstrated that sustained activation of mitochondrial ALDH2 with Alda-1 improves cardiac contractility and promotes a

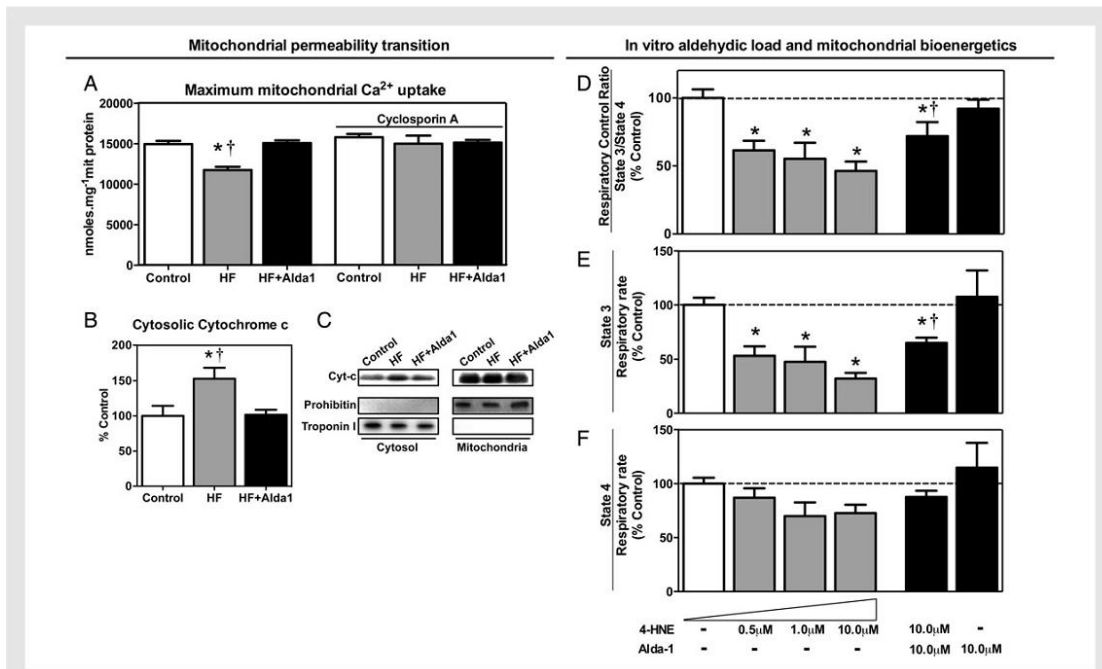


Figure 5 ALDH2 decreases sensitivity to mitochondrial permeability transition in failing hearts and preserves *in vitro* mitochondrial function upon aldehydic overload (A) Maximum mitochondrial Ca²⁺ uptake (an index of mitochondrial permeability transition) and (B) cytosolic cytochrome c levels in heart samples from control (*sham*, white bars, *n* = 10), vehicle-treated HF (HF, grey bars, *n* = 10), and Alda-1-treated HF (HF + Alda-1, grey bars, *n* = 9). Measurements were performed at 10 weeks after MI surgery. Mitochondrial cytochrome c release into the cytosol is an index of mitochondrial-mediated activation of apoptosis. Cytosolic and mitochondrial values were normalized by troponin I and prohibitin, respectively, and expressed as % of controls. (C) Representative western blots showing the levels of cytosolic and mitochondrial cytochrome c in control and age-matched post-myocardial infarction HF rats treated with Alda-1 or vehicle. Troponin I and prohibitin were used as cytosolic and mitochondrial markers, respectively. No contamination was observed between cytosolic and mitochondrial fractions. Data are means ± SEM. **P* < 0.05 vs. control (*sham*) rats. †*P* < 0.05 vs. HF + Alda-1 rats. (D) Mitochondrial respiratory rate, (E) State 3, and (F) State 4 oxygen consumption rates in isolated mitochondrial challenged with different concentrations of 4-HNE (0.5–10 μM) and Alda-1 (20 μM) (*n* = 5–6 per experiment). Cardiac mitochondria were isolated from control animals and incubated with different concentrations of 4-HNE for 10 min (0.250 mg protein mL⁻¹) in buffer containing 125 mM sucrose, 65 mM KCl, 10 mM HEPES, 2 mM inorganic phosphate, 2 mM MgCl₂, 100 μM EGTA, and 0.01% bovine serum albumin, pH 7.2, with continuous stirring at 37°C. The benefits of Alda-1 were evaluated by treating isolated mitochondria with Alda-1 (20 μM) 5 min prior to 4-HNE (10 μM) incubation. Data are means ± SEM. **P* < 0.05 vs. control. †*P* < 0.05 vs. 4-HNE (10 μM).

Downloaded from <http://cardiovascres.oxfordjournals.org/> by guest on August 30, 2014

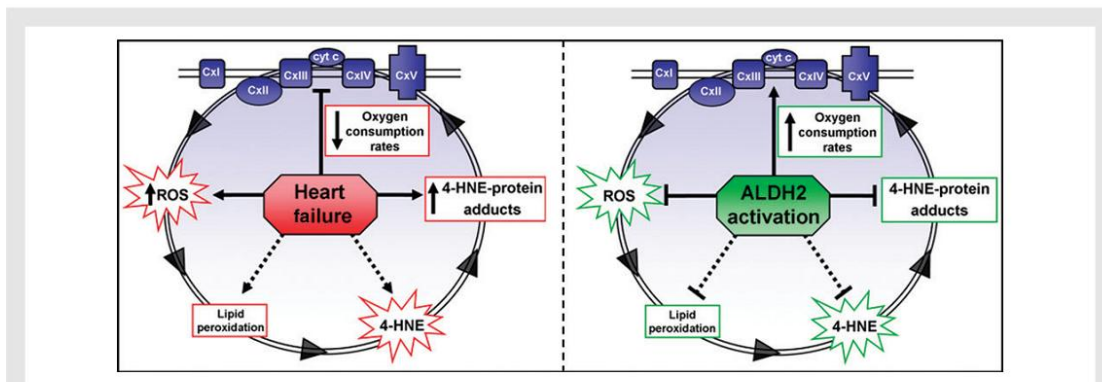


Figure 6 A proposed model for selective ALDH2 activation-mediated cardioprotection in myocardial infarction-induced HF.

cardiac anti-remodelling effect. This benefit of Alda-1 treatment can be obtained when treatment is initiated after cardiac dysfunction occurred, at 4 weeks after myocardial infarction. Alda-1-induced cardioprotection is evidenced by increased cardiac contractility, decreased LV dilation, reduced myocyte hypertrophy, and diminished cardiac fibrosis. Moreover, selective ALDH2 activation attenuated cardiac aldehydic load, mitochondrial dysfunction, and oxidative stress seen in HF. Finally, we showed that sustained treatment with Alda-1 is well tolerated in naïve rats, suggesting that chronic activation of ALDH2 may be safe.

Most of the cardiac damage occurring during HF is due to exacerbated generation of ROS, which leads to excessive oxidation of polyunsaturated fatty acids presented in biological membranes and accumulation of reactive aldehydes (i.e. 4-HNE). 4-HNE can readily interact with cysteine, histidine, and lysine residues and inactivate key proteins via Michael addition or Schiff base reactions.^{19,33} Mak *et al.*³⁴ demonstrated that 4-HNE levels are consistently elevated in the plasma of congestive HF patients and are inversely correlated with left ventricular contractility. Similar to findings in humans with failing hearts,³⁵ in the present study we found a pronounced increase in aldehydic load in the myocardium from rats with HF, characterized by accumulation of cardiac 4-HNE-protein adducts and protein carbonyls. Furthermore, sustained Alda-1 treatment strikingly corrected these changes by activating cardiac ALDH2 by 2.7-fold. These data demonstrate that selective ALDH2 activation is sufficient to produce cardioprotection against HF.

Excessive aldehyde generation during lipid peroxidation negatively affects cardiac viability by disrupting mitochondrial metabolism during acute ischaemia/reperfusion injury.^{36,37} Here, we showed that aldehydic load contributes to mitochondrial dysfunction and ROS generation in chronic HF by demonstrating that selective ALDH2 activation restored mitochondrial permeability transition, improved bioenergetics, and reduced hydrogen peroxide release in failing hearts. Moreover, acute Alda-1 treatment protected isolated mitochondria from 4-HNE-mediated dysfunction *in vitro*. We believe that reactive aldehydes lie at the centre of a positive feedback loop in HF signalling, whereby ROS produces reactive aldehydes via lipid oxidation, that then promotes mitochondrial dysfunction and lead to further ROS generation (Figure 6). In fact, disrupting this loop by reducing cardiac aldehydic load through selective ALDH2 activation enhances mitochondrial function and decreases ROS release, therefore improving the HF outcome. Unlike antioxidant treatments that aim to reduce ROS, which are unstable, and must be biologically available at the right site (e.g. inside the mitochondria) at a stoichiometric concentration, Alda-1 works catalytically on a stable product of ROS—aldehydes—within the correct microenvironment—mitochondria.

Taken together, our findings provide evidence that reducing cardiac aldehydic load via selective ALDH2 activation is sufficient to improve ventricular function in HF rats through a process mainly mediated by better cardiac mitochondrial bioenergetics and reduced ROS generation. If Alda-1-like compounds are found to be safe in humans, administration of an ALDH2 activator such as Alda-1 to HF patients may reduce the potential injury associated with aldehydic load and become a valuable tool in treating HF. However, the results of the present study should be validated in conscious AMI patients with HF.

Supplementary material

Supplementary material is available at *Cardiovascular Research* online.

Acknowledgements

We thank Katt C. Mattos, Marcelo C. Coelho, and Camille C. Caldeira-da-Silva for technical assistance.

Conflict of interest: D.M.-R. and C.-H.C. are founders of ALDEA Pharmaceuticals. C.-H.C. is also a consultant to the company. Other authors have no disclosure.

Funding

This study was supported by Fundação de Amparo à Pesquisa do Estado de São Paulo, São Paulo (FAPESP #2012/05765-2), Conselho Nacional de Pesquisa e Desenvolvimento—Brazil (CNPq #470880/2012-0) to J.C.B.F., and National Institutes of Health NIAAA 11147 to D.M.-R.. K.M.S.G. holds master's fellowship from FAPESP.

References

- Gerczuk PZ, Kloner RA. An update on cardioprotection: a review of the latest adjunctive therapies to limit myocardial infarction size in clinical trials. *J Am Coll Cardiol* 2012;**59**: 969–978.
- Roger VL, Go AS, Lloyd-Jones DM, Benjamin EJ, Berry JD, Borden WB, Bravata DM, Dai S, Ford ES, Fox CS, Fullerton HJ, Gillespie C, Halpern SM, Heit JA, Howard VJ, Kissela BM, Kittner SJ, Lackland DT, Lichtman JH, Lisabeth LD, Makuc DM, Marcus GM, Marelli A, Matchar DB, Moy CS, Mozaffarian D, Mussolino ME, Nichol G, Paynter NP, Soliman EZ, Sorlie PD, Sotoodehnia N, Turan TN, Virani SS, Wong ND, Woo D, Turner MB. Heart disease and stroke statistics—2012 update: a report from the American Heart Association. *Circulation* 2012;**125**:e2–e220.
- Chen CH, Budas GR, Churchill EN, Disatnik MH, Hurley TD, Mochly-Rosen D. Activation of aldehyde dehydrogenase-2 reduces ischemic damage to the heart. *Science* 2008;**321**:1493–1495.
- Chen CH, Sun L, Mochly-Rosen D. Mitochondrial aldehyde dehydrogenase and cardiac diseases. *Cardiovasc Res* 2010;**88**:51–57.
- Perez-Miller S, Younus H, Vanam R, Chen CH, Mochly-Rosen D, Hurley TD. Alda-1 is an agonist and chemical chaperone for the common human aldehyde dehydrogenase 2 variant. *Nat Struct Mol Biol* 2010;**17**:159–164.
- Sun L, Ferreira JC, Mochly-Rosen D. ALDH2 activator inhibits increased myocardial infarction injury by nitroglycerin tolerance. *Sci Transl Med* 2011;**3**:107ra111.
- Chen CH, Ferreira JC, Gross ER, Mochly-Rosen D. Targeting aldehyde dehydrogenase 2: new therapeutic opportunities. *Physiol Rev* 2014;**94**:1–34.
- Nakamura K, Kusano K, Nakamura Y, Kakishita M, Ohta K, Nagase S, Yamamoto M, Miyaji K, Saito H, Morita H, Emori T, Matsubara H, Toyokuni S, Ohe T. Carvedilol decreases elevated oxidative stress in human failing myocardium. *Circulation* 2002;**105**: 2867–2871.
- Johns TN, Olson BJ. Experimental myocardial infarction. I. A method of coronary occlusion in small animals. *Ann Surg* 1954;**140**:675–682.
- Campos JC, Queliconi BB, Dourado PM, Cunha TF, Zambelli VO, Bechara LR, Kowaltowski AJ, Brum PC, Mochly-Rosen D, Ferreira JC. Exercise training restores cardiac protein quality control in heart failure. *PLoS ONE* 2012;**7**:e52764.
- Ferreira JC, Koyanagi T, Palaniyandi SS, Fajardo G, Churchill EN, Budas G, Disatnik MH, Bernstein D, Brum PC, Mochly-Rosen D. Pharmacological inhibition of betallPKC is cardioprotective in late-stage hypertrophy. *J Mol Cell Cardiol* 2011;**51**:980–987.
- Palaniyandi SS, Ferreira JC, Brum PC, Mochly-Rosen D. PKC β inhibition attenuates myocardial infarction induced heart failure and is associated with a reduction of fibrosis and pro-inflammatory responses. *J Cell Mol Med* 2011;**15**:1769–1777.
- Cancherini DV, Queliconi BB, Kowaltowski AJ. Pharmacological and physiological stimuli do not promote Ca(2+)-sensitive K⁺ channel activity in isolated heart mitochondria. *Cardiovasc Res* 2007;**73**:720–728.
- Murphy AN, Bredesen DE, Cortopassi G, Wang E, Fiskum G. Bcl-2 potentiates the maximal calcium uptake capacity of neural cell mitochondria. *Proc Natl Acad Sci USA* 1996;**93**:9893–9898.
- Bueno CR Jr, Ferreira JC, Pereira MG, Bacurau AV, Brum PC. Aerobic exercise training improves skeletal muscle function and Ca²⁺ handling-related protein expression in sympathetic hyperactivity-induced heart failure. *J Appl Physiol* 2010;**109**:702–709.
- Ferreira JC, Boer BN, Grinberg M, Brum PC, Mochly-Rosen D. Protein quality control disruption by PKC β in heart failure: rescue by the selective PKC β inhibitor, betallV5–3. *PLoS ONE* 2012;**7**:e33175.
- Budas GR, Disatnik MH, Chen CH, Mochly-Rosen D. Activation of aldehyde dehydrogenase 2 (ALDH2) confers cardioprotection in protein kinase C epsilon (PKC ϵ) knockout mice. *J Mol Cell Cardiol* 2010;**48**:757–764.
- Budas GR, Disatnik MH, Mochly-Rosen D. Aldehyde dehydrogenase 2 in cardiac protection: a new therapeutic target? *Trends Cardiovasc Med* 2009;**19**:158–164.
- Lucas DT, Swzeda LI. Cardiac reperfusion injury: aging, lipid peroxidation, and mitochondrial dysfunction. *Proc Natl Acad Sci USA* 1998;**95**:510–514.

20. Petersen DR, Doorn JA. Reactions of 4-hydroxynonenal with proteins and cellular targets. *Free Radic Biol Med* 2004;**37**:937–945.
21. Figueira TR, Barros MH, Camargo AA, Castilho RF, Ferreira JC, Kowaltowski AJ, Sluse FE, Souza-Pinto NC, Vercesi AE. Mitochondria as a source of reactive oxygen and nitrogen species: from molecular mechanisms to human health. *Antioxid Redox Signal* 2013;**18**:2029–2074.
22. Kowaltowski AJ, Castilho RF, Vercesi AE. Mitochondrial permeability transition and oxidative stress. *FEBS Lett* 2001;**495**:12–15.
23. Ramachandran V, Perez A, Chen J, Senthil D, Schenker S, Henderson GI. In utero ethanol exposure causes mitochondrial dysfunction, which can result in apoptotic cell death in fetal brain: a potential role for 4-hydroxynonenal. *Alcohol Clin Exp Res* 2001;**25**:862–871.
24. Petronilli V, Penzo D, Scorrano L, Bernardi P, Di Lisa F. The mitochondrial permeability transition, release of cytochrome c and cell death. Correlation with the duration of pore openings *in situ*. *J Biol Chem* 2001;**276**:12030–12034.
25. Lee WC, Wong HY, Chai YY, Shi CW, Amino N, Kikuchi S, Huang SH. Lipid peroxidation dysregulation in ischemic stroke: plasma 4-HNE as a potential biomarker? *Biochem Biophys Res Commun* 2012;**425**:842–847.
26. Guyatt GH, Devereaux PJ. A review of heart failure treatment. *Mt Sinai J Med* 2004;**71**:47–54.
27. Bayeva M, Gheorghide M, Ardehali H. Mitochondria as a therapeutic target in heart failure. *J Am Coll Cardiol* 2012;**61**:599–610.
28. Palaniyandi SS, Qi X, Yogalingam G, Ferreira JC, Mochly-Rosen D. Regulation of mitochondrial processes: a target for heart failure. *Drug Discov Today Dis Mech* 2010;**7**:e95–e102.
29. Ferreira JC, Mochly-Rosen D. Nitroglycerin use in myocardial infarction patients. *Circ J* 2012;**76**:15–21.
30. Ma H, Yu L, Byra EA, Hu N, Kitagawa K, Nakayama KI, Kawamoto T, Ren J. Aldehyde dehydrogenase 2 knockout accentuates ethanol-induced cardiac depression: role of protein phosphatases. *J Mol Cell Cardiol* 2010;**49**:322–329.
31. Contractor H, Stottrup NB, Cunnington C, Manlihot C, Diesch J, Ormerod JO, Jensen R, Botker HE, Redington A, Schmidt MR, Ashrafian H, Kharbanda RK. Aldehyde dehydrogenase-2 inhibition blocks remote preconditioning in experimental and human models. *Basic Res Cardiol* 2013;**108**:343.
32. Zhang H, Gong DX, Zhang YJ, Li SJ, Hu S. Effect of mitochondrial aldehyde dehydrogenase-2 genotype on cardioprotection in patients with congenital heart disease. *Eur Heart J* 2012;**33**:1606–1614.
33. Hill BG, Dranka BP, Zou L, Chatham JC, Darley-Usmar VM. Importance of the bioenergetic reserve capacity in response to cardiomyocyte stress induced by 4-hydroxynonenal. *Biochem J* 2009;**424**:99–107.
34. Mak S, Lehotay DC, Yazdanpanah M, Azevedo ER, Liu PP, Newton GE. Unsaturated aldehydes including 4-OH-nonenal are elevated in patients with congestive heart failure. *J Card Fail* 2000;**6**:108–114.
35. Nakamura K, Kusano KF, Matsubara H, Nakamura Y, Miura A, Nishii N, Banba K, Nagase S, Miyaji K, Morita H, Saito H, Emori T, Ohe T. Relationship between oxidative stress and systolic dysfunction in patients with hypertrophic cardiomyopathy. *J Card Fail* 2005;**11**:117–123.
36. Churchill EN, Ferreira JC, Brum PC, Szweda LI, Mochly-Rosen D. Ischaemic preconditioning improves proteasomal activity and increases the degradation of deltaPKC during reperfusion. *Cardiovasc Res* 2010;**85**:385–394.
37. Hill BG, Awe SO, Vladykovskaya E, Ahmed Y, Liu SQ, Bhatnagar A, Srivastava S. Myocardial ischaemia inhibits mitochondrial metabolism of 4-hydroxy-trans-2-nonenal. *Biochem J* 2009;**417**:513–524.

Súmula Curricular

Dados Pessoais

Nome: Bruno Barros Queliconi

Local e data de nascimento: São Paulo, 20/06/1986

Educação

Colégio Agostiniano Mendel, São Paulo, 2004.

Universidade de São Paulo, São Paulo, 2009.

Graduação Ciências Biológicas

Ocupação

Bolsista de Doutorado, Agência FAPESP, 02/2009-02/2015

Publicações

1. Cancherini, D.V., **Queliconi, B.B.**, Kowaltowski, A.J. (2007) Pharmacological and physiological stimuli do not promote Ca^{2+} -sensitive K^+ channel activity in isolated heart mitochondria. *Cardiovascular Research* 73: 720-728 (doi: 10.1016/j.cardiores.2006.11.035).
2. Cardoso, A.R., **Queliconi, B.B.**, Kowaltowski, A.J. (2010) Mitochondrial Ion Transport Pathways: Role in Metabolic Diseases. *Biochimica et Biophysica Acta - Bioenergetics* 1797: 832-838 (doi: 10.1016/j.bbabi.2009.12.017).
3. **Queliconi, B.B.**, Wojtovich, A.P., Nadtochiy, S.M., Kowaltowski, A.J., Brookes, P.S. (2011) Redox regulation of the mitochondrial K(ATP) channel in cardioprotection. *Biochimica Biophysica Acta – Molecular Cell Research* 1813: 1309-1315 (doi: 10.1016/j.bbamcr.2010.11.005).
4. Cardoso, A.R., Chausse, B., da Cunha, F.M., Luévano-Martínez, L.A., Marazzi, T.B., Pessoa, P.S., **Queliconi, B.B.**, Kowaltowski, A.J., (2012) Mitochondrial compartmentalization of redox processes. *Free Radical Biology and Medicine* 52: 2201-2208 (doi: 10.1016/j.freeradbiomed.2012.03.008).
5. **Queliconi, B.B.**, Marazzi, T.B., Vaz, S.M., Brookes, P.S., Nehrke, K., Augusto, O., Kowaltowski, A.J., (2012) Bicarbonate modulates oxidative and functional damage in ischemia-reperfusion. *Free Radical Biology and Medicine* 55:46-53 (doi: 10.1016/j.freeradbiomed.2012.11.007).
6. Campos, J.C., **Queliconi, B.B.**, Dourado, P.M., Cunha, T.F., Zambelli, V.O., Bechara, L.R., Kowaltowski, A.J., Brum, P.C., Mochly-Rosen, D., Ferreira, J.C. (2012) Exercise training

restores cardiac protein quality control in heart failure. *PLoS One* 7:e52764 (doi: 10.1371/journal.pone.0052764).

7. **Queliconi, B.B.**, Kowaltowski, A.J., Nehrke, K. (2014) An anoxia-starvation model for ischemia/reperfusion in *C. elegans*. *J. Vis. Exp.* 7:e52764 (doi: 10.3791/51231).
8. Gomes, K.M., Campos, J.C., Bechara, L.R., **Queliconi, B.B.**, Lima, V.M., Disatnik, M.H., Magno, P., Chen, C.H., Brum, P.C., Kowaltowski, A.J., Mochly-Rosen, D., Ferreira, J.C. (2014) Aldehyde dehydrogenase 2 activation in heart failure restores mitochondrial function and improves ventricular function and remodelling. *Cardiovasc. Res.* 103:498-508 (doi: 10.1093/cvr/cvu125)

Publicações – Capítulo de Livro

1. Cardoso, A.R., **Queliconi, B.B.**, Kowaltowski, A.J. (2009) Mitochondrial reactive oxygen species in myocardial pre- and post-conditioning. In: *Studies on Cardiovascular Disorders*, H. Sauer, A. Shahand F. Laurindo, eds. Springer/Human Press.